INVESTIGATIONS INTO THE OXIDATIVE DESULFURIZATION ACTIVITY IN A FILM-SHEAR REACTOR, THE SOURCE OF ENHANCED REACTIVITY, AND OTHER POTENTIAL APPLICATIONS

by

BRANDY R. FOX

A DISSERTATION

Presented to the Department of Chemistry
and the Graduate School of the University of Oregon
in partial fulfillment of the requirements
for the degree of
Doctor of Philosophy

June 2011

DISSERTATION APPROVAL PAGE

Student: Brandy R. Fox

Title: Investigations into the Oxidative Desulfurization Activity in a Film-Shear Reactor, the Source of Enhanced Reactivity, and Other Potential Applications

This dissertation has been accepted and approved in partial fulfillment of the requirements for the Doctor of Philosophy degree in the Department of Chemistry by:

Victoria J. DeRose	Chairperson
David R. Tyler	Advisor
Kenneth M. Doxsee	Member
Catherine J. Page	Member
Mark H. Reed	Outside Member

and

Richard Linton	Vice President for Research and Graduate Studies/Dean of the Graduate School

Original approval signatures are on file with the University of Oregon Graduate School.

Degree awarded June 2011.

DISSERTATION ABSTRACT

Brandy R. Fox

Doctor of Philosophy

Department of Chemistry

June 2011

Title: Investigations into the Oxidative Desulfurization Activity in a Film-Shear Reactor, the Source of Enhanced Reactivity, and Other Potential Applications

Approved: _____
David R. Tyler

Fuel purification is an extremely active area of research in today's green world. Specifically, desulfurization of fuels is an important area of research for two reasons. First, any sulfur present in fuels generates SO_x pollutants that are hazardous to human health and contribute to acid rain. Second, even trace sulfur contaminants prohibit the use of fuel streams in fuel cells. However, achieving near-zero sulfur levels with existing technology is impractical. The work in this thesis investigates a new process for the removal of sulfur from fuel streams using a film-shear reactor (based on a process known as oxidative desulfurization) and goes on to investigate the mode of activation for the process within the reactor through a study of the reactor conditions. Additionally, other applications of the film-shear reactor, including mechanical activation of molecules and controlled nanoparticle synthesis, are explored.

Chapter I outlines the current status of oxidative desulfurization research, highlighting the strengths of the method, innovative approaches, and drawbacks to the various approaches. Chapters II and III go on to discuss the enhancement of the process in the film-shear reactor using model fuels and a variety of substrates. This method was

found to significantly enhance the oxidative desulfurization process, reducing both the time and temperature required to achieve considerable sulfur removal. Levels of desulfurization that require hours at elevated temperatures by conventional stirring methods were obtainable on the scale of seconds at or below room temperature.

Chapter IV offers investigations into the conditions within the film-shear reactor and presents studies of the ability of the high shear rates obtained in the reactor to mechanically activate molecules.

Chapter V extends the applicability of the film-shear reactor to nanoparticle synthesis through investigation of two titania synthesis methods utilizing the film-shear reactor.

Appendices A and B offer supplementary information to enhance the studies presented in Chapters II and III, and Appendices C, D, and E highlight work done investigating the ability of platinum complexes to hydrate nitriles and cyanohydrins.

This dissertation includes previously published and unpublished co-authored material.

CURRICULUM VITAE

NAME OF AUTHOR: Brandy R. Fox

GRADUATE AND UNDERGRADUATE SCHOOLS ATTENDED:

University of Oregon, Eugene
Saint Martin's University, Lacey, WA

DEGREES AWARDED:

Doctor of Philosophy, Chemistry, 2011, University of Oregon
Bachelor of Science, Chemistry, 2006, Saint Martin's University

AREAS OF SPECIAL INTEREST:

Fuel purification
Coordination chemistry
Catalytic hydration reactions

PROFESSIONAL EXPERIENCE:

Graduate Research Assistant, Department of Chemistry, University of Oregon, Eugene, 2006-2011

Graduate Teaching Assistant, Department of Chemistry, University of Oregon, Eugene, 2006-2007

Intern, Unigen Pharmaceuticals, Lacey, WA, 2005-2006

GRANTS, AWARDS, AND HONORS:

IGERT Fellowship, National Science Foundation, University of Oregon, 2010-2011

Public Impact Fellowship, University of Oregon Graduate School 2009-2010

University of Oregon Women in Graduate Sciences Travel Award, UO Women in Graduate Sciences 2009

GK-12 Fellowship, National Science Foundation, University of Oregon 2008 – 2010

James Bernard Graduate Student Travel Award, University of Oregon Chemistry Department 2009

Undergraduate Research Award, Saint Martin's University 2005

PUBLICATIONS:

Fox, B.R.; Sun, A.W.; Dauer, H.B.; Male, J.L.; Stewart, M.L. Tyler, D.R. *Fuel*, **2010**, *90*, 898.

Ahmed, T.J.; Fox, B.R.; Knapp, S.M.M.; Yelle, R.; Juliette, J.J.; Tyler, D.R. *Inorg. Chem.*, **2009**, *48*, 7828.

ACKNOWLEDGMENTS

I wish to express sincere appreciation to my advisor, Professor David R. Tyler, for his guidance in this thesis work, and his support in my academic pursuits.

I would also like to thank the several undergraduate researchers I have been fortunate enough to work with. Thank you Helen Dauer, Alexander Sun, Ryan Everett, and Benjamin Brinich for all of your efforts. Thanks also goes to Michael Strain for his NMR spectroscopy support and to Jeffrey Raber for his technical assistance with the film-shear reactor.

I am grateful to past and present members of the Tyler Lab for many stimulating scientific conversations and moral support over the years. I could not have asked for a better group of people to keep me on my toes! I would especially like to thank Takiya J. Ahmed for taking the time to help a new graduate student find her feet, and all of her advice, regarding both life and science.

I would especially like to thank my husband, Marc Fox, for being my rock while this work was being completed. I would not be where I am without his support.

This work was supported by funding from the Army Research Lab, and GK-12 (DGE-0231997) and IGERT (DGE-0549503) Fellowships from the National Science Foundation.

I dedicate this work to my mother, Dorothy Butterfield, for her dedication to raising a strong and independent daughter, and her constant reminders that I CAN.

TABLE OF CONTENTS

Chapter Page

I. FUEL PURIFICATION BY OXIDATIVE DESULFURIZATION 1

1.1. Introduction 1

1.1.1. Alternatives to HDS 5

1.2. Conventional ODS 9

1.3. Alternative Catalysts 12

1.4. Phase Transfer Catalysts 20

1.5. Use of Ionic Liquids in Desulfurization 24

1.6. Other Approaches 33

1.6.1. Alternative Oxidants 34

1.6.2. Photocatalytic Enhancement of ODS 39

1.6.3. Ultrasound-Assisted Oxidative Desulfurization 41

1.7. Summary 43

1.8. Thesis Overview 44

1.9. Acknowledgments 45

II. ENHANCED OXIDATIVE DESULFURIZATION OF MODEL FUELS USING A FILM-SHEAR REACTOR 46

2.1. Introduction 46

2.2. Experimental 48

2.2.1. Reagents 49

2.2.2. Film-Shear Reactor Trials 49

2.2.3. Sample Preparation and Analysis 49

Chapter Page

2.2.4. Conventional Mixing Control Experiments 50

2.3. Results and Discussion 50

2.4. Summary and Conclusions 55

2.5. Notes 55

III. ENHANCED OXIDATIVE DESULFURIZATION REACTIVITY IN A FILM-SHEAR REACTOR 57

3.1. Introduction 57

3.2. Experimental 59

3.2.1. General Considerations 59

3.2.2. Reagents 59

3.2.3. Film-Shear Reactor Trials 60

3.2.4. Sample Preparation and Analysis 60

3.2.5. Conventional Mixing Controls 61

3.2.6. Air as an Oxidant 61

3.3. Results and Discussion 62

3.3.1. Overview of Desulfurization 62

3.3.2. Design of Experiments 63

3.3.3. Other Thiophene Contaminants 65

3.3.4. High Combined Flow Rate 68

3.3.5. Utilization of Air as the Oxidant 69

3.4. Summary and Conclusions 71

Chapter Page

IV. INVESTIGATION INTO THE SOURCE OF ACTIVATION IN THE FILM-SHEAR REACTOR AND EXPLORATION OF POTENTIAL APPLICATIONS 72

4.1. Introduction 72

4.2. Temperature in the Film-Shear Reactor 73

4.2.1. Localized Hot Spots 73

4.2.2. Overall Temperature Conditions 75

4.3. Probes of Mechanical Activation 82

4.3.1. Benzocyclobutene Probes 84

4.3.2. Binol Probes 87

4.3.3. Azo-Functionalized Poly(ethylene glycol) Probes 89

4.4. Conclusions 92

4.5. Experimental Procedures 93

4.5.1. Reagents 93

4.5.2. Reactor Trials 93

4.5.3. Localized Hot Spot Studies 94

4.5.4. Overall Temperature Experiments 94

4.5.4.1. In the Absence of the Heat Exchanger 94

4.5.4.2. In the Presence of the Heat Exchanger 95

4.5.4.3. Reaction Rate Probe Studies 95

4.5.5. Dimethoxybenzocyclobutene Control Reactions 96

4.5.6. Dimethoxybenzocyclobutene Reactor Trials 96

Chapter Page

4.5.7. Binol-PMA Reactor Trials and Controls 96

4.5.8. Azo-PEG Trials and Analysis 97

V. CONTROLLED NANOPARTICLE SYNTHESIS WITHIN THE FILM-SHEAR REACTOR 98

5.1. Introduction 98

5.2. ODS Controls Using Commercially Available TiO_2 102

5.3. Particle Synthesis Starting with $TiOSO_4$ 103

5.4. Titania Synthesis from TEOT Precursor in the Film-Shear Reactor 105

5.5. Conclusions 108

5.6. Experimental Procedures 109

5.6.1. Reagents 109

5.6.2. Reactor Trials 109

5.6.3. ODS Trials 110

5.6.4. $TiOSO_4$-based Reactor Trials 110

5.6.5. TEOT-based Reactor Trials 110

VI. Summary and Outlook 111

APPENDICES 113

A. SUPPORTING INFORMATION FOR CHAPTER II 113

B. SUPPORTING INFORMATION FOR CHAPTER III 116

C. INVESTIGATION OF THE REACTIVITY OF PT PHOSPHINITO AND MOLYBDOCENE NITRILE HYDRATION CATALYSTS WITH CYANOHYDRINS 132

D. SUPPORTING INFORMATION TO ACCOMPANY APPENDIX C 167

Chapter Page

E. FURTHER INVESTIGATION INTO PLATINUM-BASED NITRILE HYDRATION CATALYSTS: EXPLORATION OF $[PtCl\{(PEt_2O)_2H\}]_2$; ATTEMPTED SYNTHESIS OF A BIS-DIMETHYLPHOSPHINITO PLATINUM COMPLEX; AND FURTHER EXPLORATION OF THE AQUEOUS BEHAVIOR OF $PtCl\{P(Me)_2OH\}\{P(Me)_2O\}_2H$ 215

REFERENCES CITED 227

LIST OF FIGURES

Figure Page

CHAPTER I

1. Selected sulfur-containing fuel contaminants. 3

2. Hydrodesulfurization of dibenzothiophene derivatives occurs through two pathways. 5

3. Removal of sulfur atom as sulfate in biodesulfurization 7

4. Thiophenic contaminants are oxidized to sulfone. 7

5. Oxidation of sulfides by peracid oxidants 9

6. Ionic liquids containing carboxylic acid for use in ODS 33

7. Combination of photochemical oxidation and ionic liquid extraction..... 40

CHAPTER II

1. Diagram of the film-shear reactor. 48

2. The effect of recirculation on desulfurization. 53

3. The effect of hydrogen peroxide concentration on desulfurization 54

CHAPTER III

1. Thiophenes examined in this study. 67

2. Reactor setup for oxidation by air. 71

CHAPTER IV

1. Increase in temperature through reactor in absence of heat exchanger. 76

Figure Page

2. Increase in temperature after passage of water through film-shear reactor 77

3. Change in temperature of acetone/water after passage through the reactor 79

4. Average temperature encountered by *t*-BuCl reaction system within the film-shear reactor 81

5. Unique products formed from benzocylcobutene probes 83

6. Trapping of a ring open form of benzocylcobutene 85

7. ^{1}H NMR spectra of benzocyclobutene probes 86

8. Racemization of central binol unit 88

9. Azo-PEG polymer 90

10. GPC data of azo-PEG polymer after 2 hours in the reaction zone 91

CHAPTER V

1. Species formed on titania surface in contact with hydrogen peroxide. 99

2. Effect of rotation speed in SDR on particle size 100

3. Size and distribution of $CaCO_3$ nanoparticles in RPB and conventional batch precipitation reaction conditions 101

4. Increase in color and cloudiness accompanies increase in shear rate 104

5. TEM of solid obtained after application of film-shear reactor 104

6. TEM illustrating material connecting particles 107

7. STEM image and EDX data 108

LIST OF TABLES

Table Page

CHAPTER I

1. Calculated electron densities and rate constants for selected compounds 11

2. Percent oxidation of model contaminants by V_2O_5/TiO_2 17

3. Desulfurization percentages after extraction with selected ionic liquids..... 25

4. Percent conversion of thiophene by hydrogen peroxide and formic acid under ultrasound..... 42

CHAPTER II

1. Parameters and the range over which they were surveyed 51

2. Effect of residence time on the extent of desulfurization 52

CHAPTER III

1. Parameters included in DOE and the range over which they were surveyed 64

2. DOE trials and results 66

3. Oxidation of additional thiophenes 67

4. Ultra high flow rate experiments 70

CHAPTER V

1. Percent removal of benzothiophene by ODS with and without titania catalyst 103

LIST OF SCHEMES

Scheme Page

CHAPTER I

1. Thiophenic sulfur is oxidized to sulfuric acid by TS-1..... 18

2. Sulfide oxidation products in the presence of MPHT..... 35

3. Oxidation of sulfides by O_2 with a $MnFe_{1.8}Cu_{0.15}Ru_{0.05}O_4$ catalyst..... 37

CHAPTER II

1. Thiophene contaminant is oxidized to the corresponding sulfone..... 47

CHAPTER V

1. Synthesis of titania from TEOT..... 106

CHAPTER I

FUEL PURIFICATION BY OXIDATIVE DESULFURIZATION

1.1. Introduction

Sulfur contaminants in fuel streams are detrimental for two primary reasons. First, sulfur contaminants in fuels generate SO_x compounds when the fuel is combusted. These compounds go on to react in the atmosphere to generate H_2SO_4, a major contributor to acid rain, which is hazardous to both the environment (causing damage or death to forests and marine life) and manmade artifacts.[1,2] Further, SO_2 itself has been linked to adverse respiratory effect, leading to increased rates of emergency room visits and hospital admissions even following short-term exposure.[3]

Secondly, existing fuel streams are ideal candidates for portable fuel cell applications due to their high energy densities and established infrastructures. However, even trace amounts of sulfur contaminants in these fuel streams prohibit this application.[4] This is because the sulfur contaminants so effectively poison both reforming and fuel cell electrode catalysts. Because of this sensitivity to poisoning, ppb levels of sulfur

contaminants are required to achieve a commercially viable operating life for fuel cells utilizing these fuels.[5,6]

Obtaining low sulfur fuels, however, can be challenging. Sulfur is the third most abundant element in crude petroleum, falling behind only carbon and hydrogen.[7,8] The actual identities of the sulfur contaminants found in fuels streams vary between fractions.[9,10] In general, the lighter distillates contain primarily mercaptans, sulfides and disulfides while the heavier distillates contain more of the heterocyclic aromatic sulfur species.[11-14] The middle distillates tend to contain predominantly benzothiophenes and alkylated derivatives,[15-17] while dibenzothiophene and its alkylated derivatives are the primary contaminants of diesel streams. Some of the more common sulfur contaminants that will be discussed are illustrated in Figure 1.

The most frequently applied technology currently for the desulfurization of fuels is hydrodesulfurization (HDS). In HDS, the sulfur in the contaminant is converted to H_2S and, in the case of contaminants possessing aromatic rings or olefin functionality, the rest of the molecule is hydrogenated as well. This occurs over a transition metal catalyst (typically solid supported Ni/Mo or Co/Mo sulfides, though the solid support isn't strictly necessary[18]) at high temperatures and under high pressures of hydrogen gas.[19] HDS is a well established technology and is quite effective in removing the thiol and mercaptan contaminants of lighter distillates. However, there are other contaminants (known as recalcitrant sulfur compounds) that are more resistant to this treatment and extremely difficult to remove while maintaining other fuel requirements.[20] These recalcitrant compounds consist mainly of polycyclic sulfur-containing heterocycles, primarily

benzothiophene and its alkylated derivatives.[21-23] 4-MBT and 4,6-DMBT are particularly difficult to remove.[24]

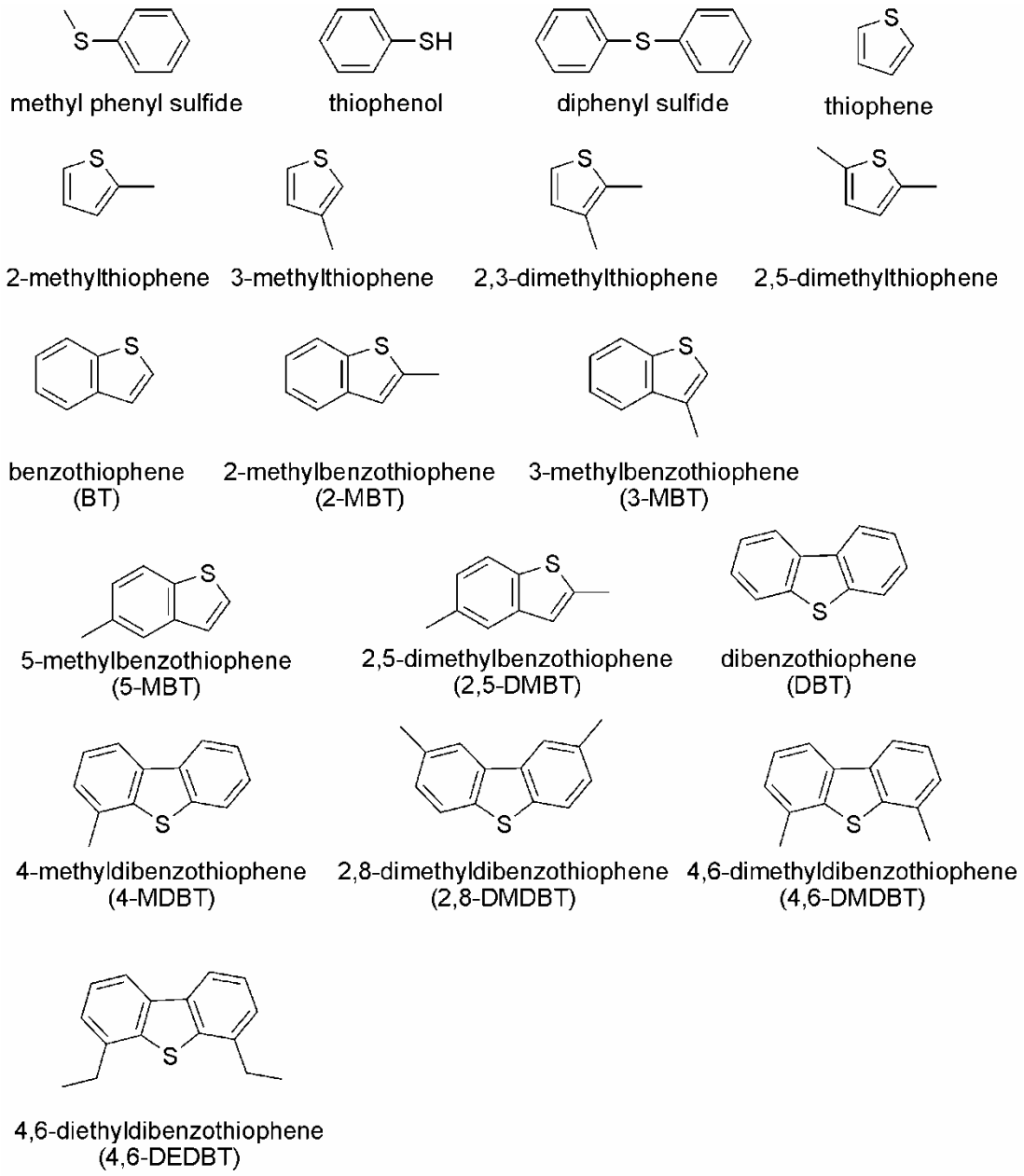

Figure 1. Selected sulfur-containing fuel contaminants.

The drastically reduced reactivity in dibenzothiophenes that are substituted at the 4 and/or 6 positions is thought to be due to a change in the dominant pathway of desulfurization.[25,26] HDS over transition metal catalyst takes place via two different pathways: hydrogenolysis and hydrogenation (Figure 2). In the hydrogenolysis pathway, the sulfur atom of the contaminant is removed prior to hydrogenation of the aromatic rings. In contrast, the hydrogenation pathway involves the hydrogenation of the aromatic rings before any reactivity of the sulfur atom occurs. In general, the hydrogenolysis pathway is the faster of the two pathways for thiophenic compounds with accessible sulfur atoms and dominates in the desulfurization process. However, this pathway requires coordination of the sulfur atom to the catalyst, and is essentially shut down by the inaccessibility of the sulfur atom in the more sterically hindered recalcitrant sulfur compounds. As a consequence, the relative amount of desulfurization occurring through the significantly slower hydrogenation pathway increases.[27-29] Upon hydrogenation of the aromatic rings (the first step in the hydrogenation pathway) the sulfur atom becomes more accessible so that rapid hydrogenolysis can then occur.[30]

This limitation of conventional HDS, in combination with the increasingly stringent sulfur regulations and need for ultra-low sulfur fuels for certain applications, has led to an increase in investigation of alternative desulfurization approaches. In addition to the investigation of novel HDS catalysts, alternatives to the HDS process are being investigated.

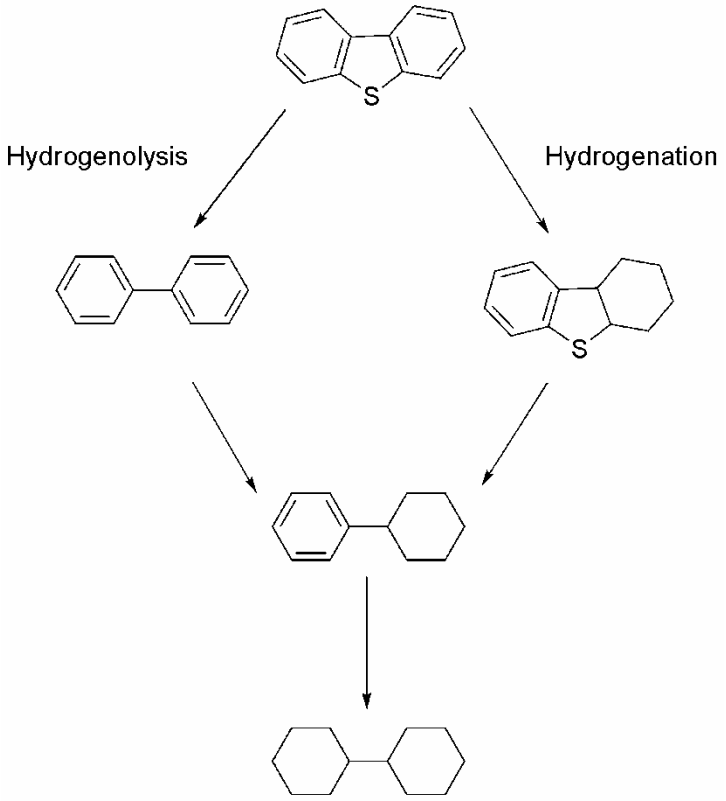

Figure 2. Hydrodesulfurization of dibenzothiophene derivatives occurs through two pathways.

1.1.1. Alternatives to HDS

One alternative to HDS that has been investigated is desulfurization by adsorption of the sulfur contaminants. Adsorptive desulfurization can take the form of H_2S removal after initial HDS or when H_2S is a contaminant of the gas, or it can involve direct adsorption of the more recalcitrant compounds.[31] Direct adsorption of the recalcitrant sulfur compounds is an especially appealing process because it can be carried out at ambient temperatures and pressures, and the sorbents may be regenerable. The sorbents

used for this process are often zeolite-based, and success has been found using materials that have been impregnated by with silver or copper. These sorbents are able to remove the sulfur contaminants via π complexation with the ring systems.[32] However, zeolites that have undergone ion exchange with Cu, Ni, Zn, Pd, and Ce have also seen success in removal of aromatic sulfur contaminants, and adsorption has found to be through direct S-adsorbent interactions (atleast in the case of Ce).[33]

Also being investigated as a potential alternative is biodesulfurization, which takes advantage of enzymes in various microorganisms that are capable of breaking down the sulfur contaminants. This process is carried out over days at low temperature under atmospheric pressure, and microorganisms capable of removing the sulfur atom from benzothiophenes as well as dibenzothiophenes have been discovered.[34,35] Many of these microorganisms (primarily rhodococci*)* are able to selectively remove only the sulfur atom from dibenzothiophene contaminants, leaving 2-hydroxybiphenyl as the product of desulfurization and minimizing the effect of desulfurization on the energy content of the fuel streams (Figure 3).[36-40] Some are capable of selectively removing above 75% of the sulfur from crude oil streams,[41] making this a potentially useful tool in fuel processing. However, the sterically hindered compounds that are most resistant to HDS are the most resistant to biodesulfurization as well, and as of yet this technology remains incapable of meeting the needs of deep desulfurization, and has not been industrially adopted.[42]

Another promising alternative to HDS is oxidative desulfurization (ODS). In ODS, the sulfide contaminants are oxidized through the sulfoxide and onto the sulfone (Figure 4). Because the resulting sulfones exhibit vastly different solubility properties,

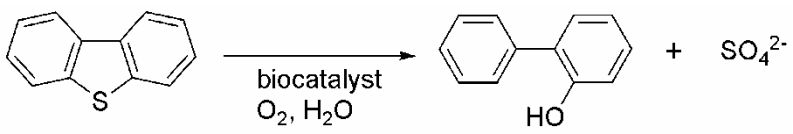

Figure 3. Removal of sulfur atom as sulfate in biodesulfurization. While biodesulfurization can digest the entire contaminatant in some cases, other microorganisms are capable of removing only the sulfur atom to leave 2-hydroxybiphenyl behind.

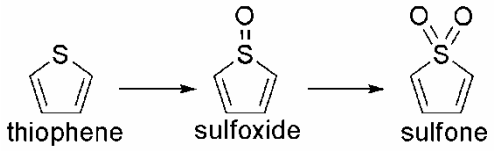

Figure 4. In ODS, thiophenic contaminants are oxidized through the sulfoxide and on to the sulfone, which is less soluble in the fuel and more easily extracted.

they are often virtually insoluble in the fuel, and therefore easily removable by extraction into a more polar cosolvent. The complementary reactivity exhibited in ODS (to be discussed) compared to HDS makes this method especially appealing.

The chemistry of this oxidation is well studied, and many techniques for ODS are inspired by established preparatory routes for the conversion of sulfides to sulfoxides or

sulfones. Common preparatory methods include oxidation by a variety of oxidants both with and without catalysts.[43-47] Peracids are the most commonly utilized oxidants, but a variety of inorganic oxidants have been used as well, including nitric acid, $NaBO_3 \bullet 4H_2O$, $Na_2Cr_2O_7,/H^+$, $KMnO_4$, Ru on alumina, MoO_5/HMPA, and $NaOCl/H^+$.[48-50] Additionally, catalysts such as $Sc(OTf)_3$, CH_3ReO_3, hydrotalcites, molybdenum, tungsten, and iron complexes have been used in conjunction with hydrogen peroxide as the oxidant to effectively convert sulfides and thiophenes to sulfoxides and sulfones.[51-55] Bicarbonate in combination with hydrogen peroxide has also been used, and even introduced as the anion of surfactants to promote aqueous phase activity of sulfides.[56] More recently, nanoparticles have also been used in the preparation of sulfoxides from sulfides.[57] Even the use of ultrasound has been employed to improve sulfone synthesis from sulfides in the presence of various catalysts.[58]

In oxidizing sulfides to sulfoxides (and then further on to sulfones), there are two primary modes.[59] One involves the formation of a sulfenium radical as the initiating step, and is observed as the primary mechanism in biological systems, but has also been invoked for some transition metal oxidations as well as oxidations where the hydroxyl radical is the oxidant and select organic acid/ H_2O_2 systems.[60,61] The second pathway, which is more commonly observed in systems utilizing electrophilic oxidants (such as peracids), is illustrated in Figure 5.[62] This mechanism proceeds through attack of a lone pair from the sulfur atom on the terminal peracid oxygen to cleave the O-O bond and has also been observed in select enzymatic systems.

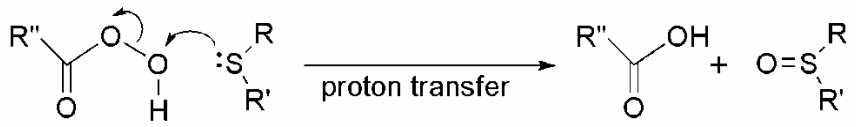

Figure 5. Oxidation of sulfides occurs through attack of the lone pair of sulfur atom on the peroxy oxygen in the case of most peracid oxidants.

However, using these well established preparatory techniques for fuel purification requires that investigators develop innovative ways to overcome the problematic matrix that the contaminants are contained in if they plan to remove the sulfur compounds based on this oxidative reactivity. Many of the oxidants are delivered as aqueous reagents and are, therefore, immiscible with the hydrocarbons that contain the sulfur-containing substrate. The result is a biphasic system that behaves quite differently than the ideal systems developed for the preparatory oxidation of sulfides to sulfones. Additionally, many of the preparatory methods are too expensive or otherwise inappropriate for large scale purifications.

1.2. Conventional ODS

The most widely studied and well understood methods of ODS employ H_2O_2 as and oxidant and require some form of catalyst. Typically this catalyst is an organic acid that forms a peroxo-acid in the presence of H_2O_2 as the active oxidant. The most commonly employed acid catalysts are formic acid, and acetic acid. The primary drawback is that conventional ODS requires that an aqueous oxidant act on a fuel-phase substrate, which translates into hours stirring at elevated temperatures. While many

methods of improving this process have been investigated, which will be discussed, this conventional ODS does effectively remove sulfur from fuel streams, and many of the fundamental studies into ODS have employed this system.

Several groups have also investigated this fundamental ODS process using catalytic formic acid in combination with aqueous H_2O_2.[63] Otsuki, et al., for example, compared rates of thiophene oxidation using aqueous H_2O_2 and formic acid to calculated electron densities on the sulfur atom and found that contaminants with a greater amount of electron density on the sulfur atom were more reactive to ODS by this method.[64] As a result, and in stark contrast to HDS, DBT and alkylated derivatives were among the most responsive contaminants to oxidation by this method. The calculated electron densities and rates are illustrated in Table 1, and it can be seen that there is a direct correlation between the two values. Furthermore, the most electron deficient thiophenes investigated (2,5-DMT, 2-MT, and thiophene) were not oxidized by this method. This was consistent with previous studies noting that the ease of oxidation was correlated to the electron density of the thiophene.[65]

Acetic acid is also commonly employed for this process.[66] In one example, Zannikos and Stournas investigated the oxidative desulfurization of straight-run gas oils (containing primarily aliphatic sulfide contaminants) by heating to 90 ˚C in the presence of an equal volume of acetic acid and aqueous hydrogen peroxide.[67] They were able to remove up to 90% of the contaminants from the fuels after approximately 30 minutes of this treatment with large amounts of acetic acid and hydrogen peroxide, but only after 3

Table 1. Calculated electron densities on sulfur atoms and rate constants for selected sulfur compounds (Ref. 64).

Thiophene	**Calculated electron density**	**k (L mol^{-1} min^{-1})**
methyl phenyl sulfide	5.915	$2.95x10^{-1}$
Thiophenol	5.902	$2.70x10^{-1}$
Diphenylsulfide	5.860	$1.56x10^{-1}$
4,6-DMDBT	5.760	$7.67x10^{-2}$
4-MDBT	5.759	$6.27x10^{-2}$
DBT	5.758	$4.60x10^{-2}$
BT	5.739	$5.74x10^{-3}$
2,5-DMT	5.716	n/a
2-MT	5.706	n/a
thiophene	5.696	n/a

extractions with polar organic solvents followed by 3 washings with water. Methanol, N-methyl pyrrolidone, and DMF were studied as extractant cosolvents, and it was found that methanol provided the greatest degree of sulfur removal among these.

Shiraishi, et al. also investigated oxidative desulfurization of model fuels (BT, 3-MBT, 2,3-MBT, DBT, 4-MDBT, 4,6-DMDBT, or 2,8-DMDBT in tetradecane) as well as actual light oils by H_2O_2 and acetic acid.[68] They correlated the electron densities of the sulfur atom of each contaminant with rate constants, and again found that increasing electron density corresponded to an increase in oxidation rate. Interestingly, they found that this relationship was linear within each series (BT and derivatives versus DBT and derivatives). They found also that a subsequent extraction step with an organic solvent was required to achieve deep desulfurization levels in the actual oils because of a slight solubility of the oxidized products in the fuel. An acetonitrile/ water mix was the solvent

of choice for this extraction. This process was also effective for the denitrification of the oils studied, but did result in some oxidation of aromatics in the light oils.

Ramirez-Verduco, et al. also studied the ability of this basic ODS system followed by extraction by a polar solvent for the removal of sulfur contaminants from actual diesel.[69] Using 30% H_2O_2 as an oxidant and acetic acid as a catalyst followed by a subsequent extraction with polar solvent, they were able to remove 60-62% of the recalcitrant sulfur contaminants (depending on the extraction solvent employed) from actual pretreated diesel fuel in 6 hours stirring at 50 ˚C.

While the above examples demonstrate that straight oxidation of the thiophene contaminants by hydrogen peroxide using a simple organic acid catalyst and organic solvent extractant is capable of removing these contaminants from fuel quite effectively, the process still requires that an aqueous oxidant act on a substrate in the fuel phase. As a result, hours of reaction time at elevated temperatures are required for effective desulfurization. Because of this, several groups have employed unique strategies to enhance this basic ODS process.

1.3. Alternative catalysts

A variety of heterogeneous catalysts have been investigated for improvement of the ODS process. The use of a heterogenous ODS catalyst typically results in a 3-phase system. The fuel phase and the oxidant/extractant occur as two liquid phases, and the catalyst comprises a third and solid phase. Introduction of heterogeneous catalysts has improved the ODS process in many cases, providing greater removal at lower reaction

temperature or shorter reaction times. Additionally, heterogeneous catalysts have the advantage of being easily recoverable and not contaminating the fuel phase.

Yu, et al. explored the use of activated carbon as a catalyst for ODS in the presence of H_2O_2 and formic acid.[70] Introduction of the activated carbon did provide a significant improvement over the conventional ODS system; in trials studying the desulfurization of actual diesel, they were able to remove up to 98% of the sulfur contaminants while recovering 96.5% of the fuel. They found that the catalytic activity of the activated carbon increased with increasing surface area, and proposed that the activated carbon promoted the decomposition of the H_2O_2 to form highly reactive hydroxyl radicals, which had been reported in other systems.[71] The authors further proposed that oxidation occurred by this hydroxyl radical after the contaminant had been activated by adsorption onto the surface of the carbon. The oxidation was most efficient at low pH, which was provided through the addition of formic acid, which also served to oxidize the sulfur through the standard performic acid route.

Polyoxometallates are fairly well established catalysts for ODS with H_2O_2 as an oxidant.[72] Commercially available phosphotungstic acid is the most widely studied, but other species have been investigated as well. For example, Te, et al. compared the reactivities of phosphotungstic acid hydrate ($H_3PW_{12}O_{40}\bullet 20H_2O$), sodium phosphotungstic hydrate ($Na_3PW_{12}O_{40}\bullet 14H_2O$), phosphomolybdic acid hydrate ($H_3PMo_{12}O_{40}\bullet 15H_2O$), sodium phosphomolybdic hydrate ($Na_3PMo_{12}O_{40}\bullet 20H_2O$), silicotungstic acid hydrate ($H_3SiW_{12}O_{40}\bullet 25H_2O$), silicomolybdenic acid hydrate ($H_3SiMo_{12}O_{40}\bullet xH_2O$).[73] They found that the phosphotungstic acid performed the best

(removing nearly all of the DBT as a model contaminant in toluene in 1 hour at 50 ˚C), followed by the Mo analogues (removing approximately half of the DBT under the same conditions) and finally the Si containing compounds (removing just over 20% in the case of the silicotungstic acid hydrate and exhibiting nearly no reactivity in the case of the silicomolybdenic acid hydrate under these conditions). The authors propose this significant drop in reactivity going from P to Si is likely due to a difference in the species formed on contact with H_2O_2. Phosphotunstic compounds and molybdenum analogues have been shown to form polyoxoperoxo compounds on treatment with H_2O_2. No similar compounds have been isolate for the Si versions. They also found that the reactivity across a series of DBT-based compounds decreased in the order: DBT > 4-MDBT > 4,6-DMDBT, suggesting that sterics play an important role in this oxidative system.

Chica, et al. investigated the oxidation of various sulfides using *t*-BuOOH over CoAPO catalysts (APO= aluminophosphate) and compared these results to a homogeneous Co acetate catalyst as well and an alumina supported molybdenum oxide.[74] They found that the CoAPO provided the greatest conversion to sulfone with *t*-BuOOH for the sulfides investigated (methylphenyl sulfide, diphenyl sulfide, 4-MDBT, and 2,5-DMT). However, while the CoAPO system was quite effective for the conversion of the first two non-thiophenic substrates, (oxidizing 99 and 98% of the methylphenyl sulfide and diphenyl sulfide after minutes at 70 ˚C) the system performed more poorly for oxidation of the 4-MDBT and 2,5-DMT substrates, providing only 73 and 30% removal of these substrates, respectively, under the same conditions. This reactivity trends with the electron density on the sulfur atom for this series of substrates and was consistent for all of the catalysts investigated.

Ramirez-Verduzco, et al. also investigated the ability of heterogeneous WO_x/ZrO_2 catalysts used with H_2O_2 to remove sulfur contaminants from an actual diesel streams with a variety of extractive cosolvents.[75] N,N-DMF, γ-butyrolactone, 2-ethoxyethanol, and acetonitrile were the cosolvents investigated, and the authors found that the γ-butyrolactone provided the best results. Using γ-butyrolactone and the solid catalyst, they were able to reduce the total sulfur content in a diesel stream from 320 to 90ppm (72% removal) in 1 hour at 60 ˚C. However, the authors did not comment on the removal of other fuel components or identify the sulfur species in the γ-butyrolactone layer, but simply reported the remaining sulfur in the fuel.

Considerable work has also gone into the investigation of supported vanadium oxide catalysts for ODS. Cedeno-Caero, et al. studied the ability of vanadium oxide on titania to remove several contaminants from a model fuel system.[76] Using hydrogen peroxide and *t*-butyl hydrogen peroxide as oxidants in a triphasic (liquid-liquid-solid) system, they evaluated the effect of temperature, solvent and amount of oxidant on the ODS process as well as the relative reactivity of the various contaminants. They found that desulfurization decreased in the order DBT > BT > 4-MDBT > 2-MT > 2,5-DMT > 4,6-DMDBT. This is not the order of reactivity that would be predicted by traditional ODS based on electron density alone, and the authors attribute this alternate order of reactivity to steric hindrance of the methyl substituents reducing catalyst access. They found that increasing the ration of the model fuel to the polar solvent (CH_3CN/H_2O) decreased the desulfurization activity, while increasing the temperature of the process increased activity. Interestingly, the best results were obtained when the oxidant was added gradually, which reduced the amount of thermal decomposition of the peroxide

that occurred. Using this system, they were able to remove more than 80% of DBT from their model fuels in minutes at 70 ˚C.

Further studies into the effect of oxidant and nitrogen-containing compounds on this process revealed that it is inhibited by nitrogen-containing compounds and that hydrogen peroxide as an oxidant allowed for more desulfurization that when *t*-butyl hydroperoxide was used.[77] The nitrogen-containing contaminants that were introduced to the model fuel were quinoline, indole and carbazole. Only indole was actually oxidized under these conditions, but a decrease in desulfurization was observed for all three compounds. Inhibition was greatest in the case of quinoline, followed by indole and finally carbazole. The authors propose that this is due to poisoning of surface catalytic sites by the nitrogen-containing compounds.

Cedeno-Caero, et al. also went on to examine the effect of the solid support on the ODS activity of these vanadium-based catalysts.[78] They studied the removal of BT, DBT, 4-MDBT, and 4,6-DMDBT from hexadecane at 60 ˚C using *t*-butyl hydroperoxide and hydrogen peroxide as oxidants, as well as the desulfurization of actual diesel fuel. They found that the identity of the solid support did, indeed, affect the desulfurization activity and that alumina and niobia provided the greatest activity. However, it was titania that showed the greatest resistance to poisoning by indole. Further studies into the methods used for preparation of these titania supported V_2O_5 catalysts revealed that the preparative method could have a significant effect on their ODS activity due to variations in pore volume, surface area, average vanadium oxidation state, and crystallinity that arise from preparative method.[79] The best activities for the oxidation of DBT, 4-MDBT,

and 4,6-DMDBT in acetonitrile after 90 minutes at 60 ˚C using these catalysts are shown in Table 2. The reactivity decreased in the order of of DBT > 4-MDBT > 4,6-DMDBT, as seen with earlier generations of these catalysts, with 68% removal of DBT under the above conditions.

Table 2. Percent oxidation of model contaminants by V_2O_5/TiO_2 after 90 minutes at 60 ˚C (Ref. 78).

Thiophene	% Oxidation
DBT	68
4-MDBT	60
4,6-DMDBT	51

Mixed metal V-Mo based catalysts on alumina supports have also been investigated as potential catalysts for ODS. Gonzalez-Garcia and Cedeno-Caero evaluated the ability of these catalysts to remove DBT, 4-MDBT, and 4,6-DMDBT from hexadecane as a model fuel as well as actual Mexican diesel fuel utilizing both H_2O_2 and *t*-butyl hydrogen peroxide as oxidants.[80,81] The catalyst was observed over several ODS cycles at 60 ˚C, and it was noted that there was a significant decrease in catalytic activity with each cycle when H_2O_2 was used as the oxidant. Activity was nearly completely lost after only 4 cycles, but this was not the case with *t*-butyl hydrogen peroxide, where there was actually a slight increase in activity with each cycle. This loss in activity was attributed to the adsorption of water onto the catalyst in the case of the H_2O_2 oxidant. Despite this loss of activity, the best desulfurization occurred during the first cycle of desulfurization using H_2O_2 rather than the *t*-butyl hydrogen peroxide. In this first cycle,

approximately 28% of DBT, 18% of 4-MDBT, and 13% of 4,6-DMDBT were converted to sulfone after an hour or reaction. After partial reduction of the catalyst, similar sulfone yields were obtained by the 4th cycle using *t*-butyl hydrogen peroxide as an oxidant as well.

With the successful application of commercially available titanium-containing zeolites to the oxidation of aliphatic thioethers,[82-84] there has been an increased interest in the synthesis and application of zeolitic materials (primarily those containing Ti and V) to the ODS process in recent years. In one example, Kong, et al. applied TS-1 (titanium silicate) to the oxidation of thiophene in *n*-octane as a model gasoline system with H_2O_2 as the oxidant.[85] Thiophene was chosen in this case as a challenging substrate for ODS due to the low electron density on the sulfur atom as compared to the larger polycyclic contaminants. Using this method, they were able to remove over 98% of the thiophene contaminant from the *n*-octane in 6 h at 60 ˚C, producing primarily sulfuric acid as the sulfur product (Scheme 1). The authors propose that activation of the thiophene for oxidation occurs through coordination of the aromatic electrons to the Ti center. This removal process represents a definite improvement over the traditional organic acid catalyzed ODS, which was unable to oxidize thiophenes with low electron densities on the sulfur molecule such as the parent molecule itself.

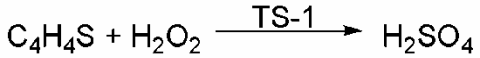

Scheme 1. Thiophenic sulfur is oxidized to sulfuric acid by TS-1.

The authors later noted that selectivity was a problem for this system because olefins in the fuels or model fuels also coordinated to the Ti sites, thereby inhibiting desulfurization activity. This challenge was addressed through addition of Ag to the TS-1 system.[86] Ag was selected because of its established ability to adsorb sulfur contaminants from fuel streams as noted above. Impregnation of the TS-1 with Ag did, indeed, increase the selectivity of the ODS system, making it possible for the authors to investigate the desulfurization of actual gasoline. They found that they were able to get up to 86% desulfurization of FCC gasoline consisting primarily of alkylated thiophenes as the sulfur contaminant, and also containing a variety of potentially competitive olefins. Further, even in the case of the model thiophene in *n*-octane, desulfurization was increased from 42% in the case of TS-1 alone to 78% for Ag/TS-1 after 30 minutes at 60 ˚C. The authors propose that the Ag sites are responsible for the selective adsorbent of the thiophene contaminants that are then oxidized by the Ti sites.

Zeolitic catalysts have also been investigated for the ODS of the more recalcitrant sulfur contaminants of the heavy distillates. For example, Hulea, et al. investigated the ability of TS-1, Ti-beta, and TI-HMS (hexagonal mesoporous silica) to catalyze the oxidation of several thiophenic compounds (including thiophenes, but also the benzothiophenes and dibenzothiophenes found in heavier distillates) by H_2O_2.[87] While these catalysts facilitated the decomposition of the H_2O_2, they were also effective catalysts for ODS. Contaminants were introduced in *n*-decane for the studies of the solid-liquid-liquid system (where the catalyst remains a third solid phase in addition to the two liquid phases traditionally observed in ODS), and nearly 94% of benzothiophene was removed by Ti-beta in 5 hours at 70 ˚C from this model fuel. Overall, the Ti-beta,

and TI-HMS performed better for desulfurization of fuels because larger molecules, such as BT and DBT, were unable to access the smaller pores of TS-1, with Ti-beta providing the best desulfurization. When the process was extended to actual kerosene, the Ti-beta was able to effectively remove up to 94% of the overall sulfur contaminants in 9 hours. However, it should be noted that for smaller molecules, such as 2,5-DMT, TS-1 exhibited the highest oxidation activity.

Wang, et al. focused on the desulfurization ability of Ti-HMS in the presence of H_2O_2. [88] They investigated the ability of this system to remove BT, DBT, and 4,6-DMDBT from *n*-octane as model fuels. They found that increasing the amount of catalyst and hydrogen peroxide both increased the desulfurization, and that after 3 hours at 60 ˚C, essentially all of the BT and DBT had been removed and that 90% of the 4,6-DMDBT had been removed under the best conditions (with a H_2O_2 : S ratio of 4:1). The order of reactivity increased as 4,6-DMDBT < BT < DBT, which does not simply trend with electron density as with conventional ODS, and suggests that sterics are playing an important role in this system.

1.4. Phase transfer catalysts

Several groups have also applied the use of phase transfer catalysts to improve the biphasic ODS process. Phase transfer catalysts have been used widely to enhance a variety of biphasic reactions including by facilitating transfer of reagents between phases. ODS, as a biphasic reaction system that is limited by the transfer of reagents between organic and aqueous phases, is an ideal candidate for enhancement by use of a phase

transfer catalyst. Phase transfer catalysts have, indeed, been explored in a variety of ODS systems.

Phase transfer catalysts have also been combined with hypochlorite oxidants for the oxidation of sulfides. While no BT-based contaminants were studied, Ramsden, et al. showed that methyltri-*n*-octyl ammonium chloride improved the oxidation of dialkyl sulfides in *n*-octane both with and without the addition of a transition metal catalyst.[89] The oxidations, which took place over 5 hours in the absence of the phase transfer catalyst, were nearly complete after only 20 minutes of reaction. Interestingly, the hypochlorite and phase transfer catalyst alone provided the sulfoxide product, while introduction of TPPMnCl (TPP= 5,10,15,20-tetraphenyl-21*H*,23*H*-porphine) into the system as an oxidation catalyst provided the fully oxidized sulfone. The authors propose that transport of the hypochlorite into the organic phase by the phase transfer catalyst is responsible for the increase in the rate of oxidation, but do not comment on the magnitude of any potential fuel contamination.

Phase transfer catalysts have also been combined with heterogeneous ODS catalysts. For example, Chen and Li effectively combined use of a phase transfer catalyst with the use of H_2O_2, formic acid and modified alumina catalysts to oxidize thiophenic sulfur in to SO_4^{2-}, thereby eliminating the sulfur from the fuel phase.[90] The alumina catalysts investigated were modified with copper oxide, iron oxide, cerium oxide, manganese oxide, or zinc oxide, with copper oxide offering the highest level of desulfurization, removing 91.2% of the thiophene from a solution in *n*-heptane after an hour of reaction time, even in the absence of a phase transfer agent. Addition of a phase

transfer catalyst increased the amount of thiophene removed even further. Emulsifier OP and a variety of ammonium bromide salts were investigated to improve the process, with emulsifier OP providing the greatest desulfurization, removing 98.5% of the thiophene from this system. However, introduction of xylene as a solvent sharply reduced the desulfurization activity of this system due to competitive reactivity of the aromatic electrons, suggesting that the use of this system on an actual fuel system would not be effective.

Collins, et al. combined the use of a phase transfer catalyst with the use of a heteropolyanion catalyst that had been shown to be effective for ODS.[91] Using phosphotungstic acid as an oxidation catalyst, H_2O_2 as an oxidant, and tetraethyl ammonium bromide as a phase transfer catalyst, they studied the oxidation of DBT in toluene as a model system for optimization. After optimization of conditions to minimize the unproductive decomposition of H_2O_2 that also occurred with these reagents, they were able to achieve nearly quantitative oxidation of DBT using this system. After optimization using DBT, the authors went on to investigate the ability of this system to remove sulfur contaminants from actual diesel fuel. They found that after 4 hours at 60 ˚C, all sulfur contaminants in the fuel stream had reacted to some extent, with the dibenzothiophene contaminants reacting to a greater extent than the benzothiophene contaminants. After oxidation and adsorption of remaining sulfur onto silica, the total sulfur in the diesel feed was reduced to as low as 50ppm.

Jiang, et al actually incorporated the catalytic polyoxometalate into a surfactant-type catalyst to take advantage of emulsions formed by the catalyst in oxidizing sulfur

contaminants.[92] They studied the removal of DBT from a model oil (*n*-octane) as well as the purification of an actual diesel stream using $[(CH_3)_3NC_{16}H_{33}]_4W_{10}O_{32}$, $[(CH_3)_3NC_{14}H_{29}]_4W_{10}O_{32}$, $[(CH_3)_3NC_{12}H_{25}]_4W_{10}O_{32}$, and $[(CH_3)_3NC_{10}H_{21}]_4W_{10}O_{32}$ in the presence of aqueous H_2O_2 followed by extraction with DMF. The chain length was determined to be an important parameter; ammonium ions with longer alkyl chains provided significantly higher levels of sulfur removal. As the length of the fourth alkyl chain on the nitrogen atom increased from 10 to 16 carbons, the degree of DBT removal from the model fuel increased from 46.5 to 99.6% in 30 minutes at 60 ˚C. The catalyst could be recycled up to six times without an appreciable drop in this reactivity. Use of $[(CH_3)_3NC_{16}H_{33}]_4W_{10}O_{32}$ for the purification of actual fuel provided 93.5% desulfurization, but was not as effective as for the model fuels and required five subsequent extractions with DMF before this level was reached. The authors do not comment on contamination of the fuel by the catalyst or the effect of the oxidation on the other fuel components.

Similarly, Li, et al. found that $[(C_{18}H_{37})_2N(CH_3)_2]_3[PW_{12}O_{40}]$ formed metastable emulsion droplets when mixed with diesel fuel.[93] The formation of these metastable droplets provided an emulsion that was effective for desulfurization without being too stable for catalyst recovery. Rather, the catalyst could be easily separated from the fuel by centrifugation for reuse. Using this catalyst with H_2O_2 as an oxidant in a model diesel composed of 4,6-DMDBT in a mixture of decahydronaphthalene, tetrahydronaphthalene and *n*-dodecane provided complete removal of the 4,6-DM DBT in 80 minutes at 30 ˚C, and this time could be reduced at higher temperatures. Further, application of this catalyst and oxidant to actual diesel (followed by extraction of oxidized products with 1-

methyl-2-pyrrolidinone) resulted in sulfur levels below 1ppm without significantly changing the properties of the diesel.

1.5. Use of ionic liquids in desulfurization

In some instances, the use of ionic liquids as an alternative to traditional organic solvents has been investigated. Ionic liquids are appealing in this capacity not only because of the volatility and flammability of traditional solvents, but also due to the tunability of ionic liquid systems.

Ionic liquids have been applied to the desulfurization of fuels in multiple ways. Perhaps the most straightforward application of ionic liquids to this process is as a simple extractant for the removal of sulfur-containing contaminants. When using ionic liquids for desulfurization in this manner, important considerations include the partition coefficients of the contaminants, ease of ionic liquid regeneration, solubility of the ionic liquid in the fuel, and vice-versa.[94]

The earliest reports of the use of ionic liquid as an extractant for deep desulfurization of fuels appear in 2001, when Bosmann, et al. investigated their ability to remove sulfur from a model fuel of 500 ppm DBT in dodecane as well as actual diesel.[95] Initial studies examined the extraction ability of [BMIm]Cl/$AlCl_3$, [EMIm]Cl/$AlCl_3$, and [$HN(C_6H_{11})Et_2$][CH_3SO_3]/ [$HNBu_3$][CH_3SO_3]. As the summary of desulfurization for the model shown in Table 3 indicates, [BMIm]Cl/$AlCl_3$ was the best performing system of the three (room temperature, model fuel: ionic liquid = 5:1). There was no observable leaching of the ionic liquids into the model fuel, and the authors report that hydrocarbons

are much less soluble in the ionic liquids than the sulfur contaminants in ionic liquids, but do not report how much of the model oil was lost in the process. Further, there is no mention of ionic liquid regeneration. However, the authors did apply the process to an actual diesel fuel and report that using the [BMIm]Cl/$AlCl_3$ system, they were able to remove 85% of the sulfur contaminants after 5 extractions in a multistage system. Additionally, they examined [BMIm] with a variety of anions and found that the effect of the chemical nature of the anion was very small, but the size did appear to play a role in the desulfurization.

Table 3. Desulfurization percentages after extraction with selected ionic liquid systems (Ref. 95).

Ionic liquid system	Percent sulfur removed
[BMIm]Cl/$AlCl_3$	45
[EMIm]Cl/$AlCl_3$	33
[$HN(C_6H_{11})Et_2$][CH_3SO_3]/ [$HNBu_3$][CH_3SO_3]	38

In another example of the use of ionic liquids as a simple extractant, Liu, et al. invested the ability of a variety of ionic liquids to extract a variety of thiophenes (500 ppmw) from n-tetradecane as a model fuel.[96] Of the ionic liquids examined, using [$(CH_2)_4SO_3$HMIm][TOS] provided the greatest degree of extraction, removing up to 56% of the contaminant (in the case of dibenzothiophene) under ideal conditions.

Interestingly, of the contaminants studied, dibenzothiophene was the most soluble in the ionic liquid, and thus exhibited the best level of extraction.

Gao, et al. investigated the ability of the pyridium-based ionic liquids N-butylpyridinium tetrafluoroborate ([BPy][BF_4]), *N*-hexylpyridinium tetrafluoroborate ([HPy][BF_4]), and *N*-octylpyridinium tetrafluoroborate ([OPy][BF_4]), to remove sulfur from both model fuels and diesel through selective extraction.[97] They found that the desulfurization activity of these ionic liquids decreased in the order [OPy][BF_4] > [HPy][BF_4], > [BPy][BF_4], noting that the larger pyridinium cations gave better extraction and that the size of the cation played an important role in the extraction activity for these ionic liquids. With respect to the removal of individual sulfur contaminants from model fuel (dodecane), removal of DBT was more efficient than BT, which was more efficient than thiophene. The authors attribute this to extraction by π-π interactions and note that aromatics occurring in the fuel matrix are also subject to this interaction. In fact, when naphthalene was added to the model fuel, it was noted that a significant amount was extracted into the ionic liquid, but that amount of DBT extracted was greater. Using [OPy][BF_4] (the best performing ionic liquid) and actual diesel (84 ppm starting sulfur levels) this method could remove 24% of the sulfur contaminants in a single extraction. This was increased to 36 and 47% with second and third extractions, respectively. However, while the ionic liquid was virtually insoluble in the fuel, the solubility of the diesel in the ionic liquid was approximately 2%, resulting in a loss of fuel and complicating ionic liquid regeneration.

Similarly, Esser, et al. studied the ability of 3 ionic liquids to extract thiophenes from both model and actual fuels. They were able to decrease the amount of DBT in a model fuel from 500 ppm to less than 10 ppm using 1-*n*-butyl-3-methylimidazoleum octylsulfate as the ionic liquid.[98] However, this required repeated treatment and additional desirable components of the actual fuel matrix were also extracted. Further, regeneration of the ionic liquid was problematic.

Other groups have taken this a step further and used room temperature ionic liquids as a cosolvent in the ODS process, where ionic liquids are touted as ideal alternatives to polar organic solvents due to their low vapor pressures, inflammability, high thermal stability, recyclability, and wide range of miscibility and solubilizing properties.[99-102] The use of ionic liquids in combination with ODS increases desulfurization relative to simple extraction because in many of the cases where ionic liquids are used as an extractant, the starting sulfur contaminant exhibits similar solubilities in the fuel and the ionic liquid extractant. In contrast, the more polar oxidized sulfur compounds are much less soluble in the fuel (as is the case for ODS in general) and are readily taken into the ionic liquid cosolvent.

In another example, Lu, et al. combined oxidative desulfurization using H_2O_2 as the oxidant and [HMIm]BF_4 as the extracting cosolvent.[103] They found that this system provided up to 93% removal of DBT from iso-octane after 6 h at 90 ˚C, and noted that higher temperatures actually led to a decrease in desulfurization reactivity (presumably due to decomposition of the peroxide, though this was not investigated). The authors also tested thiophene and BT in similar model fuel systems and noted that the reactivity

decreased in the order DBT>BT>thiophene (with 51 and 49% removal of BT and thiophene, respectively, under the above conditions), which is consistent with what has been observed in other ODS systems. Application of this system to actual diesel fuel, however, led to only 50% desulfurization even after the addition of a subsequent extraction step using acetonitrile. The $[HMIm]BF_4$ was able to be recycled 6 times prior to showing a slight decrease in desulfurization efficiency. While the authors propose that the $[HMIm]BF_4$ is acting as a catalyst, they do not speculate what its role may be. However, they were able to carry out this oxidation in the absence of the typical organic acid catalyst, which does support their assertion that the ionic liquid is acting as more than simply a cosolvent.

Li, et al. also employed an ionic liquid as the cosolvent for ODS of a model fuel (DBT in *n*-octane) with H_2O_2 and acetic acid as the oxidant.[104] However, rather than employ an imidazolium-based ionic liquid for the process, they looked at the ability of $Me_3NCH_2C_6H_5Cl•2ZnCl$ to serve this purpose. This particular ionic liquid was chosen due to the hypothesis that the first step in the ODS process with ionic liquid cosolvents is the extraction of the sulfur contaminant from the fuel into the ionic liquid. The solubility of benzothiophene was significantly greater in $Me_3NCH_2C_6H_5Cl•2ZnCl$ than in imidazolium-based ionic liquids. They found that with a 1:5 ionic liquid: fuel ratio, they were able to remove up to 94% of the DBT from this system in 30 minutes at 30 ˚C (versus 29% by extraction alone). By increasing the relative volume of the ionic liquid phase, the authors were able to achieve gradually higher levels of desulfurization up to 99% when the ratio reached 12:1. However, the increase was gradual enough that they determined 1:5 as the ideal ratio. This ionic liquid system could also be recycled 6 times

before an appreciable decrease in ODS activity was observed, but no investigations into fuel contamination, breadth of applicability, or possible interference by other components of the fuel matrix were reported.

Li, et al investigated the use of an ionic liquid as a cosolvent for an ODS process involving decatungstates that were introduced as salts with short chain ammonium ions.[105] Specifically, $[(C_4H_9)_4N]_4W_{10}O_{32}$, $[(CH_3)_4N]_4W_{10}O_{32}$, and $[(C_2H_5)_3NC_7H_7]_4W_{10}O_{32}$ were investigated as catalysts. The ionic liquid in this case was $[BMIm]PF_6$, which was not soluble in either the oil or water and instead formed a third phase. BT, DBT, and 4,6-DMDBT in *n*-octane were examined as model fuel contaminants, and aqueous H_2O_2 was used as the oxidant. This system was capable of removing up to 98% of the sulfur from the model fuel in 30 minutes at 60 ˚C (compared to 30.6% for the same system in the absence of the ionic liquid), and the catalyst/ionic liquid system could be recycled, but a slight increase in reaction time was required to reach equivalent desulfurization levels with each subsequent use. The authors proposed both the sulfur contaminants and peroxotungstates were extracted into the ionic liquid, and that the actual oxidative reactivity took place in this third phase. Interestingly, oxidation did not correlate directly with electron density, rather it decreased in the order: DBT > 4,6-DMDBT > BT. This suggests that the steric hindrance of the sulfur atom plays a role in reactivity with this system. While no contamination by the ionic liquid was detected in the model fuel, up to 8.4 ppm W was found in the fuel after this treatment.

Li, et al, went on to investigate the desulfurization of these same 3 model contaminants by phosphotungstic acid and H_2O_2 with 4 different ionic liquid

cosolvents.[106] The ionic liquids examined were [BMIm]BF_4, [BMIm]PF_6, [OMIm]BF_4, and [OMIm]PF_6. Among these, [BMIm]BF_4 provided the greatest degree of desulfurization, providing complete removal of the contaminants from the model fuel in 3 hours at 70˚C. Again, the desulfurization decreased as: DBT > 4,6-DMDBT > BT. The decrease in removal efficiency over 6 recycles was slight (down to 96.1% after 5 recycles), but the authors again noted that there was a slight contamination of the model fuel by the W.

In fact, in many cases, researchers have gone further in their use of ionic liquids, using them not only as a solvent for extraction of the sulfone products¸ but also specifically designing systems that allow the use of the ionic liquids as catalysts for sulfone formation. The tunability of the anion and cation components of ionic liquids to incorporate a variety of functionalities, as well as modify their solubility and acid/base properties[107] creates the possibility of task specific ionic liquids that can be developed specifically for use in the ODS process. Ionic liquids have been used as both phase transfer catalysts in these systems and as the actual oxidizing catalyst.

In one example of an ionic liquid acting as a phase transfer catalyst, Zhao, et al. explored the ability of the coordinated ionic liquid $(C_4H_9)_4NBr \bullet 2C_6H_{11}NO$ to assist in the ODS of both a model fuel and actual gasoline.[108] Here, the ionic liquid was not actually used as a cosolvent, but only added in small amounts to serve as a phase transfer catalyst, with water composing the majority of the second phase which contained H_2O_2/ acetic acid as the oxidant system. Nonetheless, the authors were able to demonstrate removal of 98.8% removal of thiophene in *n*-octane as a model fuel in 30 minutes at 40

˚C, but actually saw a decrease in reactivity at higher temperatures due to an increase in the unproductive decomposition of H_2O_2. The authors go on to suggest that the high reactivity is due to the ability of the alkyl chains of the ammonium ion to aid in the transport of the oxidant into the fuel phase where it can act on the thiophenic substrate, but did not address the topic of fuel contamination due to this transport of reagents into the fuel. They did, however, test the ability of this system to remove sulfur contaminants from an actual gasoline sample, and observed lower desulfurization activity (95.3% under the same conditions) due to competitive oxidation of other components of the fuel matrix.

Use of ionic liquids as oxidation catalysts as well as extractant solvents has also been investigated. For example, when N-methyl-pyrrolidinium BF_4 was used as and ionic liquid cosolvent in ODS, the N-methyl-pyrrolidinium was found to decompose H_2O_2 into hydroxyl radicals that went on to oxidize the sulfur contaminants rather than simply serve as a cosolvent.[109] This ionic liquid was used in the ODS of both model fuel (DBT in *n*-octane) as well as actual diesel, and found that essentially all of DBT in the model fuel could be removed after 60 minutes with a 3:1 O : S ratio, or 30 minutes when the ratio was doubled. This ionic liquid was also effective in the removal of sulfur from diesel fuel when followed by extraction with an equal volume of DMF, removing 99.4% of sulfur-containing compounds (3240 ppm to 20 ppm) after 2 hours at 60 ˚C. Investigation of fuel contamination by the ionic liquid was not reported, but the ionic liquid could be recycled up to 7 times without a significant decrease in reactivity.

The authors went on to investigate N-methyl-pyrrolidinium PF_6 as an cosolvent and catalyst for this transformation.[110] Again, DBT in *n*-octane was used as a model fuel,

and the N-methyl-pyrrolidinium was used to catalyze decomposition of the H_2O_2 into hydroxyl radicals for oxidation of the DBT. As before, they found that this system also was capable of removing essentially all of the sulfur from the model fuel and that the ionic liquid could be recycled up to 7 times without a significant decrease in reactivity, but oxidation of actual diesel was not investigated for this variation on the pyrrolidinium-based ionic liquid.

The carboxylic acid functionality used to for peracids in conventional ODS has also been incorporated into ionic liquids to serve as cosolvents and catalysts.[111] For example, Gui, et al. studied the series of ionic liquids containing this functional group shown in Figure 6 for their ability to remove DBT and 4,6-DMDBT from *n*-tetradecane as a model fuel in the presence of H_2O_2 as an oxidant. They found that the effectiveness of the ionic liquids for ODS trended with the formation of the corresponding peracid species (IL4 > IL5 > IL1 > IL2 > IL3), supporting the hypothesis that the formation of the peracid does aid in desulfurization activity. Starting with model fuels composed of 0.5% of the selected contaminant, they found that IL4 was able to remove up to 96.7 and 95.1% of DBT and 4,6-DMDBT from the model fuels, respectively. Again, the authors propose that the oxidation takes place after the contaminant has been extracted into the ionic liquid, and contamination of the fuel was not observed. The effect of this system on other potential substrates present in the fuel matrix was not investigated.

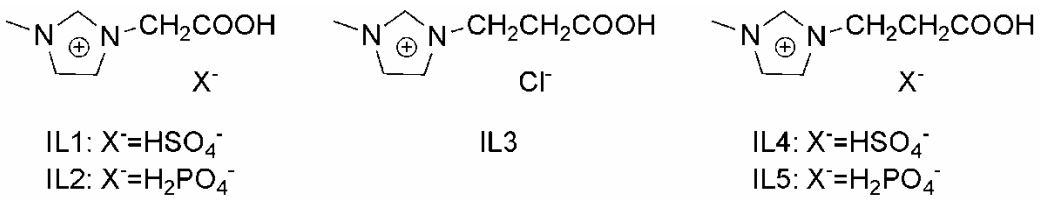

Figure 6. Ionic liquids containing the carboxylic acid functional group for formation of peracid and use in ODS (Ref 111).

Ionic liquids based on the heteropolyanions previously used as catalysts have also been developed. For example, Huang, et al. incorporated a heteropolyanion, $PW_{12}O_{40}$, as the anion of the ionic liquid [(3-sulfonic acid)propylpyridine]$_3PW_{12}O_{40}$•H_2O.[112] This ionic liquid was investigated for use as a catalyst with H_2O_2 as the oxidant in conjunction with 4 other ionic liquids ([BMIm]BF_4, [BMIm]PF_6, [OMIm]BF_4,and [OMIm]PF_6) as potential cosolvents. [OMIm]PF_6 provided the best desulfurization activity, removing 99.5% of DBT from a model fuel (500 ppm in*n*-octane) in 1 hr at 30 ˚C. Further, 4,6-DMDBT and BT were also found to be responsive to this system, with 98.8 and 69.9% removed, respectively, under the same conditions. The lower reactivity of BT was attributed to the lower electron density on the sulfur atom of BT as compared to the other two substrates. The authors went on to investigate the ability of this system to remove sulfur contaminants from actual diesel and found that the sulfur contaminants could be decreased from 360 to 70ppm after 3 hours at 30 ˚C.

1.6. Other approaches

Other approaches to the oxidative desulfurization of fuels have primarily focused on alternative oxidants or process intensification. In an attempt to improve the ODS

process, several researchers are exploring the use of alternatives to the established hydrogen peroxide (or *t*-BuOOH, in some cases) system. Alternative oxidants are being sought for the development of processes that are both more effective and greener alternatives. Many groups have also sought to improve desulfurization through the exploration of photocatalysis. Process intensification of ODS has primarily taken the form of ultrasound assisted ODS.

1.6.1. Alternative oxidants

In one example of an alternative oxidant system, Joseph, et al. explored the oxidation of various sulfides by N-Methylpyrolidin-2-one hydrotribromide (MPHT) as a potential transition-metal-free oxidant/catalyst for the ODS system.[113] The authors looked at the ability of MPHT to perform as both a stoichiometric oxidant and as a catalyst in combination with H_2O_2 as an oxidant, and found that both systems were effective for the oxidation of sulfides in CH_2Cl_2, but did not investigate any systems more closely resembling an actual fuel system. Interestingly, the oxidation of product varied between the stoichiometric and catalytic systems (Scheme 2). When stoichiometric MPHT was used, the sulfoxide was the oxidation product for all sulfides, and no sulfone was observed. In contrast, when 30% H_2O_2 was added to make the system catalytic in MPHT, the sulfone products were observed. While DBT and 4,6-DMBDT reacted less readily than the other sulfides investigated, they were oxidized in this system at 80 ˚C. 50% of the DBT had been converted to the corresponding sulfone in 210 minutes, and 4,6-DMDBT was 45% converted in 390 minutes. Interestingly, this is contrary to what

would be predicted based on S atom electron density, suggesting that steric effects factor heavily into the reactivity of this system.

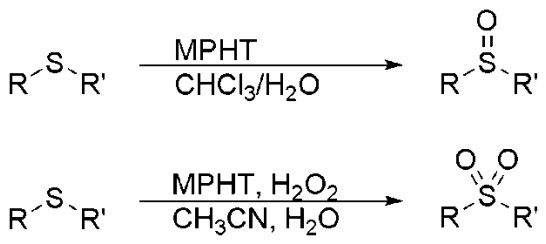

Scheme 2. Sulfide oxidation products in the presence of MPHT with and without external oxidant (Ref. 113).

In situ generation of hydrogen peroxide from H_2 and O_2 for use in an ODS system has also been investigated. For example, Song, et al. added Au particles to an established Ti/HMS ODS system to couple the desulfurization ability of the Ti system with the H_2O_2 generating capability of the Au.[114] They found that while the preparation method of the Ti supported Au did affect the efficiency of desulfurization, this system was capable of removing most BT, DBT, and 4,6-DMDBT from *n*-octane as model fuel. Removal of BT was essentially complete in 3 hours at 60 ˚C. Similarly, over 90% of the DBT was removed from a starting solution of 2700 ppm in *n*-decane. However, the removal of 4,6-DMDBT was highly dependent on the preparation method of the catalyst and retention of the large pores. In the case of the more successful catalysts, though, 80-90% of the 4,6-DMDBT could be removed from a 1980 ppm solution in 4 hours at 60˚C. However, the

authors did not report the effectiveness of this system in the presence of other potential contaminants.

Ozone would, in theory, be an appealing oxidant for the ODS process (particularly a portable process) due to the ease with which the reagent can be generated on site and the lack of hazardous waste streams.[115] However, while ozone represents an ideal oxidant for such a process, little research has been published on the use of ozone as an oxidant in ODS. Most work utilizing ozone for the oxidation of sulfur-containing compounds focuses on aliphatic sulfur-containing substrates (rather than the more difficult to remove aromatic species) and often in aqueous or gaseous environments rather than in fuel-like matrices. Gaseous oxidations with ozone focus on the oxidation of odorous emissions from industrial processes such as H_2S over solid catalysts and have been quite effective.[116] However, the gas phase reactivity of H_2S is significantly different than the solution phase chemistry of fuel contaminants.

In one example of solution phase oxidation of sulfur by ozone, Gilbert, et al. investigated the oxidation of thiodiglycolic acid in aqueous solutions, and found that the sulfide was completely absent after 9-15 minutes (depending on conditions).[117] They found that the sulfoxide was quickly formed and slowly converted to the sulfone for this substrate, and that the oxidation worked best under acidic conditions. Not only was oxidation slower under neutral or basic conditions, ozone consumption was higher as well.

Later studies of this system by Gilbert and Hodenberg expanded the list of substrates to include cysteine, cystine, and thioglycolic acid in aqueous solution.[118] They

again found that even at mild temperatures (20-25 ˚C) up to 90% of the substrates (100% in the case and thioglycolic acid) could be oxidized, but that the process required up to 160 minutes. While the authors did not examine the oxidation of any substrates in organic phase or extend the oxidation to any thiophene based contaminants, these studies could serve as a starting point for anyone wishing to do so.

Molecular oxygen represents another appealing and green oxidant for the ODS process, and has been investigated for the conversion of sulfides to sulfones for subsequent removal from fuels as well. Ji et al. were able to utilize molecular oxygen as an oxidant using a heterogeneous catalyst ($MnFe_{1.8}Cu_{0.15}Ru_{0.05}O_4$) under only 1 atm of molecular oxygen.[119] Oxidation was believed to occur through the formation of a Ru-oxo species on the catalyst surface, and this process provided complete conversion of the sulfide to the sulfoxide in 5-6 hours at 60 ˚C (Scheme 3). However, the system was applied only to methyl phenyl sulfide and diphenyl sulfide in toluene rather than an actual fuel-like system or the more recalcitrant contaminants.

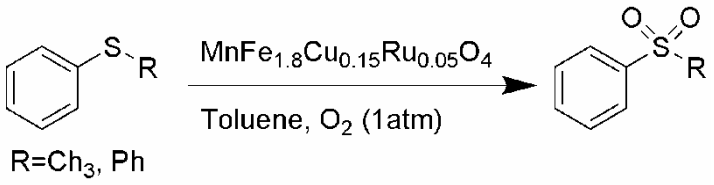

Scheme 3. Oxidation of sulfides by O_2 with a $MnFe_{1.8}Cu_{0.15}Ru_{0.05}O_4$ catalyst. (Ref. 119)

An ideal oxidant for the ODS process would be air, which is free, readily available, portable, and environmentally friendly. In fact, air has been investigated as an

oxidant in recent studies. For example, Sampanthar, et al. investigated ODS with air as the oxidant using solid supported manganese and cobalt oxide catalysts.[120] They examined not only model fuels composed of 3-MBT, DBT, 4-MDBT, 4,6-DMDBT, or 4,6-DEDBT in *n*- tetradecane, but also actual diesel fuel. They found that there was no reactivity below 110 ˚C, but that above this temperature, desulfurization using air with these catalysts was possible. The ideal range was determined to be between 130-200 ˚C, with between 80-90% of the sulfur contaminants removed from the model fuels after 8 hours at 150 ˚C followed by extraction of the fuel with a polar solvent. The order of reactivity for the compounds investigated was 4,6-DEDBT> 4,6-DMDBT>4-MDBT>DBT>3MDBT, which is consistent with other ODS systems. Further, they were able to decrease the sulfur levels of actual diesel to between 40-60 ppm using this method, but did note that the olefin and aromatic content of the fuel was decreased, suggesting that this method is not as selective as some other oxidation methods.

In another example of the use of air as an oxidant, Xu, et al. were able to oxidize thiophene, DMDBT, MDBT, DBT, and BT in a model fuel to the corresponding sulfones using only air as the oxidant.[121,122] They explored a variety of solvents (γ-butyrolactone, γ-valerolactone, δ-valerolactone, 1-methyl-2-pyrrolidinone, and ethyl heptanoate), but γ-butyrolactone provided the most efficient desulfurization among these by far. While the authors verified that the air was necessary for the oxidation to occur, and proposed that the γ-butyrolactone cosolvent could be used, they did not postulate a mechanism for the oxidation or determine why this solvent provided such superior performance relative to the others attempted. While this process represents a potentially exciting use of air as an

oxidant for the ODS process, hours at 140 ˚C were still required for the oxidation to fully occur.

One approach to the use of air as an oxidant for ODS is the in situ generation of a more conventional oxidant from air. Sundararaman, et al. have recently taken this approach, generating peroxides for the ODS process in situ from air.[123] Al_2O_3-supported CuO was used to generate the peroxides, and a SiO_2-supported MoO_3 catalyst was used to catalyze the oxidation of the fuel contaminants. The resulting sulfones were adsorbed onto β-zeolite for removal. The best results were obtained at 120 ˚C, where peroxide generation and oxidation were best balanced, and the sulfur content of actual JP-8 jet fuel could be reduced from 520-50ppm in 60 minutes. While this treatment requires 3 distinct steps for sulfur removal and does not achieve the levels required for fuel cell use, it nevertheless represents a unique approach and the utilization of the greenest of oxidants.

1.6.2. Photocatalytic enhancement of ODS

Another method that has been investigated for the enhancement of the ODS process is photochemical activation of the system. Zhao, et al. combined photochemical generation of hydroxide radicals with extraction by the ionic liquid [BMIm]PF_6 for the desulfurization of a model fuel (DBT in *n*-octane) as well as actual light oil.[124] The result was a 3 phase system (Figure 7), where the hydroxide radicals were photochemically generated in the aqueous layer, and the ionic liquid served as both an extraction solvent and as the reaction medium. Using this system, they were able to remove 99.5% of the DBT from the model fuel and 90.6% of the total sulfur from the light oil.

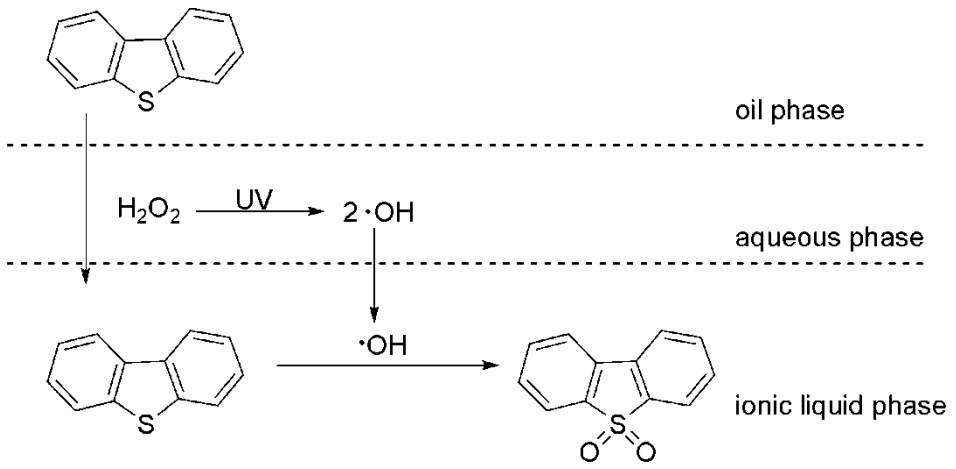

Figure 7. Combination of photochemical oxidation and ionic liquid extraction for desulfurization of DBT. (Ref. 124)

Additionally, photocatalysis using TiO_2 catalysts has been investigated. However, one of the drawbacks of TiO_2 photocatalysis is that agglomeration of the titania particles greatly reduces catalytic activity. This can be addressed through the introduction of solid supports. For example, Zhang, et al. impregnated bamboo charcoal with TiO_2 for evaluation of ODS activity.[125] They found that this solid supported system was more effective than free titania when applied to a model fuel (DBT in *n*-octane) under UV irradiation. Use of aqueous H_2O_2 as the oxidant resulted in a triphasic (liquid-solid-liquid) system featuring the solid photocatalysis between the two liquid phases and accumulating the DBT contaminant to create a DBT-rich environment at the phase boundary. The authors hypothesize that this increases the activity by facilitating mass transport. This system was capable of removing up to 80% of the DBT from the model

fuel as the corresponding sulfoxide and sulfone. However, other contaminants and potential interferences were not investigated.

Na, et al. combined the use of O_2 as an oxidant with photochemical oxidation in the presence of titanium-pillared montmorillonite as a catalyst.[126] Use of acetonitrile as an extraction solvent resulted in a three-phase system that was capable of removing 97.4% of 2,5-DMBT from a model fuel (400 ppm 2,5-DMBT in *n*-octane). However, no investigation of other fuel contaminants or potential interferences was reported.

1.6.3. Ultrasound-assisted oxidative desulfurization

Another approach to improving ODS that has been explored is the use of sonication to enhance traditional processes. The cavitation events encountered in sonochemistry are known to general hydroxyl radicals in aqueous solutions of hydrogen peroxide, and this method has been investigated for water treatment processes.[127,128] Additionally, the use of sonochemistry promotes the formation of emulsions, generating a high surface area between phases, and is believed to greatly enhance mass transport..[129,130]

Zhao, et al. combined the use of ultrasound with the benefits of a phase transfer catalyst to further improve the ODS process.[131] The use of hydrogen peroxide and formic acid as an oxidant combined with a quaternary ammonium salts as a phase transfer catalyst under ultrasound provided significant oxidative removal of thiophene from *n*-heptane in 90 minutes at 50 ˚C. The phase transfer catalysts investigated were tetramethyl ammonium bromide (TMAB), tetraethyl ammonium bromide (TEAB),

tetrapropyl ammonium bromide (TPAB), and tetrabutyl ammonium bromide (TBAB). As seen in Table 4, removal in the presence of a phase transfer catalyst ranged from 42-95% (compared to 28% in the presence of ultrasound without use of a phase transfer catalyst) with TBAB providing the best results. The authors attribute this result to the increased lipophilicity of the longer alkyl groups leading to an increased transfer of oxidant by the phase transfer catalyst into the organic phase. The effects of this process on other components of a fuel matrix and its applicability to other sulfur contaminants were not investigated.

Table 4. Percent conversion of thiophene after 90 min by hydrogen peroxide and formic acid under ultrasound at 50 ˚C in the presence of various phase transfer catalysts (Ref 131).

Phase Transfer Catalyst	None	TMAB	TEAB	TPAB	TBAB
% Thiophene Conversion	28.4	42.4	70.0	86.6	94.7

Mei, et al. further developed the process of ultrasound assisted ODS by incorporating a phosphotungstic acid catalyst as well as a phase transfer catalyst (tetraoctylammonium bromide) and investigating the desulfurization of actual diesel fuels.[132] In a model fuel composed of 0.4% DBT in toluene, complete conversion of the DBT was observed in 7 minutes at 75 ˚C (compared to just over 80% under the same

conditions in the absence of ultrasound. The authors explained the increased desulfurization as due to the formation of ultrasonic emulsions, which are composed of droplets that are smaller in size and more stable than those obtained by more conventional methods. When actual diesel was the substrate, 98-99% of the sulfur contaminants could be removed by this process, however only 83-87% of the fuel could be recovered.

Dai, et al investigated the combined use of ultrasound and Fenton's reagent (Fe^{2+}/H_2O_2) for the desulfurization of diesel fuel.[133] They found that this was more effective than the use of ultrasound with acetic acid under the same conditions, and that reactivity decrease as ultrasound/Fenton's reagent > Fenton's reagent/no ultrasound > ultrasound/ H_2O_2/acetic acid > H_2O_2/acetic acid/no ultrasound. The authors observed a 1.47 times increase in desulfurization when ultrasound was incorporated compared to the use of Fenton's reagent alone, and again attribute this to the smaller and more stable emulsion droplets that are obtained under ultrasonic conditions. They also propose that the heat generated during cavity implosion events generates additional hydroxyl radicals that further contribute to the oxidation. Use of this technique provided up to 98% desulfurization of the diesel fuel in 15 minutes at 40 'C. However, no information regarding reactivity of other matrix components was presented.

1.7. Summary

In conclusion, ODS represents a promising method of desulfurization and offers reactivity that is complementary to traditional HDS fuel processing. However, conventional preparative methods of converting sulfides to sulfones do not translate

directly into effective purification methods due to the organic environment of the sulfides and other matrix contaminants. In fuel-like systems, conventional oxidations require hours stirring at elevated temperatures.

Many approaches to the improvement of this process have been explored, but an ideal method for the production of ultra low sulfur fuels has not been found. Alternative oxidants and various catalysts have been explored, but often fuel contamination by the purification agents or incomplete removal of the sulfur contaminants hinder the process. Oxidation of other fuel components and loss of fuel can also plague the process. However, many advancements have been made in the field, and oxidative desulfurization as a method of fuel purification remains an area of active research.

1.8. Thesis overview

Studies reported in this thesis include the use of a film-shear reactor as a unique approach to enhancement of the ODS process using hydrogen peroxide and formic acid as the catalyst system. Studies into the conditions within the film-shear reactor to provide understanding of the observed enhancement, as well as ideal potential applications are also presented. Finally, the ability of titania nanoparticles to further enhance the ODS process in the film-shear reactor, and the controlled synthesis of these materials within the reactor were studied. The appendices report supplemental information corresponding to these studies, as well as work done investigating the ability of platinum catalysts to effectively hydrate nitriles and cyanohydrins.

1.9. Acknowledgments

This dissertation contains coauthored material. Authorship of Chapter II is shared with Alexander Sun, Helen Dauer, Jonathan Male, Mark Stewart, and David R. Tyler. A. Sun and H. Dauer assisted in the gathering of ODS data, and M. Stewart provided useful insight into the mixing within the reactor. J.Male and D. Tyler, my advisor, contributed significantly to the intellectual content of the chapter. Authorship of Chapter III is shared with Benjamin L. Brinich, Jonathan L. Male, and David R. Tyler. B. Brinich assisted in the collection of data regarding the oxidation of contaminants using air as an oxidant. J.Male and D. Tyler, my advisor, contributed significantly to the intellectual content of the chapter. Authorship of Chapter IV is also shared with B. Brinich, who assisted in the temperature probe studies, and David R. Tyler, my advisor. Authorship of Chapter V is shared with Ryan Everett, who assisted in the studies of TEOT hydrolysis, and my advisor David R. Tyler. Authorship of Appendices C and D are shared with Takiya J. Ahmed, who was the primary contributor of the molybdocene studies and many of the platinum catalysis studies, both intellectually and experimentally. Authorship of these appendices is also shared with Spring Melody M. Knapp (who contributed to the chapter through the Hg poisoning studies), Robert Yelle (who was responsible for the computational results), Jerrick Juliette (who provided significant intellectual contributions) and David R. Tyler.

CHAPTER II

ENHANCED OXIDATIVE DESULFURIZATION OF MODEL FUELS USING A FILM-SHEAR REACTOR

2.1. Introduction

Fuels with ultra-low sulfur levels are becoming increasingly important because fuel cells require near-zero sulfur levels and because combusting sulfur-containing fuels has negative health and environmental effects [1-5]. Current hydrodesulfurization (HDS) technologies convert the sulfur contaminants to H_2S and require high temperatures and pressures for sulfur removal [6-10]. A further decrease in sulfur levels requires increasingly harsh conditions due to recalcitrant sulfur compounds that are very difficult to remove [11-15]. A complementary alternative to HDS is oxidative desulfurization (ODS), in which thiophene contaminants are oxidized through their corresponding sulfoxide to sulfones [16-18]. The resulting sulfones are no longer soluble in the fuel phase and are therefore more easily removed (Scheme 1). ODS is also appealing because the sulfur contaminants that are most resistant to HDS are the most reactive under ODS conditions[19-21]. However, oxidative desulfurization employs an aqueous oxidant

(typically hydrogen peroxide with catalytic acid) that must react with the sulfur contaminant in the fuel phase. As a result, hours of stirring at elevated temperatures are required. In this report, we describe the application of a film-shear reactor to significantly enhance the ODS process, most noticeably through drastically reduced reaction times.

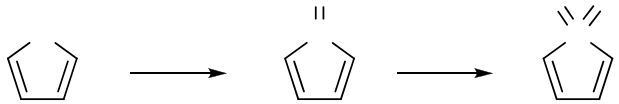

Scheme 1. In ODS, the thiophene contaminant is oxidized through the sulfoxide to the corresponding sulfone, which is no longer soluble in the fuel.

The film-shear reactor used in these experiments is illustrated in Figure 1 [22]. The reactor features a rotor plate that can be adjusted to within hundreds of microns from a stator plate. This close proximity, combined with rapid rotation of the rotor, subjects reactants between the two plates to high shear rates. The design of the reaction zone causes the non-miscible fuel and oxidant streams to encounter each other under conditions of high shear. Contact of the fluids within this narrow gap results in intense mixing and intimate contact of the two phases, promoting transport of the reactants to the interfaces. A heat exchanger allows control of the temperature in the reaction zone. Furthermore, unlike the specially designed facilities that are required to accommodate the

high temperatures and pressures required for HDS, the small size of the film-shear reactor (10 inches high) makes this technology ideal for portable applications.

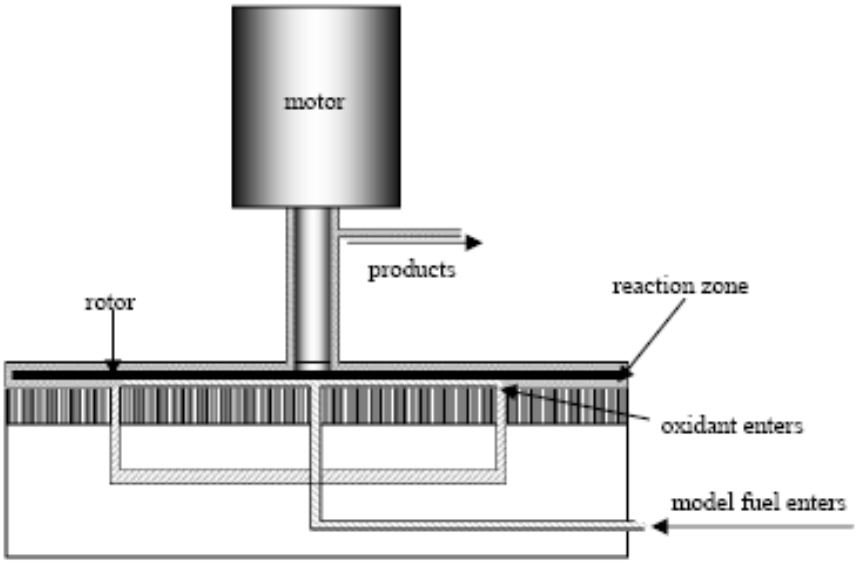

Figure 1. Diagram of the film-shear reactor (not to scale).

2.2. Experimental

For this investigation, a 0.5% solution of benzothiophene in decane was employed as a model fuel. A 5% solution of formic acid in 30% H_2O_2, mixed with an equal volume of isopropanol (to enhance product solubility), was used as the oxidant. The aqueous and decane phases separated readily upon exiting the reactor, facilitating analysis by ^{1}H NMR spectroscopy of the remaining sulfur in the decane layer. Specifically, analysis of the signal intensity in the aromatic region relative to 1,1,2,2-tetrachloroethane as an internal standard allowed calculation of the remaining thiophene (Supplemental Figure 1).

2.2.1. Reagents

Benzothiophene (99%) was obtained from Aldrich. Decane (99%) and1,1,2,2-tetrachloroethane were obtained from TCI. Hydrogen peroxide (30-32%) and isopropanol were from Mallinckdrot. Deuterated cyclohexane was obtained from Cambridge Isotope Laboratories. All reagents were used without further purification.

2.2.2. Film-shear reactor trials

All film-shear reactor trials were carried out in a KinetiChem, Inc. Synthetron^{TM} film-shear reactor. Reactant feeds were introduced at room temperature and encountered each other in the reaction zone (defined as the space within the rotor-stator gap). The bulk temperature in the reaction zone was controlled using the flow from a recirculator/chiller through the heat exchanger. The system was allowed to equilibrate at the indicated temperature for 2 or more hours prior to setting the rotor-stator gap. Reagents were delivered through Teflon tubing using independent SYR-2200 dual programmable syringe pumps obtained from J-Kem Scientific. Upon reaching the indicated reaction conditions, a minimum of two full reactor volumes was allowed to flow through the reactor prior to sample collection in order to ensure stable conditions.

2.2.3. Sample preparation and analysis

The decane phase was separated from the aqueous phase immediately upon exiting the reactor. A small sample (0.3 mL) of the decane phase was then combined in an NMR tube with 0.3mL deuterated cyclohexane containing 1,1,2,2- tetrachloroethane (10-100mM). This sample was compared to a sample of the starting solution prepared in

exactly the same way with the same internal standard solution. ^{1}H NMR spectra were recorded on a Varian 600 spectrometer at an operating frequency of 599.98 MHz.

2.2.4. Conventional mixing control experiments

A sample (10 mL) of each reactor feed was placed in a 50 mL 2-neck round-bottom flask equipped with a magnetic stir bar and reflux condenser. The apparatus was placed in an oil bath equilibrated at 80 °C and stirred vigorously. A 1 mL aliquot was withdrawn from each phase at the indicated time (in order to maintain equal volumes) and analyzed in the manner reported for the reactor trials. These results are shown in Figure 2 of Appendix A.

2.3. Results and discussion

Use of the film-shear reactor resulted in a dramatic enhancement of the ODS process, providing up to 55% removal of benzothiophene in just one pass through the reactor with residence times of only seconds to minutes. To give one example, 53% of the benzothiophene was removed from the model fuel in only 80 seconds at 10 °C using the film-shear reactor.[a] In contrast, control reactions using the same fuel and oxidant under conventional stirring conditions required four hours to achieve 60% removal of benzothiophene at 80 °C (Figure 2, Appendix A). A list of results and selected reaction conditions is found in Table 1 of Appendix A.

The degree of sulfur removal using the film-shear reactor was analyzed under a variety of conditions in an attempt to elucidate the experimental and instrumental parameters that affect the extent of desulfurization. The parameters that were varied and

the range over which they were surveyed are shown in Table 1, and a list of selected reaction conditions and results is found in Table 1 of the supporting information. The first parameter studied was the residence time (the time the reactants spend in the reaction zone of the reactor). In our initial experiments, the residence time was altered by changing the flow rate (while holding all other parameters constant). Curiously, as shown in Table 2, there was no change in the extent of desulfurization when the residence time was increased from 160 to 530 seconds by decreasing the flowrate from 1 mL/min to 0.3 mL/min. However, it is noted that the mixing of the reactants in the reaction zone could be significantly affected by changing the flow rate, which in turn could affect the extent of the ODS reaction. In other words, in these experiments the residence time was not an independent parameter.

Table 1. Parameters and the range over which they were surveyed.

Parameter	**Low**	**High**
Combined Flow Rate (mL/min)	0.3	4.0
Temperature (°C)	10	70
Rotation Speed (RPM)	740	6300
Gap (μm)	25	150
Maximum Shear (sec^{-1})	16000	840000
Residence Time (sec)	1	53
Percent Formic Acid	1	5

Table 2. Effect of residence time on extent of desulfurization

Combined Flow Rate (mL/min)	Residence Time (sec)	Percent Thiophene Removal
1.0	160	19
0.5	320	20
0.3	530	20

The effect of the residence time as an independent parameter was studied by recirculating the fuel phase for additional passes through the reactor and using a constant flow rate for each pass. The results from two such recirculation experiments are illustrated in Figure 2, which portrays two series of trials where the model fuel was recirculated (labeled as passes 2 and 3). Within each series, all of the reaction parameters remained unchanged as the fuel was recirculated. From the data in Figure 2, it is clear that each successive pass through the reactor resulted in further desulfurization of the fuel. Also note that, for each subsequent pass, the amount of sulfur removed was comparable to the desulfurization in the first pass. Comparable results could also be accomplished, in principle, by employing multiple reactors in series. From these experiments, it is concluded that increasing the residence time, while maintaining all other parameters constant, will lead to increased desulfurization.

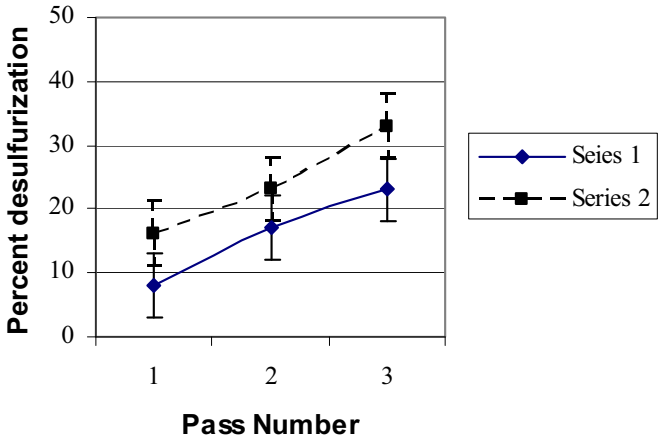

Figure 2. The effect of fuel recirculation on desulfurization. Series 1 conditions: 4mL/min, 1:1 fuel:oxidant, 30°C, 6300 RPM, 25µm gap, 10 sec residence time, 2% formic acid, 30% hydrogen peroxide. Series 2 conditions: 4mL/min, 1:1 fuel:oxidant, 30°C, 6300 RPM, 150µm gap, 60 sec residence time 5% formic acid, 30% hydrogen peroxide.

Another reaction variable that may impact the extent of desulfurization is the concentration of hydrogen peroxide. The impact of hydrogen peroxide concentration on the effectiveness of desulfurization was investigated by successively diluting the concentration of hydrogen peroxide in the oxidant feed (from 30% to 7.5%) while holding all other variables constant. As shown in Figure 3, the concentration of hydrogen peroxide over the range 7.5 - 30% had little effect on the degree of desulfurization.

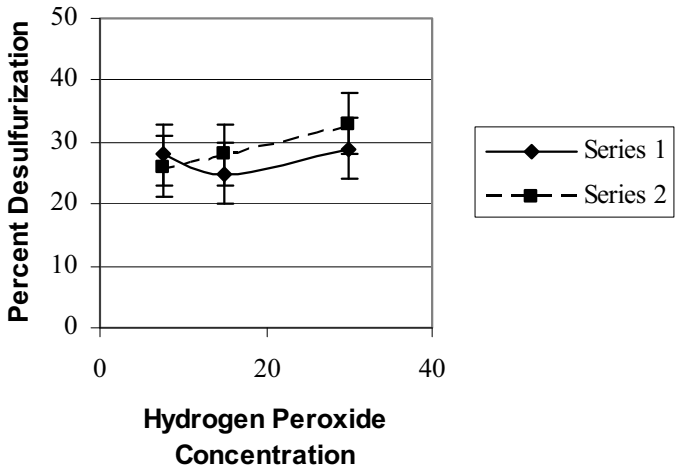

Figure 3. The effect of hydrogen peroxide concentration on desulfurization. Series 1 conditions: 0.5mL/min, 1:1 fuel:oxidant, 50°C, 6300 RPM, 80μm gap, 260 sec residence time, 1% formic acid. Series 2 conditions: 0.5mL/min, 1:1 fuel:oxidant, 50°C, 6300 RPM, 100μm gap, 320 sec residence time, 1% formic acid.

The final parameter investigated was the fuel to oxidant ratio. In these experiments, the fuel:oxidant ratio was increased from 1:1 to 10:1. Repeated trials showed that an increase in the ratio of fuel to oxidant did not impact the extent of desulfurization. To cite one example from Table S1, in run #1, 44% sulfur removal was achieved using a 10:1 ratio of fuel to oxidant (80 sec residence time at 10 °C).[b] This degree of removal is comparable to that observed with trials using 1:1 fuel:oxidant ratios. For example, run #6 had 53% removal under identical conditions except for the 1:1 fuel:oxidant ratio. It thus appears that for a given set of experiment conditions, the

efficiency cannot be improved by increasing the amount of oxidant above a certain minimum value.

2.4. Summary and conclusions

The application of a film-shear reactor provides a remarkable enhancement in the efficiency of the ODS process compared to normal stirring. Experiments reported here demonstrate that the amount of benzothiophene in a model fuel can be rapidly reduced, even at ambient temperatures and below. Recirculation experiments showed that, if the flow rate and all other experimental parameters were held constant, the extent of thiophene removal increased as the residence time increased. Experiments using various concentrations of hydrogen peroxide and different fuel:oxidant ratios showed that an increase in oxidant concentration did not lead to increased thiophene removal (above a minimum amount, of course). The source of the enhanced reactivity in the film-shear reactor was not investigated, but we speculate that it may be due to enhanced mixing of the two reaction phases in the reaction zone or possibly due to areas of localized heat generated between the rotor and stator by the shearing. Investigation into the utility and scope of this process is ongoing, as are investigations of other sulfur contaminants. An in-depth design of experiments analysis of reaction parameters and the interactions among them is also underway.

2.5. Notes

a. Conditions: 0.5mL/min, 1:1 fuel:oxidant, 10°C, 6300 RPM, 250μm gap, 80 sec residence time, 5% formic acid, 30% hydrogen peroxide.

b. Conditions: 0.5mL/min, 10°C, 6230 RPM, 250μm gap, 80 sec residence time, 5% formic acid, 30% hydrogen peroxide.

CHAPTER III

ENHANCED OXIDATIVE DESULFURIZATION REACTIVITY IN A FILM-SHEAR REACTOR

Sections of this work will be submitted for publication in *Fuel* with coauthors Benjamin L. Brinich, Jonathan L. Male, and David R. Tyler.

3.1. Introduction

The negative health and environmental effects of combusting sulfur-containing fuels provide a compelling reason to remove sulfur from fuels. Another compelling reason is that fuel cells require near-zero sulfur levels because their reforming catalysts are easily poisoned by sulfur.[1-4] Achieving near-zero sulfur levels is challenging. Current hydrodesulfurization (HDS) technologies convert the sulfur contaminants in hydrocarbon fuels to H_2S at high pressures and temperatures using heterogeneous transition metal catalysts.[5-9] Although HDS technology is able to meet current sulfur regulations, further decreases in allowable sulfur levels will require increasingly harsh conditions to remove the so-called recalcitrant thiophenes (primarily sterically hindered polycyclic aromatics).[10-17]

A complementary alternative to HDS is oxidative desulfurization (ODS), in which an aqueous oxidant (typically hydrogen peroxide with catalytic acid) reacts with the

sulfur contaminant in the fuel phase. The thiophene contaminants are oxidized to sulfones (See Chapter II, Scheme 1), which are easily removed from the fuel because they are no longer soluble in the fuel phase.[18-20] ODS is appealing because the sulfur contaminants that are most resistant to HDS are the most reactive under ODS conditions.[21-23] However, because an aqueous oxidant must act on a substrate in the fuel phase, hours of stirring at elevated temperatures are required. It was hypothesized that any technique that would enhance the mixing of the fuel and liquid phases would enhance the efficiency of the ODS process. To test this hypothesis, a film-shear reactor (a variation on the spinning-disk reactor) was employed.

The film-shear reactor used in this study is illustrated in Figure 1 of Chapter II.[24] The reactor features a rotor plate that can be adjusted down to within hundreds of microns from a stator plate. Modulation of the voltage applied to the motor provides straight-forward control over the rotation speed of the rotor, which can be as high as 6,400 rpm. This close proximity, combined with the rotation of the rotor, subjects reactants between the two plates to high shear rates. The design of the reaction zone causes the non-miscible fuel and oxidant streams to encounter each other under conditions of high shear. Contact of the fluids within the narrow gap results in intense mixing and intimate contact of the two phases, promoting transport of the reactants to the interfaces. Note that a heat exchanger allows control over bulk temperature of the reaction zone. Unlike the specially designed facilities that are required to accommodate the high temperatures and pressures required for HDS, the small size of the film-shear reactor (about 10 inches high) makes this technology ideal for portable applications.

In a previous paper, we reported significant enhancement of the ODS process using a film shear reactor.[25] For example, up to 55% of the benzothiophene in a model fuel was removed in the seconds required for a single pass of the contaminated fuel through the reactor at room temperature or below. Further desulfurization was achieved when the model fuel was recirculated through the reactor. In this report, we expand on these previously reported results, and we report on the impact of various other experimental parameters on the efficiency of the ODS process. In addition, we report the results of experiments on contaminants other than benzothiophene, and we investigate the effect on efficiencies of much higher flow rates through the reactor. Finally, results on the use of molecular oxygen rather than hydrogen peroxide as an oxidant are reported.

3.2. Experimental

3.2.1. General considerations

For this investigation, a 0.5% solution of the indicated thiophene in decane was employed as a simple model fuel. A 5% solution of formic acid (unless otherwise indicated) in 30% H_2O_2 mixed with an equal volume of isopropanol (to enhance product solubility) was used as the oxidant stream. The aqueous and decane phases separated readily upon exiting the reactor, facilitating analysis by ^{1}H NMR spectroscopy of the remaining sulfur in the decane layer. Specifically, analysis of the signal intensity in the aromatic region relative to 1,1,2,2-tetrachloroethane as an internal standard allowed calculation of the remaining thiophene (Figure S2-S6).

3.2.2. Reagents

Benzothiophene (99%), 2-methylbenzothiophene (97%), and 4,6-dimethyldibenzothiophene (97%), dibenzothiophene sulfone (97%) and γ- butyrolactone

were obtained from Sigma-Aldrich. Dibenzothiophene (98%) was from Fluka. 5-methylbenzothiophene (98%) and benzothiophene sulfone (98%) were from Alfa Aesar. Decane (99%) and1,1,2,2-tetrachloroethane were obtained from TCI. Hydrogen peroxide (30-32%) and isopropanol were from Mallinckdrot. Deuterated cyclohexane was obtained from Cambridge Isotope Laboratories. All reagents were used without further purification.

3.2.3. Film-shear reactor trials

All film-shear reactor trials were carried out in a Synthetron^{TM} film-shear reactor obtained from KinetiChem, Inc. Bulk temperature in reaction zone was controlled via recirculator flow through a heat exchanger, and the system was allowed to equilibrate at the indicated temperature for 2 or more hours prior to setting the rotor-stator gap. Reagents were delivered through Teflon tubing using independent SYR-2200 dual programmable syringe pumps obtained from J-Kem Scientific. Upon reaching indicated reaction conditions, a minimum of 2 full reaction volumes were allowed to flow through the reactor prior to sample collection in order to ensure steady conditions.

For the desulfurization studies utilizing H_2O_2, feeds were introduced at room temperature via independent syringe pumps and encountered in the reaction zone (defined as the space within the rotor-stator gap).

For the oxidation-by-air trials, the γ-butyrolactone and model fuel phases were allowed to mix in a t-joint in the absence of air flow prior to encountering the air in the reactor. Air flow was provided from a tank of Grade D breathing air (19.5-23.5% oxygen) and delivery was controlled via a flow meter.

3.2.4. Sample preparation and analysis

For both types of oxidation, the model fuel phase separated from the other phase immediately upon exiting the reactor. 0.3 mL of the decane layer was combined in an NMR tube with 0.3mL deuterated cyclohexane containing 1,1,2,2- tetrachloroethane (10-100mM). Relative integrals of the aromatic region (compared to that of a sample of the starting solution prepared in exactly the same way with the same internal standard solution) were used to calculate the percent of the initial thiophene remaining. ^{1}H NMR spectra were recorded a Varian 600 spectrometer at an operating frequency of 599.98 MHz.

For analysis of the γ-butyrolactone layer, 0.3 mL of the sample was combined in an NMR tube with 0.3 mL deuterated methanol for locking. ^{1}H NMR was obtained of this sample, which was then spiked with authentic thiophene.

3.2.5. Conventional mixing controls

For the desulfurization studies utilizing H_2O_2, 10 mL of each reactor feed was placed in a 50 mL 2-neck round bottom flask equipped with a magnetic stir bar and reflux condenser. The apparatus was placed in oil bath preheated to 80 °C and stirred vigorously. 1 mL was withdrawn from each phase at the indicated time (in order to maintain equal volumes), and the decane layer was analyzed in the manner reported for reactor trials. These results are illustrated in Figure S2.

3.2.6. Air as an oxidant

For desulfurization studies utilizing air, 15 mL of each feed was placed in a 3-neck round bottom flask equipped with a reflux condenser and stir bar. The second and third necks were sealed with septa, and air was introduced into the solutions via a needle

piercing one of these septa and penetrating into the lower γ-butyrolactone phase. Air flow was maintained at 1 mL/min using a flow meter. This apparatus was placed in a preheated oil bath (100 ˚C). At the indicated time, 1 mL was withdrawn from each phase (in order to maintain equal volumes), and the decane and γ-butyrolactone layers were both analyzed in the manner described for reactor trials. No oxidation was observed.

3.3. Results and Discussion

3.3.1. Overview of desulfurization

For this study, 0.5% benzothiophene (BT) in decane was used as a model fuel (except where indicated) and the oxidant was the indicated percentage of formic acid in 30% H_20_2, mixed 1:1 with isopropanol. The sulfone is poorly soluble in water alone;[26] the isopropanol served to prevent deposition of the sulfone product in the reactor and consequent clogging. The introduction of the isopropanol likely does influence the ODS process relative to aqueous hydrogen peroxide alone because the composition of the polar cosolvent was shown to influence the desulfurization process.[27] However, to ensure a fair comparison of the film-shear reactor results, all of the control reactions with conventional stirring also utilized isopropanol in the oxidant stream. Note that, among the common organic solvents, acetonitrile would have been an excellent choice for extracting the sufone products;[28] however, this solvent underwent unknown reactivity in the reactor and was, therefore, unsuitable for these experiments.

The fuel and oxidant feeds were introduced into the reactor separately by independent syringe pumps. Upon exiting the reactor, the phases separated readily, and the thiophene remaining in the decane layer was analyzed by ^{1}H NMR relative to an internal standard. Sulfone products were identified by TLC by comparison to authentic

samples, but the concentration of the sulfone product in the aqueous layer was not quantified. Experiments showed that the potential utility of the film-shear reactor in ODS was high, with up to 55% sulfur removal at short residence times. (See Table S1 for a summary of the experimental trials).

The degree of sulfur removal using the film-shear reactor was analyzed under a variety of conditions in an attempt to elucidate the experimental and instrumental parameters that affect the extent of desulfurization. However, the effects of the various experimental parameters on the extent of sulfur removal were not straightforward. For example, under some conditions the degree of desulfurization apparently increased with temperature; under other conditions, the opposite trend was observed. Specifically, trials 6 and7 in Table 1 of Appendix B show an increase in desulfurization from 28 to 38% with an increase in temperature from 30 to 70 ˚C with all other parameters held constant. In contrast, trials 8 and 9 show a decrease in reactivity from 53 to 37% desulfurization when the temperature was increased from 10 to 70 ˚C while all other factors remained constant. In order to more rigorously determine the effects of the experimental parameters on the degree of desulfurization, a Design of Experiment (DOE) study was undertaken.

3.3.2. Design of experiments

The DOE included an examination of 6 independently controlled variables over the range illustrated in Table 1. The bulk reactor temperature was controlled through the use of a heat exchanger, and the voltage setting allowed control over the rotation speed. The actual rotation speed corresponding to the voltage setting was measured for each trial (except where indicated), and can be found in Table 1 of Appendix B (trials 1, 2, 4, and

27-52). The ratio referred to in Table 1 refers to the ratio of model fuel to oxidant, and composition refers to the percent of formic acid in the hydrogen peroxide by volume. The combined flow rate (CFR) refers to the combined rate of both reagents for the trial, as controlled by syringe pumps, and the residence time is defined as the time spent by the fluid within the rotor-stator gap.

Table 1. Parameters included in the DOE and the range over which they were surveyed. ([a]Refers to the volumetric ratio of the fuel phase to the oxidant phase. [b] Reported as the percent formic acid in hydrogen peroxide used for the oxidant phase. [c] Flow rate of the 2 phases combined.)

Parameter	Low Value	High Value
Temperature (˚C)	10	70
Gap size (µm)	250	1500
Voltage	4	16
Ratio[a]	1	10
Composition[b]	2.5	5.0
CFR[c] (mL/min)	0.5	2.0

The initial DOE design was a resolution IV, two-level experiment with 16 trials and 3 centerpoints to give a total of 19 trials. However, as this did not isolate the potentially interesting effect of shear rate (which is determined by the interaction of gap size and applied voltage) from other two-factor interactions, trials 20-29 were added to correct for this. The full DOE and the resulting desulfurization results are shown in Table 2. Desulfurization ranged from 0-55% within the design space, with a mean sulfur removal of 19%.

DOE analysis of these trials revealed that the key parameters affecting desulfurization were the temperature and the ratio of fuel to oxidant. Overall, with increasing temperature, there was more efficient desulfurization, and interestingly, this effect showed an interaction with the fuel:oxidant ratio. Within the range studied, increasing the fuel:oxidant ratio led to a slight decrease in efficiency. However, this effect is minor and even much lower quantities of oxidant still provided highly efficient desulfurization. The exchange of the small decrease in desulfurization in a single pass for a ten-fold reduction in oxidant quantity may be a reasonable tradeoff.

Other than temperature and the amount of oxidant phase available, all other experimental parameters were found to have little to no effect in the ranges studied. However, the experiments showed significant deviation from linearity, indicating that further experiments would be required to fully optimize the process.

3.3.3. Other thiophene contaminants

The utility of the film-shear reactor in removing other thiophene contaminants was also investigated. For this study, model fuels containing 0.5% contaminant in decane (where the contaminant was one of the thiophene derivatives shown in Figure 2) were subjected to ODS in the film-shear reactor. The three sets of conditions under which each contaminant were studied are shown in Table 3. These conditions were selected for the trials because they were among the best performing conditions for benzothiophene removal. Removal of the thiophenes was monitored by ^{1}H NMR spectroscopy in the

Table 2. DOE trials and results. Ratio refers to the volumetric ratio of the fuel phase to the oxidant phase. Composition is reported as the percent formic acid in hydrogen peroxide used for the oxidant phase. Combined flow rate (CFR) indicates the rate of the 2 phases combined. Approximate error in remaining sulfur is +/- 5%.

Run	Block	Temp. (˚C)	Gap size (µm)	Voltage	Ratio	Composition	CFR (mL/min)	Remaining Sulfur (%)
1	1	40	875	10	5.5	3.75	1.25	79
2	1	10	1500	16	1.0	2.50	0.50	79
3	1	40	875	10	5.5	3.75	1.25	92
4	1	70	1500	4	1.0	2.50	2.00	49
5	1	70	1500	16	10.0	5.00	2.00	90
6	1	70	250	4	10.0	5.00	2.00	91
7	1	40	875	10	5.5	3.75	1.25	86
8	1	10	1500	4	10.0	5.00	0.50	92
9	1	10	1500	4	1.0	5.00	2.00	68
10	1	70	1500	16	1.0	5.00	0.50	78
11	1	10	250	16	10.0	5.00	0.50	56
12	1	70	1500	4	10.0	2.50	0.50	64
13	1	70	250	16	10.0	2.50	0.50	82
14	1	10	1500	16	10.0	2.50	2.00	104
15	1	70	250	16	1.0	2.50	2.00	72
16	1	10	250	16	1.0	5.00	2.00	87
17	1	10	250	4	10.0	2.50	2.00	78
18	1	70	250	4	1.0	5.00	0.50	45
19	1	10	250	4	1.0	2.50	0.50	87
20	2	10	1500	16	1.0	5.00	2.00	56
21	2	10	250	16	10.0	2.50	2.00	98
22	2	70	250	16	10.0	5.00	2.00	95
23	2	70	250	16	1.0	5.00	0.50	73
24	2	70	1500	16	1.0	2.50	2.00	87
25	2	70	1500	16	10.0	2.50	0.50	96
26	2	101	250	16	1.0	2.50	0.50	87
27	2	10	1500	16	10.0	5.00	0.50	95
28	2	40	875	10	5.5	3.75	1.25	89
29	2	40	875	10	5.5	3.75	1.25	92

aromatic region, relative to 1,1,2,2-tetrachloroethane as an internal standard.

Representative spectra for each of the thiophene contaminants are in Appendix C.

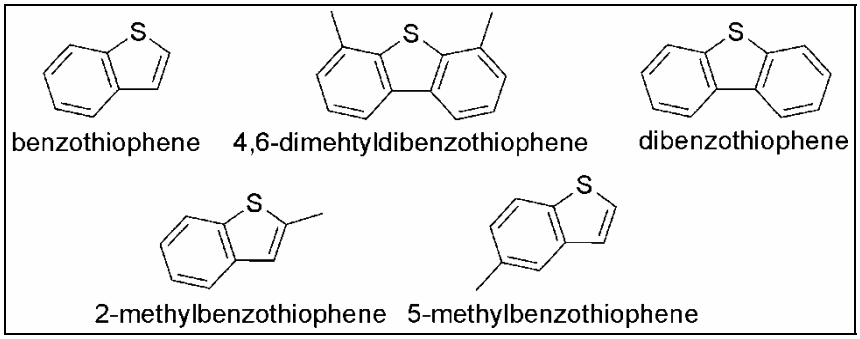

Figure 1. The 5 thiophenes examined in this study.

Table 3. Oxidation of additional thiophenes under 3 different experimental conditions.

All trials used 5% formic acid in 30% H_2O_2, 1:1 with iPrOH as oxidant.

Thiophene	Conditions A	Conditions B	Conditions C
Benzothiophene	44	51	55
Dibenzotihophene	7	17	27
5-Methylbenzothiophene	0	0	13
5-Methylbenzothiophene (series B)	0	0	21
2-Methylbenzothiophene	0	0	13
4,6-Dimethylbenzothiophene	0	0	45
Gap size (um)	250	1500	250
Temperature (° C)	10	70	70
Ratio (fuel:ox)	10	1	1
CFR (mL/min)	0.5	2	0.5
Average RPM	6300	1500	1500
Residence time (sec)	80	120	80
Average max shear rate (sec-1)	84000	3500	19000

The results for some of the thiophenes were strikingly different from those of benzothiophene. For example, 5-methylbenzothiophene, 2-methylbenzothiophene, and 4,6-dimethyldibenzothiophene were poorly removed under conditions that worked well for benzothiophene, showing essentially no desulfurization under 2 of the 3 sets of conditions. This result was surprising because these thiophenes were expected to be more reactive than benzothiophene.[21-23, 28] To verify the accuracy of the results, one set of trials (those of 5-methylbenzothiophene) was repeated. These repeated trials are denoted as series 2 in Table 3. While the three sets of conditions gave nearly identical results for benzothiophene, this was clearly not the case for the other thiophenes. The third set of conditions (250μm gap size, 6300 RPM rotor speed, 70 ˚C, 1:1 fuel:oxidant ratio, and a combined flow rate of 0.5 mL/min) was markedly better than the others, and provided especially effective desulfurization in the case of 4,6-dimethyldibenzothiophene. It is concluded that one set of conditions will not be effective in removing all types of thiophenes. For practical applications, the optimum reaction conditions would have to be determined individually for each contaminant.

3.3.4. High combined flow rate

In an attempt to increase the throughput of the ODS process in the film-shear reactor, a set of experiments at high flow rates was conducted using benzothiophene as the contaminant. For these experiments, the flow rate was varied between 100-300 mL/min, which represents an increase of approximately 2 orders of magnitude over the experiments described previously. The experimental results and the conditions are outlined in Table 4. Hydrogen peroxide and formic acid concentrations were held

constant for these experiments at 30 and 5%, respectively. Desulfurization ranged from 2 - 25%, with a mean removal of 16%. While this is slightly lower than for the slower flow rates, it is important to remember that, at these high flow rates, the residence times range from 0.1-2.4 sec. In addition, because it has already been shown that recirculation of the fuel results in further desulfurization, one could imagine a set of reactors in series operating at these high flow rates as a highly effective approach to desulfurization. The experiments outlined in Table 4 were the basis for a DOE investigation of these higher flow rates, but there were no detectable effects from the reaction variables examined in this regime. (Further details are provided in the Supporting Information.)

3.3.5. Utilization of air as the oxidant

ODS in the film-shear reactor using oxygen as the oxidant was attempted in an attempt to eliminate the need for hydrogen peroxide, thereby making this desulfurization system even more ideal for portable applications. These attempts were based on the method of Makee, et al., who were able to effectively remove thiophene contaminants from fuels using air as an oxidant when γ-butyrolactone was used as a cosolvent.[29] The necessary reagents were introduced into the reactor as illustrated in Figure 3, and the remaining sulfur in the fuel layer was quantitated by ^{1}H NMR spectroscopy as in the preceding experiments. Experiments were run at temperatures up to 80˚C. In these experiments, up to 98% of the thiophenes were removed, but the removal was found to be simply due to extraction of the thiophene into the γ-butyrolactone layer. The presence and identity of the thiophene in the γ-butyrolactone layer was confirmed by spiking the sample with a sample of authentic thiophene for each trial. Each of the thiophenes listed in Figure 2 was examined in this manner, and no sulfone formation was observed under

any of the experimental conditions. The inability to use oxygen as an oxidant is consistent with the results of control reactions using conventional stirring, which found that no detectable oxidation occurred after stirring overnight at 100 ˚C. It is noted that, in their original report, Makkee et al. reported that 140 ˚C was necessary for the ODS reaction with oxygen to occur.

Table 4. Ultra high flow rate experiments and the extent of desulfurization.

Combined Flow Rate (mL/min)	Rotation Speed (RPM)	Gap (μm)	Temp. (˚C)	Percent Sulfur Removed
300	6300	250	70	15
300	6300	250	10	2
300	1600	1500	10	3
300	1600	250	10	16
100	6300	250	10	7
100	1600	1500	70	13
100	6398	1500	70	11
200	3965	875	40	14
100	1586	250	10	12
300	6300	1500	70	18
100	1537	1500	10	11
100	6344	250	70	16
100	6260	1500	10	15
200	3919	875	40	15
300	6300	1500	10	16
300	1600	250	70	19
300	1600	1500	70	29
200	4031	875	40	24
100	1600	250	70	25
200	3930	875	40	19

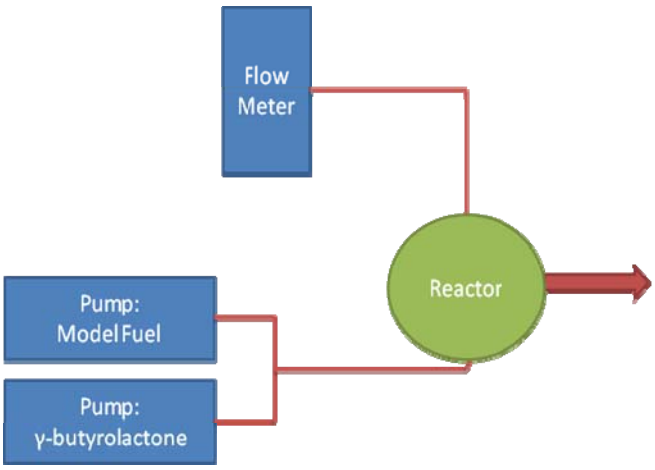

Figure 2. Schematic of the reactor setup for oxidation by air. Air delivery was controlled by way of a flow meter, and independent pumps delivered the liquid components to a t-joint for mixing in the absence of oxygen prior to entry into the reactor.

3.4. Summary and conclusions

The film-shear reactor provides a significant enhancement of the ODS process compared to conventional stirring for a variety of benzothiophene contaminants. The increased efficiency of the process is maintained even when the residence times are reduced to less than 1 second per pass. However, this system was not able to utilize air as an oxidant with γ-butyrolactone in the temperature range 10-80 °C. Experiments to further enhance the ODS process, as well as to investigate any source of enhancement beyond efficient mixing in the reactor are underway.

CHAPTER IV

INVESTIGATION INTO THE SOURCE OF ACTIVATION IN THE FILM-SHEAR REACTOR AND EXPLORATION OF POTENTIAL APPLICATIONS

Portions of the experiments in this chapter designed to probe the temperature in the reactor were performed by Benjamin L. Brinich.

4.1. Introduction

The use of a film-shear reactor to significantly enhance the oxidative desulfurization of model fuels, removing in seconds to minutes amounts of sulfur that take hours by conventional stirring methods. While this enhancement is impressive, little has been done to elucidate the source of this enhanced reactivity observed with the film-shear reactor. It is important to understand the mode of this enhancement as well as the potential modes of activation that can be achieved within the film shear reactor in order to evaluate the most advantageous potential applications of this system. These investigations are reported here. Specifically, investigations into the temperatures within the reactor and the utility of the film-shear reactor in the mechanical activation of polymer probes are reported.

4.2. Temperature in the film-shear reactor

One possible explanation for the increased reactivity seen within the film-shear reactor is an elevated temperature within the reaction zone. This elevated temperature could be due to an increase in the overall temperature due to friction within the reaction zone coupled with poor heat removal by the heat exchanger. Alternatively, the intense mixing conditions could be creating local "hot spots" (extremely localized and short lived areas of very high temperatures) analogous to those seen in sonochemistry. Both of these hypotheses were investigated.

4.2.1. Localized hot spots

One hypothesis to explain the increased reactivity seen within the film-shear reactor was the formation of localized hot spots as seen in sonochemical systems. Localized hot spots, which are very short lived, have been shown to accompany the cavitation events observed when systems are subjected to sonication. These hot spots can reach upwards of 4000 K, and can be used to promote unique chemistry in such systems.[1,2]

To investigate the possibility of similar hot spot formation within the film shear reactor, probe molecules to be used as "molecular thermometers" were introduced and subjected to reactor conditions. These molecules were used to study the local temperatures in sonochemical systems, and the reactivity observed allowed for evaluation of the conditions within the reactor.

Suslick, et al. used a set of metal carbonyls with well known activation parameters[3] as molecular thermometers in this fashion to increase understanding of the effective temperatures in the gas and liquid phases that occur during the cavitation events seen in sonochemistry. Specifically, the authors examined the dissociation of carbonyl ligands and subsequent substitution of a phosphine ligand in $Fe(CO)_5$, $Cr(CO)_6$, $Mo(CO)_6$, and $W(CO)_6$, and were able to identify hot spots up to 5200 K in the gas phase and 1900 K in the liquid phase using an effective hot spot lifetime of 2 μs, as estimated by modeling.[4]

For initial studies within the film-shear reactor, $Mo(CO)_6$ (E_a~29kcal/mol) was selected as the molecular thermometer, and $P(Ph)_3$ was selected as the incoming ligand. This system was recirculated within the reactor for 5 hours with the heat exchanger set to 23 ˚C (for a total residence time in the reaction zone of approximately 128 sec) and also mixed on the benchtop as a control. However, the formation of the phosphine complex within the reactor was not significantly greater than in the case of the control. This process was repeated with a 33 hour recirculation time (for 679 sec in the reaction zone) with the gap size reduced to 150 μm, in anticipation that the increased shear and reaction time would make any increased reactivity more noticeable. However, there was still no increase in reactivity relative to the control reaction. This lack of noticeably increased reactivity in this system suggests that hotspots are not being formed, but does not eliminate the possibility of a slight temperature increase in the overall reaction zone or reactor.

4.2.2. Overall temperature conditions

While there was no increase in reactivity consistent with what would be expected for localized hot spots, this did not eliminate the possibility of a smaller amount of less localized heating. The film-shear reactor is equipped with a heat exchanger, and the presence of the reagents as thin films should allow for highly efficient heat transfer through this heat exchanger system. However, it was observed qualitatively that the reactor felt warmer to the touch than expected for the given temperature set point on a variety of occasions. This, coupled with the observed increase in reactivity for the ODS system, led to an investigation of the temperature conditions within the reactor.

Multiple methods were employed to probe the temperature within the reactor, including use of a thermocouple as well as molecular temperature probes. The ideal method for measuring the temperature within the reaction zone would be insertion of a thermocouple probe between the rotor-stator gap. However, the small size of this gap coupled with the reactor design makes this approach impractical. Therefore, a combination of physical measurements and estimations based on observed reaction rates for a well understood and single phase reaction were used to approximate the conditions encountered by reagents within the reactor.

When the heat exchanger is not used, there is a clear increase in the temperature of the reagent feeds with increasing shear. In fact, even with the reagents entering the reactor at room temperature, and flow rates that limited the time spent in the reaction zone to seconds, boiling and subsequent recondensation of solvent in the outlet tube was observed at rotation speeds of 6300 and 4760 even at a gap size of 100 μm. The boiling

observed was greater at the higher rotation speed, and even at lower rotation speeds, a significant increase in temperature between the reagent inlet and outlet was observed. This temperature difference for the case of a decane/water/isopropanol system (based on ODS solvents) is illustrated in Figure 1. Interestingly, even at lower shear rates of approximately 5000 sec^{-1} (corresponding to the 1395 RPM data point), there is a considerable increase in temperature (over 20 ˚C) in this short residence time.

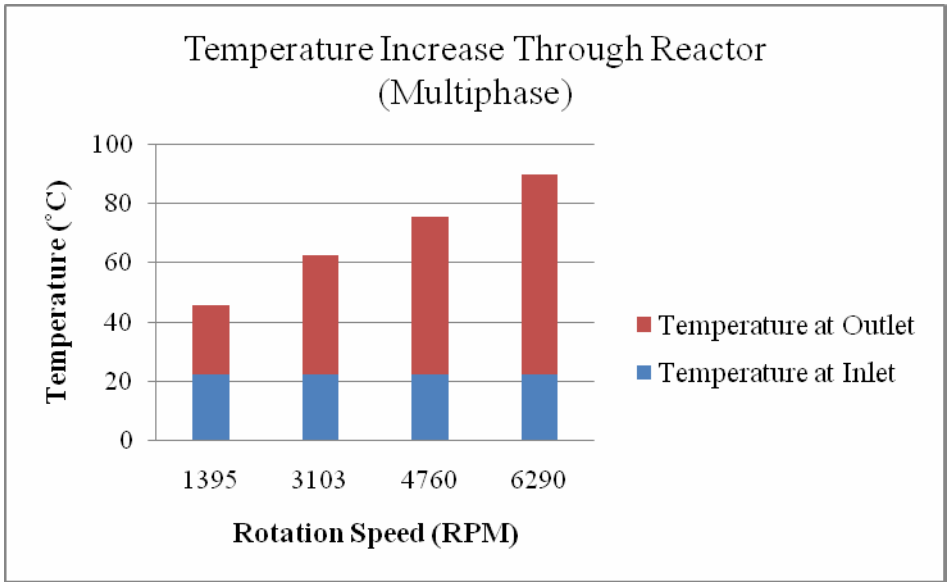

Figure 1. Increase in temperature after passage of decane, isopropanol, water mixture through film-shear reactor in absence of heat exchanger. Note that 90 ˚C after passage at 6290 RPM is an estimate, as liquid was visibly boiling. A lesser amount of boiling was observed at 4760 RPM.

Investigation of a water-only system over longer periods of time for simplification and to ensure equilibrium had been reached led to similar results (Figure 2) with vigorous boiling that led to rapid expulsion of any liquid condensed in the exit tube at 16 V (6329 RPM), but no boiling was observed at 12 V (4693 RMP), suggesting that the isopropanol was the boiling solvent in the previous system.

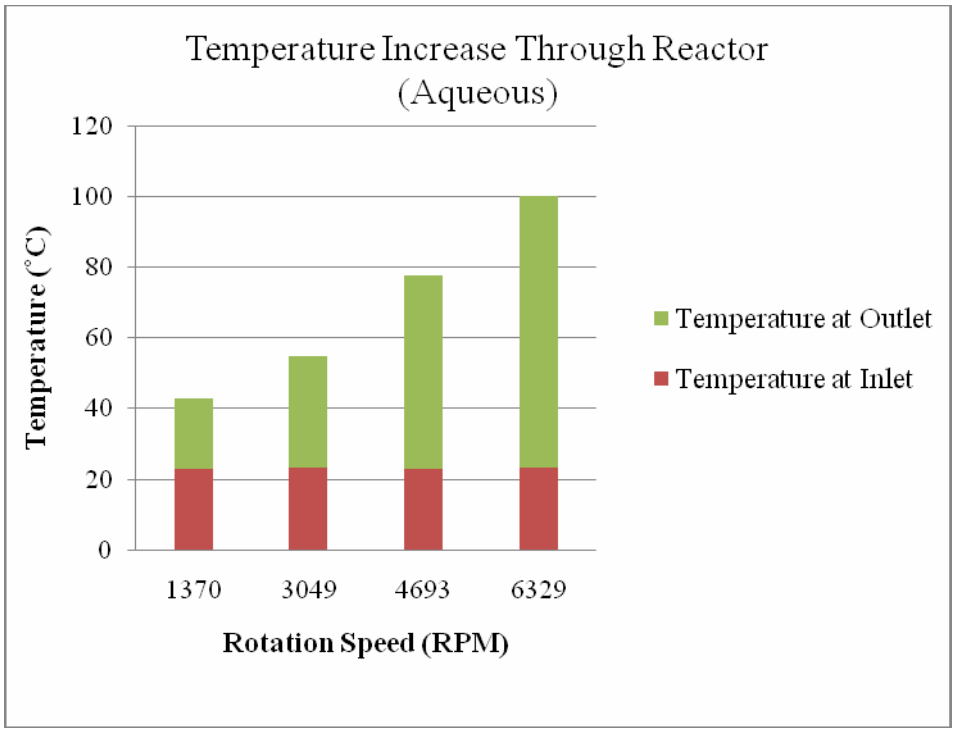

Figure 2. Increase in temperature after passage of water through film-shear reactor in absence of heat exchanger. Note that 100 ˚C after passage at 6290 RPM reflects the vigorous boiling of the solvent and may not adequately reflect the amount of heat introduced.

Clearly, these results indicated that the work done by the reactor was introducing significant heat into the system that needed to be removed by the heat exchanger in order to maintain control over the reaction temperature. Inefficient or inadequate removal of this heat would lead to an overall temperature higher than the set point. Additionally, the dependence of the temperature increase on the rotation speed correlates to a dependence of the temperature input on the shear rate, with higher shear corresponding to a greater temperature increase.

To gauge how effectively the heat introduced was being removed by the heat exchanger for a typical reactor trial, reactor conditions with the heat exchanger in use were simulated. Again, the thermocouple probes were placed at the outlet to monitor the exit temperature for comparison to the set point. However, in this case, the rotation speed was kept at the maximum (approximately 6300), and the shear rate was varied through altering the gap size (from 50-1500 μm). These results are illustrated in Figure 3.

As illustrated, the temperature at the outlet was consistently higher than the set point (from 7.4 to 14.9 ˚C), and the temperature difference was greatest at the highest and lowest gap size. While this variation in temperature from the set point confirms that the heat being introduced to the system is not entirely removed by the heat exchanger, and illustrates a general trend in the amount of temperature change based on gap size, it does not necessarily reflect the actual temperature of the liquid within the reaction zone. The fluids under shear must travel the bulk of the reactor in order to exit before the temperature can be measured, and this could result in cooling of the fluids by the reactor

parts prior to temperature measurements. To circumvent this issue in part, a single phase model reaction was used to estimate the temperature to which the reagents were exposed.

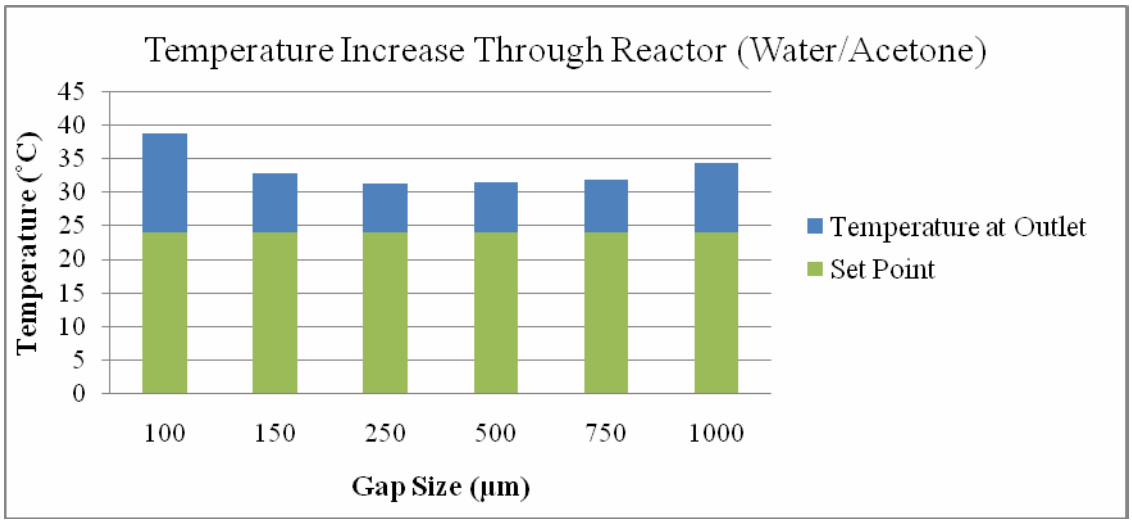

Figure 3. Change in temperature of acetone/water after passage through the reactor at maximum rotation speed and varying gap sizes as measured upon entrance into the exit tube.

The reaction selected for this analysis was the simple hydrolysis of *t*-BuCl in a 1:1 mixture of acetone:water. The reaction parameters A and E_a for this reaction are known,[5] and by measuring the rate of the reaction within the reactor, the average temperature of the reaction could be backed out of the Arrhenius equation. Comparison of the calculated temperature to the set temperature provided an estimate of the excess heat available in the reactor at a given set point and shear.

However, the treatment of the reaction time can be addressed in two ways. The first method would be to assume that any increase in reactivity only occurs in the reaction zone, and that any increase in the rate is due solely to a temperature increase there, which is quickly dissipated upon exit of the reagent from this high shear zone. Treatment two would be treatment of the reaction time as the entire time the reagents were in contact within the reactor. In reality, the scenario is likely somewhere between the two extremes, with the majority of heat being delivered within the reaction zone, but a gradual cooling leading to slightly elevated temperature throughout the reactor. This blending of the two scenarios is supported by the presence of slightly elevated temperatures even as the liquids exit the reactor.

Treatment of the reaction data by the first (reaction zone only) method results in temperatures that are elevated up to hundreds of degrees Celcius. Treatment of the data by the second (average temperature within reactor) scenario leads to average temperature elevations from 6.9-63.2 ˚C above the set point, as illustrated in Figure 4. It is, however, important to keep in mind that this average is most likely not uniform throughout the reactor, but distributed as a gradient with the highest temperatures occurring in the areas of highest shear.

It is interesting to note that the average temperature elevation appears to begin quite high at the smallest gap size and steadily decrease as the gap size is increased (and, therefore, the shear rate is increased). However, after a certain point, the temperature increase again begins to climb. This is consistent with the temperatures that were obtained when the flow was measured with a thermocouple, and can be explained by

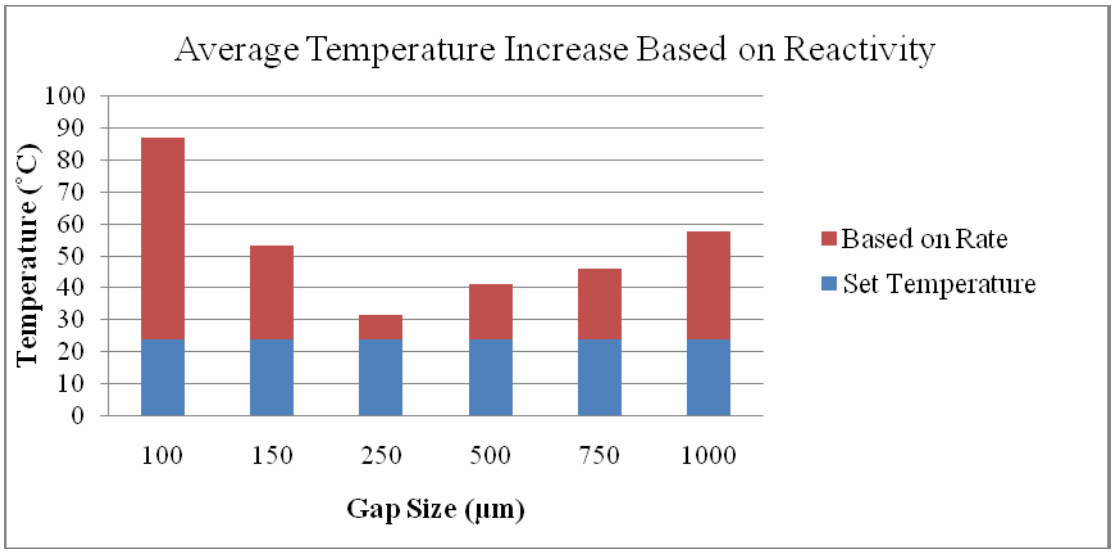

Figure 4. Average temperature encountered by *t*-BuCl reaction system within the film-shear reactor based on observed rates.

looking at the shear rate for each of the scenarios. When the gap size is small, there is very high shear in the reaction zone (between the rotor stator gap), and there is enough space above the rotor to make the shearing in the rest of the reactor negligible in comparison. As the gap size is increased, the rotor moves toward the center of the chamber, resulting in a lessening of the shear rate. However, as the rotor-stator gap is further increase, the rotor begins to become in closer proximity to the top of the reactor chamber, resulting in an increase in shearing, and therefore heat delivered in this portion of the reactor, and an overall increase in the average temperature.

4.3. Probes of mechanical activation

The mechanical activation of covalent bonds, which can sometimes lead to products unique from those obtained through thermal or photolytic activation of molecules, is one emerging and exciting area of chemistry. In one pioneering example from Jeffrey Moore's group, benzocyclobutene-based probes were used to demonstrate that mechanical activation was a unique mode of activation, and not just a result of increased temperature due to an increase in local heat due to friction or other reaction conditions. Using these benzocyclobutene probes, and mechanically activating them through the use of ultrasound, the authors were able to observe products that were distinct from those expected for thermal or photochemical activation.[6,7] Rather than mutually exclusive disrotatory or conrotatory reactivity, as would be expected under traditional activation conditions, they observed that the *cis*- functionalized isomer of their probe molecule reacted in a disrotatory fashion, while the *trans*- functionalized probe reacted to mechanical stress by undergoing a conrotatory ring opening (Figure 5).

Mechanical activation of molecules is believed to be due to physical stress on the molecules involves, and therefore, perturbation of orbital overlap, which results in changes in relative energies.[8,9] Several other mechanically activated polymers have been investigated in recent years, and an increase in reaction rate with an increase in polymer length due to greater susceptibility to these forces has been observed, but the effect of shear has not been investigated.[10] Typically, these polymer molecules are mechanically activated through the use of ultrasound, and the mechanical activation is attributed to the

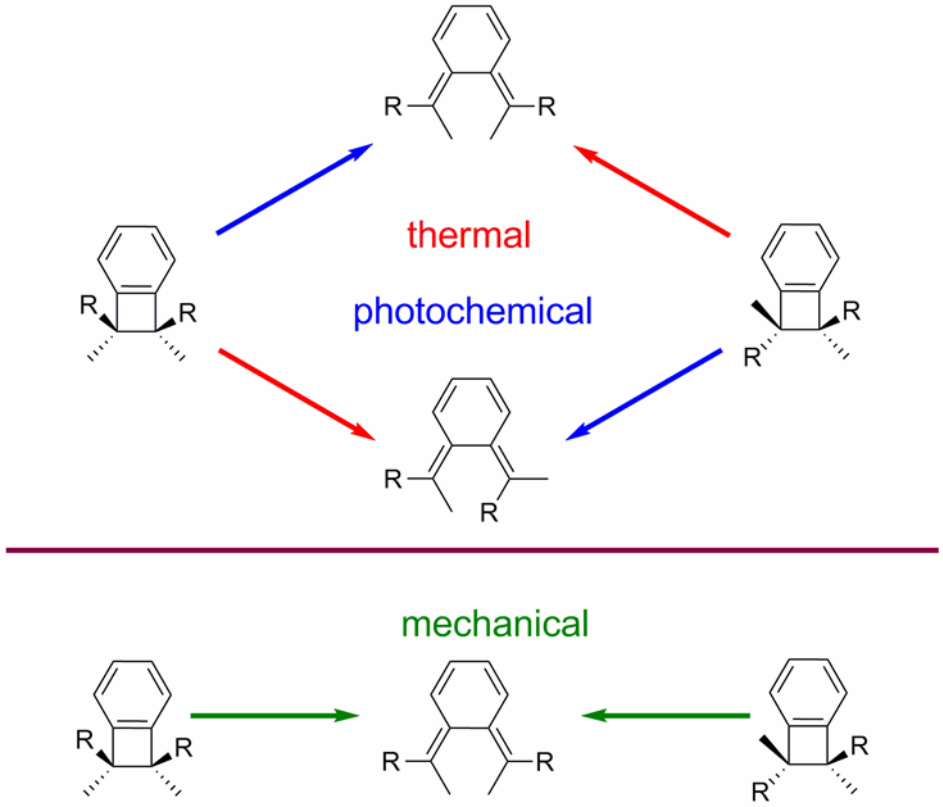

Figure 5. Unique products formed from benzocylcobutene probes under mechanical activation (Ref. 7).

shear that is provided through the cavitation events. However, the conditions upon presented with the use of ultrasound are quite intense, including very high temperatures as noted above, and the intensity of the solvodynamic shearing is not easily controlled.

It was hypothesized that the high shear rates present in the reaction zone of the film-shear reactor may be able to mechanically activate molecules as an alternative to ultrasound. This type of reactivity would not only represent an entirely new application of the film-shear reactor and a novel method of mechanically activating molecules, it

would provide a controllable and adjustable source of shearing for mechanical activation. Such a system would provide a method for the study of the effect of shear rate on mechanical activation, which was not previously studied.

4.3.1. Benzocyclobutene probes

Preliminary studies into mechanical activation within the film-shear reactor utilized probes similar to those used by the Moore group above. However, small molecule versions of these were synthesized for beginning investigations, being more relevant to the small molecules seen in ODS. Specifically, a mix of *cis*- and *trans*-dimethoxybenzocyclobutenes were introduced into the reactor in the presence of a maleic anhydride trap. The methoxybenzocyclobutene probes were an idea system because the products of thermal and photochemical ring opening followed by subsequent trapping with maleic anhydride (Figure 6) have been studied, and ^{1}H NMR shifts have been reported for convenient assignment and monitoring of the reaction products. Furthermore, any reactivity of the *cis*- isomer would be indicative of unusual activation, as it has been shown to degrade prior to undergoing thermal ring opening.[11] These probes were synthesized from , , , -tetrabromo-o-xylene through formation of the diiodobenzocylclobutene by established methods.[11-14]

To minimize any thermal reactivity, initial attempts to activate this system in the film-shear reactor were carried out at 10 ˚C under conditions of maximum shearing, but no reaction of the probe was observed. Figure 7 illustrates this, and also the key ^{1}H NMR

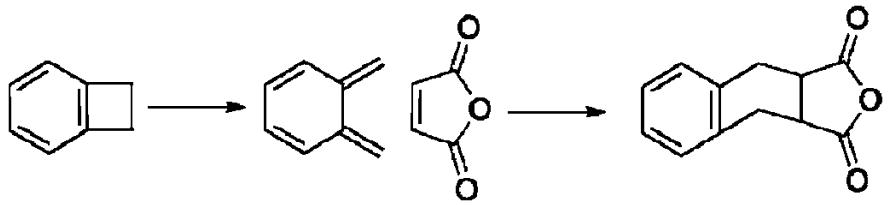

Figure 6. Trapping of a ring open form of benzocylcobutene by maleic anhydride.

resonances used in analysis of this system. However, it has been postulated and demonstrated computationally that, even in the case of mechanical activation, there is a thermal barrier that must be overcome. The key is that mechanical activation is believed to act together with thermal activation, altering the barriers and, therefore, favorable pathways, but still requiring thermal activation to overcome the resultant barrier.[15] Therefore, the same probe system was investigated at higher temperatures (40 and 80 ˚C). Even under conditions of high shear, no reactivity of the probe was observed in the trials at 40 ˚C. It should be noted, however, that the residence time was only 20 seconds in these trials due to the small gap size. Interestingly, there was significantly increased reactivity in the presence of shear compared to without shearing in the case of the trials ran at 80 ˚C. (33% reacted in the absence of shearing compared to 58% with shearing under the same conditions). However, no reactivity of the *cis*-isomer was observed, which indicates that all reactivity seen in this system could be attributed to thermal activation. This is consistent with studies showing that the temperature within the reactor is higher than the set point.

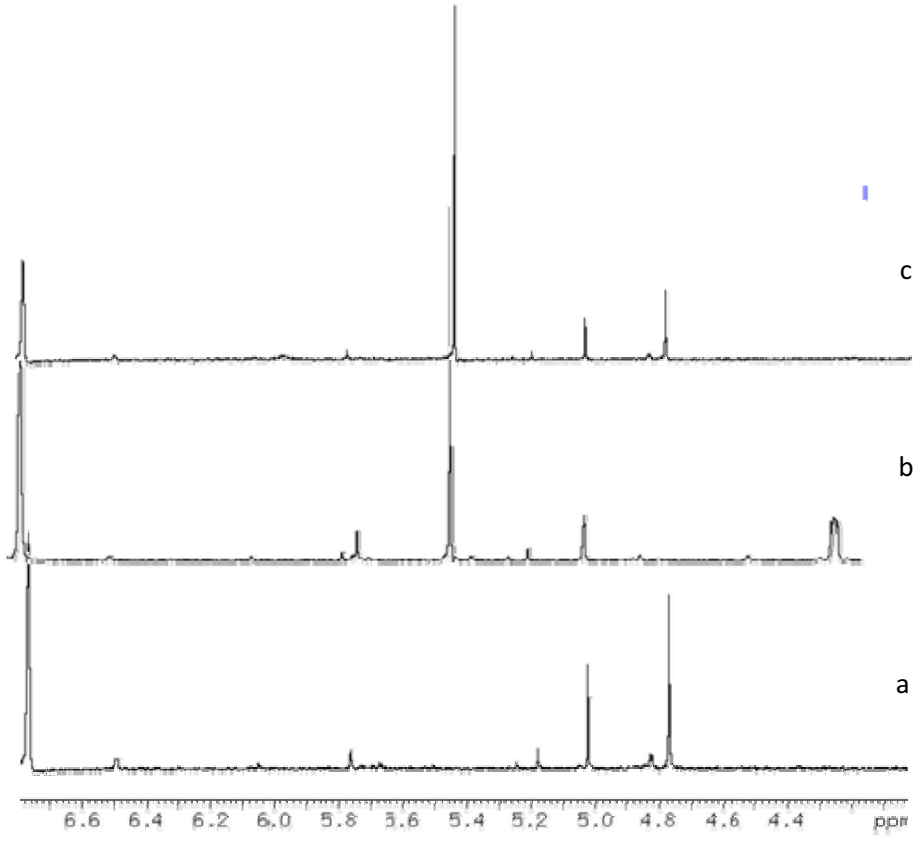

Figure 7. ^{1}H NMR spectra illustrating key resonances and the lack of reactivity of dimethoxybenzocyclobutene probes within the film shear reactor at 10 ˚C. a) Starting material, illustrating a mixture of *cis*- (5.02ppm) and *trans*-dimethoxybenzocyclobutene (δ 4.76 ppm) isomers and the mesitylene internal standard (δ 6.77 ppm). b) Thermal control reaction (80 ˚C), illustrating the disappearance of *trans*-dimethoxybenzocyclobutene and concurrent appearance of the characteristic resonance of the trapped ring opened product at δ 4.24 ppm. c) Product of film-shear reactor, showing no disappearance of either isomer under these conditions, and also no appearance of the trapped product.

The lack of mechanical activation in these probes was not surprising, as mechanical activation of small molecules has not been demonstrated in the literature, but does further suggest that the small molecule activation seen in the film-shear reactor is due to a combination of slightly elevated temperatures and unique mixing. To further investigate the possibility of mechanical activation of molecules within the reactor, two polymer systems were also studied.

4.3.2. Binol probes

The first set of polymer probes examined were the 1,1'-bi-2-naphthol (binol) derived polymers developed in the Bielawski lab. These probes consisted of a single binol unit covalently bound into the center of polymethacrylate chains (binol-PMA), and had been shown to react to the mechanical activation introduced via sonochemistry through a change of stereochemistry (Figure8).[16] While the barrier to the thermal interconversion of these types of molecules are generally in excess of 30 kcal/mol,[17,18] which prevents them from readily undergoing thermal equilibration, the authors found that the transformation took place at 0 ˚C under mechanical activation. As a result, stereochemically pure samples in CH_3CN were converted to racemic mixtures within 24 hours as monitored by circular dichroism, with over half of the signal's intensity lost within the first 2 hours. The rate of this process was also found to be dependent on chain length, the small molecule analogue showed no reactivity, and no loss in CD signal was seen when the polymer was refluxed at 257 ˚C for 72 hours, further supporting the assertion that the transformation was due to mechanical activation.

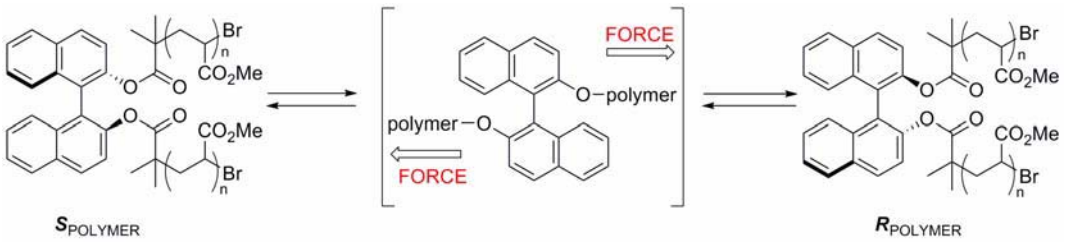

Figure 8. Racemization of central binol unit is observed when a polymer with this functionality is subjected to mechanical activation.

Initial attempts to activate these polymers focused on the highest molecular weight polymer available (100 kDa), which was expected to exhibit the greatest susceptibility to mechanical activation based on previous studies. This polymer was subjected to the film-shear reactor both with and without shear, but a single pass through the film-shear reactor provided no evidence of racemization by CD relative to the control without shearing. However, the residence time for these reactions was on the order of seconds, and it was hypothesized that the reaction may not be observable on this short time scale. To circumvent this limitation, the polymer solution was sealed off and recirculated through the reactor for 7 hours, resulting in an overall residence time of approximately 6 minutes. Interestingly, the intensity of the CD signal appeared to decrease slightly relative to the starting material and controls, but the change was not drastic enough to be conclusively outside of the noise.

To address this, the recirculation time was doubled, but racemization could still not conclusively be seen. In an attempt to limit the total volume of solution being processed, and therefore increase the proportion of time that the fluid was in the reaction

zone, additional multi-day trials were attempted without recirculation of the fuel phase, but instead leaving the solution within a sealed reactor in the absence of flow. Residence times approaching an hour were achieved by this method, but still no mechanical activation was observed. Additionally, use of the film-shear reactor in this manner damaged the rotor. Therefore, it was determined that the mechanical activation of these polymers within the film-shear reactor was impractical.

4.3.3. Azo-functionalized poly(ethylene glycol) probes

Further attempts to mechanically activate polymers within the film-shear reactor focused on the activation of azo-functionalized poly(ethylene glycol) (azo-PEG) polymers developed in the Jeffrey Moore lab. As illustrated in Figure 9, these probes feature an azo mechanophore inserted into the center of a PEG polymer. Under mechanical activation, this system has been shown to release N_2 and result in 2 polymers that are each half the length of the starting parent molecule.[19] Thus, reactivity is conveniently monitored through observation of the chain length by GPC. Again, this system exhibits rates that are dependent on chain length, as is characteristic for mechanically activated systems, and control polymers lacking the central azo functionality are unresponsive.

Initial investigations into the mechanical activation of this system using the film-shear reactor began with a 290 kDa polymer (the highest molecular weight available), and focused on much longer reaction times to increase the chance of mechanical activity

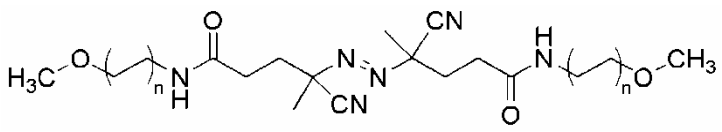

Figure 9. Azo-PEG polymer, featuring a central azo unit that is susceptible to mechanical activation.

after observartion of the lack of reactivity observed for the binol-PMA system. Interestingly, in these initial trials, a shift toward longer GPC retention times, and therefore lower molecular weights was observed in the case of one sample subjected to a residence time of over 2 hours (Figure 10). This shift was in retention time corresponded to a decrease in molecular weight from 290 kDa to 250 kDa. While this was not consistent with the clean transition from the starting polymer to polymers of one half the molecular weight, it was promising. However, this result was not conclusive evidence of mechanical activation, and could not be reproduced in subsequent trials, even with much longer residence times (with trials over the course of several days). Therefore, it was concluded that mechanical activation of these polymer probes in the film shear reactor was also impractical.

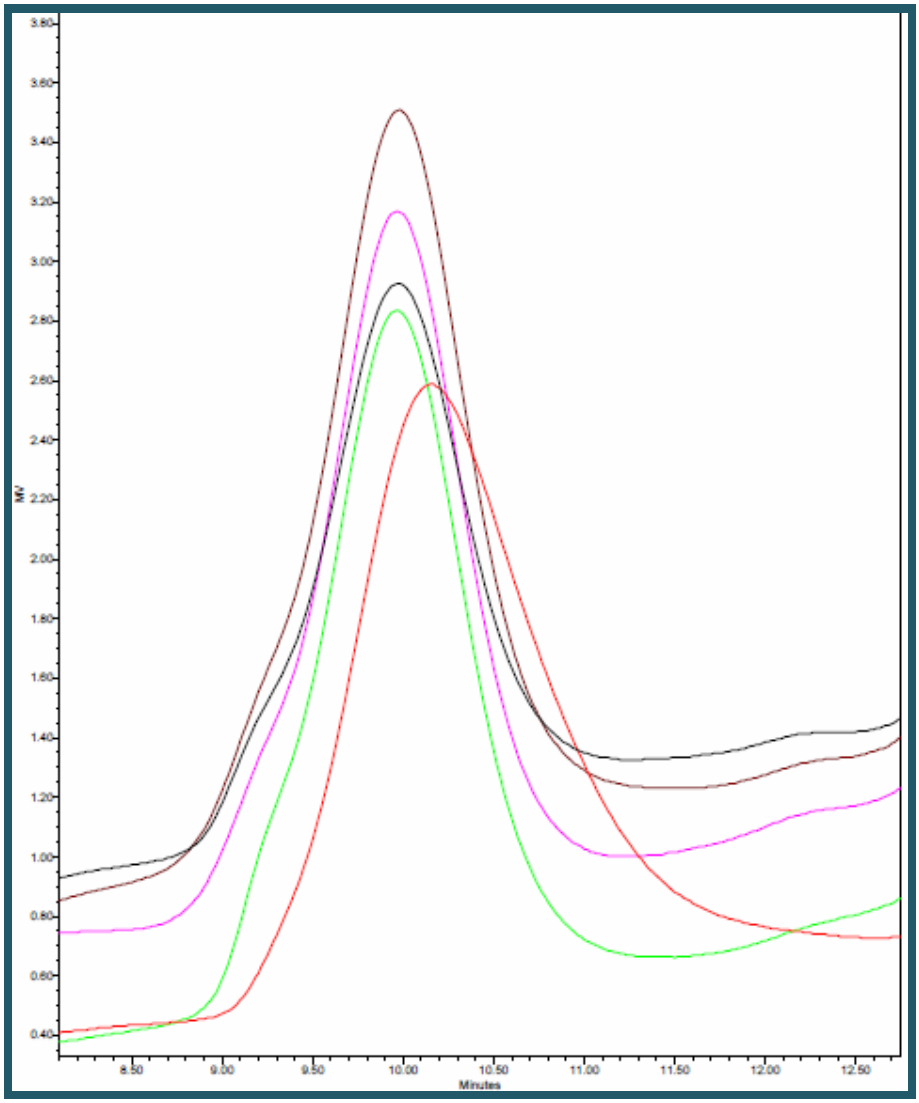

Figure 10. GPC data illustrating the shift to a lower MW in the case of azo-PEG polymer after being subjected to over 2 hours in the reaction zone of the film-shear reactor (red). Other traces represent the starting material (black), 1 pass through the reactor without shearing (pink), 1 pass through the reactor with shear (purple), and shorter recirculation time (green).

4.4. Conclusions

These experiments have provided a clearer picture of the conditions within the film-shear reactor and, therefore, ideal potential applications. The lack of mechanical activation of the probes under the conditions attempted suggests that even at the highest shear settings, the amount of shearing is not comparable to that seen in ultrasound-based experiments and that the film-shear reactor is not a practical method for the mechanical activation of such molecules. While the adjustable shear within the reactor would have provided a unique opportunity to investigate the relationship between shear rate and mechanical activation rates, mechanical activation of these molecules does not occur to an appreciable degree at shear rates in the hundreds of thousands.

Additionally, the use of a combination of physical and reactivity measurements have provided a clearer picture of the temperature conditions within the film-shear reactor. The heat exchanger does not control the temperature as efficiently as initially believed, and the actual average temperature within the reactor is potentially significantly higher than the set point. The magnitude of this temperature difference is dependent on the shear rate within the film-shear reactor, showing a dependence on both rotation speed at constant gap size and on gap size at constant rotation speeds (the two methods by which shear rate can be modified). However, the increase in reactivity observed in the ODS process cannot be explained by such temperature increase alone, suggesting that mixing also plays a key role in the unique reactivity observed in the film-shear reactor.

4.5. Experimental procedures

4.5.1. Reagents

Decane (99%), t-butyl chloride (98%), and $Mo(CO)_6$ (99%) were obtained from TCI. Isopropanol (reagent grade) was from Mallinckdrot. Deuterated toluene was obtained from Cambridge Isotope Laboratories. UV grade acetonitrile and THF were obtained from Burdick and Jackson. Binol-PMA probe was obtained from the lab of Christopher Bielawski, and the azo-functionalized PEG was obtained from the lab of Jeffrey Moore. All reagents were used without further purification

4.5.2. Reactor trials

All film-shear reactor trials were carried out in a KinetiChem, Inc. Synthetron^{TM} film-shear reactor. Reactant feeds were introduced at room temperature and encountered each other in the reaction zone (defined as the space within the rotor-stator gap). The bulk temperature in the reaction zone was controlled using the flow from a recirculator/chiller through the heat exchanger unless otherwise noted. The system was allowed to equilibrate at the indicated temperature for 2 or more hours prior to setting the rotor-stator gap. Reagents were delivered through Teflon tubing using independent SYR-2200 dual programmable syringe pumps obtained from J-Kem Scientific. Upon reaching the indicated reaction conditions, a minimum of two full reaction volumes was allowed to flow through the reactor prior to sample collection in order to ensure stable conditions. The rotation speed of the rotor was measured using a tachometer directed on the shaft

extending into the reactor, and measurements were taken at random intervals and averaged to arrive at the reported value.

4.5.3. Localized hot spot studies

Feeds 1 and 2 were a mixture of 1.2mmol $Mo(CO)_6$ and $P(Ph)_3$ that were sealed and recirculated as collected from the reactor for 5 hours at 19 ˚C with a gap size of 200 μm and spin rate of 6300 RPM. Aliquots were obtained every 30 minutes for analysis by monitoring of the IR for appearance of the phosphine substituted product (2072 cm^{-1}), and compared to a benchtop mixture of the reagents.

4.5.4. Overall temperature experiments

4.5.4.1. In the absence of the heat exchanger

Temperature of reagent feeds at inlet and upon entering the exit tube were measured via thermocouple. Reagent feeds were either feed 1 as 50:50 isopropanol : water and feed 2 as decane (the solvent system used in the ODS system) or simply water, as indicated. For outlet temperature, the probe was inserted into the exit tube to measure the temperature of the fluids just as they exited the reactor. Boiling was observed by the appearance of slugs of gas between liquid phases within the exit tube and visible condensation of liquid droplets. Recordings for inlet temperature, rotation speed, and outlet speed were measured at random intervals over 15 minutes (25 minutes in the case of the aqueous feed only) and averaged to arrive at reported values.

4.5.4.2. In the presence of the heat exchanger

Temperature of the overall reactor was controlled via recirculation of water and ethylene glycol through the heat exchanger system. Temperature of a 1:1 mixture of acetone and water upon entering the exit tube was measured via thermocouple. Each measurement was taken as part of a separate trial, where the reactor was allowed to fully equilibrate at the given temperature prior to setting of the gap. The exit temperature was monitored periodically over the run after allowing for equilibration of shearing conditions, and the points were averaged. Additionally, each trial was duplicated and the measured temperatures for each trial averaged to arrive at reported values.

4.5.4.3. Reaction rate probe studies

Feed 1 was a 0.3 M solution of *t*-BuCl in acetone, and feed 2 was water. Both feeds were introduced at the same rate to obtain equal volumes in collection reservoir. After collection of a reservoir of reagents, the feeds were recirculated, and 1 mL aliquots were taken periodically and quenched using acetone to measure the rate. Titration of HCl was used to determine the percent completion at each point. The rates obtained were compared to rates of control reactions run concurrently on the benchtop to confirm temperature calculation method. Each gap size was repeated twice, allowing for equilibration of temperature and resetting of rotor-stator gap between trials. Reported temperature increases are an average of these trials.

4.5.5. Dimethoxybenzocyclobutene control reactions

For controls of the thermal of dimethoxybenzocylcobutene, 0.5 mL dimethoxybenzocyclobutene (mixture of isomers) anhydride and 0.02 M mesitylene in toluene-d_8 was combined in an amber NMR tube (to exclude any incident light) with 0.5 mL of a 0.03 M solution of maleic anhydride in toluene-d_8. NMR tube was placed in a preheated oil bath and monitored by ^{1}H NMR.

4.5.6. Dimethoxybenzocyclobutene reactor trials

Feed 1 was a 0.02 M solution of dimethoxybenzocyclobutenes in d-8 toluene and 0.01 M mesitylene internal standard. Feed 2 was a 0.03 M solution of maleic anhydride also in d-8 toluene. General reactor conditions: 250 μm gap size, variable rotation speed (6300 RPM max), and 2mL/min CFR. Products were collected, transferred to amber NMR tube and immediately analyzed by ^{1}H NMR.

4.5.7. Binol-PMA reactor trials and controls

Both inlet feeds were from the same solution of 75 mg/mL solution of binol. A small aliquot of this solution was sealed and set aside for CD analysis as a starting material comparison. Reactor flow was at 0.5 mL/min combined, and a sample of the product was obtained as a control prior to introduction of shear (6300 RPM at 250 μm). After shear sample was collected, all samples were analyzed by CD with a 0.2 cm path length against a CH_3CN background (observed 400-180nm).

For recirculation studies, the inlet tubes were transferred directly into the collection vessel after the sample to be recirculated had been collected. The inlet tubes

were introduced through pierced septa inserted into a 2-hole rubber stopper to minimize changes in the sample due to evaporation. In the cases where flowing was stopped, the same setup was employed to keep the system closed, but the pumps were not operated.

4.5.8. Azo-PEG trials and analysis

Experimental setup was similar to that used for recirculation experiments using binol-PMA probes. Both feeds were azo-PEG polymer in CH_3CN, the gap size was 150 μm, and the rotation rate was 6300 RPM. Samples were collected as indicated for GPC analysis, and molecular weights are reported versus calibration with polystyrene standards.

CHAPTER V

CONTROLLED NANOPARTICLE SYNTHESIS WITHIN THE FILM-SHEAR REACTOR

Portions of the experiments regarding TEOT hydrolysis reported herein were performed by Ryan Everett.

5.1. Introduction

In a further attempt to further improve the oxidative desulfurization (ODS) process and explore other potential applications of the unique system, controlled synthesis of titania nanoparticles within the film-shear reactor was explored. While control of size and dispersion in any nanoparticle system would serve as proof of principle that the reactor could be used in this manner, titania particles were investigated as a starting point due to their potential applicability to the ODS process.

Upon contact with the TiO_2 surfaces, hydrogen peroxide immediately decomposes to give peroxo and superoxide radicals on the metal oxide surface that can be used to catalyze selective oxidations (Figure 1).[1]

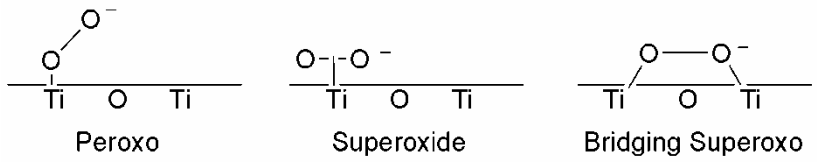

Figure 1. Species formed on titania surface in contact with hydrogen peroxide.

The resultant functionalized titania has been shown to catalyze ODS in fuel systems,[2] and maximum thiophene oxidation was seen when the catalyst and oxidant was introduced in water (as compared to other immiscible cosolvents for the process).[3] The ability of such particles to further enhance ODS reactivity previously demonstrated within the film-shear reactor was expected to provide and even more efficient desulfurization system.

Outside of this potential application of the titania nanoparticles produced, the useful applications of titania are many. TiO_2 has been explored for a variety of applications including photocatalysis,[4,5] solar cells,[6,7] water purification,[8] coatings, and pigments.[9]

Current syntheses of titania nanoparticles result in significant variations in size, structure, and stoichiometry, and hence, optical and electronic properties.[10] These variations limit usefulness, particularly in applications that depend on the very size-dependent photoactive properties of the particles. Thus, achieving control of nanoparticle size will contribute to the variety of fields in which titania particles are useful. Even catalytic processes that can be performed with the current dispersity often have an ideal particle size, and the ability to "dial up" a particle size would be incredibly useful even beyond ODS applications. Furthermore, achieving efficient size and dispersion control via the film-shear reactor will set an important precedent for the production of other useful and difficult to generate particles.

It is expected that synthesis of the nanoparticles in the reactor will allow for control of size and dispersion by modulation of reaction conditions. Precedent for this is based on experiments utilizing other reactor systems to achieve control of nanoparticle synthesis. For example, the synthesis of submicron particles of $BaCO_3$ using a spinning-disk reactor.[11] Prior to this study, submicron particles of $BaCO_3$ had not been obtainable using any conventional methods. The spinning-disk reactor, however, not only was able to facilitate production of nanoparticles, but also allow control of particle size and dispersion through modulation of disk rotation speed and reagent concentration. A summary of their results regarding the dependence of particle size on rotation rate can be seen in Figure 2. Clearly, the mean particle size decreased with increasing rotation rate.

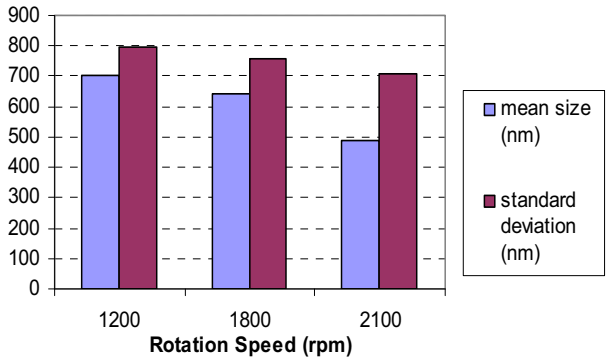

Figure 2. Summary of results illustrating effect of rotation speed in SDR on particle size (Ref. 11).

Additionally, Chen, et al. investigated the use of another high gravity (higee) device in the control of nanoparticle size and dispersion.[12] Using a rotating packed bed (RPB) reactor, it was found that the gravity level induced by the rotating bed, flow rate, and concentrations of

reagents strongly influenced the mean particle size for the formation of $CaCO_3$. As can be seen in Figure 3, a significant decrease in mean particle size as well as dispersion relative to traditional precipitation methods was observed. The authors were also able to synthesize nanoparticles of aluminum hydroxide and $SrCO_3$ in the RPB, but did not report detailed dependence on change in condition for these systems.

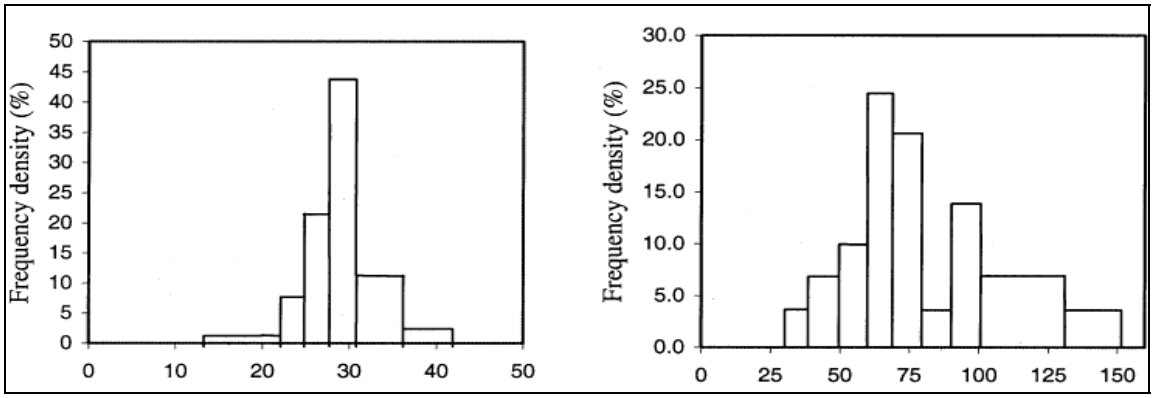

Figure 3. Size and distribution of $CaCO_3$ nanoparticles in RPB (left) and conventional batch precipitation reaction conditions (right) illustrate smaller particle size and polydispersity in RPB. X-axis is in nm (Taken from Ref. 12).

While much of the mechanism of nanoparticle formation is still poorly understood, the unique behavior observed in these reactors has been attributed to highly efficient micromixing. The local concentration of reagents plays an important role in the reaction and nucleation processes in conventional nanoparticle synthesis by precipitation. Because the time scale of micromixing is much larger that the time scale of the nucleation event in conventional reactors (in water, 5-50 ms for the former and t<1ms for the latter), it is not possible to control particle formation based on intrinsic kinetics without impedance from the much slower micromixing

process and resulting lack of uniformity. However, if the time scale of micromixing is made very small so that it is less than the timescale of the nucleation event, the solution remains highly uniform. Therefore, nucleation is uniform, resulting in a much smaller polydispersity, and allowing control of the reaction by other factors.[11] The improved control over size and dispersion that has been observed when higee reactors have been applied to nanoparticle synthesis has been attributed to intense micromixing conditions that allow for this uniform nucleation.[13]

Based on the above precedents, it is expected that the film-shear reactor will exhibit unique behavior in the synthesis of nanoparticles. Further, because of the availability of many other controllable variables in the film-shear reactor relative to the precedents, it is expected that even more control of particle size and dispersion may be accessible. The effect of residence time, gap size, shear rate, ratios of reagents, reagent concentration, and reaction temperature in the synthesis of titania nanoparticles are among the parameters that may affect particle formation.

5.2. ODS controls using commercially available TiO_2

To demonstrate that titania particles were, indeed, capable of enhancing the ODS process in the film-shear reactor, commercially available titania nanoparticles were obtained and incorporated into the ODS process. Three different sets of trials, each of which were identical except for the absence or presence of TiO_2 verified that introduction of titania was, indeed, effective in increasing the ODS of benzothiophene from a model fuel compared to H_2O_2 alone (Table 1). The uncatalyzed removal with hydrogen peroxide alone under the conditions examined was consistently around 10%, while introduction of a 0.1 wt% solution of TiO_2 doubled to tripled the removal rate, depending on temperature in the case of the commercially available particles.

Table 1. Percent removal of benzothiophene by ODS with H_2O_2 with and without introduction of titania catalyst illustrating improvement of desulfurization. Conditions: combined flow rate: 2mL/min, 6300RPM, 100μm gap size.

Temperature (˚C)	Percent Removal Without TiO_2	Percent Removal With TiO_2
10	11	23
40	11	36
80	10	30

5.3. Particle synthesis starting with $TiOSO_4$

For initial studies, a modification of an established synthesis by Karuppuchamy, and Jeong using aqueous $TiOSO_4$, which is an extremely attractive starting material due to its low cost, and hydrogen peroxide precursors was applied. TiO_2 was formed under traditional conditions by way of a peroxo-titanium precursor, and calcination of the initially amorphous product was found to yield particles that averaged 28-50nm depending on conditions employed.[24]

Preliminary data suggests that there is a significant difference in the products of this reaction with and without shear. Qualitiatively, an increase in color and cloudiness can be seen as the shear rate within the reactor increases (Figure 4). Additionally, while there was no isolable solid in the absence of rotation and the resultant shear, TEM of the isolable solid from the high shear conditions showed the presence of particles with an average size near 6nm (Figure5).

However, while this difference in apparent behavior when the shear rate was varied was quite promising, it was difficult to say that the difference in the product formed was due to differences created by the variation of shear within the reactor rather than simply due to the low starting material solubility. While $TiOSO_4$ had been reported to be a convenient water

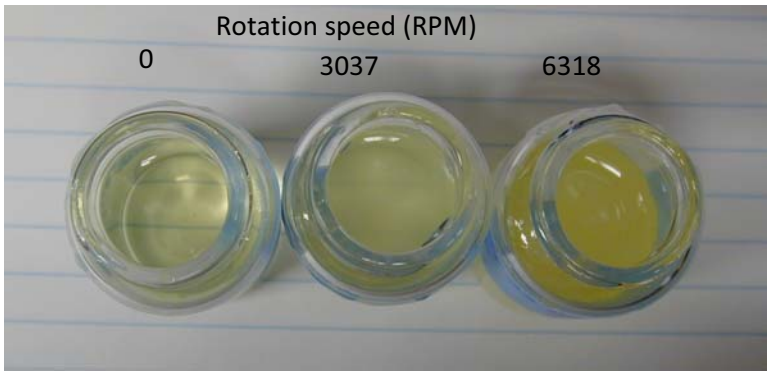

Figure 4. An increase in color and cloudiness accompanied an increase in shear rate (as determined by rotation speed). Increasing shear from left to right.

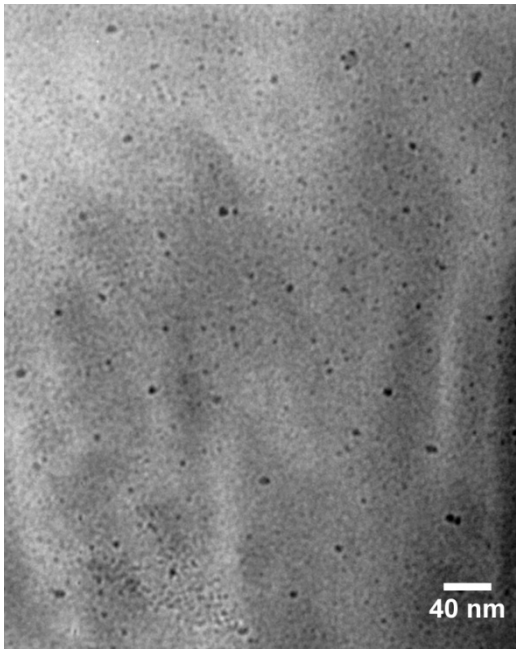

Figure 5: TEM of solid obtained after application of the film-shear reactor.

soluble precursor, it was very poorly soluble in reality. As a result, the precursor $TiOSO_4$ solution was introduced into the reactor system as a vigorously stirred suspension. It is possible that under conditions of little to no shear, the majority of the starting material or product formed was simply

crashing out before exiting the reactor, and therefore not observed. In contrast, the higher shear conditions were keeping any solids present in the reactor suspended, allowing them to be removed from the reactor and observed in the product. Due to this potential complication, another method of titania synthesis was attempted.

5.4. Titania synthesis from TEOT precursor in the film-shear reactor

Synthesis of titania through the hydrolysis of orthotitanates is a fairly common approach.[15] A variety of alkoxide precursors, have been explored, and syntheses by this method typically employ a polymer such as HPC or electrolytes as a dispersant that is easily removed from the final product based on solubility.[16]

For initial investigation of this synthesis method within the reactor, tetraethyl orthotitanate (TEOT) was selected as the titanium precursor (Scheme 1). This was an especially appealing method of synthesis because it was well established, required only water as the second reagent, and could be carried out in ethanol. Additionally, synthesis of nanoparticles by this method in a continuous aging tube reactor (where reagents are simply allowed to mix in small diameter tube for an established period of time) showed that even the small degree of change in the uniformity of mixing provided by introducing a slug of air between segments of reaction solutions (versus continuous flow) had an effect on particle formation.[17,18] By altering reaction conditions, the authors were able to obtain particles with a mean diameter as low as 40 nm over 300 nm. This suggested that particle formation for this system is very sensitive to changes in mixing and the system should therefore, be susceptible to the effects of small changes in reaction conditions achieved through alteration of reactor parameters.

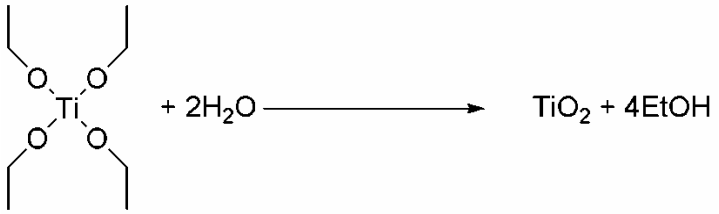

Scheme 1. Synthesis of titania from tetraethyl orthotitanate (TEOT).

Initial trials based on the literature preparations cited above (see experimental procedures for details) did not yield solid titania that could be isolated as expected after being passed through the reactor. However, this was remedied by increasing the water concentration from 0.64 to 4.6 % (v/v) of solution, which produced a cloudy white solution within 3 seconds of mixing.

However, TEM analysis of the reactor product showed networks of solid that were connected by what was initially thought to be HPC dispersant that had not been removed (Figure 6). This material persisted despite increased washings intended to remove the HPC, and further analysis by EDX determined that it was composed of Ti and O rather than organic species (Figure 7).

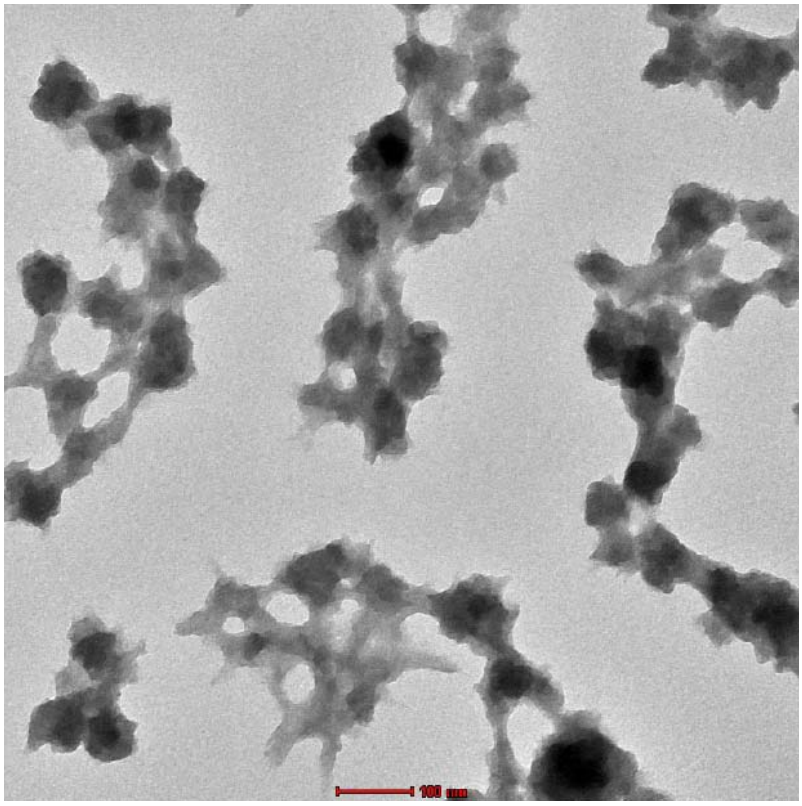

Figure 6. TEM illustrating material connecting particles. Scale bar: 100nm.

The formation of these "necks" between particles has been demonstrated for this system under conditions of mild shearing,[19-21] and apparently persists into the high shear realm (up to 200,000 sec^{-1}, as applied in these trials). The formation of these structures from the TEOT and water precursors under shear suggests that another synthesis method may be present to obtain discrete particles that will allow direct observation of the effect of reactor parameters on nanoparticle formation. However, synthesis of titania in this manner, does provide material that is potentially useful for enhancement of the ODS process. Further, the formation of these unusual structures in the presence of shear illustrates an example of the surprising effect that shearing and mixing can provide in nanoparticle syntheses.

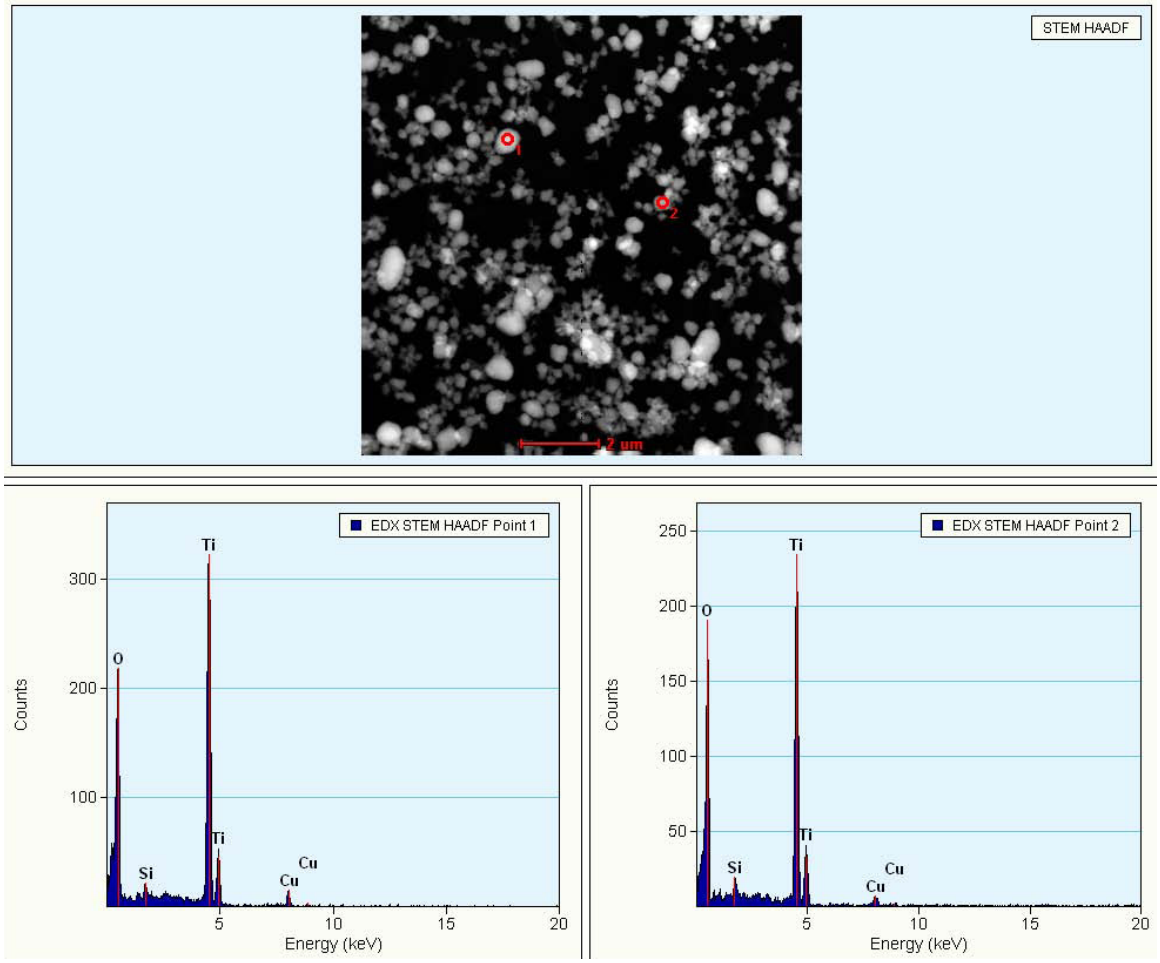

Figure 7. STEM image and EDX data indicating that particles as well as connecting areas are composed of Ti and O.

5.5. Conclusions

Improvement of the ODS process within the reactor by introduction of titania (compared to hydrogen peroxide alone) has been demonstrated, making synthesis of titania materials in the reactor (in order to provide a portable method for catalyst synthesis as well as subsequent ODS) an appealing application of the film-shear reactor.. Controlled synthesis of titania nanoparticles within the film-shear reactor was explored by two different methods. While neither provided the ideal route for an investigation of the effect of various reactor parameters on nanoparticle size and

dispersion, synthesis of potentially catalytic titania material within the reactor was successful in both cases. Interestingly, however the synthesis of titania by the hydrolysis of TEOT led to the formation of titania "necks" bridging the particles, and illustrates the potential effects of mixing and shear on nanoparticle syntheses.

5.6. Experimental procedures

5.6.1. Reagents

Benzothiophene (99%), TiO_2 (99.5%, <100nm), and titanium oxysulfate hydrate were obtained from Aldrich. Decane (99%) and1,1,2,2-tetrachloroethane were obtained from TCI. Hydrogen peroxide (30-32%) and isopropanol were from Mallinckdrot. Deuterated cyclohexane was obtained from Cambridge Isotope Laboratories. Ethanol (anhydrous) was from Pharmco-Aaper, stored over molecular sieves and filtered prior to use. All reagents were used without further purification.

5.6.2. Reactor trials

All film-shear reactor trials were carried out in a KinetiChem, Inc. Synthetron^{TM} film-shear reactor. Reactant feeds were introduced at room temperature and encountered each other in the reaction zone (defined as the space within the rotor-stator gap). The bulk temperature in the reaction zone was controlled using the flow from a recirculator/chiller through the heat exchanger. The system was allowed to equilibrate at the indicated temperature for 2 or more hours prior to setting the rotor-stator gap. Reagents were delivered through Teflon tubing using independent SYR-2200 dual programmable syringe pumps obtained from J-Kem Scientific. Upon reaching the indicated reaction conditions, a minimum of two full reaction volumes was allowed to flow through the reactor prior to sample collection in order to ensure stable conditions. The rotation speed of the rotor was measured using a tachometer directed on the shaft extending

into the reactor, and measurements were taken at random intervals and averaged to arrive at the reported value.

5.6.3. ODS trials

Feed 1 was, in all cases, a 0.5% (wt) solution of benzothiophene in decane. In trials without TiO_2 feed 2 contained 30% H_2O_2 (aq) mixed 1:1 with isoprpoanol. In trials incorporating TiO_2, feed 2 was introduced after t-mixing of 0.1 % (wt) TiO_2 in iPrOH with 30% H_2O_2 (aq). Upon exiting the reactor, the organic phase was analyzed by ^1H NMR of remaining benzothiophene relative to 1,1,2,2-tetracholoroethane as an internal standard. ^1H NMR spectra were recorded on a Varian 600 spectrometer at an operating frequency of 599.98 MHz.

5.6.4. $TiOSO_4$-based reactor trials

Feed 1 (central inlet) was composed of a suspension of 0.008M $TiOSO_4$ kept suspended through vigorous stirring and delivered at a rate of 0.8 mL/min. Feed 2 was composed of 30% H_2O_2 (aq) and delivered at a rate of 0.2 mL/min. Reactor product was collected, transferred to a centrifuge tube, and centrifuged 3 x 10 minutes, with washing and resuspension in fresh ethanol with each pass. The resultant solid was suspended in methanol and dropped onto TEM grid for analysis.

5.6.5. TEOT-based reactor trials

Feed 1 (central inlet) was composed of 0.2M TEOT and HPC (0.25g/100mL) in ethanol under N_2 atmosphere and delivered at a rate of 1.5 mL/min. Feed 2 was composed of indicated water concentration (typically 4.6% v), and delivered at a rate of 0.5 mL/min. Reactor product was collected, transferred to a centrifuge tube, and centrifuged 3 x 10 minutes, with washing and resuspension in fresh ethanol between each round. The resultant solid was suspended in methanol and dropped onto TEM grid for analysis.

CHAPTER VI

SUMMARY AND OUTLOOK

The use of a film-shear reactor as a route to a convenient and portable method to low sulfur fuels has been shown to significantly enhance the oxidative desulfurization process in model fuels. Application of the film-shear reactor has taken a process that typically requires hours stirring at elevated temperatures and demonstrated the same reactivity in seconds to minutes at or below room temperature. The temperature and amount of oxidant were found to be key parameters affecting the amount of desulfurization observed, but even when the amount of oxidant used is reduced, the desulfurization observed remains far superior to conventional stirring methods. This process has been shown to be effective in oxidizing a variety of recalcitrant sulfur contaminants.

Trials investigating the synthesis of titania nanoparticles for further improvement of this process have also been promising. Initial trials have demonstrated that titania nanoparticles can be used to improve the ODS of model fuels relative to the use of H_2O_2 alone. Further, synthesis of the titania nanoparticles for this application within the reactor has been explored with two different methods. Interestingly, the hydrolysis of TEOT results in the formation of unusual "necks" between the particles due to the high shear conditions, but this material may still be effective for enhancement of the ODS

process, providing a portable method for synthesis of ideal catalysts as well as purification of fuel streams. Further, the parameters available for control of the reaction zone in the film-shear reactor may provide a route to a high degree of control in these and other nanoparticle syntheses.

Investigations into the conditions within the film-shear reactor have provided significant insight into the source of activation and ideal potential applications of the film-shear reactor. Exploration of known mechanophores demonstrated that, even in the case of molecules that have been shown to be susceptible to mechanical activation, the shear forces reached within the film-shear reactor are not great enough to induce mechanochemical activation. The lack of mechanically induced reactivity seen in these ideal systems also suggests that mechanical activation is not responsible for the small molecule substrates examined. It was also demonstrated, through both physical measurements and studies using molecular thermometers, that somewhat elevated temperatures (relative to the set point) are present within the reaction zone of the film-shear reactor. However, the magnitude of these temperature differences was not great enough to fully explain the enhancement seen in the ODS process, suggesting that the unique mixing also plays an important role, and that a variety of biphasic systems may show enhanced reactivity within the film-shear reactor. While much understanding of the reactivity within the film-shear reactor and the capabilities of the system regarding ODS has been gained, there are a wide variety of such biphasic systems that may be worthy of investigation. Additionally, control of size and dispersion in other nanoparticle syntheses may be an ideal way to take full advantage of the unique mixing within the film-shear reactor.

APPENDIX A

SUPPORTING INFORMATION FOR CHAPTER II

A.1. Sample ^{1}H NMR spectrum

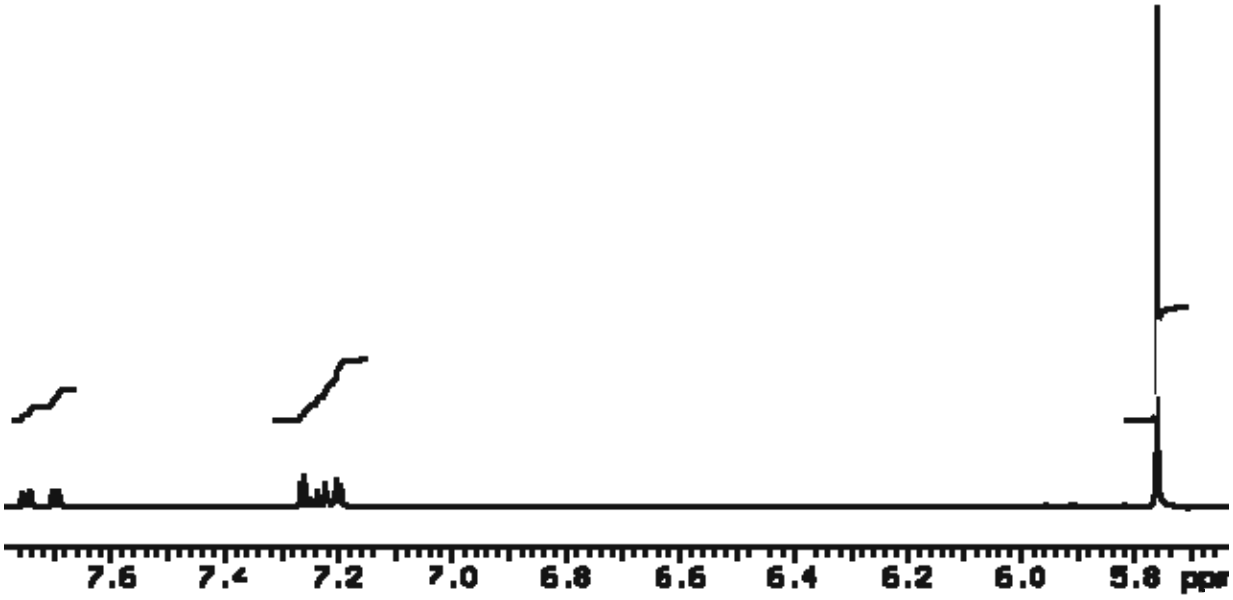

Figure 1. Sample ^{1}H NMR spectra (aromatic region used for analysis).

A.2. Conventional stirring control data

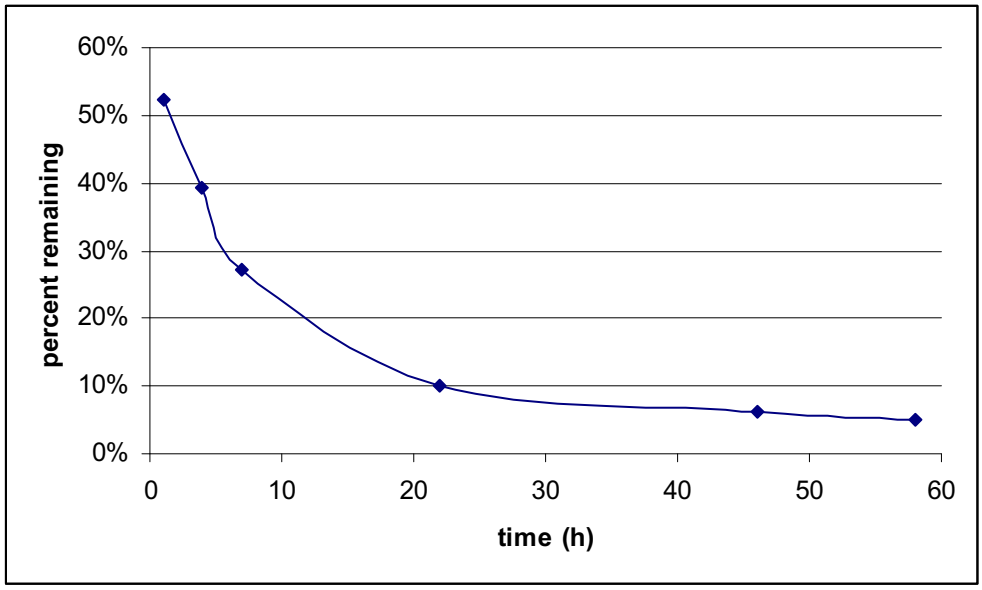

Figure S2. Conventional stirring control data illustrating percent remaining thiophene versus time.

A.3. Selected trials, conditions, and degree of desulfurization

Run #	Combined Flow Rate (mL/min)	Fuel: Oxidant	Temperature (°C)	Rotation Speed (RPM)	Gap Size	Max. Shear	Residence Time (sec)	Percent Formic Acid	Percent H2O2	Percent Removed	Pass
1	0.5	10	10	6230	250	83000	80	5	30	44	1
2	2	10	10	6210	1500	14000	120	2.5	30	0	1
3	0.5	1	70	6364	250	84000	80	2.5	30	17	1
4	0.5	1	70	1470	250	20000	80	5	30	55	1
5	0.2	1	50	740	250	9800	200	5	30	43	1
6	0.5	1	10	6300	250	84000	80	5	30	53	1
7	2	1	70	6300	250	84000	20	5	30	40	1
8	0.5	1	80	740	1500	1600	480	5	30	47	1
9	1	1	30	6300	1000	21000	160	5	30	19	1
10	0.5	1	30	6300	1000	21000	320	5	30	20	1
11	0.3	1	30	6300	1000	21000	530	5	30	20	1
12	4	1	30	6300	250	84000	10	2	15	8	1
13	4	1	30	6300	250	84000	10	2	15	17	2
14	4	1	30	6300	250	84000	10	2	15	23	3
15	4	1	30	6300	1500	14000	60	5	30	16	1
16	4	1	30	6300	1500	14000	60	5	30	23	2
17	4	1	30	6300	1500	14000	60	5	30	33	3
18	0.5	1	50	6300	800	26000	260	1	30	29	1
19	0.5	1	50	6300	800	26000	260	1	15	25	1
20	0.5	1	50	6300	800	26000	260	1	7.5	28	1
21	0.5	1	50	6300	1000	21000	320	1	30	33	1
22	0.5	1	50	6300	1000	21000	320	1	15	28	1
23	0.5	1	50	6300	1000	21000	320	1	7.5	26	1

APPENDIX B

SUPPORTING INFORMATION FOR CHAPTER III

B.1. Experimental details

Full experimental details for each reported trial are given in Table 1.

Table 1. Expanded details for each reported trial

Run #	CFR (mL/min)	Fuel: oxidant	Temp. (°C)	(RPM)	Gap size (um)	Max. shear (sec-1)	Residence time (sec)	Percent formic acid	Percent H2O2	% Removed	Pass	Thiophene[1]
1	0.5	10	10	6230	250	83000	80	5	30	44	1	BT
2	2	10	10	6210	1500	14000	120	2.5	30	0	1	BT
3	0.5	1	70	6364	250	84000	80	2.5	30	17	1	BT
4	0.5	1	70	1470	250	20000	80	5	30	55	1	BT
5	0.2	1	50	740	250	9800	200	5	30	43	1	BT
6	1.0	1	30	6300[2]	250	83000	40	5	30	28	1	BT
7	1.0	1	70	6300[b]	250	83000	40	5	30	38	1	BT
8	0.5	1	10	6300[b]	250	84000	80	5	30	53	1	BT
9	0.5	1	70	6300[b]	250	84000	80	5	30	37	1	BT
10	2	1	70	6300[b]	250	84000	20	5	30	40	1	BT
11	0.5	1	80	740	1500	16000	480	5	30	47	1	BT
12	1	1	30	6300[b]	1000	21000	160	5	30	19	1	BT
13	0.5	1	30	6300[b]	1000	21000	320	5	30	20	1	BT
14	0.3	1	30	6300[b]	1000	21000	530	5	30	20	1	BT
15	4	1	30	6300[b]	250	84000	10	2	15	8	1	BT
16	4	1	30	6300[b]	250	84000	10	2	15	17	2	BT
17	4	1	30	6300[b]	250	84000	10	2	15	23	3	BT
18	4	1	30	6300[b]	1500	14000	60	5	30	16	1	BT
19	4	1	30	6300[b]	1500	14000	60	5	30	23	2	BT
20	4	1	30	6300[b]	1500	14000	60	5	30	33	3	BT
21	0.5	1	50	6300[b]	800	26000	260	1	30	29	1	BT

[1] Benzothiophene (BT), dibenzothiophene (DBT), 5-methylbenzothiophne (5-MeBT), 2-methylbenzothiophene (2-MeBT), or 4,6-dimethyldibenzothiophene.
[2]Indicates that an average rotation speed based on a typical run at the reported setting is given, rather than an empirical value for the specific trial.

22	0.5	1	50	6300[b]	800	26000	260	1	15	25	1	BT
23	0.5	1	50	6300[b]	800	26000	260	1	7.5	28	1	BT
24	0.5	1	50	6300[b]	1000	21000	320	1	30	33	1	BT
25	0.5	1	50	6300[b]	1000	21000	320	1	15	28	1	BT
26	0.5	1	50	6300[b]	1000	21000	320	1	7.5	26	1	BT
27	1.25	5.5	40	3881	875	15000	110	1.25	30	21	1	BT
28	0.5	1	10	6230	1500	14000	480	0.5	30	21	1	BT
29	1.25	5.5	40	3918	875	15000	110	1.25	30	8	1	BT
30	2	1	70	1586	1500	3500	120	2	30	51	1	BT
31	2	10	70	6378	1500	14000	150	2	30	10	1	BT
32	2	10	70	1562	250	19000	20	2	30	9	1	BT
33	1.25	5.5	40	3868	875	15000	110	1.25	30	14	1	BT
34	0.5	10	10	1460	1500	3400	480	0.5	30	8	1	BT
35	2	1	10	1415	1500	3400	120	2	30	32	1	BT
36	0.5	1	70	6373	1500	14000	480	0.5	30	22	1	BT
37	0.5	10	70	1505	1500	3400	480	0.5	30	63	1	BT
38	0.5	10	70	6406	250	83000	80	0.5	30	18	1	BT
39	2	1	70	6417	250	83000	20	2	30	28	1	BT
40	2	1	10	6247	250	83000	20	2	30	13	1	BT
41	2	10	10	1493	250	19000	20	2	30	22	1	BT
42	0.5	1	10	1387	250	18000	80	0.5	30	13	1	BT
43	2	1	10	6300[b]	1500	14000	120	2	30	4	1	BT
44	2	10	10	6330	250	83000	20	2	30	2	1	BT
45	2	10	70	6387	250	83000	20	2	30	5	1	BT
46	0.5	1	70	6365	250	83000	80	0.5	30	27	1	BT
47	2	1	70	6364	1500	14000	120	2	30	13	1	BT
48	0.5	10	70	6300[b]	1500	14000	480	0.5	30	4	1	BT
49	0.5	1	10	6300[b]	250	83000	80	0.5	30	13	1	BT

50	0.5	10	10	6300[b]	1500	14000	480	0.5	30	5	1	BT
51	1.25	5.5	40	3890	875	15000	110	1.25	30	11	1	BT
52	1.25	5.5	40	3922	875	15000	110	1.25	30	8	1	BT
53	300	1	70	6300[b]	250	83000	0.1	5	30	85	1	BT
54	300	1	10	6300[b]	250	83000	0.1	5	30	98	1	BT
55	300	1	10	1600	1500	4000	0.8	5	30	97	1	BT
56	300	1	10	1600	250	21000	0.1	5	30	84	1	BT
57	100	1	10	6300[b]	250	83000	0.4	5	30	93	1	BT
58	100	1	70	1600	1500	4000	2.4	5	30	87	1	BT
59	100	1	70	6398	1500	83000	2.4	5	30	89	1	BT
60	200	1	40	3965	875	15000	0.7	5	30	86	1	BT
61	100	1	10	1586	250	21000	0.4	5	30	88	1	BT
62	300	1	70	6300[b]	1500	14000	0.8	5	30	82	1	BT
63	100	1	10	1537	1500	4000	2.4	5	30	89	1	BT
64	100	1	70	6344	250	83000	0.4	5	30	84	1	BT
65	100	1	10	6260	1500	14000	2.4	5	30	85	1	BT
66	200	1	40	3919	875	15000	0.7	5	30	85	1	BT
67	300	1	10	6300	1500	14000	0.8	5	30	84	1	BT
68	300	1	70	1600	250	21000	0.1	5	30	81	1	BT
69	300	1	70	1600	1500	4000	0.8	5	30	71	1	BT
70	200	1	40	4031	875	15000	0.7	5	30	76	1	BT
71	100	1	70	1600	250	21000	0.4	5	30	75	1	BT
72	200	1	40	3930	875	15000	0.7	5	30	81	1	BT
73	0.5	10	10	6300	250	84000	80	5	30	7	1	DBT
74	2	1	70	1500	1500	3500	120	5	30	17	1	DBT
75	0.5	1	70	1500	250	19000	80	5	30	27	1	DBT
76	0.5	10	10	6300	250	84000	80	5	30	0	1	5-MeBT
77	2	1	70	1500	1500	3500	120	5	30	0	1	5-MeBT

78	0.5	1	70	1500	250	19000	80	5	30	13	1	5-MeBT
79	0.5	10	10	6300	250	84000	80	5	30	0	1	5-MeBT
80	2	1	70	1500	1500	3500	120	5	30	0	1	5-MeBT
81	0.5	1	70	1500	250	19000	80	5	30	21	1	5-MeBT
82	0.5	10	10	6300	250	84000	80	5	30	0	1	2-MeBT
83	2	1	70	1500	1500	3500	120	5	30	0	1	2-MeBT
84	0.5	1	70	1500	250	19000	80	5	30	13	1	2-MeBT
85	0.5	10	10	6300	250	84000	80	5	30	0	1	4,6-DMDBT
86	2	1	70	1500	1500	3500	120	5	30	0	1	4,6-DMDBT
87	0.5	1	70	1500	250	19000	80	5	30	45	1	4,6-DMDBT

B.2. Full details of DOE experiments

Table 2. H_2O_2 DOE experiments. 6 variables were analyzed over 2 levels.

Run	Block	Temp. (˚C)	Gap size (µm)	Voltage	Ratio	Composition	CFR (mL/min)	Remaining Sulfur (%)
1	1	40	875	10	5.5	3.75	1.25	79
2	1	10	1500	16	1.0	2.50	0.50	79
3	1	40	875	10	5.5	3.75	1.25	92
4	1	70	1500	4	1.0	2.50	2.00	49
5	1	70	1500	16	10.0	5.00	2.00	90
6	1	70	250	4	10.0	5.00	2.00	91
7	1	40	875	10	5.5	3.75	1.25	86
8	1	10	1500	4	10.0	5.00	0.50	92
9	1	10	1500	4	1.0	5.00	2.00	68
10	1	70	1500	16	1.0	5.00	0.50	78
11	1	10	250	16	10.0	5.00	0.50	56
12	1	70	1500	4	10.0	2.50	0.50	64
13	1	70	250	16	10.0	2.50	0.50	82
14	1	10	1500	16	10.0	2.50	2.00	104
15	1	70	250	16	1.0	2.50	2.00	72
16	1	10	250	16	1.0	5.00	2.00	87
17	1	10	250	4	10.0	2.50	2.00	78
18	1	70	250	4	1.0	5.00	0.50	45
19	1	10	250	4	1.0	2.50	0.50	87
20	2	10	1500	16	1.0	5.00	2.00	56
21	2	10	250	16	10.0	2.50	2.00	98
22	2	70	250	16	10.0	5.00	2.00	95
23	2	70	250	16	1.0	5.00	0.50	73
24	2	70	1500	16	1.0	2.50	2.00	87
25	2	70	1500	16	10.0	2.50	0.50	96
26	2	101	250	16	1.0	2.50	0.50	87
27	2	10	1500	16	10.0	5.00	0.50	95
28	2	40	875	10	5.5	3.75	1.25	89
29	2	40	875	10	5.5	3.75	1.25	92

DOE Output

6 Factors: A, B, C, D, E, F

Design Matrix Evaluation for Factorial Reduced 3FI Model

Factorial Effects Aliases

[Est. Terms] Aliased Terms

[Intercept] = Intercept - 0.727 * ABE - 0.727 * BDF + 0.785 * ADEF + 0.0574 * BCDF

[Block] = Block + 0.727 * ABE + 0.727 * BDF + 0.0574 * ADEF + 0.785 * BCDF

[A] = A + BCE + DEF + ABCDF

[B] = B + ACE + CDF + ABDEF

[C] = C + 0.818 * ABE + 0.818 * BDF + 0.0909 * ADEF - 0.0909 * BCDF + ACDEF

[D] = D + AEF + BCF + ABCDE

[E] = E + ABC + ADF + BCDEF

[F] = F + ADE + BCD + ABCEF

[AB] = AB + ABC + BDEF + BCDEF

[AC] = AC - BCE + CDEF - ABCDF

[AD] = AD + EF + ABCF + BCDE

[AE] = AE + DF + ACE + CDF

[AF] = AF + DE + ABCD + BCEF

[BC] = BC - ACE - CDF + ABCDEF

[BD] = BD + BCD + ABEF + ABCEF

[BE] = BE + BCE + ABDF + ABCDF

[BF] = BF + BCF + ABDE + ABCDE

[CD] = CD - BCF + ACEF - ABCDE

[CE] = CE - ABC + ACDF - BCDEF

[CF] = CF - BCD + ACDE - ABCEF

[ABD] = ABD + BEF + ABCD + BCEF

[ABF] = ABF + BDE + ABCF + BCDE

[ACD] = ACD + CEF - ABCF - BCDE

[ACF] = ACF + CDE - ABCD - BCEF

Design Matrix Evaluation Performed Omitting Aliased Terms

Aliases are calculated based on your response selection,
taking into account missing datapoints, if necessary.
Watch for aliases among terms you need to estimate.

Response 1 Remaining Sulfur
ANOVA for selected factorial model (Aliased)

Ignored terms are ABC ABD ABE ABF ACD ACE ACF
SS: 2273.54 df: 9

Analysis of variance table [Partial sum of squares - Type III]

Source	**Sum of Squares**	**df**	**Mean Square**	**F Value**	**p-value Prob > F**
Block	914.74	1	914.74		
Model	2305.97	14	164.71	5.64	0.0900
A-Temp.	*397.34*	*1*	*397.34*	*13.60*	*0.0346*
B-Gap Size	*42.98*	*1*	*42.98*	*1.47*	*0.3119*
C-Voltage	*145.82*	*1*	*145.82*	*4.99*	*0.1116*
D-Ratio	*507.33*	*1*	*507.33*	*17.37*	*0.0251*
E-Composition	*6.40*	*1*	*6.40*	*0.22*	*0.6716*
F-CFR	*193.67*	*1*	*193.67*	*6.63*	*0.0821*
AB	*4.66*	*1*	*4.66*	*0.16*	*0.7162*
AC	*228.91*	*1*	*228.91*	*7.84*	*0.0679*
AD	*345.65*	*1*	*345.65*	*11.83*	*0.0412*
AE	*117.21*	*1*	*117.21*	*4.01*	*0.1389*
AF	*6.34*	*1*	*6.34*	*0.22*	*0.6730*
BC	*92.55*	*1*	*92.55*	*3.17*	*0.1731*
BD	*119.22*	*1*	*119.22*	*4.08*	*0.1366*
BE	*8.68*	*1*	*8.68*	*0.30*	*0.6235*
BF	*90.09*	*1*	*90.09*	*3.08*	*0.1773*
CD	*33.24*	*1*	*33.24*	*1.14*	*0.3643*
CE	*75.34*	*1*	*75.34*	*2.58*	*0.2066*
CF	*20.72*	*1*	*20.72*	*0.71*	*0.4615*
204.89	*204.89*	*1*	*7.01*	*0.0771*	

Curvature	204.89 1	204.89	7.01	0.0771
Pure Error	87.63 3	29.21		
Cor Total	3513.2319			

The Model F-value of 5.64 implies there is a 9.00% chance that a "Model F-Value" this large could occur due to noise.

Values of "Prob > F" less than 0.0500 indicate model terms are significant.
In this case A, D, AD are significant model terms.
Values greater than 0.1000 indicate the model terms are not significant.
If there are many insignificant model terms (not counting those required to support hierarchy),
model reduction may improve your model.

The "Curvature F-value" of 7.01 implies there is curvature (as measured by difference between
the average of the center points and the average of the factorial points) in the design space.
There is only a 7.71% chance that a "Curvature F-value" this large could occur due to noise.

Std. Dev.	5.40	R-Squared	0.9634
Mean	81.93	Adj R-Squared	0.7925
C.V. %	6.60	Pred R-Squared	N/A
PRESS	N/A	Adeq Precision	11.544

Case(s) with leverage of 1.0000: Pred R-Squared and PRESS statistic not defined

"Adeq Precision" measures the signal to noise ratio. A ratio greater than 4 is desirable. Your
ratio of 11.544 indicates an adequate signal. This model can be used to navigate the design space.

Factor	Coefficient Estimate	df	Standard Error	95% CI Low	95% CI High	VIF
Intercept	79.01	1	2.81	70.06	87.96	
Block 1	-2.58	1				
Block 2	2.58					
A-Temp.	-4.98	1	1.35	-9.28	-0.68	1.50
B-Gap Size	1.64	1	1.35	-2.66	5.94	1.50
C-Voltage	6.28	1	2.81	-2.67	15.24	5.90
D-Ratio	5.63	1	1.35	1.33	9.93	1.50
E-Composition	-0.63	1	1.35	-4.93	3.67	1.50
F-CFR	3.48	1	1.35	-0.82	7.78	1.50
AB-0.54	1	1.35	-4.84	3.76	1.50	
AC3.78	1	1.35	-0.52	8.08	1.50	
AD4.65	1	1.35	0.35	8.95	1.50	

AE2.71	1	1.35	-1.59	7.01	1.50
AF0.63	1	1.35	-3.67	4.93	1.50
BC2.41	1	1.35	-1.89	6.71	1.50
BD2.73	1	1.35	-1.57	7.03	1.50
BE0.74	1	1.35	-3.56	5.04	1.50
BF-2.37	1	1.35	-6.67	1.93	1.50
CD-1.44	1	1.35	-5.74	2.86	1.50
CE-2.17	1	1.35	-6.47	2.13	1.50
CF-3.21	1	1.35	-7.51	1.09	1.50

ALIASED E, AB, CE

Final Equation in Terms of Coded Factors:

Remaining Sulfur	=
+79.01	
-4.98	* A
+1.64	* B
+6.28	* C
+5.63	* D
-0.63	* E
+3.48	* F
-0.54	* A * B
+3.78	* A * C
+4.65	* A * D
+2.71	* A * E
+0.63	* A * F
+2.41	* B * C
+2.73	* B * D
+0.74	* B * E
-2.37	* B * F
-1.44	* C * D
-2.17	* C * E
-3.21	* C * F

B.3. Sample ^{1}H NMR spectra for thiophenes

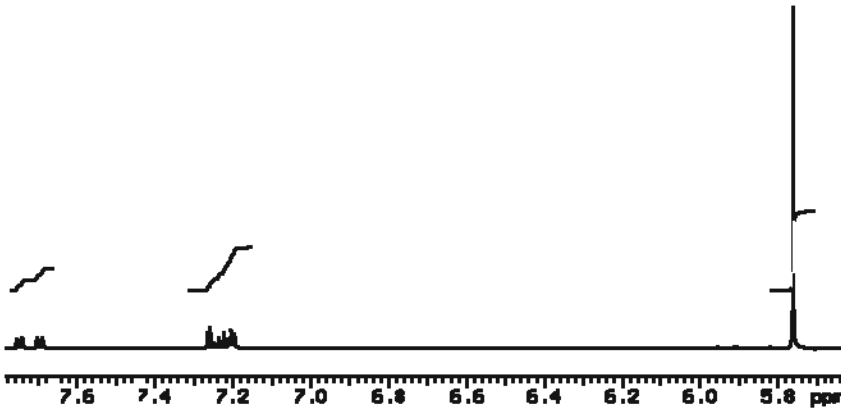

Figure 2. Sample ^{1}H NMR spectrum (aromatic region used for analysis) for benzothiophene. Samples were analyzed relative to 1,1,2,2-tetrachloroethane signal (furthest upfield) as an internal standard.

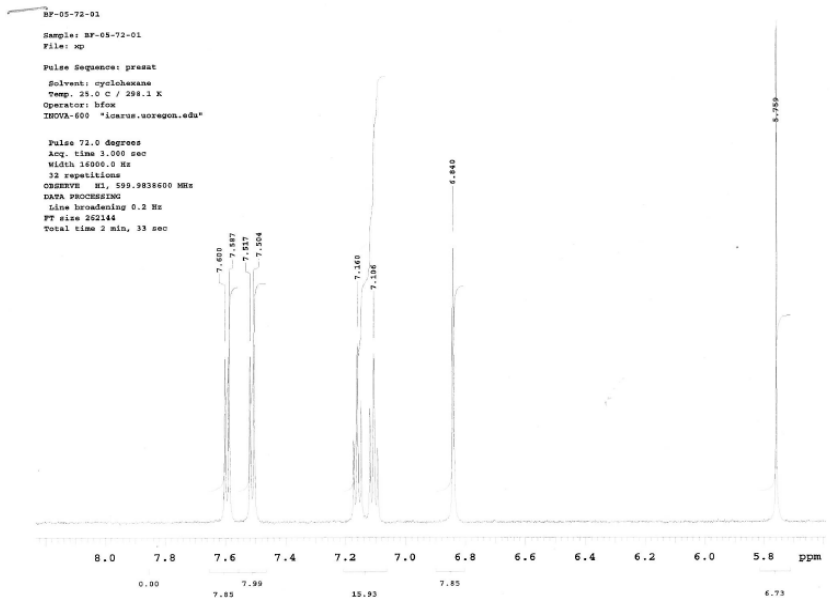

Figure 3. Sample ^{1}H NMR spectrum (aromatic region used for analysis) for 2-methylbenzothiophene. Samples were analyzed relative to 1,1,2,2-tetrachloroethane signal (furthest upfield) as an internal standard.

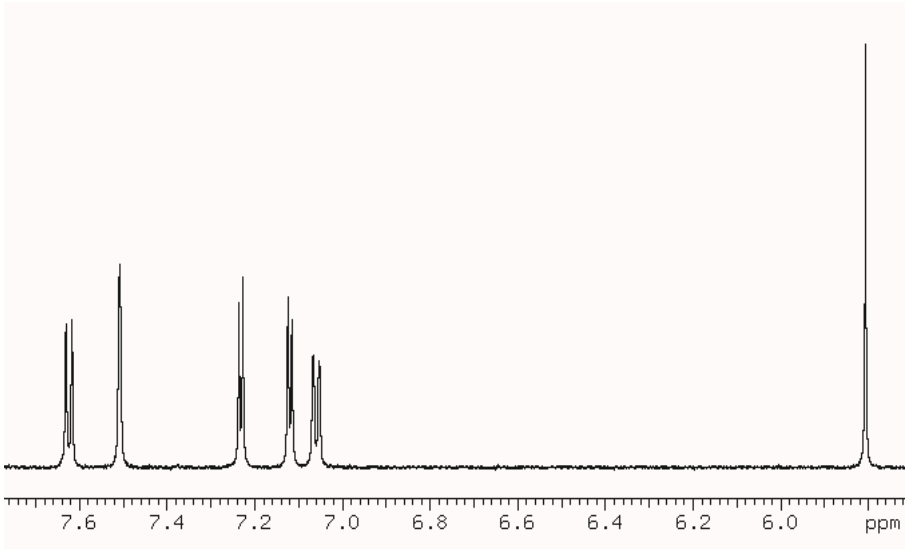

Figure 4. Sample ^{1}H NMR spectrum (aromatic region used for analysis) for 5-methylbenzothiophene. Samples were analyzed relative to 1,1,2,2-tetrachloroethane signal (furthest upfield) as an internal standard.

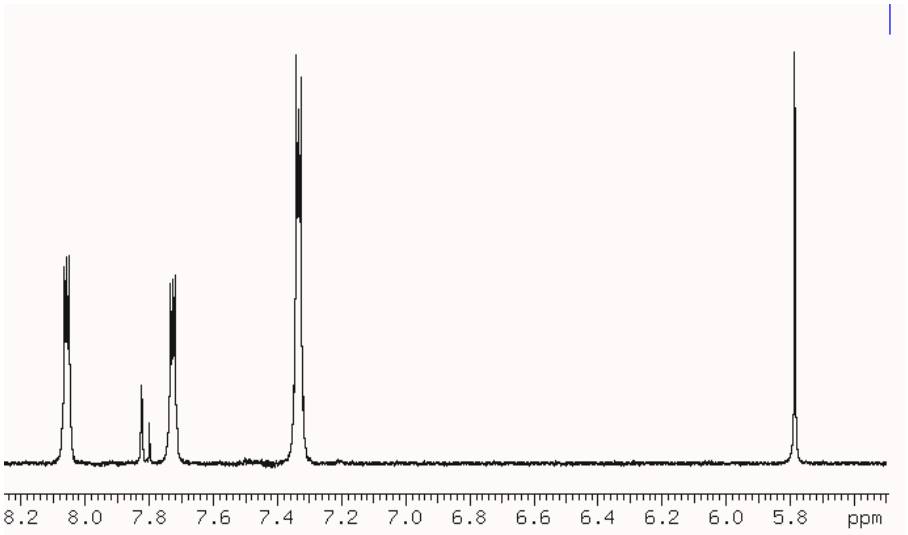

Figure 5. Sample ^{1}H NMR spectrum (aromatic region used for analysis) for dibenzothiophene. Samples were analyzed relative to 1,1,2,2-tetrachloroethane signal (furthest upfield) as an internal standard.

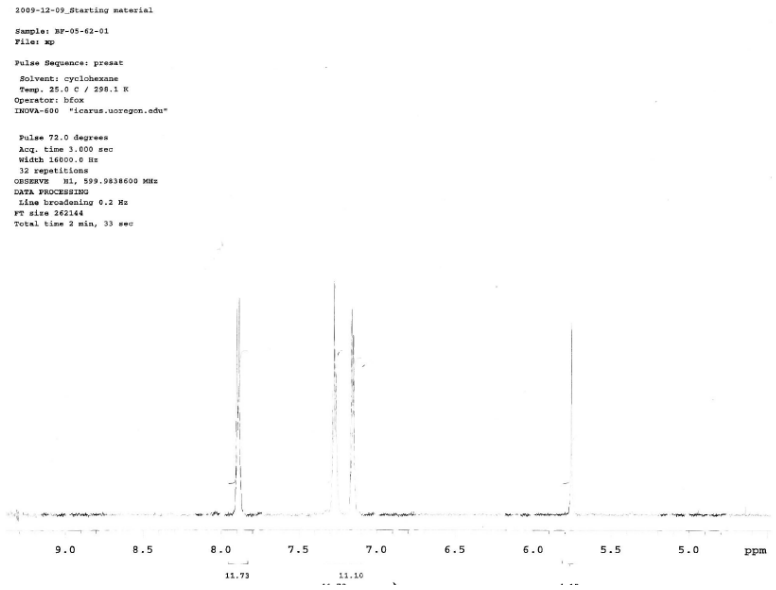

Figure 6. Sample ^{1}H NMR spectrum (aromatic region used for analysis) for 4,6-dimethyldibenzothiophene. Samples were analyzed relative to 1,1,2,2-tetrachloroethane signal (furthest upfield) as an internal standard.

B.4. Ultra high CFR DOE trials

Table 3. H_2O_2 (ultra-high flow rate) DOE experiments.

Combined Flow Rate (mL/min)	Rotation Speed (RPM)	Gap (µm)	Temp. (˚C)	Percent Sulfur Removed
300	6300	250	70	15
300	6300	250	10	2
300	1600	1500	10	3
300	1600	250	10	16
100	6300	250	10	7
100	1600	1500	70	13
100	6398	1500	70	11
200	3965	875	40	14
100	1586	250	10	12
300	6300	1500	70	18
100	1537	1500	10	11
100	6344	250	70	16
100	6260	1500	10	15
200	3919	875	40	15
300	6300	1500	10	16
300	1600	250	70	19
300	1600	1500	70	29
200	4031	875	40	24
100	1600	250	70	25
200	3930	875	40	19

High CFR DOE output:

Analysis of variance table [Partial sum of squares - Type III]

Source	Sum of Squares	df	Mean Square	F Value	p-value Prob > F
Model	509.00	10	50.90	1.40	0.3218
A-CFR	*4.00*	*1*	*4.00*	*0.11*	*0.7483*
B-V	*49.00*	*1*	*49.00*	*1.35*	*0.2785*
C-gap	*1.00*	*1*	*1.00*	*0.028*	*0.8722*
D-temp	*256.00*	*1*	*256.00*	*7.06*	*0.0289*
AB1.00	*1*	*1.00*	*0.028*	*0.8722*	
AC36.00	*1*	*36.00*	*0.99*	*0.3482*	
AD36.00	*1*	*36.00*	*0.99*	*0.3482*	
BC81.00	*1*	*81.00*	*2.23*	*0.1733*	

BD36.00	*1*	*36.00*	*0.99*	*0.3482*	
CD	*9.00*	*1*	*9.00*	*0.25*	*0.6317*
Curvature	45.00	1	45.00	1.24	0.2976
Residual	290.00	8	36.25		
Lack of Fit	*228.00*	*5*	*45.60*	*2.21*	*0.2736*
Pure Error	*62.00*	*3*	*20.67*		
Cor Total	844.00	19			

The "Model F-value" of 1.40 implies the model is not significant relative to the noise. There is a 32.18 % chance that a "Model F-value" this large could occur due to noise.

B.5. Conventional stirring control experiments

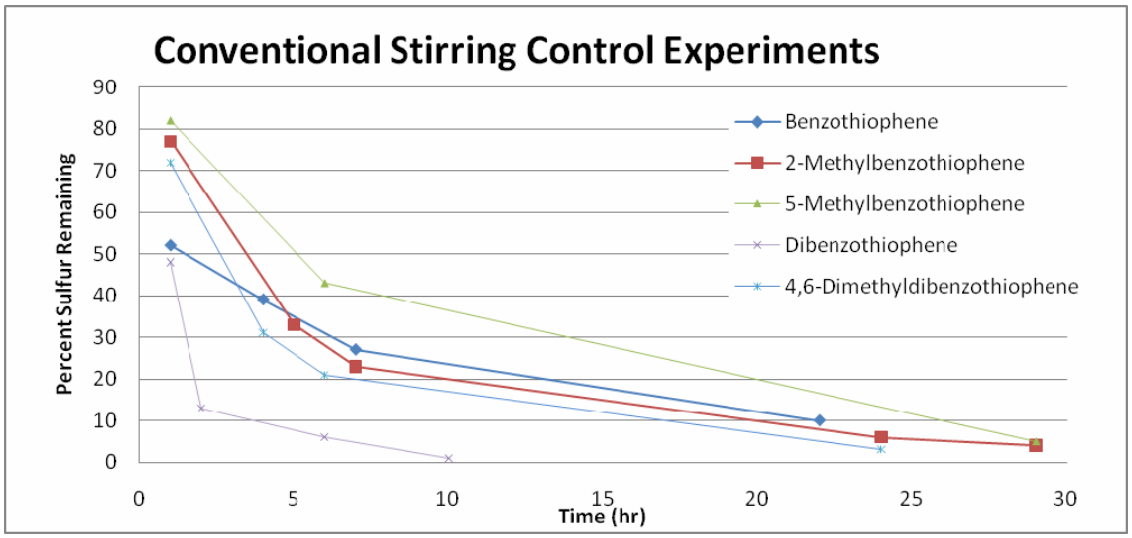

Figure 7. H_2O_2 conventional stirring controls. Desulfurization occurred on the time scale of hours.

B.6. Sample ^{1}H NMR spectra for thiophenes in γ-butyrolactone

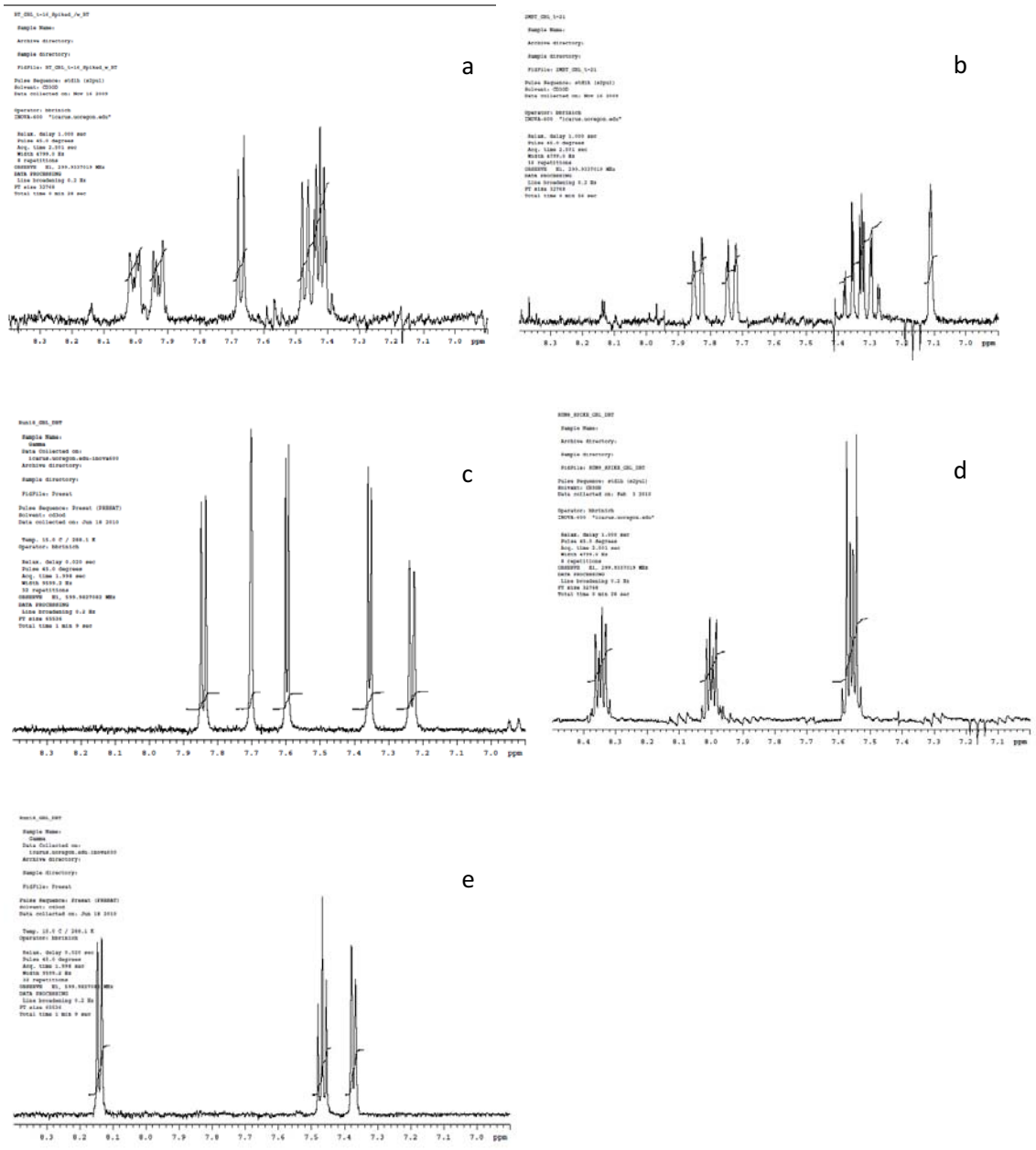

Figure 8. ^{1}H NMR spectra (aromatic) for thiophenes in γ-butyrolactone. a) benzothiophene b) 2-methylbenzothiophene c) 5-methylbenzothiophene d) dibenzothiophene e) 4,6-dimethyldibenzothiophene.

APPENDIX C

INVESTIGATION OF THE REACTIVITY OF PT PHOSPHINITO AND MOLYBDOCENE NITRILE HYDRATION CATALYSTS WITH CYANOHYDRINS

C.1. Introduction

The catalytic hydration of cyanohydrins (eq 1) is an important transformation in many chemical and pharmaceutical processes because it provides an atom economical route to high-value -hydroxyamides, -hydroxycarboxylic acids, and -hydroxycarboxylic esters.[1,2]

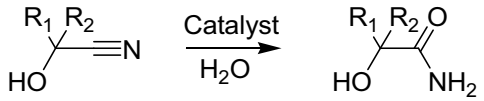

(1)

Classical methods of using concentrated acid to promote the hydration of cyanohydrins present several disadvantages. For example, when sulfuric acid is used, the amide sulfate salt is generated as opposed to the -hydroxyamide. Although the amide sulfate salt can be hydrolyzed or esterified to afford value-added carboxylic acids and esters in high yield (> 92 %), the reaction also produces undesired sulfonates, oligomers, polymers, and ammonium bisulfate.[1] The production of by-product ammonium bisulfate is a major economic and environmental drawback of a large-scale sulfuric acid mediated process because its disposal is typically not permitted and its recycle to virgin sulfuric acid requires additional high-energy processing steps. Anhydrous HCl can also be used to hydrate cyanohydrins, but stoichiometric quantities of undesirable alkyl chloride byproduct are generated. For these reasons, our goal is to develop an acid-free process for the hydration of cyanohydrins using a low-cost homogeneous, transition metal catalyst that will allow direct access to the -hydroxyamide product.[a] In principle, the electronic and structural environment of such a catalytic system could be tailored to afford a general synthetic route by which a range of chiral and achiral -hydroxyamides, -hydroxycarboxylic acids, and -hydroxycarbocylic esters could be accessed.

A host of organometallic and coordination complexes of early and late transition metals have been shown to catalyze the conversion of nitriles to amides.[3] In general, these activate the nitrile by removing electron density from the nitrile carbon, making it more susceptible to intramolecular or intermolecular nucleophilic attack by water or hydroxide (Figure 1). In doing so, the metal center lowers the activation barrier to hydration of the nitrile relative to hydrolysis of the amide, and in many cases further hydrolysis of the amide functionality is not observed. However, none of these catalytic

systems have been applied to cyanohydrins. Of the transition metal complexes reported in the literature, the Pt phosphinito complexes, $[PtX(PR_2OH)\{(PR_2O)_2H\}]$ where X = Cl or H, first developed by Parkins and coworkers,[4-6] are the most reactive and versatile in hydrolytic nitrile conversions. For example, acrylonitrile is hydrated regioselectively to acrylamide in refluxing aqueous ethanol at a turnover frequency of 0.5 s^{-1} using only 0.015 mol % of $[PtCl(PMe_2OH)\{(PMe_2O)_2H\}]$.[5] In related work, Cobley et al. demonstrated that the Pt complexes are also effective in the hydrolytic amidation of nitriles to N-substituted amides using alkylamines.[7] Further work by Jiang et al. demonstrated that the Pt phosphinito complexes are also efficient in the hydration of bulky nitriles and in nitriles containing acid- or base-sensitive functionalities (i.e., ether and carbohydrate functionalities),[8] which typically show very low reactivity and selectivity with other nitrile hydration catalysts.

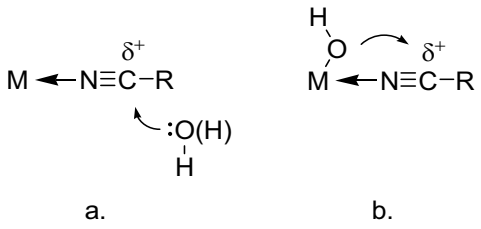

Figure 1. Intermolecular (a) and intramolecular (b) pathways for the metal-catalyzed hydration of nitriles.

The broad applicability and high activity of the Pt phosphinito complexes toward nitrile substrates makes them excellent candidates for catalytic conversions of

cyanohydrins. In this report, the reactivity of the [PtCl(PMe_2OH){$(PMe_2O)_2H$}] (**1**) complex toward variously substituted cyanohydrins is described. In addition, the catalytic reactivity of $Cp_2Mo(OH)(OH)_2^+$ (**2**) with cyanohydrins is reported. In prior work, our laboratory demonstrated the utility of molybdocene complexes, such as (**2**),[9-11] in the hydration of nitrile substrates. Like the Pt phosphinito complexes, the molybdocenes are slightly water-soluble, effective toward the regioselective hydration of acrylonitrile (TOF = 3.8 x 10^{-4} s^{-1} using 1.4 % (η^5-$C_5H_4Me)_2Mo(OH)(OH_2)^+$ in D_2O at 75 ^oC),[9] and reactive with bulky nitriles. Furthermore, although molybdocenes are much less reactive than the Pt phosphinito complexes, they show improved reactivity with nitriles containing electron-withdrawing substituents, which bodes well for cyanohydrin substrates.

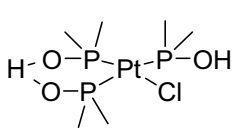

1

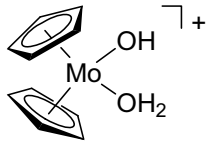

2

C.2. Experimental

C.2.1. General considerations

Experiments were performed using standard air-free techniques in an atmosphere of N_2 unless otherwise stated. The complexes [PtCl(PMe_2OH){$(PMe_2O)_2H$}] (**1**),[5] $[Cp_2Mo(\mu\text{-}OH)]_2[OTs]_2$ (**2**),[12] 2-methoxypriopionitrile,[13] and 2-methoxyisobutyronitrile[13] were synthesized according to procedures previously reported in the literature. Reagent

grade nitriles (> 97 % purity) were purchased from Sigma-Aldrich. Cyanohydrins were distilled before use, except cyclohexanone cyanohydrin (a solid) and glycolonitrile (purchased as a 55 % solution in water). Glycolamide was obtained from Sigma-Aldrich, and 2-hydroxyisobutyramide was obtained from TCI Japan Organic Chemicals. All hydrolysis and hydration reaction samples were prepared in a glovebox under an atmosphere of N_2 in Wilmad 9 in. precision NMR tubes or Wilmad J-Young screw cap NMR tubes, except where noted. Reactions carried out in the Wilmad 9 in. NMR tubes were flame sealed while frozen. Reaction tubes were heated in an oil bath. ^{1}H NMR spectra were obtained using a Varian Inova 500 MHz (500.104 MHz for ^{1}H and 125.764 MHz for ^{13}C) or 600 MHz NMR spectrometer (599.982 MHz for ^{1}H and 150.879 MHz for ^{13}C). Cyanohydrin hydration reactions were performed using a plethora of reaction conditions. Representative procedures that yielded the best results are given below.

C.2.2. Preparation of stock solutions of 1.

Stock solutions of **1** were prepared by adding **1** and thallium triflate to 10 mL of D_2O and heating to 80 ^{o}C. After 8 hours, the solutions were allowed to cool to room temperature and filtered using 0.22 μm filters to remove grey or white precipitate. The concentration of [PtX(PMe_2OH){$(PMe_2O)_2H$}] and degraded Pt was determined using an using a known amount of tetrabutylphosphonium bromide as an internal standard. (The identity of X in [PtX(PMe_2OH){$(PMe_2O)_2H$}] is discussed in the last section of the Results and Discussion section.)

C.2.3. General procedures for the hydration of cyanohydrins catalyzed by 1

Note that the procedures using catalyst **2** were identical to the procedures described below; however, no Tl salt was added.

C.2.3.1. Glycolonitrile

Catalyst **1** (0.0054 g, 0.012 mmol) and TlOTf (0.0036 g, 0.010 mmol) were added to a solution of 55 % glyconitrile (3.55 mmol) in H_2O and allowed to react at 25 °C. After 3 days, the ^1H NMR spectrum showed a mixture of glycolonitrile at 4.50 ppm (s, 2H, (HO)C*H*$_2$CN) and glycolamide at 4.30 ppm (s, 2H, (HO)C*H*$_2$C(O)NH_2).

C.2.3.2. Lactonitrile

Lactonitrile (250 μL, 3.49 mmol), catalyst **1** (0.0102 g, 0.0220 mmol), and TlOTf (0.0110 g, 0.0311 mmol) were added to 250 μL of D_2O. The mixture was allowed to react at 25 °C for 13 days, over which time 69.0 % of lactonitrile was hydrated to 2-hydroxypropionamide. In the ^1H NMR spectrum, resonances (D_2O) for lactonitrile were observed at 4.66 ppm (q, J = 6.5 Hz, 1H, (HO)(CH_3)C*H*CN) and 1.48 ppm (d, J = 6.5 Hz, 3H, (HO)(C*H*$_3$)CHCN), and resonances for 2-hydroxypropionamide were observed at 4.22 ppm (m, 1H, (HO)(CH_3)C*H*C(O)ND_2) and 1.29 ppm (d, J = 7.0 Hz, 3H, (HO)(CH_3)C*H*C(O)ND_2). The generation of 2-hydroxypropionamide was also observed in the ^{13}C NMR spectrum at 183.5 ppm (s, (HO)(CH_3)CH*C*(O)ND_2), 70.3 ppm (s, (HO)(CH_3)*C*HC(O)ND_2), 22.4 ppm (s, (HO)(*C*H_3)CHC(O)ND_2). Less intense resonances for acetaldehyde were observed at 9.61 ppm.

C.2.3.3. 2-Hydroxybutyronitrile

A solution containing catalyst **1** (0.0165 g, 0.0356 mmol), TlOTf (0.0150 g, 0.0424 mmol), 2-hydroxybutyronitrile (250 μL, 2.83 mmol), 50 μL H_2O, and 200 μL methanol was prepared. Over 5 days at 25 °C, ^{1}H NMR resonances for 2-hydroxybutyronitrile at 4.57 ppm (t, J = 6.9 Hz, 1H, $CH_3(HO)(CH_2)C\mathit{H}CN$), 1.91 ppm (quintet, J = 7.0 Hz, 2H, $CH_3(HO)(CH_2)C\mathit{H}CN$), and 1.14 ppm (t, J = 7.2 Hz, 3H, $C\mathit{H}_3(HO)(CH_2)CHCN$) disappeared, and the appearance of 2-hydroxybutyramide at 7.52 ppm (s, 1H, $CH_3(HO)(CH_2)CHCON\mathit{H}_2$), 7.11 ppm (s, 1H, $CH_3(HO)(CH_2)CHCON\mathit{H}_2$), 4.12 ppm (m, 1H, $CH_3(HO)(CH_2)C\mathit{H}CONH_2$), 1.74 ppm (m, 2H, $CH_3(HO)(C\mathit{H}_2)CHCONH_2$), and 1.06 ppm (t, J = 7.0 Hz, 3H, $C\mathit{H}_3(HO)(CH_2)C\mathit{H}CONH_2$) was observed. 2-Hydroxybutyramide was also observable in the ^{13}C NMR spectrum at 182.1 ppm (s, $CH_3(HO)(CH_2)CH\mathit{C}ONH_2$), 75.4 ppm (2, $CH_3(HO)(CH_2)\mathit{C}HCONH_2$), 30.2 ppm (s, $CH_3(HO)(\mathit{C}H_2)CHCONH_2$), and 11.6 ppm (s, $\mathit{C}H_3(HO)(\mathit{C}H_2)CHCONH_2$).

C.2.3.4. Mandelonitrile

A solution containing catalyst **1** (0.0183 g, 0.0395 mmol), TlOTf (0.0170 g, 0.0481 mmol), mandelonitrile (250 μL, 2.10 mmol), 50 μL H_2O, and 200 μL methanol was prepared. Initially, ^{1}H NMR resonances for mandelonitrile appeared at 7.46 ppm (m, 2H, $C_5\mathit{H}_5(HO)CHCN$), 7.32 ppm (m, 3H, $C_5\mathit{H}_5(HO)CHCN$), and 5.59 ppm (s, 1H, $C_5H_5(HO)C\mathit{H}CN$). After 3 days at 25 °C, benzaldehyde signals were noted at 9.77 ppm (s, 1H, $C_5H_5(HO)CHC(O)\mathit{H}$) in the ^{1}H NMR spectrum and 197.1 ppm in the ^{13}C spectrum (s, $C_5H_5(HO)CH\mathit{C}(O)H$). A signal attributable to mandelamide was detected in the ^{13}C NMR spectrum at 180.2 ppm (s, $C_5H_5(HO)CH\mathit{C}(O)NH_2$).

C.2.3.5. Cyclohexanone cyanohydrin

Cyclohexanone cyanohydrin (0.0901 g, 0.720 mmol), catalyst **1** (0.0162 g, 0.0349 mmol), TlOTf (0.0150 g, 0.0424 mmol) were added to a mixture of 50 μL H_2O and 450 μL methanol. After 3 days at 25 °C, amide protons were apparent at 7.59 ppm and 7.01 ppm in the ^1H NMR spectrum. 2-hydroxy-2-cyclohexanoic acid amide was also observed in the ^{13}C NMR spectrum at 185.3 ppm ($C_6H_{10}CH\mathit{C}(O)ND_2$), 77.6 ppm ($C_6H_{10}\mathit{C}C(O)ND_2$), 36.6 ppm ($\mathit{C}_6H_{10}CC(O)ND_2$), 27.9 ppm ($\mathit{C}_6H_{10}C(O)ND_2$), and 23.7 ppm ($\mathit{C}_6H_{10}C(O)ND_2$).

C.2.3.6. Acetone cyanohydrin

A solution containing catalyst **1** (0.0232 g, 0.0500 mmol), TlOTf (0.0200 g, 0.0566 mmol), acetone cyanohydrin (500 μL, 5.48 mmol), and 500 μL D_2O was prepared. The mixture was allowed to react for 7 days at 25 °C. During this time, the acetone cyanohydrin was hydrated to 2-hydroxyisobutyramide (2.73 % yield) and dissociated to give 0.93 % of acetone. ^1H NMR resonances for the acetone cyanohydrin appeared at 1.51 ppm (s, 6H, $HO(C\mathit{H}_3)_2CCN$) and 2-hydroxyisobutyramide was observed at 1.44 ppm (s, 6H, $HO(C\mathit{H}_3)_2CCOND_2$). A less intense resonance was observed for acetone at 2.01 ppm (s, 6H, $(CH_3)_2CO$. The presence of 2-hydroxyisobutyramide was confirmed in the ^{13}C spectrum at 182.3 ppm (s, 6H, $HO(CH_3)_2C\mathit{C}OND_2$), 73.1 ppm (s, 6H, $HO(CH_3)_2\mathit{C}COND_2$), 28.6 ppm (s, 6H, $HO(\mathit{C}H_3)_2CCOND_2$). The amide deuterium atoms were observable in the ^2H spectrum at 7.46 ppm and 6.76 ppm.

C.2.4. Hydration of other nitriles catalyzed by 1

C.2.4.1. 3-Hydroxypropionitrile

3-Hydroxypropionitrile (16 μL, 0.24 mmol) was added to 0.60 mL of catalyst solution (0.24 μmol) and 0.10 mL of PBu_4Br (0.32 μmol). Over 10 hours at 43 °C, ^1H NMR resonances (D_2O) for the 3-hydroxypropionitrile at 3.78 ppm (t, J = 6.0 Hz, 2H, $HOC\mathit{H}_2CH_2CN$) and 2.67 ppm (t, J = 6.0 Hz, 2H, $HOCH_2C\mathit{H}_2CN$) disappeared, and the appearance of 3-hydroxypropionamide at 3.76 ppm (t, J = 6.0 Hz), 2H, $HOCH_2C\mathit{H}_2CONH_2$) and 2.45 ppm (t, J = 6.0 Hz), 2H, $HOC\mathit{H}_2CH_2CONH_2$) was observed.

C.2.4.2. 2-Methoxypropionitrile

Catalyst stock solution (0.60 mL, 0.24 μmol), PBu_4Br (0.10 mL, 0.32 μmol), and 2-methoxypropionitrile (22 μL, 0.24 mmol) were added to a nine-inch NMR tube. The ^1H NMR resonances (D_2O) before heating appeared at 4.39 ppm (q, J = 6.8 Hz, 1H, $(CH_3O)(CH_3)C\mathit{H}CN$), 3.44 ppm (s, 3H, $(C\mathit{H}_3O)(CH_3)CHCN$), and 1.49 (d, J = 6.8 Hz, 3H, $(CH_3O)(C\mathit{H}_3)CHCN$). Over 15 hours at 43 °C, the ^1H NMR resonances corresponding to 2-methoxypropionitrile decreased in intensity, and resonances for 2-methoxypropionamide increased at 3.82 ppm (q, J = 6.8 Hz, 1H, $(CH_3O)(CH_3)C\mathit{H}C(O)ND_2$), 3.33 ppm (s, 3H, $(C\mathit{H}_3O)(CH_3)CHC(O)ND_2$), and 1.29 (d, J = 6.8 Hz, 3H, $(CH_3O)(C\mathit{H}_3)CHC(O)ND_2$).

C.2.4.3. 2-Bromopropionitrile

2-Bromopropionitrile (21 μL, 0.24 mmol) was added to a mixture of catalyst stock solution (0.60 mL, 0.24 μmol) and PBu_4Br (0.10 mL, 0.32 μmol). 2-Bromopropionitrile was sparingly soluble in D_2O and formed a white layer at the bottom of the NMR tube. The sample was heated at 43 °C for 24 hours. During this time, all of the 2-bromoproionitrile dissolved and the ^1H NMR resonances (D_2O) for the 2-bromopropionitrile at 4.69 ppm (q, J = 7.2 Hz, 1H, (Br)(CH_3)C*H*CN) and 1.90 ppm (d, J = 7.1 Hz, 3H, (Br)(C*H*$_3$)CHCN) were replaced by resonances for 2-bromopropionamide at 4.49 ppm (q, J = 6.9 Hz, 1H, (Br)(CH_3)C*H*C(O)ND_2) and 1.71 ppm (d, J = 6.9 Hz, 3H, (Br)(C*H*$_3$)CHC(O)ND_2). Less intense resonances attributed to 2-hydroxypropionamide were also observed at 4.37 ppm and 1.33 pppm.

C.2.4.4. Acetonitrile

Acetonitrile (12.5 μL, 0.24 mmol) was added to a mixture of catalyst stock solution (0.60 mL, 0.24 μmol) and PBu_4Br (0.10 mL, 0.32 μmol). The resulting mixture was heated at 43 °C for 45 hours. During this time, acetonitrile was converted to acetamide. The production of acetamide was monitored in the ^1H NMR spectrum (D_2O) by disappearance of the acetonitrile protons at 2.01 (s, C*H*$_3$CN) and the appearance of acetamide at 1.93 ppm (s, C*H*$_3$C(O)ND_2).

C.2.4.5. Propionitrile

Catalyst stock solution (0.60 mL, 0.24 μmol), PBu_4Br (0.10 mL, 0.32 μmol), and propionitrile (17 μL, 0.24 mmol) were added to a nine-inch NMR tube. Over 3 days at 43 °C, ^1H NMR resonances (D_2O) for the propionitrile at 2.38 ppm (q, J = 7.6 Hz, 2H, CH_3C*H*$_2$CN) and 1.18 ppm (t, J = 7.6 Hz, 3H, C*H*$_3CH_2$CN) disappeared, and the

appearance of propionamide at 2.21 ppm (q, J = 7.6 Hz), 2H, $CH_3CH_2C(O)ND_2$) and 1.05 ppm (t, J = 7.7 Hz), 3H, $CH_3CH_2C(O)ND_2$) was observed.

C.2.4.6. Isobutyronitrile

Catalyst stock solution (0.60 mL, 0.24 μmol), PBu_4Br (0.10 mL, 0.32 μmol), and isobutyronitrile (22 uL, 0.24 mmol) were added to a nine-inch NMR tube. ^1H NMR resonances (D_2O) were observed at 2.81 ppm (heptet, J = 7.0 Hz, 1H, $(CH_3)_2CHCN$) and 1.26 ppm (d, J = 7.0 Hz, 6H, $(CH_3)_2CHCN$) before heating. Over three weeks at 43 °C, the ^1H NMR resonances corresponding to isobutyronitrile decreased in intensity, and resonances for 2- isobutyroamide appeared at 2.49 ppm (heptet, J = 7.0 Hz, 1H, $(CH_3)_2CHC(O)ND_2$) and 1.07 ppm (d, J = 7.0 Hz, 6H, $(CH_3)_2CHC(O)ND_2$).

C.2.4.7. Trimethylacetonitrile

Catalyst stock solution (0.60 mL, 0.24 μmol), PBu_4Br (0.10 mL, 0.32 μmol), and 2-methoxypropionitrile (26 μL, 0.24 mmol) were added to a nine-inch NMR tube. The resulting mixture was heated on an oil bath at 80 °C two days. During this time, trimethylacetonitrile was converted to trimethylacetamide. The production of trimethylacetamide was monitered by ^1H NMR (D_2O) by the disappearance of the trimethylacetonitrile protons at 1.31 (s, $(CH_3)_3CN$) and the appearance of trimethylacetamide at 1.35 ppm (s, $(CH_3)_3C(O)ND_2$).

C.2.4.8. 2-Methoxyisobutyronitrile

2-Methoxyisobutyronitrile (35 μL, 0.34 mmol), **1** (0.0010 g, 2.2 μmol), and excess $NaBPh_4$ in D_2O were added to a nine-inch NMR tube. The solution was heated to

60 °C for 14 hours, during which time the 2-methoxyisobutyronitrile was hydrated. The hydration was monitored by the disappearance of ^{1}H NMR resonances (D_2O) at 3.36 ppm (s, 3H, (C*H*$_3$O)(CH$_3$)$_2$CCN) and 1.51 ppm (s, 6H, (C*H*$_3$O)(CH$_3$)$_2$CCN) and by the appearance of resonances at 3.18 (s, 3H, (C*H*$_3$O)(CH$_3$)$_2$CC(O)ND$_2$) and 1.28 ppm (s, 6H, (CH$_3$O)(C*H*$_3$)$_2$CC(O)ND$_2$).

C.2.5. Control experiment for the H/D exchange reaction

7.00 μL of acetone cyanohydrin (77.0 μmol) was added to 0.800 mL of D_2O containing NBu$_4$BF$_4$ (6.96 μmol) and CD$_3$SO$_3$D (1.13 μmol) as internal standards (pH 3.5). The disappearance of ACH was monitored at 1.62 ppm (s, 6H, HO(C*H*$_3$)$_2$CCN), and the appearance of acetone and HCN were monitored at 2.23 ppm (s, 6H, (C*H*$_3$)$_2$CO) and 5.29 ppm (*H*CN) in the ^{1}H NMR spectrum. The appearance of deuterated ACH, acetone, and hydrocyanic acid were monitored in the ^{2}H NMR spectra at 1.62 ppm (DO(C*D*$_3$)$_2$CCN), 2.25 ppm ((C*D*$_3$)$_2$CO), and 5.28 ppm (*D*CN). After 25 days, 90.5 % of the ACH was fully deuterated, and a total of 43.3 % of the ACH was dissociated to acetone and HCN.

C.2.6. Tests for substrate inhibition

PBu$_4$Br (100 μL, 0.398 μmol), an aliquot of stock solution of **1** (400 μL, 0.195 μmol), and 3-hydroxyproponitrile (17.0 μL, 0.250 mmol) were added to each of three nine-inch NMR tubes. After 50 minutes of reaction, one reaction mixture was spiked with lactonitrile (18.0 μL, 0.250 mmol), and acetone cyanohydrin (23.0 μL, 0.250 mmol) was added to a second. The reaction solutions spiked with lactonitrile and ACH showed an abrupt halt in reactivity.

C.2.7. Tests for product inhibition

Acetonitrile (28.0 mL, 0.536 mmol), 2-hydroxyisobutryonitrile (0.0135 g, 0.184 μmol), and PBu_4Br (100 μL, 0.44 μmol) were added to 400 μL of **1** (0.24 μmol) in D_2O and heated to 35 °C in oil bath and monitored for three days. In a separate trial, acetonitrile (12.5 μL, 0.239 mmol), glycolamide (0.0244 g, 0.325 mmol), and PBu_4Br (100 μL, 0.32 μmol) were added to 600 μL of **1** (0.24 μmol) in D_2O and heated to 35 °C in oil bath and monitored for three days. In both cases, the acetonitrile hydration was monitored by ^1H NMR spectroscopy as noted above. The rate of acetamide production was identical to that observed for the control reactions performed using identical concentrations of reactants (and internal standard) and no added amide.

C.2.8. Titration with KCN

Aliquots of KCN dissolved in D_2O (2 – 60 μL; 8.91 μmol – 0.913 mmol) were added to reaction mixtures containing 28.0 μL acetonitrile (0.536 mmol), 400 μL of **1** (0.205 μmol), and 100 μL of PBu_4Br (0.398 μmol) in 9 inch NMR tubes. The mixtures were heated at 35 °C in an oil bath for three days, over which time the production of acetamide was monitored as noted above. Complete cessation of catalytic reactivity was observed above 3.5 equivalents. The rate of acetonitrile hydration was calculated from the percent conversion at 22 hours of reaction and plotted as a function of KCN equivalents with respect to dissolved Pt. The resulting linear plot was described by $y = -0.012x + 0.033$.

C.2.9. Hg poisoning test

1 (13 mg, 0.028 mmol) was added to a stirred mixture of acetonitrile (6.5 mL, 0.12 mol) and H_2O (4.0 mL, 0.22 mol). $AgBF_4$ (7.4 mg, 0.038 mmol) was added to the reaction mixture, and the mixture was refluxed at 85 °C for 3 hours. Hg^0 (3 drops) was added to the reaction mixture, and the reaction was stirred under reflux for another 21 hours. Aliquots (0.25mL) of the reaction were taken at 3 hr, 4 hr, 5 hr, 6 hr and 23 hr, being careful not to remove any Hg^0. Aliquots were added to an internal standard (3.32 mM $[NMe_4][PF_6]$ in D_2O, 0.25mL) in an NMR tube, and quantitated by ^1H NMR.

C.2.10. Computational methods

To compare the reactivities of cyanohydrins with other nitriles toward catalytic hydration, DFT calculations were performed on various reaction intermediates of the isomeric compounds lactonitrile and 3-hydroxypropionitrile (3-HPN). The molybdocene catalyst **2** was used in the calculations, and the intermediates are based on the mechanism proposed by Breno (Figure 8).[9] The building and modeling of $Cp_2Mo(OH)NCR$ and all related intermediates were performed using the program Ecce v3.2.4.[14,15] Each intermediate has a +1 charge. Calculations were performed on singlet states of each intermediate. All density functional calculations were performed using NWChem version 5.0.[16,17]

Geometry optimizations were performed on all structures, and frequency and single-point energy calculations were performed on the optimized structures. All structures yielded zero imaginary frequencies. For some structures, a fine grid and tighter convergence criteria were needed to obtain a minimum energy structure. For all

atoms except molybdenum, the 6-31G* basis set[18] was used for the geometry optimizations and frequency calculations, and the 6-311G** basis set[19] was used for the final energy calculations. For molybdenum, a triple-zeta valence basis set and effective core potential developed by Andrae et al,[20] augmented with one diffuse f function (zeta=0.338) determined by Martin and Sundermann[21] resulting in a (8s7p6d1f)/[6s5p3d1f] contraction, was used for both the optimizations and single-point energy calculations. Final energies include solvation energies as well as thermal and entropic corrections. All calculations employed the B3LYP functional.[22-25]

Solvation contributions were approximated by employing the COSMO reaction field[26] on the gas-phase optimized structures. Solvent effects were not incorporated into geometry optimizations, because it was found to be very difficult to obtain converged structures with this approach. In addition, it is possible that hydrogen bonding from the solvent may participate in the reaction. Since both nitriles can utilize hydrogen bonding, it is unlikely to account for the observed differences between them, thus the effects of hydrogen bonding are not considered here. A dielectric constant of 78.4 corresponding to H_2O was used for the solvation energy calculations. The atomic radii used for the solvation energy calculations were those developed by Stefanovich and Truong,[27] except for molybdenum, where an approximate cavity radius of 2.0 Å was used. Radii for sp/sp^2-carbon atoms (1.635 Å) were used for the cyclopentadienyl- and nitrile-carbons, and radii for sp^3-carbon atoms (2.096 Å) were used for treating the aliphatic carbons. A solvent probe radius of 0.2 Å was used because it gave the closest agreement with experimental solvation energies of H_2O, acetonitrile, and acetamide (which are representative of the system).

C.3. Results and discussion

C.3.1. Hydration reactions of cyanohydrins using catalysts 1 and 2

The cyanohydrins in Figure 2 were reacted with catalytic amounts of **1** and **2** under a variety of hydration reaction conditions. Selected reaction conditions and results illustrating the range of reactivity are listed in Table 1. In general, species **2** was a very poor catalyst for the hydration reactions, while the catalytic activity of **1** varied greatly with catalyst concentration, substrate concentration, and volume of cosolvent. With catalyst **1**, lactonitrile and 2-hydroxybutryonitrile produced the highest yields of amide product (> 50%), while glycolonitrile and cyclohexanone cyanohydrin yielded only 4% and 14 % of the respective -hydroxyamides. Of the various nitriles, acetone cyanohydrin (ACH) and mandelonitrile showed the lowest reactivity with **1**, producing only a few percent of -hydroxyisobutyramide (< 3 %) and trace amounts of - mandelamide, respectively. Note also in Table 1 that, in many cases, dissociation of the cyanohydrin to give an equilibrium mixture of the cyanohydrin, HCN, and the parent aldehyde or ketone (eq 2) was the only reactivity observed.

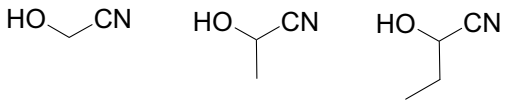

3

4

5

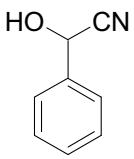

6

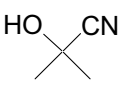

7

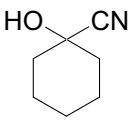

8

Figure 2. Structures of glycolonitrile (**3**); lactonitrile (**4**); 2-hydroxybutyronitrile (**5**); mandelonitrile (**6**); acetone cyanohydrin, ACH (**7**); and cyclohexanone cyanohydrin (**8**).

Because the reaction mixtures were acidified using triflic-, methyl sulfonic-, or tosic-acid, the extent of cyanohydrin dissociation observed in the dilute reaction mixtures was surprisingly larger than expected. It was expected that acidic conditions would help to stabilize the cyanohydrin species because acid is produced upon its dissociation (eq 2). However, even at pH 1, extensive dissociation (> 80 %) was observed in dilute reaction mixtures of ACH. In fact, note in Table 1 that aldehyde or ketone from the dissociation of cyanohydrin was always observed by ^{1}H NMR spectroscopy in all of the reaction mixtures. A control experiment showed that the dissociation is not metal mediated. Thus, cyanohydrin dissociation occurred without **1** or **2** present (in water with or without cosolvents; see Table 1), even under acidic conditions. For example, at pH 3 and 23 °C, 76.1 % dissociation of ACH was observed in five days without either catalyst present.

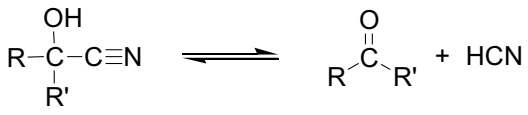

(2)

Cyanohydrin	Catalyst	Cosolvent	mL Cyanohdyrin	mL water	mL Other Cosolvent	[Cyanohydrin] (M)	% Catalyst	Reaction Temp (oC)	% Dissociation	% Hydration	Rxn Time (hrs)
Glycolonitrile	1	H_2O	0.275	0.225	0.000	8.68	0.06%	25	1.00%	3.98%	52.6
Lactonitrile	1	D_2O	0.025	1.000	0.000	0.34	0.29%	80	1.07%	68.00%	1896.0
Lactonitrile	1	D_2O	0.250	0.250	0.000	6.97	0.63%	25	0.25%	68.95%	143.8
Lactonitrile	2	H_2O	0.250	0.25	0.000	6.97	1.04%	25	0.21%	0.82%	74.8
2-Hydroxybutyronitrile	1	D_2O	0.500	0.100	0.000	9.42	0.20%	50	< 0.5 %	0.00%	24.0
2-Hydroxybutyronitrile	1	H_2O, CH_3OH	0.250	0.050	0.200	5.65	1.26%	25	< 0.5 %	51.35%	99.5
Mandelonitrile	1	D_2O	0.500	0.100	0.000	7.01	0.20%	50	2.86%	0.00%	24.0
Mandelonitrile	1	H_2O, CH_3OH	0.200	0.050	0.250	3.36	2.35%	25	2.86%	Trace	74.4
Cyclohexanone Cyanohydrin	1	D_2O	0.030 g	0.500	0.000	0.40	0.20%	50	--	0.00%	24.0
Cyclohexanone Cyanohydrin	1	H_2O, CH_3OH	0.0901	0.450	0.050	1.26	4.71%	25	--	14.00%	74.4
Acetone Cyanohydrin	1	D_2O	0.032	1.000	0.000	0.34	0.33%	25	5.30%	0.00%	24.2
Acetone Cyanohydrin	1	D_2O, $(CH_3)_2CO_2H$	1.000	0.426	1.000	4.51	0.05%	80	47.85%	0.00%	24.0
Acetone Cyanohydrin	1	D_2O, $(CH_3)_2CO$	0.640	0.426	0.815	3.73	0.08%	80	68.60%	0.00%	24.0
Acetone Cyanohydrin	1	D_2O	0.500	0.100	0.000	9.13	0.20%	50	25.00%	0.00%	328.2
Acetone Cyanohydrin	1	CH_3OH	0.500	0.000	0.100	9.13	0.19%	50	1.57%	0.00%	328.6
Acetone Cyanohydrin	1	IPA	0.500	0.000	0.100	9.13	0.10%	50	0.90%	0.00%	328.5
Acetone Cyanohydrin	1	D_2O	0.900	0.100	0.000	9.86	0.02%	25	0.32%	0.00%	170.7
Acetone Cyanohydrin	1	D_2O	0.500	0.500	0.000	5.48	0.04%	25	0.60%	0.00%	170.7
Acetone Cyanohydrin	1	D_2O	0.100	0.900	0.000	1.10	0.20%	25	2.98%	0.00%	170.7
Acetone Cyanohydrin	1	D_2O	0.500	0.500	0.000	5.48	0.91%	25	0.93%	2.72%	144.8
Acetone Cyanohydrin	1	H_2O, CH_3OH	0.250	0.050	0.200	5.48	1.34%	25	0.90%	2.00%	163.9
Acetone Cyanohydrin	1	H_2O, CH_3OH	0.250	0.250	0.000	5.48	1.34%	25	1.27%	1.06%	163.9
Acetone Cyanohydrin	2	D_2O, Acetic Acid	0.500	0.200	0.500	4.56	0.19%	80	80.00%	0.52%	38.6
Acetone Cyanohydrin	2	H_2O	0.250	0.250	0.000	5.48	1.76%	25	6.42%	1.00%	75.0

Table 1. Summary of selected cyanohydrin hydration results using $PtCl(PMe_2OH)\{(PMe_2O)_2H\}$ (1) and $Cp_2Mo(OH)(OH_2)^+$ (2) Nitrile Hydration Catalysts.

Although the metal complex does not appear to mediate degradation, it does influence the position of the cyanohydrin-HCN equilibrium. As shown in Table 1, a higher percentage of degradation was observed when a higher concentration of catalyst was used but with all other conditions identical (i.e., solvent composition, reaction temperature, and substrate concentration). Over time, the percent degradation always approached or exceeded the percent catalyst. The experimental consequences of the cyanohydrin dissociation are discussed later.

In several of the ACH reaction mixtures where no reactivity was observed, scrambling of the ketone and cyanohydrin protons with solvent deuterium occcurred, as indicated in the ^{1}H NMR spectrum by the appearance of triplet and quintet resonances on the shoulder of the parent resonance (Figure 3). The presence of the deuterated species was also confirmed in the ^{2}H spectrum of the ACH, which showed resonances at 1.62 ppm (DO(C*D*$_3$)$_2$CCN), 2.25 ppm ((C*D*$_3$)$_2$CO), and 5.28 ppm (*D*CN). The mechanism of H/D exchange is not metal mediated because H/D exchange was also observed in a control reaction performed at pH 3 without **1** present.[b] It is suggested that H/D exchange proceeds by the keto-enol tautomerism of the acetone under acidic conditions (Scheme 1). At high ACH concentration when no acid was added to the reaction mixture, no deuterated acetone or cyanohydrin was observed, a result consistent with the proposed acid catalyzed mechanism. Note that the HCN present in the reaction mixture is not acidic enough to protonate the acetone.

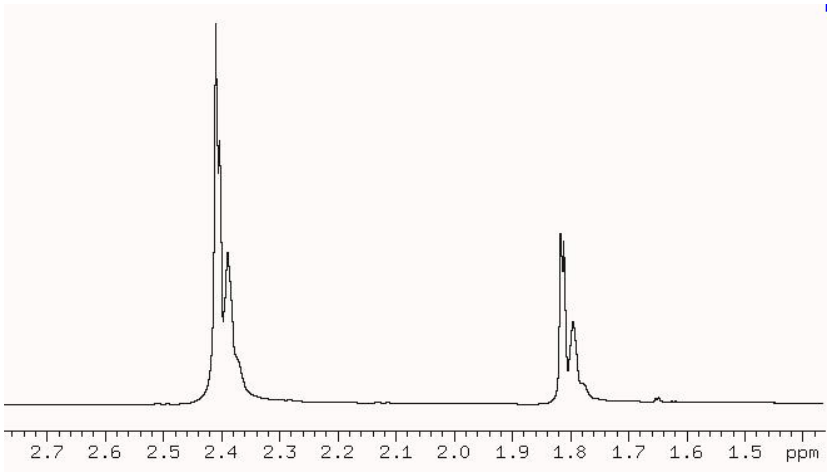

Figure 3. ^{1}H NMR spectrum of ACH reaction mixture showing appearance of deuterated acetone and ACH.

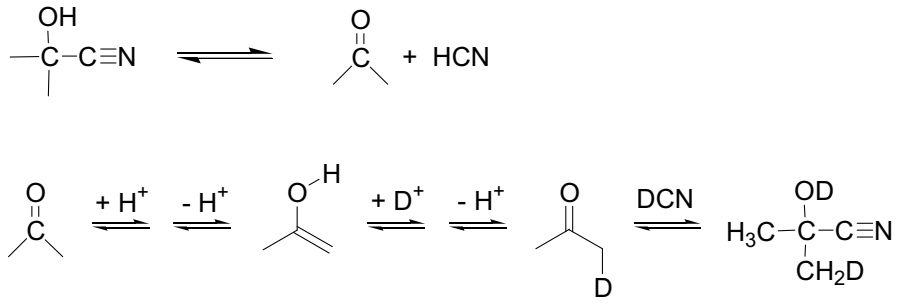

Scheme 1. Proposed mechanism of H/D exchange for cyanohydrins under acidic reaction conditions.

C.3.2. Comparison of cyanohydrins to other nitriles

The -hydroxy substituent in cyanohydrins was expected to increase the reactivity of the nitrile group by increasing the partial positive charge on the nitrile carbon. This expectation was based on prior work that showed molybdocene catalysts

were most reactive toward nitriles containing electron-withdrawing substituents.[9] (An increase in the reaction rate with increasing electron withdrawing ability of the substrate is expected for a mechanism involving nucleophilic attack of the hydroxo ligand on the coordinated substrate.) Interestingly, lactonitrile (an -hydroxynitrile) is essentially unreactive with catalyst **2**, whereas a prior study found that the hydration of 3-hydroxypropionitrile (3-HPN; -hydroxynitrile) was the fastest molybdocene-catalyzed nitrile hydration of the nitriles studied.[9] To explain this result, it was initially hypothesized that the nitrile carbon of cyanohydrins may be more electron rich (i.e., have more cyanide-like character) than other nitrile substrates. Such an electron-rich carbon center would be much less susceptible to nucleophilic attack and would, therefore, be less reactive by typical metal-mediated nitrile hydration pathways. However, comparison of the ^{13}C NMR resonance frequencies of selected nitriles shows that the nitrile carbons of ACH and 2-hydroxypropionitrile resonate at a frequency similar to that of other nitriles (Table 2), which suggests that the electronic charge on the nitrile carbon in cyanohydrins is not unusual.

Table 2. Comparison of nitrile ^{13}C NMR resonate frequencies for selected nitriles

Nitrile	**δ (NCR)**
Acetonitirile	118.1
3-hydroxypropionitrile	120.7
2-hydroxypropionitrile	121.5
acetone cyanohydrins	123.3
Propionitrile	123.7

To gain insight into the sluggish reactivity of the cyanhydrins and the electronic and steric influences of the -hydroxy group on the rate, an investigation of variously substituted nitriles (Figure 4) was conducted using the more reactive catalyst **1**. A summary of the results appears in Table 3.[c,d] An interesting point, not shown in the table, is that the rate of lactonitrile hydration declined rapidly from an initial rate of 0.062 M/hr[e] to 1.9 x 10^{-4} M/hr within nine hours of reaction (Figure 5). This behavior is typical of product inhibition. Interestingly, the substrates 2-methoxypropionitrile and 2-methoxyisobutyronitrile,[f] which are electronically similar to lactonitrile and acetone cyanohydrin (σ_m = 0.10 and 0.13 for MeO and OH, respectively) but more sterically encumbered, reacted rapidly in excellent yield and showed no signs of inhibition. Based on the results in Table 3, it is clear that: a) electron-withdrawing substituents facilitate the hydration reaction, and b) cyanohydrins are initially as reactive to hydration by catalyst **1** as the other nitriles tested. The lack of longterm rapid reactivity noted for the cyanohydrins is apparently due to some type of inhibition, which among the nitriles is unique to the cyanohydrins. The possible causes of inhibition are discussed in the following section.

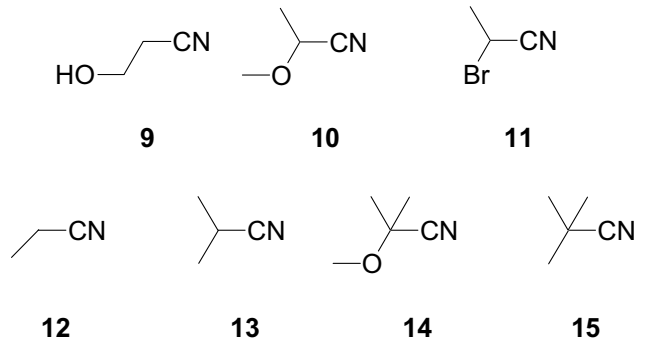

Figure 4. Structures of 3-hydroxypropionitrile (3-HPN; **9**); 2-methoxypropionitrile (**10**); 2-bromopropionitrile (**11**); propionitrile (**12**); isobutryonitrile (**13**); 2-methoxyisobutyronitrile (**14**); and trimethylacetonitrile (**15**).

Table 3. Rate data for hydration of various nitriles catalyzed by **1**.

Substrate	**[Substrate] (M)**	**% Catalyst**	**Rxn Temp. (^{o}C)**	**Rate (M/hr)**	**% Conversion**
3-hydroxypropionitrile[a]	0.34	0.10	43	9.4×10^{-2}	100
2-methyoxypropionitrile[a]	0.34	0.10	43	5.5×10^{-2}	100
2-bromopropionitrile[a]	0.34	0.10	43	2.5×10^{-2}	90
lactonitrile[a]	0.34	0.10	43	2.2×10^{-2}	12
acetonitrile[a]	0.34	0.10	43	1.3×10^{-2}	100
propionitrile[a]	0.34	0.10	43	8.0×10^{-3}	100
isobutyronitrile[a]	0.34	0.10	43	2.2×10^{-3}	100
Trimethylacetonitrile	0.34	0.25	80	1.1×10^{-1}	100

[a] Reaction mixtures also contained 0.45 mM PBu_4Br as an internal standard.

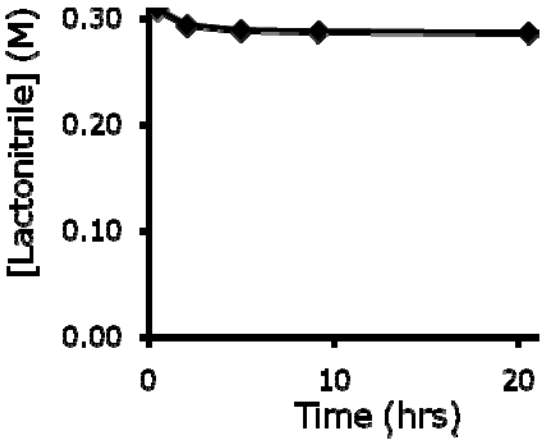

Figure 5. Plot of [Lactonitrile] versus time for the hydration of lactonitrile (0.34 M) catalyzed by **1**.

C.3.3. Catalyst inhibition tests

Although the -hydroxy group of cyanohydrins is electronically similar to an -methoxy substituent, the substrates differ in that the cyanohydrins can be deprotonated. The consequences of cyanohydrin deprotonation are formation of an alkoxide species, which is a better ligand than a nitrile, and dissociation of the cyanohydrinate to form HCN and the parent aldehyde or ketone. Based on this possible reactivity, three hypotheses were formulated to explain the inhibition of catalytic activity observed with cyanohydrin substrates: 1) Following nucleophilic attack of water or hydroxide on the nitrile carbon, catalysis may be inhibited by irreversible formation of an inert iminol or iminolate species, which is perhaps chelated (Figure 6). In support of this hypothesis, it

is known that molybdocene-catalyzed nitrile hydration is inhibited by irreversible coordination of amides[9] and that coordination of amides to transition metals stabilizes the iminol tautomer.[3] Once the iminol tautomer is formed, the -hydroxy group could coordinate, resulting in the formation of a more stable five-membered ring species that may be even more inert. (This mechanism was explored by DFT calculations. See the Supporting Information.) 2) The cyanohydrin preferentially binds through the alcohol functionality leading to formation of an alkoxide ligand. Binding of the cyanohydrin through the oxygen may lead to inadequate activation of the nitrile carbon and decreased reactivity. Furthermore, if the resulting alkoxide ligand is relatively inert, the formation of the metal-alkoxide complex will be a thermodynamic sink, resulting in acute substrate inhibition. 3) The HCN produced in the dissociation of the cyanohydrin may poison the catalyst by coordination of cyanide to the metal center.

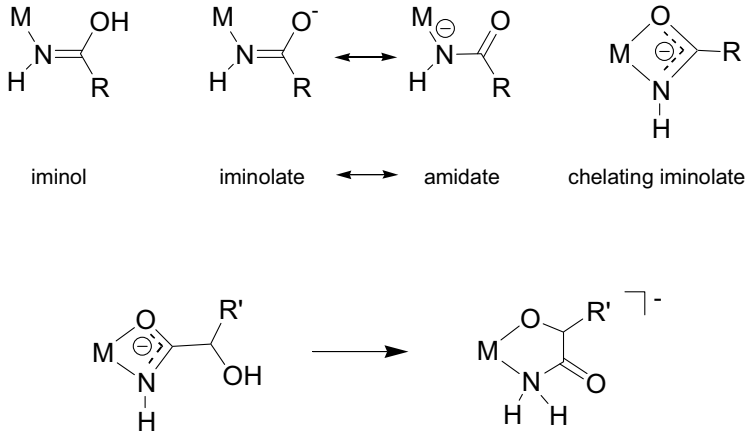

Figure 6. Stabilization of iminol and iminolate (amidate) ligands by metal coordination. Rearrangement of the chelating iminolate would result in a more stable species with a five-membered ring.

Experimental tests of hypotheses 1 and 2 were negative and are reported in the Supporting Information. Hypothesis 3 suggests that free cyanide generated from dissociation of the cyanohydrin may bind irreversibly to the Pt center and deactivate the catalyst. Indeed, the addition of excess KCN to 3-HPN prevented hydration of the nitrile (see details in the Supporting Information). Instead of hydration, substitution of the hydroxy group in the 3-HPN occurred to give succinonitrile. In order to determine the efficiency of cyanide poisoning, substoichiometric aliquots of potassium cyanide were added to reaction mixtures containing acetonitrile substrate (Figure 7). Catalytic activity did not cease until the $[CN^-]/[Pt]_{total}$ ratio reached 3:1.[g] The identity of the resulting Pt cyanide complex(es) was not determined; however, it is apparent that three cyanide ligands are required to deactivate the catalyst. Furthermore, the rate of acetonitrile hydration versus cyanide equivalents gives a linear relationship, which indicates that cyanide binding is irreversible.

Hypothesis 3 is also consistent with the results summarized in Table 1. As noted previously, at least trace amounts of ketone or aldehyde were detected in the ^{1}H NMR spectra of all of the reaction mixtures, indicating equivalent levels of HCN. In addition, the highest yields of hydration were observed using lactonitrile and 2-hydroxybutyronitrile, which are more robust to dissocation than acetone cyanohydrin and mandelonitrile. These latter two substrates showed little reactivity.[28] Close scrutiny of Table 1 shows that hydration was only observed when the percent dissociation was less than the percent of catalyst in solution, except in the cases of lactonitrile and

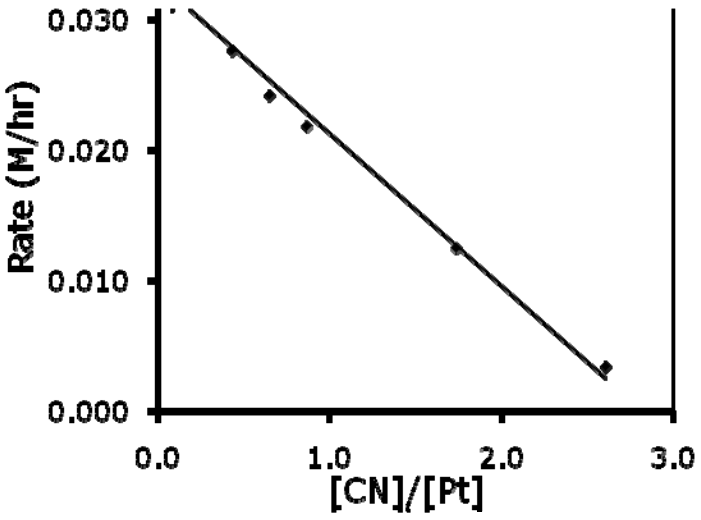

Figure 7. Plot of acetonitrile hydration rate versus $[CN^-]/[Pt]$ showing the effect of CN^- on the catalytic activity of the $[PtCl(PMe_2OH)\{(PMe_2O)_2H\}]$ ($y = -0.012x + 0.033$).

glycolonitrile. This result may be rationalized after considering that the equilibrium between cyanohydrins and HCN/aldehyde(ketone) in solution occurs at different rates. The apparent inconsistency in the cases of glycolonitrile and lactontrile is most likely due to slower dissociation of these more robust substrates, which leads to slower catalyst poisoning. In general, note that lower yields (or no yield in the case of ACH) were observed at higher reaction temperatures, consistent with faster cyanohydrin dissociation at higher temperatures and concomitant faster catalyst poisoning.

It is interesting that three equivalents of HCN were not required to inhibit hydration of the cyanohydrins, as was the case in acetonitrile hydration. The relative acuteness of cyanide poisoning in the cyanohydrin reaction mixtures may be due to the inferiority of the cyanohydrins as ligands in comparison to acetonitrile. That is, acetonitrile is sterically less hindered and more electron-donating relative to the -hydroxynitriles. As such, the acetonitrile substrate will be more competitive versus cyanide for Pt binding than the cyanohydrins. The high oxidation state molybdocene catalyst (**2**) is even more susceptible to cyanide poisoning because it is a much stronger Lewis acid than the Pt catalyst (**1**).[11]

C.3.4. DFT analysis of molybdocene catalyzed nitrile hydration

The calculated reaction profiles for the molybdocene-catalyzed hydration of lactonitrile (LN) and 3-hydroxyproprionitrile (3-HPN) are shown in Figure 8. The intermediates in these profiles are based on the mechanism for nitrile hydration reported in a previous paper.[9] In the first step, energy comparisons show that binding of either LN or 3-HPN to the molybdenum center is reversible. In the next step, attack of the hydroxo ligand on the substrates occurs to form the iminolate complexes. This step is slightly more favorable for LN (by 2 kcal/mol). Optimizations of the next step (H_2O coordination to the metallocycle; step 3) resulted in a proton transfer to the carbonyl oxygen in both cases, yielding the iminol form of the ligand. Step 3 is slightly endergonic for both LN and 3-HPN (+1 and +4 kcal/mol, respectively); note it is more favorable by 3 kcal/mol for LN. The net reactions of the iminol intermediates to give the final products are slightly favorable (-1 kcal/mol) for both nitriles, but the calculation suggests that this reaction may not proceed by way of the coordinated amide species due to the high barrier

to reach the amides (+9 kcal/mol for LN, +11 kcal/mol for 3-HPN). (Note that the molybdocene stabilizes the iminol over the amide. However, should the amides form, the dissociation of the amide is favorable for both cases (-10 kcal/mol for LN, -12 kcal/mol for 3-HPN).) Overall the free energies of hydration are calculated to be -15 kcal/mol for LN and -9 kcal/mol for 3-HPN.

The first important point to come from the calculations is that the formation of most intermediates and the overall reaction itself are more favorable for LN than for 3-HPN. Thus, from an electronic standpoint, there appears to be no reason for the lack of reactivity observed for lactonitriles. These findings corroborate the experimental finding that the initial rates of the metal-mediated hydration reactions of cyanohydrins are comparable to the rates of the other nitriles. The second important point concerns inhibition of the hydration reaction. In previous studies, it was shown that the rate of molybdocene-catalyzed nitrile hydration decreased with increasing substrate concentration or with the intentional addition of amide product.[9] It was proposed that the amide binds irreversibly to the molybdocene catalyst and deactivates it. Amides in general are not strongly bonding ligands, but according to the computational analysis presented here, amide inhibition occurs because coordination is stabilized by isomerization to the iminol tautomer.

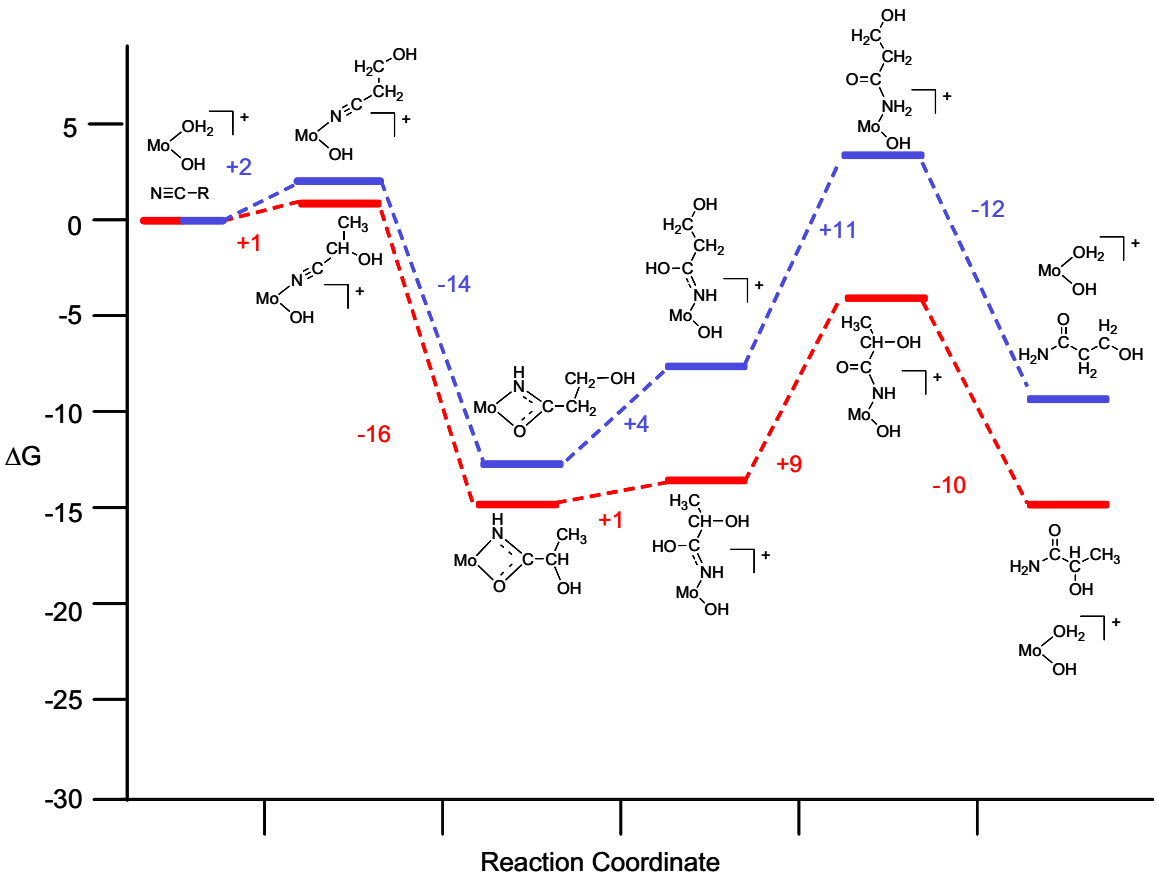

Figure 8. Reaction profiles for proposed catalytic cycle of molybdocene-catalyzed lactonitrile and 3-hydroxypropionitrile hydration. Free energies are in kcal/mol. The Cp_2Mo fragment is abbreviated as Mo.

Additional DFT calculations computationally tested the three hypothesis described above in the section on catalyst inhibition. The results support hypothesis 3, namely, that cyanide poisoning is responsible for the low amide yields in the case of molybdocene catalyzed hydration of cyanohydrin. The results and further discussion of these calculations are found in the Supporting Information.

C.3.5. Aqueous behavior of [PtCl(PMe$_2$OH){(PMe$_2$O)$_2$H}]

Previous studies prepared the active catalyst from complex **1** by abstracting the chloride ligand in aqueous solution.[5] In the present study, however, partial to complete degradation of the [PtCl(PMe$_2$OH){(PMe$_2$O)$_2$H}] complex (due to dissociation of the dimethyl phosphinito ligands) was always observed when **1** was treated with Ag^+, Tl^+, or Na^+ salts. For example, upon treatment of complex **1** with one of the aforementioned salts, the resonances in the ^{31}P NMR spectrum sharpened (δ 96 (d, 2 P) and δ 58 (t, 1 P)) and new resonances appeared at δ 35 (t) and δ53 (s), due to free ligand and dimethylphosphinic acid, respectively. Note that dimethylphosphinic acid is generated by disproportionation (eq 4) of dimethylphosphine oxide (the tautomer of the dimethylphosphinito ligand).

$$2\ P(O)(CH_3)_2H \longrightarrow P(O)(CH_3)_2(OH) + P(CH_3)_2H \quad (4)$$

The gaseous dimethylphosphine byproduct is typically not observed; however, spiking with an authentic sample decisively identified the dimethylphosphinic acid. (The resonance for dimethyl phosphinic acid was observed at δ 53 but no additional resonances.) Little or no dimethylphosphinic acid was observed when oxygen was excluded from the reaction vessel.

Degradation of the catalyst is more extensive at high temperatures or when using Ag^+ salts. In fact, no resonances due to **1** were detectable by ^{31}P NMR spectroscopy after

12 hours of reflux in water solution in the presence of AgOTf or $AgBF_4$. Quantification of the resulting phosphine oxide and/or dimethylphosphinic acid accounted for only 67 % of **1**; however, analysis of the remaining solid indicated undissolved **1**. Note that stock solutions of catalyst prepared using Ag^+ salts were less reactive toward nitriles in general, especially the bulky 2° and 3° nitriles. Furthermore, in some cases, the reaction mixtures changed colors after several hours of reaction time. The color changes were inconsistent and appeared blue, pink, purple, red, yellow, and amber in different trials, and several reaction mixtures continued to change in color from colorless to blue to pink if left on the heat source. In many of the experiments where the solid formed upon treatment with Ag^+ was removed prior to addition of the nitrile (the solid was presumed to be AgCl), an abrupt halt in the hydration of the substrate accompanied this color change. The reaction rates were also inconsistent when Ag^+ salts were used to abstract the chloride from **1**, which is suggestive of heterogeneous catalysis. However, no evidence was collected in support of heterogeneous catalysis. For example, addition of mercury to the acetonitrile hydration reaction catalyzed by **1** did not affect the rate of the reaction. (Rate data for the Hg poisoning experiment are found in the Supporting Information.)

It was not possible to determine the identity of the catalyst that formed when $[PtCl(PMe_2OH)\{(PMe_2O)_2H\}]$ was treated with chloride abstraction reagents. Repeated attempts to crystallize the catalyst from stock solutions after treatment with a chloride abstraction agent merely resulted in crystallization of $[PtCl(PMe_2OH)\{(PMe_2O)_2H\}]\cdot 0.5H_2O$.

C.4. Summary and key insights

Comparison of the hydration reactivity of cyanohydrins to that of other nitriles demonstrated that the low reactivity of the -hydroxynitrile substrates is not due to the steric or electronic consequences of the hydroxy group on the carbon. In fact, the cyanohydrin lactonitrile exhibits initial rates that are comparable to those of other nitriles containing electron-withdrawing substituents, demonstrating that the electronic character of the nitrile carbon in cyanohydrins is not unusual in comparion with other nitriles. The low reactivity of cyanohydrins is instead due to liberation of HCN from the cyanohydrin substrate, the coordination of which leads to deactivation of the catalyst. Unfortunately, because water is necessary for the hydration reaction, generation of some small equilibrium amount of HCN is inevitable. No evidence of metal-mediated dehydrocyanation was observed; however, coordination of the free cyanide to the transition metal encourages greater dehydrocyanation by removing HCN from the equilibrium. Irreversible binding of cyanide ensures complete catalyst poisoning. Deactivation due to cyanide poisoning occurred for both catalysts **1** and **2**, and such deactivation may explain the lack of cyanohydrin hydration noted for other transition metal nitrile hydration catalysts. Overall, this work provides a more thorough understanding of the challenges associated with transition metal catalyzed nitrile hydration. Furthermore, the results obtained using the α-methoxy-substituted nitriles indicated that protected cyanohydrins provide a viable route to access α-hydroxyamides. This knowledge is being used to develop new cyanohydrin hydration catalysts that are less susceptible to cyanide poisoning.

C.5. Notes

a. Several noteworthy acid-free synthetic methods for the hydration of cyanohydrins utilizing boron, metal oxides, and nitrile hydratase enzymes as mediators have been disclosed in patents and in the literature. These methods are summarized in the Supporting Information.

b. Prior studies showed that H/D exchange in alcohols occurs by a mechanism involving coordination through the oxygen atom, followed by β-hydride elimination. (See Balzarek, C.; Weakley, T.J.R.; Tyler, D. R. *J. Amer. Chem. Soc.* **2000**, *122*, 9427.) However, beta-hydride elimination is not possible from coordinated ACH because it is a tertiary alcohol.

c. The rates shown in the table were calculated for the nitrile substrates based on the percent conversion after two hours of reaction. No carboxylic acid product was observed in the reaction mixtures of these systems, even after prolonged heating. Note that all of the reactions proceeded to completion and displayed first- or zero-order dependence on the substrate and eventually proceeded to completion.[31]

d. For the reactions carried out at 43 °C, nitriles containing electron-withdrawing groups displayed psuedo-first order kinetics. In contrast, psuedo-zero-order kinetics were observed for electron-donating nitriles, indicating a change in the rate-determining step. This inconsistency precluded generation of a Hammett plot. Kinetic traces for each substrate are available in the Supporting Information.

e. This value was the rate after 30 minutes of reaction.

f. Unfortunately, rate data could not be obtained for the 2-methoxyisobutyronitrile. However, the reaction of ~0.50 M 2-methoxyisobutyronitrile did proceed to completion.

g. Note that the concentration of **1** does not account for all of the Pt in solution, as some free ligand is observed in solution due to degradation of the Pt complex. The aqueous behavior of $[PtCl(PMe_2OH)\{(PMe_2O)_2H\}]$ is described in more detail in a following section.

APPENDIX D

SUPPORTING INFORMATION

TO ACCOMPANY APPENDIX C

D.1. Additional information on cyanohydrin hydration catalysts

Several noteworthy acid-free synthetic methods for the hydration of cyanohydrins utilizing boron,[1-3] metal oxides,[4] and nitrile hydratase enzymes[5-12] as mediators have been disclosed in patents and in the literature. The use of nitrile hydratase enzymes (commonly denoted as NHases) to promote cyanohydrin hydration has received the most attention by far, and these enzymes show promise for large-scale synthesis of α-hydroxyamides. NHases contain Fe(III) or Co(III) centers[13-15] and are used by microorganisms to hydrolyze nitriles exuded from plant biomass for the generation of essential carboxylic metabolites.[15] A wide range of NHases (including those belonging to the genera *Rhodococcus*,[8,9] *Corynebacterium*,[11] *Pseudomonas*,[7] *Arthrobacter*,[11] *Alcaligenes*,[12] *Brevibacterium*,[11] and *Nocardia*[11]) have been used, often in combination with amidase, to prepare α-hydroxyamides and carboxylic acids. The main disadvantages of these systems are the limited availablility of enzyme and coenzyme sources and the sensitivity of these enzymes to the unstable cyanohydrin substrates, aldehydes, and/or HCN.[11] However, efficient reactivity and optical resolution has been noted in several cases, and the use of NHases has been applied to the enantioselective

syntheses of fine chemicals containing amide and carboxylic acid functionalities. Furthermore, the successful application of microbial NHases in the industrial production of acrylamide demonstrates the viability of the biocatalytic approach in the manufacture of amides.[16,17]

The use of modified MnO_2 has proven the most successful in sulfuric acid-free cyanohydrin hydration, as it is currently being used by Mitsubishi Gas Chemical Company in the manufacture of methyl methacrylate.[18] Although MnO_2 generates α-hydroxyamides cleanly in high yield and eliminates the need for harsh acidic conditions, the process is less cost effective than the current sulfuric acid chemistry employed. The manufacturing costs are increased partly because the MnO_2 must be treated to modify its structure for optimal activity. Interestingly, other heterogeneous metal oxides that have found use in the industrial-scale synthesis of amides (such as Cu/Cr oxides, Cu/Mo oxides, and Raney Cu) were found to be ineffective in the hydrolytic conversion of cyanohydrins.[4] Because mechanistic investigations of heterogeneous catalytic systems are often ambiguous, the factors that affect the reactivity of these complexes toward cyanohydrins have not been delineated.

D.2. Catalytic inhibition; experimental and computational tests of hypotheses 1 and 2

To test for the occurrence of product inhibitition (hypothesis 1), α-hydroxyisobutyramide and glycolamide were added to reaction mixtures containing acetonitrile and catalyst **1**. Addition of one equivalent (with respect to acetonitrile) of the α-hydroxyamides to a reaction mixture of acetonitrile and **1** did not affect the rate of acetamide production (see rate data below), which suggests that product inhibition does

not occur and therefore that hypothesis 1 is not applicable to catalyst **1**. Note that, even though molybdocene-mediated nitrile hydration reactions showed product inhibition in other experiments, the low levels of amide detected in those reaction mixtures could not be solely responsible for inactivating the catalyst. Thus, even though product inhibition does occur in the case of catalyst **2,** other factors must be contributing to the low reactivity observed.

In a test of hypothesis 2, acetone cyanohydrin or lactonitrile was added to reaction mixtures of catalyst **1** and 3-HPN. An abrupt halt in the hydration of the 3-HPN was observed when either acetone cyanohydrin or lactonitrile was added to the reaction mixture, which suggests that the cyanohydrin substrates inhibit catalysis. However, because the cyanohydrins dissociate to give HCN, this cessation in catalytic activity could be due to either the cyanohydrin (hypothesis 2) or the HCN (hypothesis 3). The applicability of hypothesis 2 can be ruled out, however, based on results previously obtained for the molybdocene-catalyzed hydration of 3-HPN, which are inconsistent with the hypothesis 2.[10] The key result from this earlier study is that, in the presence of molybdocene catalysts in D_2O solvent, 3-HPN undergoes H/D exchange of the protons α to the alcohol, in addition to nitrile hydration (eq 1).

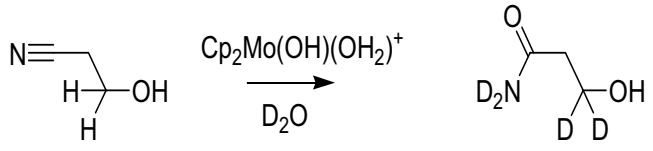

(1)

The accepted pathway of molybdocene catalyzed H/D exchange of alcohols involves β-hydride elimination of the coordinated alkoxide, which indicates oxygen-

coordination of the 3-HPN substrate. Coordination of 3-HPN does not compromise the reactivity of its nitrile functionality; on the contrary, the hydration of 3-HPN is one of the fastest nitrile hydration reactions noted for the molybdocene catalysts. If the nitrile carbon of β-hydroxynitrile is aptly activated for hydration despite preferential binding through the alcohol group, O-coordination of α-hydroxynitriles should be even less problematic. Accordingly, hypothesis 2 can be ruled out.

To further understand the metal-mediated cyanohydrin hydration, the three hypotheses described above and in the main body of the paper on catalyst inhibition were also computationally tested. To test hypothesis 1, calculations were performed on the two cyclic intermediates that can form when an iminolate coordinates to a metal (Figure 1). Rearrangement of the four-membered metallocycle iminolate to the larger cyclic structure was computed to be unfavorable (+7 kcal/mol) for 3-HPN, but thermoneutral (-1 kcal/mol) for lactonitrile (LN). While the difference between 3-HPN and LN is relatively large (8 kcal/mol), the fact that the reaction is reversible for LN makes this pathway an unlikely reason for the low amide yields observed for lactonitrile.

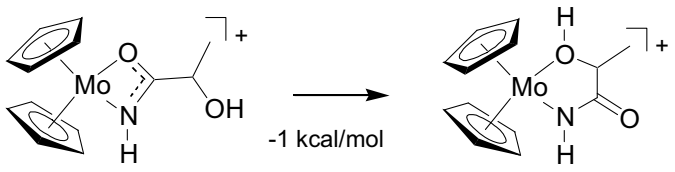

Figure 1. Rearrangement of four-membered metallocycle intermediate of lactonitrile hydration to cyclic molybdocene amidate bound through the alcohol functionality of the lactonitrile substrate. $\Delta G° = +7$ kcal/mol for 3-HPN.

To test hypothesis 2, calculations were performed on structures where the molybdocene coordinated the alcohol rather than the nitrile substituent. Binding of the nitrile to the molybdocene via the hydroxyl substituent was found to be slightly unfavorable for both cases (+5 for LN, +4 for 3-HPN). Additional calculations were performed in which the proton was transferred from the alcohol to the hydroxide ligand, resulting in an alkoxide bound to the molybdocene, as illustrated in Figure 2 for 3-HPN. This was found to be slightly favorable (-5 for LN, -3 for 3-HPN). The net reaction is thus found to be reversible for both reactions. Therefore, hypothesis 2 is likely not the reason for the low amide yields observed for lactonitrile.

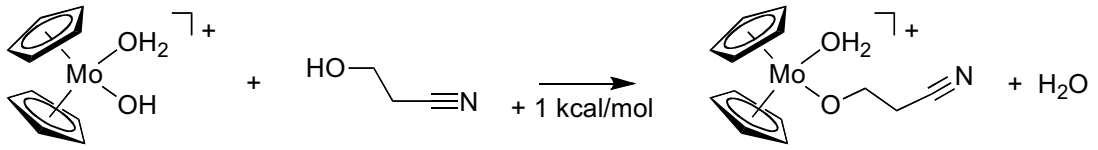

Figure 2. Coordination of 3-HPN via the alcohol functionality with transfer of alcohol proton. $\Delta G° = 0$ kcal/mol for LN.

Finally, calculations were also done in which the bound water was replaced by HCN (Figure 3). The lowest energy configuration for this reaction has the cyanide bonded through the carbon to the molybdenum, and the proton transferred to the hydroxide. This reaction is favorable by 11 kcal/mol, which is much lower than the

binding of either nitrile ligand. In summary, the calculations support hypothesis 3; namely that cyanide poisoning is most likely responsible for the low amide yields in the case of molybdocene catalyzed hydration of cyanohydrin.

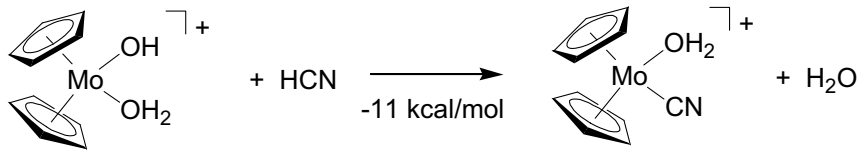

Figure 3. Energetics of cyanide binding to molybdocene catalyst.

D.3. Concentration versus time for selected nitrile hydration trials

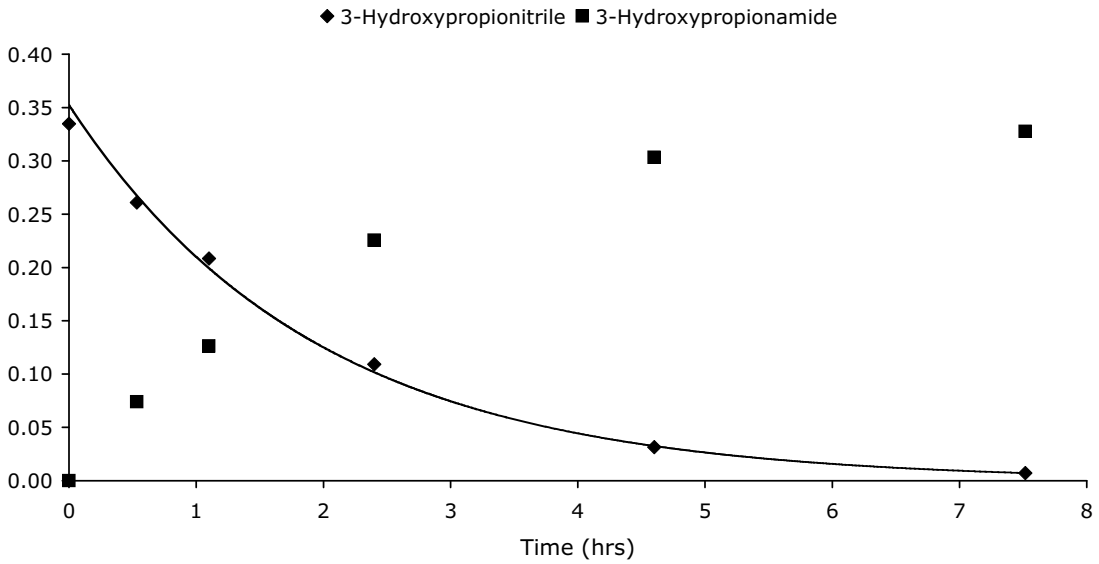

Figure 4. Plot of concentration versus time for the hydration of 3-hydroxypropionitrile catalyzed by $[PtCl(PMe_2OH)\{(PMe_2O)_2H\}]$ at 43 °C ($y = 0.353e^{-0.518}x$; $R^2 = 0.999$)

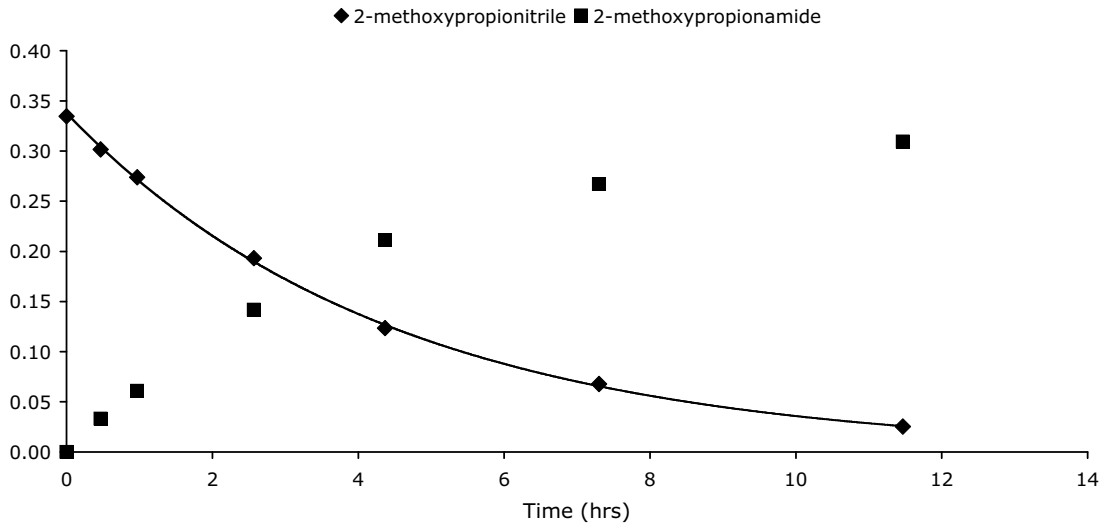

Figure 5. Plot of concentration versus time for the hydration of 2-methoxypropionitrile catalyzed by $[PtCl(PMe_2OH)\{(PMe_2O)_2H\}]$ at 43 °C ($y = 0.338e^{-0.225}x$; $R^2 = 0.9995$)

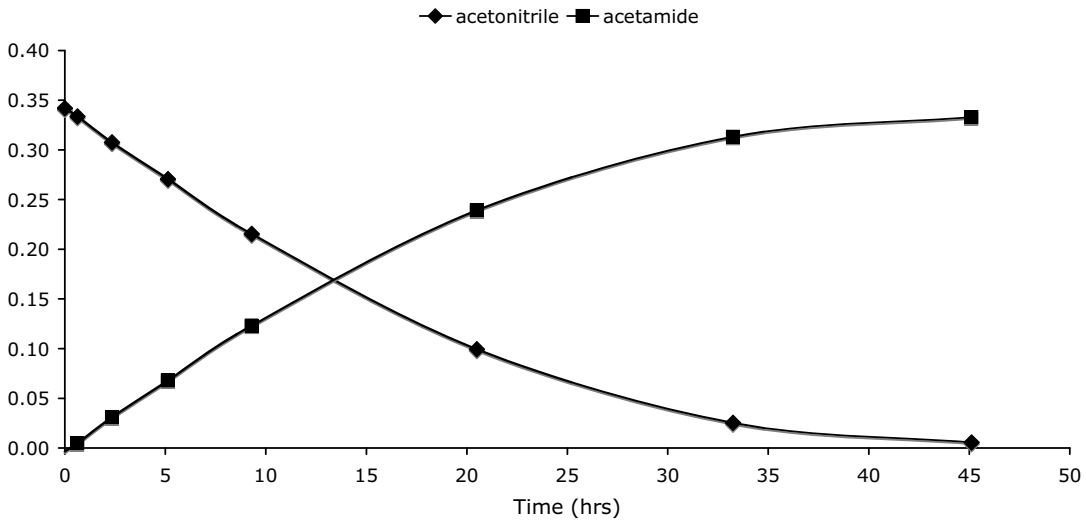

Figure 6. Plot of concentration versus time for the hydration of acetonitrile catalyzed by $[PtCl(PMe_2OH)\{(PMe_2O)_2H\}]$ at 43 °C (does not fit to first or second order decay)

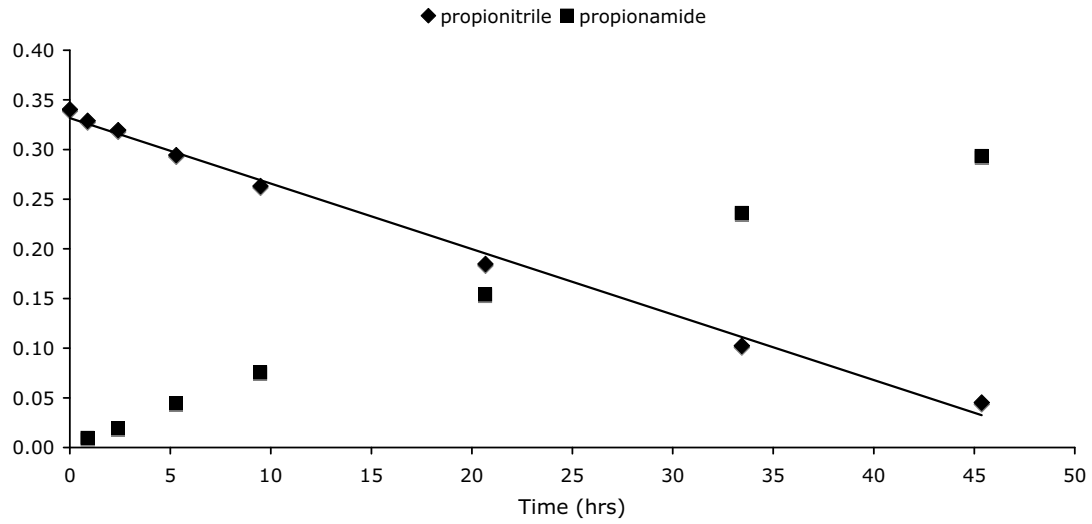

Figure 7. Plot of concentration versus time for the hydration of propionitrile catalyzed by [PtCl(PMe$_2$OH){(PMe$_2$O)$_2$H}] at 43 °C (y = -0.00660x + 0.332; R^2 = 0.994)

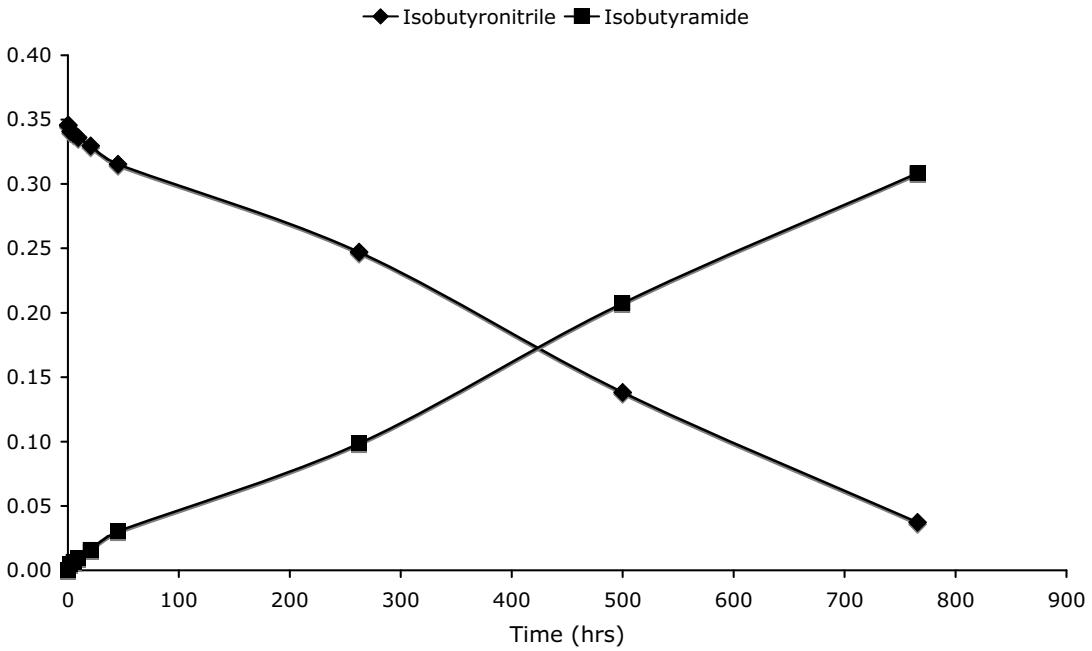

Figure 8. Plot of concentration versus time for the hydration of isobutyronitrile catalyzed by [PtCl(PMe$_2$OH){(PMe$_2$O)$_2$H}] at 43 °C (y = -3.97E10^{-4}x + 0.342, R^2 = 0.998)

D.4. Effect of -hydroxyamides on nitrile hydration

Table 1. Rate data for acetamide production promoted by [PtCl(PMe_2OH){$(PMe_2O)_2H$}] with and without one equivalent of the listed α-hydroxyamide.

Amide	[CH_3CN] (M)	[Amide] (M)	Temp	% Cat	Rate (mol nitrile/s)
--	0.34	--	43	0.10	0.023
Glycolamide	0.34	0.46	43	0.10	0.024
--	1.0	--	65	0.03	0.035
HIBAM	1.0	1.0	65	0.03	0.034

D.5. Effect of Hg on catalysis

Table 2. Rate data for acetamide production promoted by [PtCl(PMe_2OH){$(PMe_2O)_2H$}] with and without Hg.

	[CH_3CN] (M)	Temp	% Cat	Rate (mol nitrile/sec)
no Hg(0)	5.5	85	0.03	0.0002
with Hg(0)	5.9	85	0.02	0.00008

D.6. Calculated energies in molybdocene-mediated hydrolysis

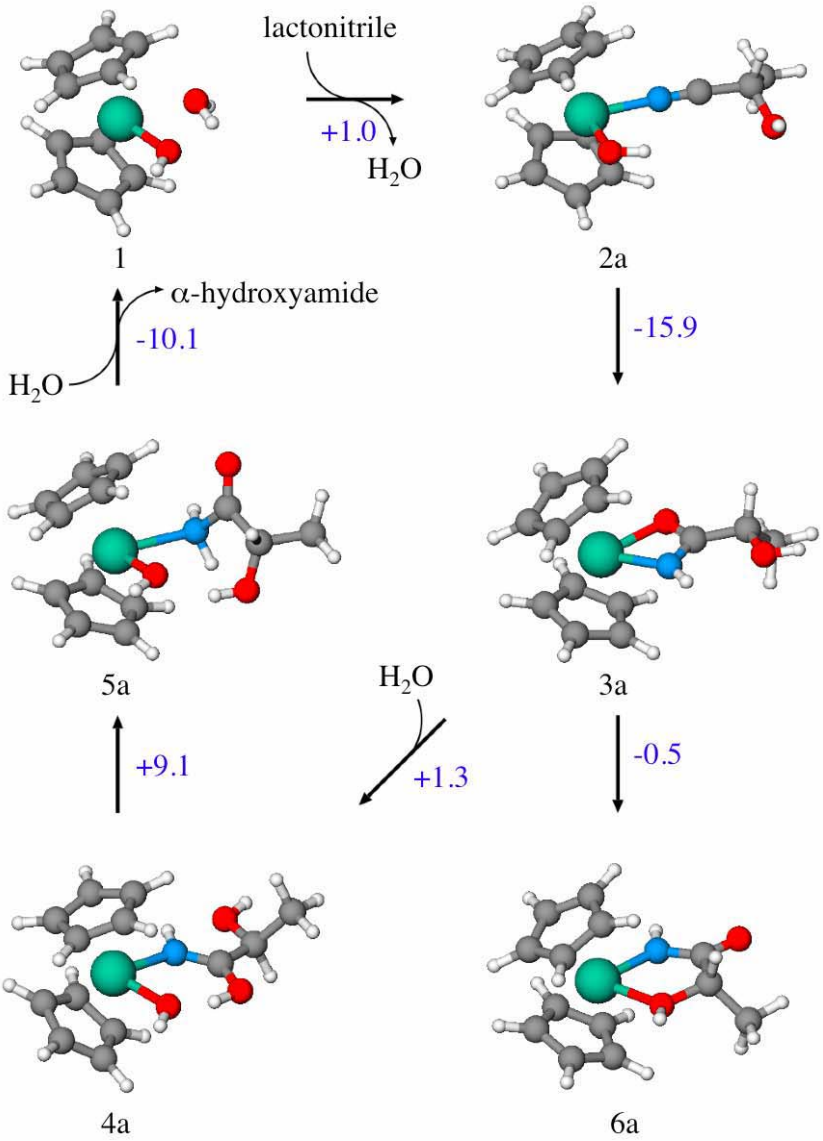

Figure 9. Calculated intermediate structures for the hydrolysis of lactonitrile by $Mo(Cp)_2(OH)OH_2$.

Reaction energies are in kcal/mol.

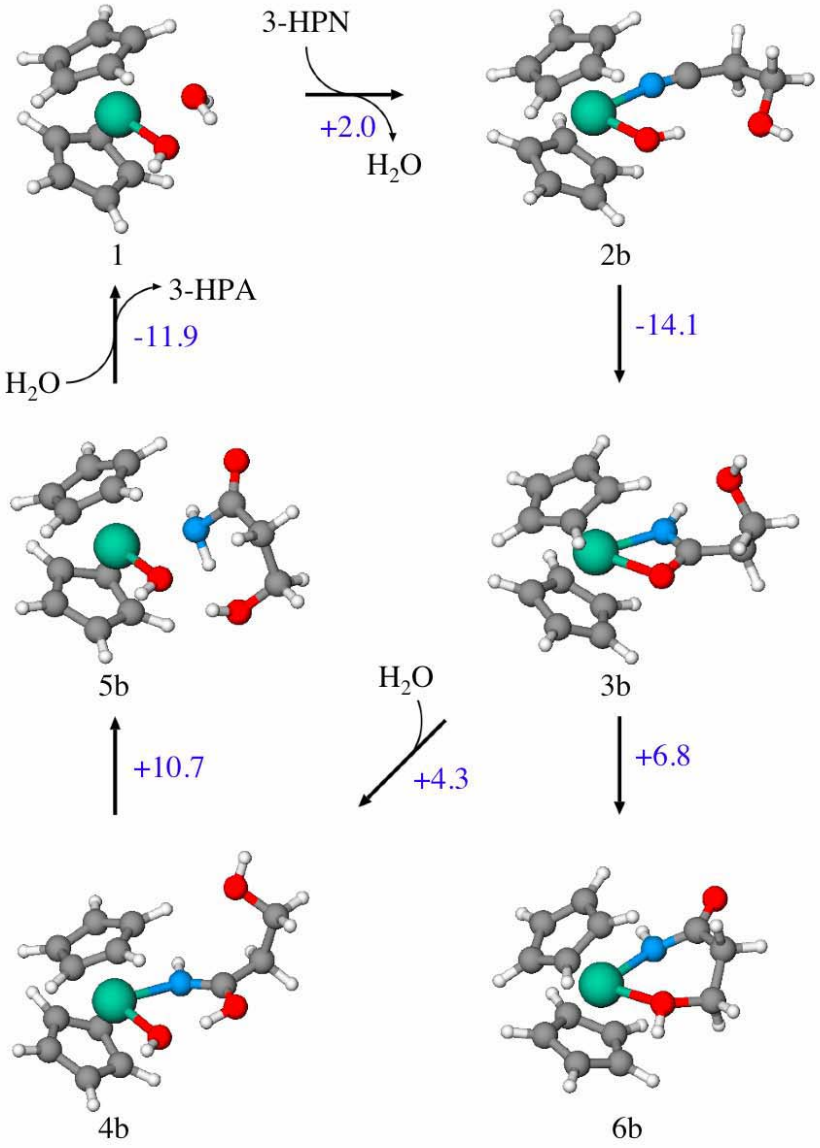

Figure 10. Calculated intermediate structures for the hydrolysis of 3-HPN by

$Mo(Cp)_2(OH)OH_2$. Reaction energies are in kcal/mol.

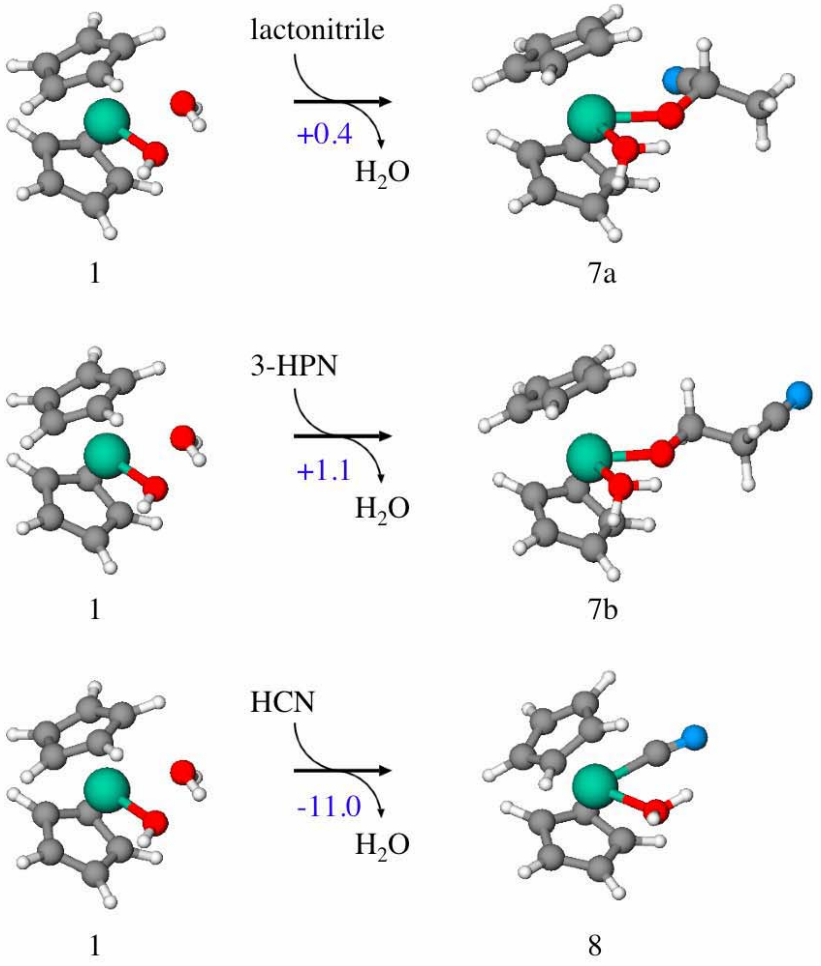

Figure 11. Calculated intermediate structures for the side reactions for nitrile hydrolysis

by $Mo(Cp)_2(OH)OH_2$. Reaction energies are in kcal/mol.

Table 3. Reaction energies (kcal/mol) for the formation of various intermediates in the molybdocene-mediated hydrolysis of lactonitrile. ΔE_{gas} are the gas-phase electronic energies, ΔE_{sol} are the solution phase energies (electronic plus solvation), and ΔG are the free energies (solution phase plus thermal corrections plus entropy) at 298.15 K.

Hydrolysis of lactonitrile by $MoCp_2(OH)(OH_2)$:	ΔE_{gas}	ΔE_{sol}	ΔG
1 + lactonitrile → 2a + H_2O	-0.4	1.5	1.0
2a → 3a	-25.0	-19.9	-15.9
3a + H_2O → 4a	-16.3	-11.2	1.3
4a → 5a	13.8	6.5	9.1
5a + H_2O → 1 + 2-HPA	-5.1	-5.4	-10.1
Cyclic side-reaction:			
3a → 6a	9.3	-1.7	-0.5

Table 4. Reaction energies (kcal/mol) for the formation of various intermediates in the molybdocene-mediated hydrolysis of 3-HPN. ΔE_{gas} are the gas-phase electronic energies, ΔE_{sol} are the solution phase energies (electronic plus solvation), and ΔG are the free energies (solution phase plus thermal corrections plus entropy) at 298.15 K.

Hydrolysis of 3-HPN by $MoCp_2(OH)(OH_2)$:	ΔE_{gas}	ΔE_{sol}	ΔG
1 + 3-HPN → 2b + H_2O	-2.1	1.6	2.0
2b → 3b	-21.4	-18.3	-14.1
3b + H_2O → 4b	-13.9	-8.3	4.3
4b → 5b	13.6	9.2	10.7
5b + H_2O → 1 + 3-HPA	-2.1	-5.6	-11.9
Cyclic side-reaction:			
3b → 6b	19.0	6.6	6.8

Table 5. Reaction energies (kcal/mol) for the formation of various side-reactions in the molybdocene-mediated hydrolysis of lactonitrile and 3-HPN. ΔE_{gas} are the gas-phase electronic energies, ΔE_{sol} are the solution phase energies (electronic plus solvation), and ΔG are the free energies (solution phase plus thermal corrections plus entropy) at 298.15 K.

Binding of hydroxyl group of lactonitrile to Mo:	ΔE_{gas}	ΔE_{sol}	ΔG
1 + lactonitrile $\rightarrow$ $MoCp_2(OH)(OHCHCH_3CN)$ + H_2O	3.8	4.3	5.2
$MoCp_2(OH)(OHCHCH3CN)$ $\rightarrow$ 7a	0.7	-1.5	0.4
Binding of hydroxyl group of 3-HPN to Mo:			
1 + 3-HPN $\rightarrow$ $MoCp_2(OH)(OHCH_2CH_2CN)$ + H_2O	6.8	3.2	3.7
$MoCp_2(OH)(NCCH_2CH_2OH)$ $\rightarrow$ 7b	5.8	0.5	1.1
Reactions with HCN:			
1 + HCN $\rightarrow$ $MoCp_2(OH)(NCH)$ + H_2O	6.6	5.5	3.8
1 + HCN $\rightarrow$ 8 + H_2O	2.1	-10.5	-11.0

D.7. NWChem inputs.

Sample NWChem inputs are listed below. The first is a typical input for a geometry optimization used in this work. The second input is for a vibrational frequency calculation, which was performed on the optimized geometry. The third input is for calculating the single-point energies (including the solvent contribution) of the optimized structures. For brevity, only the coordinates of the Fe are given in the optimization and frequency calculations, but the complete coordinates are given for the single-point energy (and bond-order) calculation.

==========

===

```
Title "MoCp2OHOH2_opt"

Start MoCp2OHOH2_opt

echo

charge 1

geometry noautosym noautoz units angstrom
…
end

ecce_print ecce.out

basis "ao basis" spherical print
  H library "6-31G*"
  O library "6-31G*"
  C library "6-31G*"
  Mo library "Stuttgart RSC 1997 ECP"
  Mo    F
        0.33800000         1.00000000
END
ECP
  Mo library "Stuttgart RSC 1997 ECP"
END
```

```
dft
  mult 1
  direct
  noio
  XC b3lyp
  iterations 300
  mulliken
  grid fine
  convergence energy 1e-7 density 1e-6 gradient 5e-5
  tolerances accCoul 9
end

driver
  gmax 0.000045
  grms 0.00003
  xmax 0.00018
  xrms 0.00012
  maxiter 200
end

task dft optimize
================================================================================
Title "MoCp2OHOH2_frq"

Start MoCp2OHOH2_frq

echo

Memory 250 mw

charge 1

geometry autosym noautoz units angstrom
 C     -0.52055523    -2.26171620     0.23658269
 C      0.33437865    -1.83594715     1.31548309
 C      1.56475130    -1.46024323     0.72572662
 C      1.47789653    -1.65177423    -0.69443006
 C      0.20493691    -2.17711155    -0.98493578
 Mo    -0.15405915    -0.01431887    -0.02675386
 C      0.80199408     1.74201229     1.16646656
 C     -0.33113065     2.32421186     0.52374804
 C     -0.15618407     2.25613556    -0.87486127
 C      1.07607170     1.60717950    -1.14951263
 C      1.68870593     1.32687172     0.12399047
```

```
 H    -1.54097952   -2.61029515    0.32591787
 H     0.11776537   -1.87228510    2.37471891
 H     2.43243320   -1.10487365    1.26374310
 H     2.25936888   -1.44162008   -1.41347657
 H    -0.17980219   -2.41107948   -1.96810318
 H     0.98962302    1.71270241    2.23105895
 H    -1.21552547    2.69338898    1.02570718
 H    -0.88774322    2.56260853   -1.60975512
 H     1.51715317    1.45460075   -2.12540291
 H     2.68605578    0.93481302    0.25817222
 O    -1.75151084   -0.04910450   -1.27128626
 H    -1.60404421   -0.05470349   -2.22829320
 O    -2.09333015    0.18517271    1.07196952
 H    -2.69923918    0.05005139    0.30136820
 H    -2.34369822   -0.41064471    1.79651382
end

ecce_print ecce.out

basis "ao basis" spherical print
  H library "6-31G*"
  O library "6-31G*"
  C library "6-31G*"
  Mo library "Stuttgart RSC 1997 ECP"
  Mo    F
        0.33800000         1.00000000
END
ECP
  Mo library "Stuttgart RSC 1997 ECP"
END

dft
  mult 1
  direct
  noio
  XC b3lyp
  iterations 300
  mulliken
  grid fine
  tolerances accCoul 9
end

task dft energy
task dft freq
```

```
================================================================================
Title "MoCp2OHOH2_snrg"

Start MoCp2OHOH2_snrg

echo

charge 1

geometry autosym noautoz units angstrom
 C     -0.52055523    -2.26171620     0.23658269
 C      0.33437865    -1.83594715     1.31548309
 C      1.56475130    -1.46024323     0.72572662
 C      1.47789653    -1.65177423    -0.69443006
 C      0.20493691    -2.17711155    -0.98493578
 Mo    -0.15405915    -0.01431887    -0.02675386
 C      0.80199408     1.74201229     1.16646656
 C     -0.33113065     2.32421186     0.52374804
 C     -0.15618407     2.25613556    -0.87486127
 C      1.07607170     1.60717950    -1.14951263
 C      1.68870593     1.32687172     0.12399047
 H     -1.54097952    -2.61029515     0.32591787
 H      0.11776537    -1.87228510     2.37471891
 H      2.43243320    -1.10487365     1.26374310
 H      2.25936888    -1.44162008    -1.41347657
 H     -0.17980219    -2.41107948    -1.96810318
 H      0.98962302     1.71270241     2.23105895
 H     -1.21552547     2.69338898     1.02570718
 H     -0.88774322     2.56260853    -1.60975512
 H      1.51715317     1.45460075    -2.12540291
 H      2.68605578     0.93481302     0.25817222
 O     -1.75151084    -0.04910450    -1.27128626
 H     -1.60404421    -0.05470349    -2.22829320
 O     -2.09333015     0.18517271     1.07196952
 H     -2.69923918     0.05005139     0.30136820
 H     -2.34369822    -0.41064471     1.79651382
end

ecce_print ecce.out

basis "ao basis" spherical print
  H library "6-311G**"
  O library "6-311G**"
  C library "6-311G**"
```

```
  Mo library "Stuttgart RSC 1997 ECP"
  Mo    F
        0.33800000          1.00000000
END
ECP
  Mo library "Stuttgart RSC 1997 ECP"
END

dft
  mult 1
  direct
  noio
  XC b3lyp
  iterations 300
  mulliken
  grid fine
end

cosmo
  rsolv 0.2
  radius 1.635
         1.635
         1.635
         1.635
         1.635
         2.000
         1.635
         1.635
         1.635
         1.635
         1.635
         1.172
         1.172
         1.172
         1.172
         1.172
         1.172
         1.172
         1.172
         1.172
         1.172
         1.576
         1.172
         1.576
         1.172
```

```
        1.172
end

property
  mulliken
  dipole
  quadrupole
end

task dft property
```

D.8. Coordinates

The complete Cartesian coordinates for all optimized structures are provided below.

==========

MoCp2OHOH2

C	-0.52055523	-2.26171620	0.23658269
C	0.33437865	-1.83594715	1.31548309
C	1.56475130	-1.46024323	0.72572662
C	1.47789653	-1.65177423	-0.69443006
C	0.20493691	-2.17711155	-0.98493578
Mo	-0.15405915	-0.01431887	-0.02675386
C	0.80199408	1.74201229	1.16646656
C	-0.33113065	2.32421186	0.52374804
C	-0.15618407	2.25613556	-0.87486127
C	1.07607170	1.60717950	-1.14951263
C	1.68870593	1.32687172	0.12399047
H	-1.54097952	-2.61029515	0.32591787
H	0.11776537	-1.87228510	2.37471891
H	2.43243320	-1.10487365	1.26374310
H	2.25936888	-1.44162008	-1.41347657
H	-0.17980219	-2.41107948	-1.96810318
H	0.98962302	1.71270241	2.23105895
H	-1.21552547	2.69338898	1.02570718
H	-0.88774322	2.56260853	-1.60975512
H	1.51715317	1.45460075	-2.12540291
H	2.68605578	0.93481302	0.25817222
O	-1.75151084	-0.04910450	-1.27128626
H	-1.60404421	-0.05470349	-2.22829320
O	-2.09333015	0.18517271	1.07196952
H	-2.69923918	0.05005139	0.30136820
H	-2.34369822	-0.41064471	1.79651382

MoCp2OH-NCCHOHCH3

C	2.16861357	0.11645714	-0.40368072
C	1.97267039	0.59535038	0.94240461
C	1.68221957	1.97976404	0.83131173
C	1.68723544	2.34754177	-0.56505144
C	2.03769906	1.20270271	-1.30268571
Mo	-0.06327998	0.77819622	-0.12963522
C	-1.54172519	0.91954129	1.63952122
C	-2.31094167	0.49871036	0.49513549
C	-2.35945165	1.55662196	-0.44355690
C	-1.57475537	2.61757048	0.04441013
C	-1.09811620	2.23732229	1.35349392
H	2.39808550	-0.90187925	-0.68648176
H	2.11449833	0.03318851	1.85494268
H	1.55494471	2.66382389	1.65651757
H	1.50536296	3.33487449	-0.96857007
H	2.05640934	1.13116393	-2.38071532
H	-1.41433638	0.37795963	2.56652453
H	-2.79018998	-0.46325298	0.37554847
H	-2.79766123	1.50201909	-1.42974432
H	-1.40682562	3.56578245	-0.44887162
H	-0.56016059	2.88196722	2.03170626
O	-0.47612246	0.37217324	-2.06062282
H	-0.56081709	-0.57944066	-2.23473106
N	-0.20385071	-1.33743760	0.06539836
C	-0.25519038	-2.49334246	0.14890759
C	-0.24696417	-3.98807656	0.20145445
C	0.65509583	-4.47892274	1.33719577
H	1.69155472	-4.18466775	1.15071379
H	0.32925214	-4.07767669	2.30134216
H	-1.28328482	-4.30374756	0.38867102
H	0.60305012	-5.57003454	1.36722662
O	0.25229237	-4.48764968	-1.01906294
H	-0.46431895	-4.54457297	-1.67190241

MoCp2OH-NCCH2CH2OH

C	-0.07298	0.37916	-2.31642
C	-1.41435	0.21996	-1.81337
C	-1.50945	-1.12320	-1.36317
C	-0.23914	-1.77894	-1.57423
C	0.61148	-0.85502	-2.20738
Mo	0.00000	0.00000	0.00000
C	-1.43345	0.39748	1.77105

C	-0.10032	0.63706	2.26342
C	0.60981	-0.58635	2.29308
C	-0.21741	-1.59227	1.75978
C	-1.49826	-0.98948	1.47068
H	0.34364	1.28706	-2.73052
H	-2.21355	0.94646	-1.86453
H	-2.40631	-1.60289	-1.00192
H	-0.00317	-2.80998	-1.34525
H	1.65600	-1.01557	-2.43435
H	-2.24719	1.10864	1.73982
H	0.29270	1.59441	2.57713
H	1.65589	-0.70035	2.54023
H	0.04089	-2.63720	1.64777
H	-2.38197	-1.52530	1.15919
O	2.01551	0.00000	0.00000
H	2.38486	0.89117	-0.12804
N	0.35441	2.09850	-0.11616
C	0.74043	3.18312	-0.24204
C	1.36798	4.48774	-0.44636
C	2.87206	4.40831	-0.11732
H	3.33839	5.34231	-0.45644
H	3.01073	4.32681	0.96966
H	1.22703	4.75722	-1.49990
O	3.37841	3.27444	-0.80002
H	4.34360	3.25056	-0.70710
H	0.87079	5.24911	0.16442

MoCp2ONH-CCHOHCH3

C	-0.32645	0.49933	-2.31265
C	-1.38074	-0.32888	-1.83740
C	-0.78001	-1.57675	-1.46111
C	0.63898	-1.49482	-1.66658
C	0.89764	-0.20949	-2.20893
Mo	0.00000	0.00000	0.00000
C	-1.61549	-0.34409	1.63689
C	-0.65176	0.50492	2.24527
C	0.58889	-0.17959	2.30883
C	0.42962	-1.47298	1.74566
C	-0.94661	-1.58196	1.35123
H	-0.43467	1.51840	-2.65767
H	-2.43666	-0.09724	-1.85763
H	-1.31920	-2.46424	-1.16595
H	1.36359	-2.28339	-1.51735
H	1.87800	0.18779	-2.43586

H	-2.66792	-0.13123	1.50984
H	-0.82398	1.52363	2.56420
H	1.52189	0.23788	2.66300
H	1.18115	-2.24916	1.70319
H	-1.42449	-2.48092	0.99193
O	1.88289	1.08272	0.11401
N	0.00000	2.14686	0.00000
C	1.30071	2.24235	0.06601
C	2.09065	3.53414	0.07235
C	3.00957	3.63328	1.29491
H	2.42124	3.65085	2.21828
H	3.70683	2.79127	1.32633
H	2.70961	3.52763	-0.84085
H	-0.56816	2.98485	-0.05143
H	3.59731	4.55643	1.24471
O	1.11556	4.56396	0.01670
H	1.56424	5.42364	0.03225

MoCp2ONH-CCH2CH2OH

C	2.18779509	1.16394891	1.01236526
C	1.27551402	2.23712029	1.20801568
C	0.95800588	2.74573333	-0.09727687
C	1.64762888	1.96197327	-1.08551323
C	2.41095971	0.99711047	-0.37792609
Mo	0.06905179	0.65985960	0.01060016
C	-1.99090613	1.85313463	0.36041718
C	-2.19867681	0.50842931	0.71882741
C	-1.95506068	-0.29751984	-0.43761472
C	-1.63759831	0.56874077	-1.53944143
C	-1.65443568	1.89199575	-1.03418970
H	2.60476196	0.54322747	1.79314653
H	0.95954109	2.64550571	2.15802257
H	0.35495790	3.62051935	-0.29439346
H	1.64599308	2.11617128	-2.15585206
H	3.00708409	0.21620539	-0.83063180
H	-2.06396686	2.70768402	1.02109648
H	-2.45175640	0.14464341	1.70560511
H	-2.00337500	-1.37965697	-0.46841116
H	-1.45014383	0.26889319	-2.56113442
H	-1.45721139	2.78689523	-1.60924668
O	0.72391061	-1.24562060	-0.77449706
N	0.34170983	-1.00448782	1.33596192
C	0.63960783	-1.84436803	0.37434192
C	0.82283011	-3.33142304	0.48388511

C	-0.21621246	-4.07006683	-0.36634080
H	-0.05252488	-3.84449966	-1.42840727
H	-0.09424379	-5.15029461	-0.21630067
H	1.82649124	-3.59295822	0.12729779
O	-1.50309759	-3.62773412	0.06266815
H	-2.17696672	-4.19600183	-0.34225126
H	0.73762451	-3.63693588	1.53145457
H	0.18000381	-1.31638639	2.28613177

MoCp2OH2ONH-CCHOHCH3

C	-2.30818902	0.54516980	-0.37057709
C	-1.70275092	1.32223148	-1.40245637
C	-1.26995880	2.54258789	-0.78982329
C	-1.56202014	2.48748461	0.61688098
C	-2.22964275	1.25460600	0.84610691
Mo	0.03833598	0.88414971	0.07599869
C	1.76761964	0.86404266	-1.43533415
C	2.27930181	0.26640837	-0.23315081
C	2.33973575	1.25490740	0.77872879
C	1.82500516	2.46034919	0.26176969
C	1.49712403	2.22613042	-1.11984672
H	-2.71982154	-0.44721684	-0.48994529
H	-1.67651379	1.07913474	-2.45600163
H	-0.87637631	3.40431487	-1.30666270
H	-1.40365045	3.27609305	1.34006791
H	-2.55040028	0.87768418	1.80755845
H	1.70352884	0.40036276	-2.41018569
H	2.56421521	-0.76877237	-0.11146567
H	2.62927038	1.07815536	1.80541016
H	1.73806577	3.39956768	0.79210774
H	1.17464303	2.97673272	-1.82559715
O	-0.31552883	-2.33345640	1.67412401
N	-0.13261244	-1.25688947	-0.35430859
C	-0.27811981	-2.32795589	0.37332184
C	-0.42411397	-3.69985235	-0.26813981
C	0.74253215	-4.61724120	0.11431925
H	1.68849476	-4.21691349	-0.26589568
H	0.80951392	-4.72526088	1.19998160
H	-1.36227431	-4.12221677	0.12349381
H	-0.14532543	-1.50904360	-1.34116199
H	0.58929391	-5.61301005	-0.31622740
O	-0.51866931	-3.47864528	-1.66880880
H	-0.49308415	-4.33340990	-2.12546496
O	0.07942610	0.07809282	1.98318430

H	-0.17369267	-1.35842365	2.00717163
H	0.03835195	0.69448156	2.72763533

MoCp2OH2ONH-CCH2CH2OH

C	-0.15592	-0.33075	-2.27082
C	1.21882	-0.51379	-1.88621
C	1.69186	0.75119	-1.45573
C	0.63191	1.71170	-1.58792
C	-0.48845	1.04525	-2.11288
Mo	0.00000	0.00000	0.00000
C	1.60102	-0.30575	1.66050
C	0.38829	-0.72758	2.27994
C	-0.49562	0.37066	2.33799
C	0.13096	1.50682	1.75309
C	1.45183	1.08985	1.36765
H	-0.82436	-1.10055	-2.62916
H	1.79964	-1.42152	-1.97593
H	2.69584	0.95810	-1.11193
H	0.68711	2.76255	-1.33200
H	-1.46344	1.48214	-2.28060
H	2.49350	-0.90254	1.52916
H	0.15180	-1.73987	2.58505
H	-1.51157	0.33199	2.70476
H	-0.27267	2.50961	1.70230
H	2.22610	1.74633	0.99813
O	-2.65891	-2.34217	0.44781
N	-0.41916	-2.14769	-0.00265
C	-1.48149	-2.86413	0.26792
C	-1.40855	-4.35958	0.45325
C	-1.43871	-4.72041	1.94210
H	-2.39011	-4.39370	2.38404
H	-1.36671	-5.81186	2.04034
H	-2.27255	-4.81646	-0.03989
O	-0.32780	-4.07363	2.56925
H	-0.29956	-4.36232	3.49637
H	-0.49532	-4.75571	-0.00369
H	0.41053	-2.72867	-0.06791
O	-2.07824	0.00000	0.00000
H	-2.51238	0.83098	0.23996
H	-2.59125	-1.30526	0.30878

MoCp2OHNH2-OCCHOHCH3

C	1.71336417	1.19161096	1.45814569

C	1.19551693	2.46506425	1.12370387
C	1.40564642	2.69885237	-0.27740305
C	2.07350549	1.58113253	-0.80755923
C	2.23836831	0.62925313	0.23924119
Mo	-0.04114319	0.78876649	0.00001932
C	-1.89417717	1.36201272	1.30949542
C	-2.35697434	0.28244747	0.50170969
C	-2.29318619	0.66511913	-0.85618918
C	-1.78172196	1.98795414	-0.93840163
C	-1.56740788	2.43017424	0.41617234
H	1.77485303	0.76657264	2.45118722
H	0.73699657	3.15575090	1.81784214
H	1.10995938	3.58398840	-0.82614524
H	2.35593668	1.43842600	-1.84166439
H	2.71111733	-0.33808933	0.12530851
H	-1.88911411	1.39862459	2.39084683
H	-2.65447853	-0.69889079	0.84819795
H	-2.51982815	0.01801914	-1.69221986
H	-1.68197463	2.58485253	-1.83525101
H	-1.28083118	3.43127158	0.70359502
O	-1.75805115	-2.72458715	0.36839460
N	0.04994210	-1.36796983	0.90494822
C	-0.58763569	-2.49197160	0.20322130
C	0.37800702	-3.30688781	-0.65831580
C	0.69799882	-4.63555242	0.03276740
H	1.21334797	-4.46946207	0.98530601
H	-0.21708158	-5.20509133	0.21551718
H	-0.14644672	-3.50492522	-1.60296509
H	1.35950744	-5.21698795	-0.61448755
O	1.57906709	-2.58921171	-0.87136450
H	1.31248664	-1.80795593	-1.41178385
O	0.18433744	-0.44184484	-1.62151762
H	0.13641038	0.01917648	-2.47250029
H	1.05059119	-1.57723705	0.94076730
H	-0.33713970	-1.30616920	1.84618138

MoCp2OHNH2-OCCH2CH2OH

C	-1.25283	0.578828	-1.85614
C	-1.70926	-0.699926	-1.44916
C	-0.646425	-1.65297	-1.62377
C	0.453662	-0.968823	-2.16927
C	0.111651	0.405651	-2.28296
Mo	0.00000	0.00000	0.00000
C	-1.63638	0.226252	1.67628

C	-0.428430	0.632386	2.30650
C	0.474300	-0.455706	2.31069
C	-0.144081	-1.57015	1.67984
C	-1.47197	-1.14846	1.31702
H	-1.84668	1.48034	-1.92607
H	-2.70900	-0.927592	-1.10836
H	-0.696239	-2.71108	-1.40077
H	1.42238	-1.39540	-2.39128
H	0.775006	1.17461	-2.65981
H	-2.53220	0.823332	1.57372
H	-0.221320	1.62753	2.67729
H	1.49310	-0.421309	2.67091
H	0.261016	-2.56996	1.59657
H	-2.23645	-1.79541	0.913094
O	0.825487	3.48214	1.95838
N	0.586625	2.28103	0.00667113
C	1.38858	2.93407	1.03998
C	2.88980	2.85126	0.870833
C	3.41747	3.04588	-0.566196
H	3.18884	4.04984	-0.937297
H	4.50822	2.93484	-0.554657
H	3.33132	3.59001	1.54570
O	2.05415	0.00000	0.00000
H	2.42949	-0.892609	0.0399102
H	3.18876	1.85391	1.22118
O	2.82631	2.13231	-1.49511
H	2.85055	1.23483	-1.08396
H	1.13171	2.32630	-0.872676
H	-0.296210	2.78879	-0.0580966

MoCp2OH-OHCHCH3CN

C	-0.27162	0.70465	-2.29440
C	-1.54089	0.45320	-1.69643
C	-1.56555	-0.94014	-1.37564
C	-0.29605	-1.52439	-1.72441
C	0.47570	-0.49195	-2.32148
Mo	0.00000	0.00000	0.00000
C	-1.17993	0.61832	1.89803
C	0.16523	0.26229	2.27074
C	0.34187	-1.13618	2.07330
C	-0.85185	-1.64755	1.52974
C	-1.79565	-0.56946	1.44014
H	0.08777	1.67282	-2.61548
H	-2.34597	1.16686	-1.58440

H	-2.41647	-1.48782	-0.99816
H	-0.02331	-2.56860	-1.65093
H	1.49897	-0.58156	-2.65909
H	-1.65887	1.58178	2.00492
H	0.92315	0.93262	2.65326
H	1.25354	-1.69142	2.24658
H	-1.03046	-2.67579	1.24208
H	-2.81698	-0.64841	1.09458
O	2.03035	0.00000	0.00000
H	2.50351	-0.84281	-0.05622
C	1.50403	4.42134	-0.01639
C	0.53506	3.35350	0.49170
H	0.56326	3.30686	1.58813
H	1.48603	4.47448	-1.10796
O	0.88017	2.05403	-0.04573
H	2.52052	4.19108	0.31971
C	-0.85419	3.61108	0.08008
N	-1.95318	3.79529	-0.24130
H	1.22471	5.39798	0.38961
H	1.83620	1.81806	0.05563

MoCp2OH-OHCH2CH2CN

C	-0.26067	0.82950	-2.25350
C	-1.53270	0.54440	-1.67561
C	-1.55841	-0.86463	-1.43103
C	-0.28794	-1.42768	-1.80807
C	0.48544	-0.36417	-2.34504
Mo	0.00000	0.00000	0.00000
C	-1.18336	0.49779	1.92932
C	0.16359	0.13192	2.28394
C	0.35135	-1.25115	2.00721
C	-0.83639	-1.74102	1.43253
C	-1.78900	-0.66727	1.40263
H	0.10269	1.81316	-2.51829
H	-2.34903	1.24129	-1.54300
H	-2.41148	-1.43283	-1.09058
H	-0.01577	-2.47458	-1.79237
H	1.51017	-0.43454	-2.68280
H	-1.66801	1.44819	2.10459
H	0.91359	0.78520	2.70895
H	1.26680	-1.80811	2.15256
H	-1.00607	-2.75253	1.08618
H	-2.80975	-0.73754	1.05339
O	2.02847	0.00000	0.00000

H	2.50185	-0.83924	-0.09524
C	1.32955	4.44830	0.25761
C	0.52636	3.25333	0.79557
H	0.71295	3.11206	1.86553
H	1.13860	4.57837	-0.81386
O	0.86586	2.05722	0.06708
H	2.40621	4.27595	0.38298
H	1.81404	1.78821	0.15498
H	-0.54198	3.40642	0.63852
C	0.95191	5.66767	0.97511
N	0.61973	6.60740	1.56806

MoCp2OH2-OCH3CHCN

C	-0.64022	0.79605	-2.21940
C	-1.75466	0.23594	-1.55628
C	-1.45930	-1.15764	-1.34103
C	-0.13943	-1.43089	-1.80971
C	0.35508	-0.19826	-2.34975
Mo	0.00000	0.00000	0.00000
C	-1.08693	0.51248	1.97635
C	0.28083	0.18872	2.25329
C	0.48246	-1.20649	1.99195
C	-0.73140	-1.73459	1.52198
C	-1.69731	-0.67553	1.49996
H	-0.53199	1.83748	-2.48611
H	-2.67081	0.75760	-1.31491
H	-2.14513	-1.89001	-0.93959
H	0.34531	-2.39700	-1.85221
H	1.33359	-0.04454	-2.78783
H	-1.57987	1.46282	2.12570
H	1.03575	0.87243	2.61683
H	1.41540	-1.74392	2.09562
H	-0.89875	-2.75621	1.20589
H	-2.73152	-0.76785	1.19528
O	2.23786	0.00000	0.00000
H	2.77454	-0.47674	-0.65392
C	1.12559	4.28485	-0.08194
C	0.23202	3.13343	0.39664
H	0.17081	3.17199	1.49688
H	1.19062	4.29367	-1.17371
O	0.77704	1.89801	-0.01351
H	2.12898	4.15586	0.33453
C	-1.15573	3.29214	-0.10541
N	-2.24432	3.35474	-0.50473

H	0.72812	5.24702	0.25534
H	2.35816	0.97711	-0.10607

MoCp2OH2-OCH2CH2CN

C	2.27491	0.35910	0.06400
C	2.04865	-0.30008	-1.16496
C	1.96481	-1.71001	-0.87684
C	2.07453	-1.90311	0.53173
C	2.26071	-0.60086	1.10025
Mo	0.10595	-0.76445	0.08670
C	-1.47351	-0.57003	-1.57869
C	-2.14286	-0.85693	-0.34746
C	-1.81745	-2.19269	0.04955
C	-0.93000	-2.72600	-0.90051
C	-0.70798	-1.72573	-1.90078
H	2.34627	1.42938	0.20184
H	2.02811	0.16067	-2.14385
H	1.89148	-2.49862	-1.61192
H	2.12402	-2.84956	1.05294
H	2.36833	-0.37676	2.15444
H	-1.57035	0.32253	-2.18042
H	-2.79027	-0.18194	0.19497
H	-2.15318	-2.68269	0.95371
H	-0.47524	-3.70769	-0.86643
H	-0.09336	-1.83979	-2.78366
O	-0.54957	-0.76353	2.22539
H	-0.03280	-1.15041	2.95096
C	-0.65370	3.48271	0.88924
C	-0.54986	2.25796	-0.04248
H	-1.46943	2.18809	-0.64144
H	0.25057	3.56097	1.50463
O	-0.36563	1.09820	0.73483
H	-1.50363	3.36008	1.57085
H	0.28651	2.40472	-0.74096
C	-0.82145	4.71306	0.11360
N	-0.94854	5.66094	-0.54333
H	-0.61931	0.21657	2.33874

MoCp2OH2-CN

C	0.60044487	2.21218820	-0.00679316
C	0.04152338	1.94853134	1.28336892
C	-1.31730263	1.61751653	1.09572484
C	-1.62186163	1.73196009	-0.30263032

C	-0.44646047	2.10331941	-0.98918952
Mo	0.00653646	0.01130591	-0.06913434
C	-1.08257022	-1.61947174	1.17234602
C	0.04056289	-2.30051857	0.62916802
C	-0.06342493	-2.27171512	-0.78268814
C	-1.26363710	-1.59629371	-1.15545063
C	-1.90666422	-1.21340297	0.06794694
H	1.62908826	2.48426406	-0.19962495
H	0.57592339	1.96146521	2.22328730
H	-2.01465407	1.33934507	1.87569529
H	-2.58963560	1.55802399	-0.75523529
H	-0.35562789	2.29454840	-2.04979008
H	-1.30391880	-1.50303476	2.22473395
H	0.85641149	-2.72805445	1.19519811
H	0.67159592	-2.68188827	-1.46399481
H	-1.66187719	-1.49124730	-2.15576282
H	-2.87869431	-0.74735483	0.14953627
O	1.59600583	0.03610267	-1.65126021
H	2.47755487	-0.22596123	-1.31782340
C	1.81668467	-0.24703547	0.96438084
N	2.91484820	-0.37946405	1.34562095
H	1.48431757	-0.29138125	-2.55854468

==========
===

D.9. NWChem partial output

Total gas phase and solution phase energies, and gross orbital populations from NWChem outputs are listed below for structures.

The Mulliken population analysis listed here gives the total atomic charge and each individual shell charge for each atom in the system. Each shell charge represents the contributions of all atomic orbitals (basis functions) in a particular shell to the total charge of the atom. For instance, a P shell is the sum of atomic orbitals $p_x + p_y + p_z$. The shell charges are read as follows:

Mo: columns 1-6 are S shells, 7-11 are P shells, 12-14 are D shells, 15 is F
O: 1 S, 2 S, 3 P, 4 S, 5 P, 6 S, 7 P, 8 is D
N: 1 S, 2 S, 3 P, 4 S, 5 P, 6 S, 7 P, 8 is D
C: 1 S, 2 S, 3 P, 4 S, 5 P, 6 S, 7 P, 8 D
H: (1-3) S, 4 P

==========

MoCp2OHOH2

gas phase energy = -607.5319163602
sol phase energy = -607.6155373340

Total Density - Mulliken Population Analysis

Atom	Charge	Shell Charges
1 C 6	6.10	1.10 0.89 0.64 0.77 1.50 0.48 0.66 0.06
2 C 6	6.10	1.10 0.89 0.64 0.76 1.49 0.50 0.65 0.06
3 C 6	6.10	1.10 0.89 0.64 0.77 1.48 0.51 0.65 0.06
4 C 6	6.07	1.10 0.89 0.64 0.77 1.48 0.49 0.64 0.06
5 C 6	6.06	1.10 0.89 0.64 0.77 1.48 0.48 0.63 0.06
6 Mo 14	13.76	-0.41 1.48 0.91 0.38 0.06 0.01 0.72 4.75 0.71 0.15 0.06 3.55 1.06 0.16 0.16

7 C	6	6.11	1.10	0.89	0.64	0.76	1.49	0.50	0.66	0.06
8 C	6	6.06	1.10	0.89	0.64	0.78	1.48	0.48	0.63	0.06
9 C	6	6.04	1.10	0.89	0.64	0.78	1.47	0.47	0.63	0.06
10 C	6	6.10	1.10	0.89	0.64	0.77	1.49	0.50	0.66	0.06
11 C	6	6.10	1.10	0.89	0.64	0.77	1.48	0.50	0.66	0.07
12 H	1	0.83	0.27	0.46	0.07	0.03				
13 H	1	0.84	0.27	0.47	0.08	0.03				
14 H	1	0.83	0.27	0.46	0.07	0.03				
15 H	1	0.84	0.27	0.46	0.08	0.03				
16 H	1	0.83	0.27	0.46	0.07	0.03				
17 H	1	0.85	0.27	0.47	0.08	0.03				
18 H	1	0.83	0.27	0.46	0.07	0.02				
19 H	1	0.84	0.27	0.46	0.07	0.03				
20 H	1	0.84	0.27	0.46	0.08	0.03				
21 H	1	0.83	0.28	0.46	0.07	0.03				
22 O	8	8.61	1.08	0.91	0.98	0.99	2.01	0.86	1.77	0.01
23 H	1	0.71	0.27	0.33	0.05	0.06				
24 O	8	8.45	1.08	0.91	0.99	0.99	2.06	0.79	1.62	0.01
25 H	1	0.65	0.25	0.31	0.03	0.06				
26 H	1	0.65	0.26	0.31	0.02	0.06				

MoCp2OH-NCCHOHCH3

gas phase energy = -778.4297009715
sol phase energy = -778.5145325798

Total Density - Mulliken Population Analysis

Atom		Charge	Shell Charges							
1 C	6	6.11	1.10	0.89	0.64	0.77	1.49	0.49	0.67	0.06
2 C	6	6.11	1.10	0.89	0.64	0.76	1.49	0.50	0.65	0.06
3 C	6	6.10	1.10	0.89	0.64	0.77	1.48	0.50	0.66	0.06
4 C	6	6.09	1.10	0.89	0.64	0.77	1.48	0.49	0.66	0.06
5 C	6	6.00	1.10	0.89	0.64	0.78	1.47	0.45	0.61	0.06
6 Mo	14	13.75	-0.41	1.48	0.91	0.41	0.00	0.02	0.72	4.75
0.72	0.12	0.06	3.55	1.12	0.12	0.17				
7 C	6	6.11	1.10	0.89	0.64	0.76	1.49	0.50	0.66	0.06
8 C	6	6.09	1.10	0.89	0.64	0.77	1.49	0.48	0.65	0.06
9 C	6	6.00	1.10	0.89	0.64	0.78	1.47	0.45	0.60	0.06
10 C	6	6.11	1.10	0.89	0.64	0.77	1.48	0.50	0.66	0.06
11 C	6	6.11	1.10	0.89	0.64	0.77	1.48	0.51	0.66	0.06

12 H	1	0.83	0.27	0.46	0.07	0.03					
13 H	1	0.85	0.27	0.47	0.08	0.03					
14 H	1	0.83	0.27	0.46	0.07	0.03					
15 H	1	0.84	0.27	0.47	0.08	0.03					
16 H	1	0.84	0.27	0.46	0.07	0.03					
17 H	1	0.85	0.27	0.47	0.08	0.03					
18 H	1	0.84	0.27	0.46	0.08	0.03					
19 H	1	0.84	0.27	0.46	0.07	0.03					
20 H	1	0.84	0.27	0.46	0.08	0.03					
21 H	1	0.83	0.28	0.46	0.07	0.03					
22 O	8	8.55	1.08	0.91	0.98	1.00	2.00	0.86	1.72	0.01	
23 H	1	0.73	0.27	0.35	0.06	0.06					
24 N	7	7.36	1.09	0.90	0.77	0.91	1.67	0.80	1.18	0.03	
25 C	6	5.69	1.10	0.88	0.64	0.81	1.33	0.30	0.55	0.07	
26 C	6	5.94	1.10	0.89	0.62	0.77	1.51	0.35	0.59	0.12	
27 C	6	6.29	1.10	0.89	0.66	0.75	1.53	0.46	0.86	0.04	
28 H	1	0.86	0.27	0.46	0.10	0.02					
29 H	1	0.86	0.27	0.46	0.10	0.02					
30 H	1	0.81	0.27	0.45	0.06	0.02					
31 H	1	0.86	0.27	0.46	0.10	0.02					
32 O	8	8.41	1.08	0.91	0.98	1.00	2.03	0.82	1.56	0.01	
33 H	1	0.70	0.26	0.34	0.04	0.06					

MoCp2OH-NCCH2CH2OH

gas phase energy = -778.4364384657
sol phase energy = -778.5179585441

Total Density - Mulliken Population Analysis

Atom	Charge	Shell Charges								
1 C 6	6.10	1.10	0.89	0.64	0.77	1.49	0.49	0.66	0.06	
2 C 6	6.10	1.10	0.89	0.64	0.76	1.49	0.50	0.65	0.06	
3 C 6	6.10	1.10	0.89	0.64	0.77	1.48	0.51	0.66	0.06	
4 C 6	6.11	1.10	0.89	0.64	0.77	1.48	0.50	0.66	0.06	
5 C 6	6.00	1.10	0.89	0.64	0.78	1.47	0.46	0.60	0.07	
6 Mo 14	13.75	-0.41	1.48	0.91	0.41	0.00	0.02	0.72	4.75	0.72	0.11	0.07	3.55	1.12	0.12	0.17
7 C 6	6.10	1.10	0.89	0.64	0.76	1.49	0.50	0.65	0.06	
8 C 6	6.10	1.10	0.89	0.64	0.77	1.48	0.49	0.66	0.06	
9 C 6	6.00	1.10	0.89	0.64	0.78	1.47	0.46	0.60	0.07	

10 C	6	6.11	1.10	0.89	0.64	0.77	1.48	0.50	0.67	0.06
11 C	6	6.10	1.10	0.89	0.64	0.77	1.48	0.51	0.66	0.06
12 H	1	0.83	0.27	0.46	0.07	0.03				
13 H	1	0.85	0.27	0.47	0.08	0.03				
14 H	1	0.84	0.28	0.46	0.07	0.03				
15 H	1	0.84	0.27	0.46	0.08	0.03				
16 H	1	0.83	0.27	0.46	0.07	0.02				
17 H	1	0.85	0.27	0.47	0.08	0.03				
18 H	1	0.83	0.27	0.46	0.07	0.03				
19 H	1	0.83	0.27	0.46	0.07	0.02				
20 H	1	0.84	0.27	0.46	0.08	0.03				
21 H	1	0.84	0.28	0.46	0.07	0.03				
22 O	8	8.55	1.08	0.91	0.97	1.00	2.00	0.86	1.72	0.01
23 H	1	0.76	0.27	0.35	0.07	0.06				
24 N	7	7.36	1.09	0.90	0.77	0.91	1.67	0.80	1.17	0.03
25 C	6	5.72	1.10	0.88	0.65	0.80	1.33	0.32	0.56	0.08
26 C	6	6.18	1.10	0.89	0.65	0.76	1.56	0.40	0.77	0.06
27 C	6	6.01	1.10	0.89	0.62	0.77	1.49	0.38	0.67	0.09
28 H	1	0.86	0.28	0.47	0.09	0.02				
29 H	1	0.86	0.28	0.48	0.09	0.02				
30 H	1	0.80	0.27	0.45	0.07	0.02				
31 O	8	8.44	1.08	0.91	0.99	0.99	2.04	0.82	1.60	0.01
32 H	1	0.69	0.26	0.32	0.04	0.06				
33 H	1	0.80	0.27	0.45	0.06	0.02				

MoCp2ONH-CCHOHCH3

gas phase energy = -778.4695893411
sol phase energy = -778.5462768148

Total Density - Mulliken Population Analysis

Atom	Charge	Shell Charges											
1 C	6	6.05	1.10	0.89	0.64	0.78	1.47	0.48	0.62	0.06			
2 C	6	6.12	1.10	0.89	0.64	0.76	1.49	0.51	0.66	0.06			
3 C	6	6.11	1.10	0.89	0.64	0.77	1.48	0.50	0.66	0.07			
4 C	6	6.12	1.10	0.89	0.64	0.76	1.49	0.51	0.66	0.06			
5 C	6	6.05	1.10	0.89	0.64	0.78	1.48	0.48	0.62	0.06			
6 Mo	14	13.70	-0.41	1.48	0.91	0.41	0.06	0.01	0.72	4.75	0.73	0.04	0.06	3.57	1.14	0.06	0.16
7 C	6	6.12	1.10	0.89	0.64	0.76	1.49	0.51	0.66	0.06			

8 C	6	6.05	1.10	0.89	0.64	0.78	1.47	0.48	0.62	0.06
9 C	6	6.04	1.10	0.89	0.64	0.78	1.48	0.48	0.62	0.06
10 C	6	6.11	1.10	0.89	0.64	0.76	1.49	0.51	0.66	0.06
11 C	6	6.11	1.10	0.89	0.64	0.77	1.48	0.51	0.66	0.07
12 H	1	0.83	0.27	0.46	0.07	0.03				
13 H	1	0.84	0.27	0.46	0.08	0.03				
14 H	1	0.83	0.27	0.46	0.07	0.03				
15 H	1	0.84	0.27	0.46	0.08	0.03				
16 H	1	0.83	0.27	0.46	0.08	0.03				
17 H	1	0.84	0.27	0.46	0.08	0.03				
18 H	1	0.83	0.27	0.46	0.07	0.03				
19 H	1	0.83	0.27	0.46	0.08	0.03				
20 H	1	0.84	0.27	0.46	0.08	0.03				
21 H	1	0.83	0.27	0.46	0.07	0.03				
22 O	8	8.44	1.08	0.91	0.97	1.00	2.01	0.90	1.55	0.01
23 N	7	7.47	1.09	0.90	0.80	0.86	1.77	0.73	1.29	0.02
24 C	6	5.54	1.10	0.89	0.62	0.80	1.40	0.29	0.28	0.16
25 C	6	5.97	1.10	0.89	0.62	0.77	1.51	0.35	0.62	0.11
26 C	6	6.31	1.10	0.89	0.66	0.75	1.53	0.46	0.88	0.04
27 H	1	0.87	0.28	0.46	0.11	0.02				
28 H	1	0.87	0.27	0.46	0.11	0.02				
29 H	1	0.84	0.28	0.47	0.08	0.02				
30 H	1	0.74	0.27	0.38	0.05	0.04				
31 H	1	0.87	0.28	0.46	0.11	0.02				
32 O	8	8.45	1.08	0.91	0.99	0.99	2.04	0.82	1.61	0.01
33 H	1	0.70	0.27	0.34	0.04	0.06				

MoCp2ONH-CCH2CH2OH

gas phase energy = -778.4705552004
sol phase energy = -778.5470517978

Total Density - Mulliken Population Analysis

Atom		Charge	Shell Charges							
1 C	6	6.05	1.10	0.89	0.64	0.78	1.47	0.49	0.63	0.06
2 C	6	6.11	1.10	0.89	0.64	0.76	1.49	0.50	0.66	0.06
3 C	6	6.11	1.10	0.89	0.64	0.77	1.48	0.50	0.67	0.07
4 C	6	6.11	1.10	0.89	0.64	0.76	1.49	0.50	0.66	0.06
5 C	6	6.03	1.10	0.89	0.64	0.78	1.47	0.48	0.61	0.06

6 Mo 14 13.76 -0.41 1.48 0.91 0.41 0.08 0.02 0.72 4.75 0.73 0.05 0.07 3.58 1.15 0.09 0.16
7 C 6 6.03 1.10 0.89 0.64 0.77 1.47 0.47 0.63 0.06
8 C 6 6.07 1.10 0.89 0.64 0.77 1.47 0.49 0.64 0.06
9 C 6 6.11 1.10 0.89 0.64 0.77 1.49 0.48 0.67 0.06
10 C 6 6.11 1.10 0.89 0.64 0.77 1.49 0.50 0.66 0.06
11 C 6 6.10 1.10 0.89 0.64 0.77 1.47 0.50 0.66 0.06
12 H 1 0.84 0.27 0.46 0.07 0.03
13 H 1 0.84 0.27 0.46 0.08 0.03
14 H 1 0.82 0.27 0.45 0.07 0.03
15 H 1 0.84 0.27 0.46 0.08 0.03
16 H 1 0.84 0.27 0.46 0.08 0.03
17 H 1 0.85 0.27 0.47 0.08 0.03
18 H 1 0.84 0.27 0.46 0.08 0.03
19 H 1 0.85 0.27 0.45 0.10 0.03
20 H 1 0.84 0.27 0.46 0.08 0.03
21 H 1 0.83 0.27 0.46 0.07 0.03
22 O 8 8.45 1.08 0.91 0.97 1.00 2.01 0.89 1.56 0.01
23 N 7 7.48 1.09 0.90 0.80 0.86 1.77 0.74 1.29 0.02
24 C 6 5.55 1.10 0.89 0.62 0.80 1.40 0.30 0.29 0.16
25 C 6 6.25 1.10 0.89 0.65 0.76 1.55 0.44 0.81 0.05
26 C 6 6.02 1.10 0.89 0.63 0.77 1.49 0.38 0.68 0.09
27 H 1 0.87 0.28 0.47 0.09 0.02
28 H 1 0.86 0.28 0.47 0.09 0.02
29 H 1 0.83 0.27 0.45 0.08 0.02
30 O 8 8.45 1.08 0.91 0.98 0.99 2.04 0.83 1.60 0.01
31 H 1 0.70 0.27 0.33 0.04 0.06
32 H 1 0.84 0.28 0.45 0.09 0.02
33 H 1 0.73 0.27 0.38 0.04 0.04

MoCp2OH2ONH-CCHOHCH3

gas phase energy = -854.9430183359
sol phase energy = -855.0220738296

Total Density - Mulliken Population Analysis

Atom		Charge	Shell Charges							
1 C	6	6.06	1.10	0.89	0.64	0.78	1.47	0.48	0.64	0.06
2 C	6	6.11	1.10	0.89	0.64	0.76	1.49	0.49	0.66	0.06
3 C	6	6.10	1.10	0.89	0.64	0.77	1.48	0.50	0.66	0.07

4 C	6	6.12	1.10	0.89	0.64	0.76	1.49	0.50	0.67	0.06				
5 C	6	6.05	1.10	0.89	0.64	0.77	1.48	0.48	0.63	0.06				
6 Mo	14	13.64	-0.41	1.48	0.91	0.39	0.02	0.02	0.72	4.76	0.71	0.09	0.07	3.54
1.05	0.13	0.16												
7 C	6	6.12	1.10	0.89	0.64	0.76	1.49	0.50	0.67	0.06				
8 C	6	6.08	1.10	0.89	0.64	0.77	1.48	0.48	0.66	0.06				
9 C	6	6.04	1.10	0.89	0.64	0.78	1.47	0.47	0.63	0.07				
10 C	6	6.10	1.10	0.89	0.64	0.77	1.48	0.50	0.66	0.06				
11 C	6	6.10	1.10	0.89	0.64	0.77	1.48	0.50	0.66	0.06				
12 H	1	0.84	0.27	0.46	0.08	0.02								
13 H	1	0.85	0.27	0.47	0.08	0.03								
14 H	1	0.83	0.28	0.46	0.07	0.03								
15 H	1	0.84	0.27	0.46	0.08	0.03								
16 H	1	0.83	0.27	0.46	0.07	0.02								
17 H	1	0.85	0.27	0.47	0.08	0.03								
18 H	1	0.84	0.27	0.46	0.08	0.03								
19 H	1	0.83	0.27	0.46	0.07	0.02								
20 H	1	0.84	0.27	0.46	0.08	0.03								
21 H	1	0.83	0.28	0.46	0.07	0.03								
22 O	8	8.39	1.08	0.91	0.99	1.00	2.06	0.82	1.52	0.01				
23 N	7	7.48	1.09	0.90	0.80	0.87	1.76	0.72	1.33	0.03				
24 C	6	5.61	1.10	0.89	0.62	0.80	1.40	0.28	0.36	0.16				
25 C	6	5.95	1.10	0.89	0.62	0.77	1.51	0.34	0.61	0.11				
26 C	6	6.31	1.10	0.89	0.66	0.75	1.53	0.46	0.89	0.04				
27 H	1	0.87	0.28	0.46	0.11	0.02								
28 H	1	0.87	0.27	0.46	0.11	0.02								
29 H	1	0.84	0.28	0.46	0.08	0.02								
30 H	1	0.72	0.27	0.37	0.04	0.04								
31 H	1	0.86	0.28	0.46	0.11	0.02								
32 O	8	8.46	1.08	0.91	0.99	0.99	2.04	0.82	1.61	0.01				
33 H	1	0.69	0.26	0.33	0.04	0.06								
34 O	8	8.66	1.08	0.91	0.98	0.98	2.03	0.86	1.80	0.01				
35 H	1	0.66	0.22	0.31	0.05	0.09								
36 H	1	0.69	0.27	0.32	0.05	0.06								

MoCp2OH2ONH-CCH2CH2OH

gas phase energy = -854.9401504045
sol phase energy = -855.0181416927

Total Density - Mulliken Population Analysis

Atom	Charge	Shell Charges								
1 C	6	6.10	1.10	0.89	0.64	0.77	1.49	0.48	0.66	0.06
2 C	6	6.11	1.10	0.89	0.64	0.76	1.49	0.50	0.66	0.06
3 C	6	6.10	1.10	0.89	0.64	0.77	1.48	0.50	0.66	0.06
4 C	6	6.07	1.10	0.89	0.64	0.77	1.48	0.49	0.64	0.06
5 C	6	6.05	1.10	0.89	0.64	0.77	1.48	0.48	0.63	0.06
6 Mo	14	13.71	-0.41	1.48	0.91	0.40	0.02	0.02	0.72	4.75
0.71	0.11	0.06	3.56	1.09	0.13	0.16				
7 C	6	6.11	1.10	0.89	0.65	0.76	1.49	0.49	0.66	0.06
8 C	6	6.07	1.10	0.89	0.64	0.78	1.47	0.48	0.65	0.06
9 C	6	6.06	1.10	0.89	0.64	0.77	1.48	0.48	0.64	0.06
10 C	6	6.11	1.10	0.89	0.64	0.76	1.49	0.49	0.67	0.06
11 C	6	6.11	1.10	0.89	0.64	0.77	1.48	0.50	0.67	0.07
12 H	1	0.84	0.27	0.46	0.07	0.03				
13 H	1	0.84	0.27	0.46	0.08	0.03				
14 H	1	0.83	0.27	0.46	0.07	0.03				
15 H	1	0.84	0.27	0.46	0.08	0.03				
16 H	1	0.84	0.27	0.46	0.08	0.03				
17 H	1	0.85	0.27	0.47	0.08	0.03				
18 H	1	0.85	0.27	0.45	0.10	0.03				
19 H	1	0.84	0.27	0.46	0.07	0.03				
20 H	1	0.84	0.27	0.47	0.08	0.03				
21 H	1	0.83	0.27	0.45	0.07	0.03				
22 O	8	8.38	1.08	0.91	0.99	1.00	2.06	0.82	1.51	0.01
23 N	7	7.48	1.09	0.90	0.80	0.86	1.76	0.72	1.33	0.02
24 C	6	5.60	1.10	0.89	0.62	0.80	1.40	0.29	0.35	0.16
25 C	6	6.26	1.10	0.89	0.65	0.76	1.55	0.44	0.81	0.05
26 C	6	6.00	1.10	0.89	0.62	0.77	1.49	0.37	0.67	0.09
27 H	1	0.87	0.28	0.48	0.10	0.02				
28 H	1	0.87	0.28	0.48	0.09	0.02				
29 H	1	0.84	0.27	0.45	0.09	0.02				
30 O	8	8.44	1.08	0.91	0.98	0.99	2.03	0.83	1.60	0.01
31 H	1	0.71	0.27	0.34	0.04	0.06				
32 H	1	0.84	0.28	0.45	0.09	0.02				
33 H	1	0.73	0.27	0.38	0.03	0.04				
34 O	8	8.64	1.08	0.91	0.98	0.98	2.03	0.86	1.78	0.01
35 H	1	0.70	0.27	0.32	0.05	0.06				
36 H	1	0.66	0.22	0.31	0.04	0.09				

MoCp2OHNH2-OCCHOHCH3

gas phase energy = -854.9210241009
sol phase energy = -855.0117161569

Total Density - Mulliken Population Analysis

Atom		Charge	Shell Charges											
1 C	6	6.10	1.10	0.89	0.64	0.76	1.49	0.50	0.65	0.06				
2 C	6	6.09	1.10	0.89	0.64	0.77	1.48	0.50	0.64	0.06				
3 C	6	6.07	1.10	0.89	0.64	0.77	1.47	0.49	0.64	0.06				
4 C	6	6.05	1.10	0.89	0.64	0.77	1.48	0.47	0.63	0.06				
5 C	6	6.12	1.10	0.89	0.64	0.77	1.49	0.49	0.67	0.06				
6 Mo	14	13.74	-0.41	1.48	0.91	0.40	0.01	0.02	0.72	4.75	0.71	0.13	0.07	3.57
1.11	0.12	0.15												
7 C	6	6.08	1.10	0.89	0.64	0.76	1.49	0.49	0.65	0.06				
8 C	6	6.09	1.10	0.89	0.64	0.78	1.47	0.50	0.65	0.06				
9 C	6	6.04	1.10	0.89	0.64	0.78	1.48	0.47	0.62	0.06				
10 C	6	6.10	1.10	0.89	0.64	0.77	1.49	0.49	0.66	0.06				
11 C	6	6.10	1.10	0.89	0.64	0.77	1.48	0.50	0.66	0.07				
12 H	1	0.84	0.27	0.46	0.08	0.03								
13 H	1	0.83	0.27	0.46	0.07	0.03								
14 H	1	0.83	0.27	0.46	0.07	0.03								
15 H	1	0.83	0.27	0.46	0.07	0.03								
16 H	1	0.83	0.27	0.46	0.08	0.03								
17 H	1	0.85	0.27	0.47	0.08	0.03								
18 H	1	0.84	0.27	0.45	0.09	0.03								
19 H	1	0.83	0.27	0.46	0.07	0.03								
20 H	1	0.84	0.27	0.47	0.08	0.03								
21 H	1	0.82	0.27	0.45	0.07	0.03								
22 O	8	8.35	1.08	0.91	0.98	1.01	1.99	0.86	1.50	0.02				
23 N	7	7.52	1.09	0.90	0.80	0.87	1.79	0.69	1.36	0.02				
24 C	6	5.62	1.10	0.89	0.61	0.81	1.36	0.30	0.39	0.16				
25 C	6	5.99	1.10	0.89	0.62	0.77	1.51	0.36	0.63	0.11				
26 C	6	6.29	1.10	0.89	0.66	0.75	1.53	0.45	0.87	0.04				
27 H	1	0.87	0.28	0.46	0.11	0.02								
28 H	1	0.87	0.28	0.46	0.11	0.02								
29 H	1	0.84	0.28	0.46	0.08	0.02								
30 H	1	0.87	0.28	0.46	0.11	0.02								
31 O	8	8.45	1.08	0.91	0.98	0.99	2.04	0.84	1.60	0.01				
32 H	1	0.69	0.25	0.33	0.05	0.07								
33 O	8	8.63	1.08	0.91	0.98	0.99	2.01	0.88	1.77	0.01				
34 H	1	0.71	0.27	0.33	0.05	0.06								
35 H	1	0.68	0.26	0.35	0.03	0.04								
36 H	1	0.69	0.27	0.35	0.04	0.04								

MoCp2OHNH2-OCCH2CH2OH

gas phase energy = -854.9184505075
sol phase energy = -855.0035032137

Total Density - Mulliken Population Analysis

Atom		Charge	Shell Charges														
1 C	6	6.09	1.10	0.89	0.64	0.76	1.49	0.50	0.64	0.06							
2 C	6	6.10	1.10	0.89	0.64	0.77	1.48	0.51	0.66	0.06							
3 C	6	6.08	1.10	0.89	0.64	0.77	1.48	0.50	0.64	0.06							
4 C	6	6.04	1.10	0.89	0.64	0.78	1.47	0.48	0.62	0.06							
5 C	6	6.12	1.10	0.89	0.64	0.77	1.49	0.50	0.67	0.06							
6 Mo	14	13.73	-0.41	1.48	0.91	0.41	0.00	0.01	0.72	4.75	0.71	0.15	0.07	3.57	1.11	0.11	0.15
7 C	6	6.08	1.10	0.89	0.64	0.76	1.49	0.49	0.65	0.06							
8 C	6	6.08	1.10	0.88	0.64	0.78	1.47	0.49	0.64	0.06							
9 C	6	6.05	1.10	0.89	0.64	0.77	1.48	0.48	0.63	0.06							
10 C	6	6.10	1.10	0.89	0.64	0.76	1.49	0.49	0.66	0.06							
11 C	6	6.11	1.10	0.89	0.64	0.77	1.48	0.50	0.66	0.07							
12 H	1	0.84	0.27	0.46	0.08	0.03											
13 H	1	0.83	0.27	0.46	0.07	0.03											
14 H	1	0.84	0.27	0.46	0.08	0.03											
15 H	1	0.83	0.27	0.46	0.07	0.03											
16 H	1	0.83	0.27	0.46	0.07	0.03											
17 H	1	0.84	0.27	0.47	0.08	0.03											
18 H	1	0.84	0.27	0.45	0.08	0.03											
19 H	1	0.83	0.27	0.46	0.07	0.03											
20 H	1	0.84	0.27	0.46	0.07	0.03											
21 H	1	0.82	0.28	0.46	0.07	0.03											
22 O	8	8.35	1.08	0.91	0.98	1.01	1.99	0.85	1.51	0.02							
23 N	7	7.50	1.09	0.90	0.80	0.87	1.79	0.69	1.34	0.02							
24 C	6	5.63	1.10	0.89	0.61	0.80	1.36	0.30	0.40	0.16							
25 C	6	6.29	1.10	0.89	0.65	0.76	1.55	0.46	0.83	0.05							
26 C	6	6.03	1.10	0.89	0.63	0.76	1.49	0.39	0.68	0.09							
27 H	1	0.86	0.28	0.47	0.09	0.02											
28 H	1	0.86	0.28	0.47	0.09	0.02											
29 H	1	0.85	0.27	0.45	0.09	0.02											
30 O	8	8.62	1.08	0.91	0.98	0.99	2.01	0.88	1.77	0.01							
31 H	1	0.72	0.27	0.34	0.05	0.06											
32 H	1	0.81	0.27	0.44	0.08	0.02											

33 O	8	8.47	1.08	0.91	0.98	0.99	2.04	0.83	1.61	0.01
34 H	1	0.69	0.25	0.33	0.05	0.07				
35 H	1	0.71	0.26	0.37	0.04	0.05				
36 H	1	0.70	0.27	0.35	0.04	0.04				

MoCp2OH-OHCHCH3CN

gas phase energy = -778.4229696461
sol phase energy = -778.5100059954

Total Density - Mulliken Population Analysis

Atom	Charge	Shell Charges								
1 C	6	6.07	1.10	0.89	0.64	0.78	1.48	0.49	0.64	0.06
2 C	6	6.10	1.10	0.89	0.64	0.76	1.49	0.49	0.66	0.06
3 C	6	6.10	1.10	0.89	0.64	0.77	1.48	0.49	0.66	0.07
4 C	6	6.09	1.10	0.89	0.64	0.77	1.49	0.49	0.65	0.06
5 C	6	6.05	1.10	0.89	0.64	0.78	1.48	0.47	0.63	0.06
6 Mo	14	13.70	-0.41	1.48	0.91	0.40	0.02	0.02	0.72	4.75
0.71	0.12	0.07	3.56	1.07	0.13	0.16				
7 C	6	6.11	1.10	0.89	0.64	0.76	1.49	0.51	0.66	0.06
8 C	6	6.10	1.10	0.89	0.64	0.77	1.50	0.48	0.66	0.06
9 C	6	6.02	1.10	0.89	0.64	0.78	1.47	0.46	0.62	0.06
10 C	6	6.07	1.10	0.89	0.64	0.77	1.48	0.49	0.64	0.06
11 C	6	6.09	1.10	0.89	0.64	0.77	1.47	0.50	0.65	0.06
12 H	1	0.83	0.27	0.46	0.08	0.02				
13 H	1	0.84	0.27	0.46	0.08	0.03				
14 H	1	0.83	0.28	0.46	0.07	0.03				
15 H	1	0.84	0.27	0.46	0.08	0.03				
16 H	1	0.84	0.27	0.46	0.07	0.03				
17 H	1	0.84	0.27	0.46	0.08	0.03				
18 H	1	0.83	0.27	0.46	0.07	0.03				
19 H	1	0.84	0.27	0.46	0.08	0.03				
20 H	1	0.84	0.27	0.46	0.08	0.03				
21 H	1	0.83	0.27	0.46	0.07	0.03				
22 O	8	8.62	1.08	0.91	0.98	0.99	2.01	0.86	1.78	0.01
23 H	1	0.71	0.27	0.33	0.05	0.06				
24 C	6	6.31	1.10	0.89	0.66	0.75	1.53	0.47	0.87	0.04
25 C	6	5.92	1.10	0.89	0.62	0.77	1.50	0.34	0.59	0.11
26 H	1	0.79	0.27	0.45	0.05	0.02				
27 H	1	0.85	0.27	0.46	0.09	0.02				

28 O	8	8.47	1.08	0.91	0.99	0.99	2.06	0.82	1.61	0.01
29 H	1	0.84	0.27	0.46	0.09	0.02				
30 C	6	5.84	1.10	0.88	0.65	0.80	1.34	0.32	0.67	0.06
31 N	7	7.31	1.10	0.90	0.75	0.95	1.58	0.83	1.18	0.03
32 H	1	0.85	0.27	0.46	0.09	0.02				
33 H	1	0.65	0.24	0.30	0.04	0.06				

MoCp2OH-OHCH2CH2CN

gas phase energy = -778.4222552194
sol phase energy = -778.5154144728

Total Density - Mulliken Population Analysis

Atom		Charge	Shell Charges							
1 C	6	6.06	1.10	0.89	0.64	0.78	1.48	0.48	0.64	0.06
2 C	6	6.10	1.10	0.89	0.64	0.76	1.49	0.49	0.66	0.06
3 C	6	6.09	1.10	0.89	0.64	0.77	1.48	0.49	0.66	0.07
4 C	6	6.10	1.10	0.89	0.64	0.77	1.49	0.49	0.66	0.06
5 C	6	6.05	1.10	0.89	0.64	0.78	1.48	0.47	0.63	0.06
6 Mo	14	13.69	-0.41	1.48	0.91	0.39	0.03	0.01	0.72	4.75
0.71	0.12	0.06	3.56	1.06	0.13	0.16				
7 C	6	6.12	1.10	0.89	0.64	0.76	1.49	0.51	0.66	0.06
8 C	6	6.10	1.10	0.89	0.64	0.77	1.49	0.48	0.66	0.06
9 C	6	6.02	1.10	0.89	0.64	0.78	1.47	0.46	0.62	0.06
10 C	6	6.08	1.10	0.89	0.64	0.77	1.48	0.49	0.64	0.06
11 C	6	6.09	1.10	0.89	0.64	0.77	1.48	0.50	0.65	0.06
12 H	1	0.84	0.27	0.46	0.08	0.03				
13 H	1	0.84	0.27	0.47	0.08	0.03				
14 H	1	0.83	0.28	0.46	0.07	0.03				
15 H	1	0.84	0.27	0.47	0.08	0.03				
16 H	1	0.84	0.27	0.46	0.07	0.03				
17 H	1	0.84	0.27	0.46	0.08	0.03				
18 H	1	0.83	0.27	0.46	0.07	0.03				
19 H	1	0.84	0.27	0.46	0.08	0.03				
20 H	1	0.84	0.27	0.46	0.08	0.03				
21 H	1	0.83	0.27	0.46	0.07	0.03				
22 O	8	8.61	1.08	0.91	0.98	0.99	2.01	0.86	1.77	0.01
23 H	1	0.71	0.27	0.33	0.05	0.06				
24 C	6	6.21	1.10	0.89	0.65	0.76	1.56	0.42	0.77	0.06
25 C	6	6.00	1.10	0.89	0.62	0.77	1.48	0.39	0.65	0.09

26 H	1	0.83	0.28	0.46	0.07	0.02				
27 H	1	0.80	0.27	0.45	0.06	0.02				
28 O	8	8.46	1.08	0.91	0.99	0.99	2.06	0.82	1.61	0.01
29 H	1	0.80	0.27	0.45	0.06	0.02				
30 H	1	0.66	0.25	0.31	0.04	0.06				
31 H	1	0.82	0.28	0.46	0.06	0.02				
32 C	6	5.92	1.10	0.88	0.65	0.80	1.33	0.33	0.75	0.07
33 N	7	7.30	1.10	0.90	0.75	0.95	1.58	0.74	1.25	0.03

MoCp2OH2-OCH3CHCN

gas phase energy = -778.4279255558
sol phase energy = -778.5191800151

Total Density - Mulliken Population Analysis

Atom	Charge	Shell Charges									
1 C	6	6.02	1.10	0.89	0.64	0.78	1.47	0.48	0.60	0.07	
2 C	6	6.05	1.10	0.89	0.64	0.77	1.48	0.50	0.60	0.06	
3 C	6	6.10	1.10	0.89	0.64	0.77	1.48	0.50	0.66	0.07	
4 C	6	6.10	1.10	0.89	0.64	0.76	1.49	0.49	0.66	0.06	
5 C	6	6.08	1.10	0.89	0.64	0.77	1.48	0.48	0.65	0.06	
6 Mo	14	13.72	-0.41	1.48	0.91	0.39	0.04	0.02	0.72	4.75	0.71
0.11	0.07	3.56	1.09	0.11	0.16						
7 C	6	6.10	1.10	0.89	0.64	0.77	1.49	0.50	0.65	0.06	
8 C	6	6.09	1.10	0.89	0.64	0.77	1.50	0.48	0.65	0.06	
9 C	6	6.06	1.10	0.89	0.64	0.77	1.48	0.49	0.63	0.06	
10 C	6	6.05	1.10	0.89	0.64	0.77	1.47	0.48	0.62	0.06	
11 C	6	6.10	1.10	0.88	0.64	0.77	1.47	0.50	0.66	0.07	
12 H	1	0.84	0.27	0.47	0.08	0.03					
13 H	1	0.85	0.27	0.47	0.09	0.03					
14 H	1	0.82	0.27	0.45	0.07	0.03					
15 H	1	0.84	0.27	0.46	0.08	0.03					
16 H	1	0.84	0.27	0.46	0.07	0.03					
17 H	1	0.84	0.27	0.46	0.08	0.03					
18 H	1	0.83	0.27	0.46	0.07	0.03					
19 H	1	0.83	0.27	0.46	0.07	0.03					
20 H	1	0.84	0.27	0.46	0.08	0.03					
21 H	1	0.82	0.27	0.46	0.07	0.03					
22 O	8	8.45	1.08	0.91	0.99	0.99	2.06	0.79	1.61	0.01	
23 H	1	0.65	0.26	0.31	0.02	0.06					

24 C	6	6.29	1.10	0.89	0.65	0.75	1.53	0.46	0.87	0.04
25 C	6	5.91	1.10	0.89	0.62	0.77	1.50	0.32	0.59	0.12
26 H	1	0.83	0.28	0.46	0.08	0.02				
27 H	1	0.86	0.28	0.46	0.10	0.02				
28 O	8	8.57	1.08	0.91	0.97	0.99	2.01	0.88	1.71	0.01
29 H	1	0.86	0.28	0.46	0.10	0.02				
30 C	6	5.86	1.10	0.88	0.65	0.81	1.32	0.35	0.68	0.07
31 N	7	7.35	1.10	0.90	0.75	0.94	1.58	0.83	1.21	0.03
32 H	1	0.87	0.27	0.46	0.11	0.02				
33 H	1	0.66	0.25	0.31	0.04	0.06				

MoCp2OH2-OCH2CH2CN

gas phase energy = -778.4237909228
sol phase energy = -778.5196988358

Total Density - Mulliken Population Analysis

Atom		Charge	Shell Charges										
1 C	6	6.04	1.10	0.89	0.64	0.78	1.47	0.47	0.63	0.06			
2 C	6	6.09	1.10	0.89	0.64	0.77	1.48	0.49	0.65	0.06			
3 C	6	6.10	1.10	0.89	0.64	0.77	1.48	0.50	0.66	0.07			
4 C	6	6.09	1.10	0.89	0.64	0.76	1.49	0.49	0.65	0.06			
5 C	6	6.09	1.10	0.89	0.64	0.77	1.48	0.49	0.65	0.06			
6 Mo	14	13.69	-0.41	1.48	0.91	0.39	0.05	0.02	0.72	4.75	0.71	0.11	0.06	3.56	1.08	0.10	0.16
7 C	6	6.11	1.10	0.89	0.64	0.76	1.49	0.50	0.66	0.06			
8 C	6	6.09	1.10	0.89	0.64	0.77	1.50	0.48	0.65	0.06			
9 C	6	6.05	1.10	0.89	0.64	0.78	1.48	0.49	0.62	0.06			
10 C	6	6.05	1.10	0.89	0.64	0.77	1.48	0.48	0.63	0.06			
11 C	6	6.09	1.10	0.89	0.64	0.77	1.47	0.50	0.65	0.07			
12 H	1	0.84	0.27	0.46	0.07	0.03							
13 H	1	0.84	0.27	0.46	0.08	0.03							
14 H	1	0.82	0.27	0.46	0.07	0.03							
15 H	1	0.84	0.27	0.46	0.08	0.03							
16 H	1	0.83	0.27	0.46	0.07	0.03							
17 H	1	0.84	0.27	0.46	0.08	0.03							
18 H	1	0.83	0.27	0.46	0.07	0.03							
19 H	1	0.83	0.27	0.46	0.07	0.03							
20 H	1	0.84	0.27	0.46	0.08	0.03							
21 H	1	0.83	0.27	0.46	0.07	0.02							

22 O	8	8.45	1.08	0.91	0.99	0.99	2.06	0.79	1.62	0.01
23 H	1	0.65	0.26	0.31	0.02	0.06				
24 C	6	6.21	1.10	0.89	0.65	0.76	1.56	0.42	0.78	0.06
25 C	6	5.98	1.10	0.89	0.62	0.76	1.48	0.37	0.66	0.10
26 H	1	0.87	0.28	0.47	0.10	0.02				
27 H	1	0.82	0.27	0.45	0.07	0.02				
28 O	8	8.57	1.08	0.91	0.98	0.99	2.02	0.87	1.71	0.01
29 H	1	0.82	0.27	0.45	0.07	0.02				
30 H	1	0.87	0.28	0.47	0.10	0.02				
31 C	6	5.94	1.10	0.88	0.65	0.80	1.33	0.34	0.76	0.07
32 N	7	7.31	1.10	0.90	0.75	0.95	1.58	0.74	1.27	0.03
33 H	1	0.66	0.25	0.31	0.04	0.06				

MoCp2OH2-CN

gas phase energy = -624.5330482617
sol phase energy = -624.6355236667

Total Density - Mulliken Population Analysis

Atom	Charge	Shell Charges											
1 C	6	6.09	1.10	0.89	0.64	0.77	1.49	0.49	0.64	0.06			
2 C	6	6.05	1.10	0.89	0.64	0.78	1.47	0.49	0.62	0.06			
3 C	6	6.07	1.10	0.89	0.64	0.77	1.48	0.49	0.63	0.06			
4 C	6	6.07	1.10	0.89	0.64	0.78	1.47	0.50	0.64	0.06			
5 C	6	6.09	1.10	0.89	0.64	0.77	1.49	0.50	0.64	0.06			
6 Mo	14	13.87	-0.41	1.48	0.91	0.43	0.02	0.02	0.72	4.75	0.73	0.07	0.08	3.61	1.17	0.15	0.14
7 C	6	6.07	1.10	0.89	0.64	0.77	1.49	0.49	0.63	0.06			
8 C	6	6.04	1.10	0.89	0.64	0.78	1.47	0.49	0.61	0.06			
9 C	6	6.06	1.10	0.89	0.64	0.78	1.48	0.49	0.62	0.06			
10 C	6	6.09	1.10	0.89	0.64	0.77	1.49	0.50	0.65	0.06			
11 C	6	6.09	1.10	0.89	0.64	0.77	1.48	0.50	0.64	0.07			
12 H	1	0.82	0.27	0.46	0.07	0.03							
13 H	1	0.83	0.27	0.46	0.07	0.03							
14 H	1	0.83	0.27	0.46	0.07	0.03							
15 H	1	0.82	0.27	0.46	0.07	0.03							
16 H	1	0.83	0.27	0.46	0.07	0.03							
17 H	1	0.84	0.27	0.46	0.07	0.03							
18 H	1	0.83	0.27	0.46	0.07	0.03							
19 H	1	0.83	0.27	0.46	0.07	0.03							

20 H	1	0.84	0.27	0.46	0.08	0.03				
21 H	1	0.82	0.27	0.45	0.07	0.03				
22 O	8	8.46	1.08	0.91	0.99	0.98	2.07	0.79	1.63	0.01
23 H	1	0.64	0.25	0.31	0.02	0.06				
24 C	6	6.00	1.10	0.88	0.62	0.82	1.28	0.53	0.71	0.06
25 N	7	7.39	1.10	0.90	0.76	0.93	1.59	0.85	1.24	0.03
26 H	1	0.65	0.26	0.31	0.02	0.06				

APPENDIX E

FURTHER INVESTIGATION INTO PLATINUM-BASED NITRILE HYDRATION CATALYSTS: EXPLORATION OF $[PtCl\{(PEt_2O)_2H\}]_2$; ATTEMPTED SYNTHESIS OF A BIS-DIMETHYLPHOSPHINITO PLATINUM COMPLEX; AND FURTHER EXPLORATION OF THE AQUEOUS BEHAVIOR OF $PtCl\{P(Me)_2OH\}\{P(Me)_2O\}_2H$

E.1. Catalytic behavior of $[PtCl\{(PEt_2O)_2H\}]_2$ toward nitrile hydration

E.1.1. Results and discussion

The novel Pt dimer, $[PtCl\{(PEt_2O)_2H\}]_2$,(**1**) was obtained unexpectedly following the procedure for the preparation of $PtCl\{P(Me)_2OH\}\{P(Me)_2O\}_2H$ (**2**) with the substitution of diethylphosphine oxide (DEPO) for the dimethylphophine oxide (DMPO) ligand (Scheme 1, see Ref. 1 for full synthesis and characterization details).[1,2] The catalytic activity of this complex (after treatment with a chloride abstractor as required for the DMPO-based catalyst) toward the hydration of acetonitrile, propionitrile, 3-hydroxypropionitrile (3-HPN), and isobutyronitrile (iBuN) was explored.

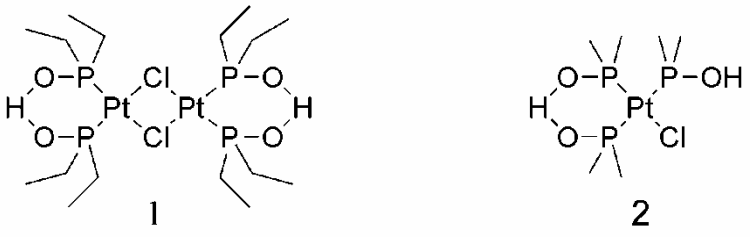

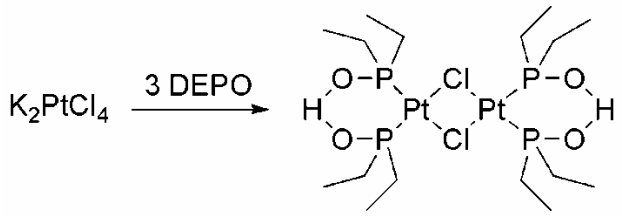

Scheme 1. Synthesis of [Pt*Cl*{$(PEt_2O)_2H$}]$_2$ from K_2PtCl_4.

While the identity of the species formed upon treatment of 1 with silver was not conclusively identified, ^{1}H NMR data for the resultant species is illustrated in Figure 1. The disappearance of the signals at 1.25 and 1.32 ppm that were observed in the starting material and appearance of signals at 1.0 and 1.65 ppm indicate a change in the identity of the complex up on treatment with silver. The low solubility of the resultant complex prohibited acquisition of ^{31}P and ^{195}Pt NMR spectra for further comparison to starting material and determination of structure.

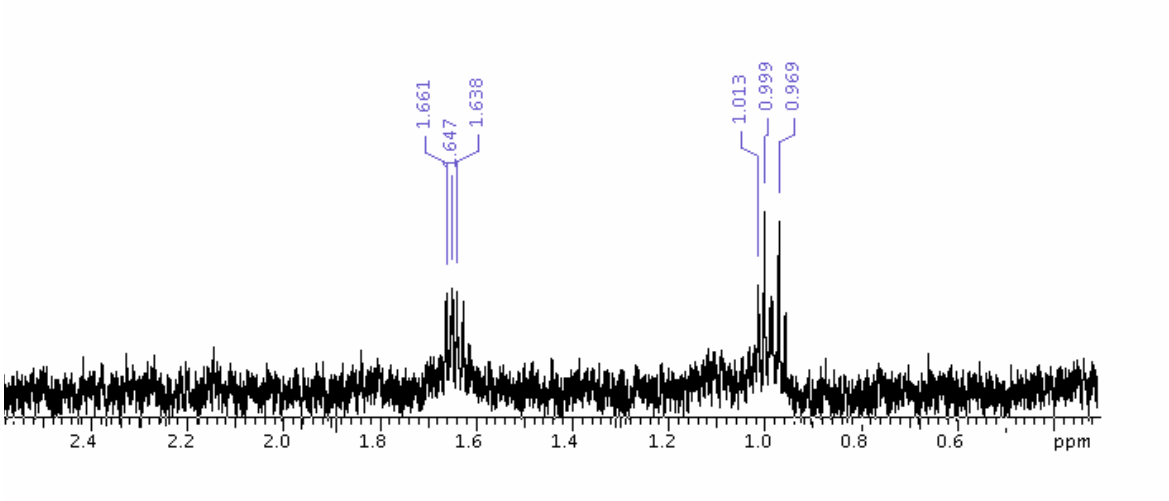

Figure 1. ^{1}H NMR spectrum of **1** following reflux with silver triflate. Disappearance of resonances at 1.25 and 1.32 ppm and appearance of multiplets centered around 1.0 and 1.65 ppm indicate a change in the complex upon treatment with silver.

This species was found to catalyze the hydration of acetonitrile and 3-HPN (as illustrated in Figure 2), however, even after several days of reaction, essentially no hydration of iBuN or propionitrile was observed. While no accurate kinetic data could be obtained due to a change in concentrations over time (likely due to evaporation of solvent, nitrile or both from the NMR tube), the rate of hydration of acetonitrile for **1** was slightly slower than those found for **2,** but still comparable to some trials (note that the rates for catalysis by **2** were highly variable, as reported in previous chapters). Interestingly, the small increase in steric hindrance from acetonitrile to propionitrile resulted in an effective halt in hydration reactivity, suggesting that this dimer may be more sensitive to steric effects than **2.** Furthermore, addition of the hydroxyl group to the propionitrile in the case of 3-HPN restored a small amount of reactivity, which

suggests that the addition of an electron withdrawing group to the substrate promotes hydration activity. This result is consistent with previous nitrile hydration studies.[1,3,4] Interestingly, some hydrolysis of the resultant amide to yield the carboxylic acid was also observed in the case of acetonitrile. Also consistent with the behavior of **2** was the abrupt halt in reactivity prior to the completion of the reaction (possibly due to product inhibition) that was observed in the hydration of acetonitrile.

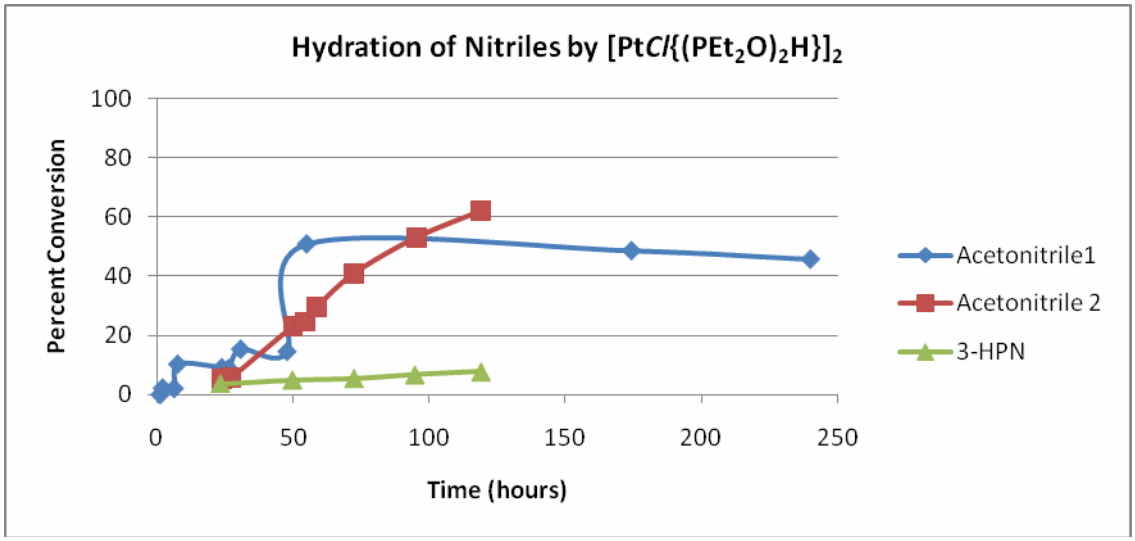

Figure 2. Hydration of acetonitrile and 3-HPN over time.

E.1.2. Experimental procedures

For preparation of catalyst stock solution, 33 mg **1** (synthesized as reported in reference 1) was placed in 25 mL round bottom flask equipped with a magnetic stir bar and reflux condenser. 11 mL D_2O and 19 mg silver triflate were added to the vessel. The mixture was then brought to reflux and left stirring overnight. After 14 hours, the

mixture was removed from heat and allowed to cool to room temperature before the resultant solid was removed from the mixture via filtration through a 0.2 μm acrodisc.

For hydration trials, 1 mL of catalyst stock solution was added to a 7 in. NMR tube. 0.35 mmol of the appropriate nitrile was then added to this solution via volumetric syringe. NMR tube was kept in an oil bath maintained at 80 ˚C when NMR spectra were not being actively obtained. Reaction progress was monitored by observation of the protons adjacent to the nitrile carbon by ^{1}H NMR spectroscopy.

E.2. Attempts to cleave [Pt*Cl*{$(PEt_2O)_2H$}]$_2$ dimer

E.2.1. Results and discussion

Cleavage of the [Pt*Cl*{$(PEt_2O)_2H$}]$_2$ dimer to give Pt Cl_2 $(PEt_2O)_2H$ prior to treatment with silver was attempted to investigate two hypotheses. First, it was suggested in the initial report of **2** that the free hydroxyl group of the third dimethylphosphinito group was responsible for intramoleular attack of the nitrile carbon in the mechanism of catalysis (Figure 3).[2,5] Generation of a *cis*-dimethylphospinito platinum complex lacking this third phosphinito ligand was expected to serve as a route to investigation of this proposal. Second, the activity of the dimer toward nitrile hydration suggests that another mechanism may be at play. Cleaving the dimer was expected to increase access of the nitrile substrate to the metal center, potentially increasing catalytic activity.

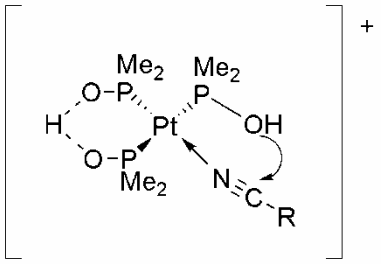

Figure 3. Intramolecular attack of the hydroxyl on the nitrile carbon proposed in 2.

Unfortunately, attempts to cleave the dimer with DCl to yield **3** were unsuccessful. While ^{1}H, ^{31}P and ^{195}Pt NMR spectroscopy indicated that some reaction had occurred, the spectra were inconsistent with **3**.

E.2.2. Experimental procedures

[Pt*Cl*{$(PEt_2O)_2H$}]$_2$ was added to 0.75 mL 3M DCl in D_2O in NMR tube and the mixture was left to stand at room temperature for 3 days. However, poor solubility prevented spectroscopic analysis of this mixture. To increase solubility, an additional 0.2 mL 3M DCl in D_2O and 0.8 mL MeOH was added to the mixture in the NMR tube. The mixture was allowed to stand at room temperature over night before spectroscopic analysis.

E.3. Further attempts to synthesize a *cis*-phosphinito Pt complex

E.3.1. Results and discussion

Several attempts to synthesize Pt Cl_2 $(PMe_2O)_2H$ (**3**) as a precursor to complexes useful for the investigation of the intramolecular attack mechanism mentioned in the previous section were undertaken. Decreasing the amount of dimethylphosphinito ligand

used in the synthesis to 2 equivalents relative to the platinum simply yielded the triply substituted **2**, with no evidence of the target **3**, or any other disubstituted species.

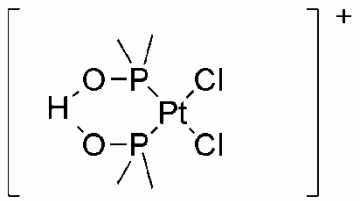

3

Attempts to synthesize **3** through the precursor $(Me_2S)_2PtCl_2$ (synthesized as published in the literature) were also unsuccessful. This precursor has been used to obtain *cis*-bisphosphine platinum complexes upon treatment with 2 equivalents of the appropriate phosphine.[6] However, treatment of $(Me_2S)_2PtCl_2$ with 2 equivalents of dimethylphosphine oxide (Scheme 2) at room temperature led to no reaction, and gently heating the mixture to 36 ˚C led to the formation of the triply substituted product $PtCl\{P(Me)_2OH\}_3$ as determined by ^{31}P NMR spectroscopy (Figure 4). Interestingly, the fully protonated form (**4**) was obtained under these reaction conditions, as the CH_2Cl_2 solvent did not effectively facilitate deprotonation to form the proton bridge between two of the dimethylphosphinito ligands (as indicated by the slight shift and sharpening of the phosphorus resonances due to the two trans phosphinito ligands). Even when conditions were diluted significantly from those reported for the phosphine complex synthesis (in an attempt to suppress coordination of the third phosphinito ligand), the triply substituted product was the only species containing Pt-bound phosphorus that was observed.

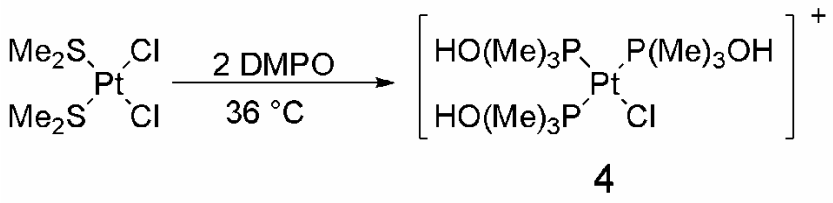

4

Scheme 2. Synthesis of fully protonated form of triply substituted catalyst in CH_2Cl_2, despite limiting DMPO to 2 equivalents.

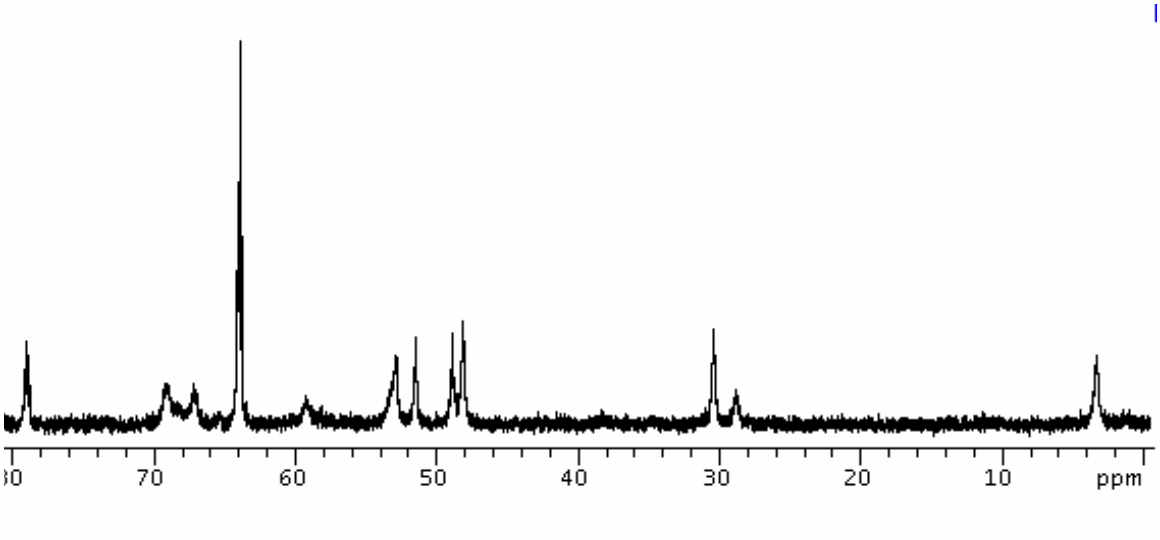

Figure 4. ^{31}P NMR spectrum of $PtCl\{P(Me)_2OH\}_3$. Synthesis in CH_2Cl_2 prevented deprotonation to form **2**.

E.3.2. Experimental procedures

*E.3.2.1. Attempt to synthesize **3** via $(Me_2S)_2PtCl_2$*

$(Me_2S)_2PtCl_2$ (39 mg, 0.1 mmol, synthesized as published in 5) was dissolved in 0.4mL CH_2Cl_2 in a scintillation vial. A stir bar and dimethylphosphine oxide (16 mg, 0.2 mmol) was added to the mixture, followed by 7 drops methanol to complete dissolution of dimethylphosphine oxide. Mixture was left to stir at room temperature for an hour and entire volume was transferred to an NMR tube. ^{31}P NMR spectroscopy indicated that no reaction had occurred.

Mixture in NMR tube was placed in oil bath at 36 ˚C. ^{31}P of this sample after 100 minutes indicated that $PtCl\{P(Me)_2OH\}_3$ was the primary phosphorus-containing product, and no evidence of the desired product was observed.

*E.3.2.2. Attempt to synthesize **3** via $(Me_2S)_2PtCl_2$ under dilute conditions*

$(Me_2S)_2PtCl_2$ (39 mg, 0.1 mmol) was added to 3 mL CH_2Cl_2 in a 2-neck round bottom flask equipped with a stir bar and addition funnel. Dimethylphosphine oxide (16 mg, 0.2 mmol) was added in 2 mL of a 1:1 CH_3OH: CH_2Cl_2 dropwise over an hour to the solution at 38 ˚C. After 6 hours, no reaction was apparent by ^{31}P NMR spectroscopy. Reaction mixture was left stirring overnight. ^{31}P NMR spectroscopy indicated that the triply substituted product was the major product, and no free dimethylphosphine oxide remained in the mixture. While other phosphorus species were present, none possessed the platinum satellites indicative of binding to the Pt center.

E.4 More on the aqueous behavior of of PtCl{P(Me)$_2$OH}{P(Me)$_2$O}$_2$H

E.4.1. Results and discussion

Treatment of **2** with silver is reported to simply extract the chloride from the complex to yield **4**, which presents an open coordination site for binding of the nitrile substrate (Scheme 3).[2] However, evidence indicated that this simple extraction to give the hypothesized active catalyst was not occurring upon treatment of **2** silver salts. Much of the observed behavior was discussed in the last chapter. The unusual aqueous behavior observed for this system is expanded upon here.

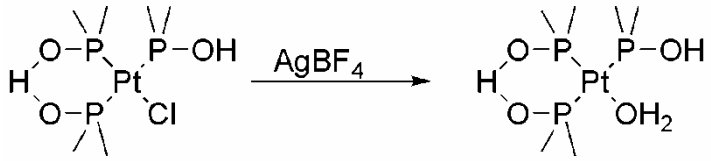

Scheme 3. Simple abstraction of the chloride ligand is reported to yield the active catalyst.

When the treatment of **2** with silver triflate was performed in an NMR tube for spectroscopic observation, for example, changes in the ^{31}P NMR spectrum inconsistent with a simple chloride extraction were observed. If a simple chloride extraction were occurring, and an aquo ligand was occupying the vacant coordination site, the ^{31}P NMR spectrum should remain quite similar to that of the starting **2**, with 2 different phosphorus environments, both exhibiting Pt satellites indicating that they are still bound to the platinum center. However, after treatment with silver at room temperature, there is a significant change in the ^{31}P NMR spectrum within 3 minutes. Specifically, only one

resonance appears in the spectrum exhibiting the platinum satellites indicative of binding (87 ppm with satellites appearing at 93 and 81 ppm) rather than the 2 signals expected for a simple extraction. Additionally, a new resonance appears at 55 ppm, which lacks these satellites and indicates a phosphorus species that is no longer bound to the platinum center. Over time, bound phosphorus signal disappeared and this signal was the only one remaining. Spiking the sample with authentic dimethylphosphinic acid confirmed the identity of this species as dimethylphosphinic acid reported as a disproportionation product of dimethylphosphine oxide. While elevated temperatures are usually required for this disproportionation to occur,[7] this process occurs here at room temperature in the process of forming the active catalytic species.

The presence of dimethylphosphinic acid as the only observable species observable by ^{31}P NMR spectroscopy is not consistent with a simple chloride extraction to yield the active catalyst as proposed by Parkins. Either the catalytic species obtained lacks phosphorus ligands, or it has undergone a large enough change to render any remaining phosphorus atoms undetectable by ^{31}P NMR spectroscopy (perhaps due to significant broadening). It should be noted that quantification of the resultant dimethylphosphinic acid did account for the majority of the phosphorus introduced as **2**.

E.4.2 Experimental procedures

In a typical NMR observation experiment, 3 mg silver triflate was added to and NMR tube containing 3 mg **2** in 1 mL D_2O. Almost immediately, the tube became cloudy, and ^{31}P NMR spectroscopy (observed on an INOVA-500 spectrometer) was initiated within 3 minutes of this addition. An array was used to monitor the ^{31}P NMR spectrum over time. The temperature within the spectrometer was raised after 5 hours to

40 ˚C for an additional 10 hours. After this time, the NMR tube was coated with an unidentified brown and metallic material, which appeared consistently in additional trials, whether the sample was heated or not, and whether or not the sample was exposed to light.

REFERENCES CITED

CHAPTER I

(1) Lelieveld, J.; Roelofs, G.T.; Ganzeveld, L.; Feichter, J.; Rodher, H. *Phil. Trans. R. Soc. Lond. B.,* **1997**, *352*, 149.

(2) Cox, R.A.; *Phil. Trans. R. Soc. Lond. B.,* **1997**, *352*, 251.

(3) U.S. Environmental Protection Agency. http://epa.gov/air/sulfurdioxide/health.html (accessed March 14, 2011).

(4) Song, C.; Ma, X. *Appl. Catal., B*, **2003**, *41*, 207.

(5) Ahmed, K.; Foger, K. *Ind. Eng. Chem. Res.* **2010**, *49*, 7239.

(6) Fukunaga, T.; Katsuno, H.; Matsumoto, H.; Takahashi, O.; Akai, Y. *Catal. Today*, **2003**, *84*, 197.

(7) Kropp, K.G.; Fedorak, P.M. *Can. J. Microbiol.***1998**, *44*, 605.

(8) Seyfried, W.D. *Chem. Eng. News*, **1949**, *27*, 2482.

(9) Long, R.B.; Speight, J.G. *Petroleum Chemistry and Refining*; Taylor & Francis: Washington, DC, 1998; pp 1-38.

(10) Del Bianco, A.; Anelli, M.; Riva, A. *Fuel Sci. Tech. Int.*, **1992**, *10*, 323.

(11) Masohan, A.; Kaur, S.; Bhatia, V.K. *J. Sci. Ind. Res.*, **1983**, *42*, 166.

(12) Thompson, C.J.; Coleman, H.J.; Hopkins, R.L.; Rall, H.T. . *J. Chem. Eng. Data*, **1965**, *10*, 279.

(13) Thompson, C.J.; Coleman, H.J.; Hopkins, R.L.; Rall, H.T. *J. Chem. Eng. Data*, **1964**, *9*, 473.

(14) Czogalla, C.; Boberg, F. *Sulfur Reports*, **1983**, *3*, 121.

(15) Coleman, H.J.; Thompson, C.J.; Hopkins, R.L.; Foster, N.G.; Whisman, M.L.; Richardson, D.M. *J. Chem. Eng. Data*, **1961**, *6*, 464.

(16) Hopkins, R.L.; Coleman, H.J.; Thompson, C.J.; Rall, H.T. *Anal. Chem.*, **1969**, *41*, 2041.

(17) Stumpf, A.; Tolvaj, K.; Juhasz, M. *J. Chromatogr., A*, **1998**, *819*, 67.

(18) Eijsbouts, S.; Mayo, S.W.; Fujita, K. *Appl. Catal., A,* **2007**, *322*, 58.

(19) Song, C.; Reddy, K.M. *Appl. Catal., A*, **1999**, *176*, 1.

(20) Babich, I.V.; Moulijn, J.A. *Fuel*, **2003**, *82*, 607.

(21) Girgis, M.J.; Gates, B.C. *Ind. Eng. Chem. Res.*, **1991**, *30*, 2021.

(22) Ma, X.; Sakanishi, K.; Mochida, *Ind. Eng. Chem. Res.*, **1994**, *33*, 218.

(23) Song, C. *Catal. Today*, **2003**, *86*, 211.

(24) Knudsen, K.G.; Cooper, B.H.; Topsoe, H. *Appl. Catal.*, **1999**, *189*, 205.

(25) Rothlisberger, A.; Prins, R.; *Jour. Catal.,.* **2005**, *235*, 229.

(26) Gates, B.C.; Topsoe, H. *Polyhedron*, **1997**, *16*, 3213.

(27) Whitehurst, D.D.; Isoda, T.; Mochida, I. *Adv. In Catal.* **1998**, *42*, 345.

(28) Ma, X.; Sakanishi, K.; Isoda, T.; Mochida, I. *Energy Fuels*, **1995**, *9*, 33.

(29) Wang, H.; Prins, R. *Jour. Catal.* **2008**, *258*, 153.

(30) Farag, H.; Whitehurst, D.D.; Sakanishi, K.; Mochida, I.*Catal. Today*, **1999**, *50*, 49.

(31) Bao, W.; Zhang, Z.; Ren, X.; Li, F.; Chang, L. *Energy Fuels*, **2009**, *23*, 3600.

(32) Yang, R.T.; Hernandez-Maldonado, A.J.; Yang, F.H. *Science*, **2003**, *301*, 79.

(33) Velu, S.; Ma, X.; Song, C. *Ind. Eng. Chem. Res.*, **2003**, *42*, 5293.

(34) Shennan, J.L. *J. Chem. Tech. Biotechnol.* **1996**, *67*, 109.

(35) McFarland, B.L.; Boron, D.J.; Deever, W.; Meyer, J.A.; Johnson, A.R.; Atlas, R.M. *Crit. Rev. Microbiol.* **1998**, *24*, 99.

(36) Vazquez-Duhalt, R.; Torres, E.; Valerrama, B.; Le Borge, S. *Energy Fuels*, **2002**, *16*, 1239.

(37) Gray, K.A.; Mrachko, G.T.; Squires, C.H. *Curr. Opin. Microbiol.*, **2003**, *6*, 229.

(38) Soleimani, M.; Bassi, M.; Margaritis, A. *Biotechnol. Adv.*, **2007**, *25*, 570.

(39) Kertesz, M.A. *FEMS Microbiol. Rev.*, **1999**, *24*, 135.

(40) Monticello, D.J. *Chemtech*, **1998**, *28*, 38.

(41) Torkamani, S.; Shayegan, J.; Yaghmaei, S.; Alemzadeh, I. *Ind. Eng. Chem. Res.* **2008**, *47*, 7476.

(42) McFarland, B.L. *Curr. Opin. Microbiol.* **1999**, *2*, 257.

(43) Block, E. Introduction. In *Reactions of Organosulfur Compounds*; Blomquist, A.T., Wasserman, H.H., Eds.; Organic Chemistry: A Series of Monographs 37; Academic Press, Inc.; New York, NY, 1978; pp. 15-18.

(44) Rigau, J.J.; Bacon, C.C.; Johnson, C.R. *J. Org. Chem.*, **1970**, *35*, 3655.

(45) Gilman, H.; Esmay, D.L. *J. Am. Chem. Soc.*, **1952**, *74*, 2021.

(46) Aleksanyan, V.T.; Kimel'fel'd, Y.M.; Shostakovskii, S.M.; L'vov, A.I. *J. Appl. Spectrosc.* **1965**, *3*, 355.

(47) Schlesinger, A.H.; Mowry, D.T. *J. Am. Chem. Soc.*, **1951**, *73*, 2614.

(48) Nakayama, J.; Sugihara, Y. Chemistry of Thiophene 1,1-Dioxides in *Organosulfur Chemistry II*; Page, P.C.B., Ed.; Topics in Current Chemistry 205; Springer-Verlag: Germany, 1999; pp 131-195.

(49) Truce, W. E.; Klingler, T.C.; Brand, W.W. Sulfones and Sulfoximines. In *Organic Chemistry of Sulfur*; Oae, S., Ed.; Plenum Press: New York, 1977; pp 527-602.

(50) Geneste, P.; Grimaud, J.; Olive, J. – L.; Ung, S.N. *Bull. Chem. Soc. France*, **1977**, *3*, 271.

(51) Matteucci, M.; Bahalay, G.; Bradley, M. *Org. Lett.*, **2003**, *5*, 235.

(52) Oae, S.; Watanabe, Y.; Fujimori, K. *Tetrahedron Lett.,* **1982**, *23*, 1189.

(53) Bortolini, O.; Di Furia, F.; Modena, G.l Seraglia, R. *J. Org. Chem.*, **1985**, *50,* 2688.

(54) Palomeque, J.; Clacens, J.M.; Figueras, F. *J. Catal.*, **2002**, *211*, 103.

(55) Vassel, K.A.; Espenson, J.H. *Inorg. Chem.*, **1994**, *33*, 5491.

(56) Yao, H.; Richardson, D.E. *J. Am. Chem. Soc.*, **2003**, *125*, 6211.

(57) Veerakumar, P.; Lu, Z.; Velayudham, M.; Lu, K,; Rajagopal, S. *J. Mol. Catal. A: Chem.*, **2010**, *332*, 128.

(58) Kelkar, M.A.; Gagate, P.R.; Pandit, A.B. *Ultrasonics Sonochemistry*, **2006**, *13*, 523.

(59) Oae, S. Historical Development of Sulfur Bonding: A View of an Experimental Sulfur Chemist. In *Organic Sulfur Chemistry*; Bernardi, F., Csizmadia, I.G., Mangini, A. Eds.; Studies in Organic Chemistry 19; Elsevier; New York, NY, 1985; pp 28-29.

(60) Watanabe, Y.; Numata, T.; Iyanagi, T.; Oae, S. *Bull. Chem. Soc. Jpn.*, **1981**, *54*, 1163.

(61) Watanabe, Y.; Oae, S.; Iyanagi, T. *Bull. Chem. Soc. Jpn.*, **1982**, *55*, 188.

(62) Di Furia, F.; Modena, G. *Pure & Appl. Chem.*, **1982**, *54*, 1853.

(63) DeFillipis, p.; Scarsella, M.; Verdone, N. *Ind. Eng. Chem. Res.* **2010**, *49*, 4594.

(64) Otsuki, S.; Nonaka, T.; Takashimi, N.; Qian, W.; Ishihara, A.; Imai, T.; Kabe, T. *Energy Fuel*, **2000**, *14*, 1232.

(65) Bordwell, F.G.; Albisetti, C.J. Jr.; *J. Am. Chem. Soc.*, **1948**, *70*, 1955.

(66) Shiraishi, Y.; Tachinaba, K.; Hirai, T.; Komasawa, I. *Energy Fuel*, **2003**, *17*, 95.

(67) Zanniko, F.; Stournas, L.S. *Fuel Process. Technol.*, **1995**, *42*, 35.

(68) Shiraishi, Y.; Tachibana, K.; Hirai, T.; Komasawa, I. *Ind. Eng. Chem. Res.*, **2002**, *41*, 4362.

(69) Ramirez-Verduco, L.F.; Murrieta-Guevara, F.; Garcia-Gutierrez, J.L.; Saint Martin-Castanon, R.; Martinez-Gerreno, M.C.; Montiel-Pacheco, M.C.; Mata-Diaz, R. *Petr. Sci. & Eng.*, **2004**, *22*, 129.

(70) Yu, G.; Lu, S.; Chen, H.; Zhu, Z. *Energy Fuels*, **2005**, *19*, 447.

(71) Firth, J.B.; Watson, F.S. *J. Phys. Chem.*, **1925**, *29*, 987.

(72) Liu, G.; Cao, Y.; Jiang, R.; Wang, L.; Zhang, X.; Mi, Z. *Energy Fuel*, **2009**, *23*, 5978.

(73) Te, M.; Fairbridge, C.; Ring, Z. *Appl. Catal., A*, **2001**, *219*, 267.

(74) Chica, A.; Gatti, G.; Moden, B.; Marchese, L.; Iglesia, E. *Chem. Eur. J.* **2006**, *12*, 1960.

(75) Ramirez-Verduzco, L.F.; Torres-Garcia, E.; Gomez-Quintana, R.; Gonzalez-Pena, V.; Murrieta,-Guevara, F. *Catal. Today*, **2004**, *98*, 289.

(76) Cedeno-Caero, L.; Hernandez, E.; Pedraza, F.; Murrieta, F. *Catal. Today*, **2005**, *107*, 564.

(77) Cedeno-Caero, L.; Jorge, F.; Navarro, A.; Gutierrez-Alejandro, A. *Catal. Today*, **2006**, *116*, 562.

(78) Cedeno-Caero, L.; Gomez-Bernal, H.; Frausto-Cuevas, A.; Guerra-Gomez, H.D.; Cuevas-Garcia, R. *Catal. Today* **2008**, *133*, 244.

(79) Ramos-Luna, M.A.; Cedeno-Caero, L. *Ind. Eng. Chem. Res.* **2011**, *50*, 2641.

(80) Gonzalez-Garcia, O.; Cedeno-Caero, L. *Catal. Today* **2009**, *148*, 42.

(81) Gonzalez-Garcia, O.; Cedeno-Caero, L. *Catal. Today* **2010**, *150*, 237.

(82) Hulea, V.; Moreau, P.; Di Renzo, F. *Jour. of Mol. Catal. A* **1996**, *111*, 325.

(83) Hulea, V.; Moreau, P.; *Jour. of Mol. Catal. A* **1996**, *113*, 499.

(84) Moreau, P.; Hulea, V.; Gomez, S.; Brunel, D.; Di Renzo, F. *Appl. Catal. A* **1997**, *155*, 253.

(85) Kong, L.; Li, G.; Wang, X. *Catl. Lett.* **2004**, *92*, 163.

(86) Kong, L.; Li, G.; Wang, X.; Wu, B. *Energy Fuels* **2006**, *20*, 896.

(87) Hulea, V. Fajula, F.; Bousquet, J. *J. Catal.* **2001**, *198*, 179.

(88) Wang, Y.; Li, G.; Wang, X.; Jin, C. *Energy Fuel*, **2007**, *21*, 1415.

(89) Ramsden, J.H.; Drago, R.S.; Riley, R. *JACS*, **1989**, *111*, 3958.

(90) Chen, L.; Li, F. *Energy Fuel*, **2010**, *24*, 3443.

(91) Collins, F.M.; Lucy, A.R.; Sharp, C. *J. Mol. Catal. A: Chem.,* **1997**, *117*, 397.

(92) Jiang, X.; Li, H.; Zhu, W.; He, L.; Shu, H.; Lu, J. *Fuel*, **2009**, *88*, 431.

(93) Li, C.; Jiang, Z.; Gao, J.; Wang, S.; Tian, F.; Sun, F.; Sun, X.; Ying, P.; Han, C. *Chem. Eur. J.* **2004**, *10*, 2279.

(94) Kulkanari, P.S.; Afonso, C.A.M. *Green Chem.* **2010**, *12*, 1139.

(95) Bosmann, A.; Datsevich, L.; Jess, A.; Lauter, A.; Schmitz, C.; Wasserceid, P. *Chem. Commun.* **2001**, *23*, 2494.

(96) Liu, D.; Gui, J.; Song, L.; Zhang, X.; Sun, Z. *Petr. Sci. & Tech.* **2008**, *26*, 973.

(97) Gao, H.; Luo, M.; Xing, J.; Wu, Y.; Li, Y.; Liu, Q.; Liu, H. *Ind. Eng. Chem. Res.* **2008,** *47*, 8384.

(98) Esser, J.; Wasserceid, P.; Jess, A. *Green Chem.* **2004**, *6*, 316.

(99) Opperman, S.; Stein, F.; Kragl, U. *Appl. Microbiol. Biotechnol.* **2011**, *89*, 493.

(100) Rosa, J. N.; Afonso, C. A. M.; Santos, A.G. *Tetrahedron*, **2001**, *57*, 4189.

(101) Earle, M.J.; Seddon, K.R. *Pure Appl. Chem.* **2000**, *72*, 1391.

(102) Handy, S. *Chem. Eur. J.* **2003**, *9*, 2938.

(103) Lu, L.; Cheng, S.; Gao, J.; He, M. *Energy Fuels*, **2007**, *21*, 383.

(104) Li, F.; Liu, R.; Wen, J.; Zhao, D.; Sun, Z.; Liu, Y. *Green Chem.*, **2009**, *11*, 883.

(105) Li, H.; Jiang, X.; Zhu, W.; Lu, J.; Shu, H.; Yan, Y. *Ind. Eng. Chem. Res.*, **2009**, *48*, 9034.

(106) Li, H.; He, L.; Lu, J.; Zhu, W.; Jiang, X.; Wang, Y.; Yan, Y. *Energy Fuels*, **2009**, *23*, 1354.

(107) Scammels, P.J.; Scott, J.L.; Singer, R.D. *Aust. J. Chem*. **2005**, *58*, 155.

(108) Zhao, D.; Sun, Z.; Li, F.; Liu, R.; Shan, H. *Energy Fuels*, **2008**, *22*, 3065.

(109) Zhao, D.; Wang, J.; Zhou, E. *Green Chem.*, **2007**, *9*, 1219.

(110) Wang, J.; Zhao, D.; Li, K. *Energy Fuels*, **2009**, *23*, 3831.

(111) Gui, J.; Liu, D.; Sun, Z.; Liu, D.; Min, D.; Song, B.; Peng, X. *J. Mol. Catal. A: Chem.*, **2010**, *331*, 64.

(112) Huang, W.; Zhu, W.; Li, H.; Shi, H.; Zhu, G.; Liu, H.; Chen, G. *Ind. Eng. Chem. Res.* **2010**, *49*, 8998.

(113) Joseph, J.K.; Jain, S.L.; Sain, B. *Synth. Commun.,* **2006**, *36,* 2743.

(114) Song, H.Y.; Li, G.; Wang, X.; Xu, Y.; *Catal. Today*, **2010**, *149*, 127.

(115) Oyama, S.T. C*atal. Rev.- Sci. Eng.,* **2000**, *42*, 279.

(116) Sahle-Demessie, E.; Devulapelli, V.G. *Appl. Catal,. B*, **2008**, *84*, 408.

(117) Gilbert, E.; Hoffman-Gleve, S. *Ozone: Sci. Eng.*, **1990**, *12*, 315.

(118) Gilbert, E.; Hodenberg, S.V. *Ozone: Sci. Eng.*, **1997**, *19*, 145.

(119) Ji, H.; Wang, T.T.; Wang, L.; Fang, Y.X. *React. Kinet. Catal. Lett.*, **2007**, *90*, 259.

(120) Sampanthar, J.T.; Xiao, J.T.; Dou, J.; Nah, T.Y.; Rong, X.; Kwan, W.P. *Appl. Catal., B* **2006**, *63*, 85.

(121) Xu, X.; Moulijn, J.A.; Ito, E.; Wagemans, R.; Makkee, M. *ChemSusChem*, **2008**, *1*, 817.

(122) Ito, E.; Makkee, M.; Moulijn, J.A.; Wagemans, R.W.; Xu, X. Process for Oxidative Desulphurization of a Hydrocarbon Fuel. PCT Int. Appl. WO2009098264, 2009.

(123) Sundararaman, R.; Ma, X.; Song, C. *Ind. Eng. Chem. Res.*, **2010**, *49*, 5561.

(124) Zhao, D.; Liu, R.; Wang, J.; Liu, B. *Energy Fuels*, **2008**, *22*, 1100.

(125) Zhang, J.; Zhao, D.; Wang, J.; Yang, L.; *J. Mater. Sci.*, **2009**, *44*, 3112.

(126) Na, P.; Zhao, B.; Gu, L.; Liu, J.; Na, J. *J. Phys. Chem. Solids*, **2009**, *70*, 1465.

(127) Adewuyi, Y.G. *Environ. Sci. Technol.*, **2005**, *39*, 8557.

(128) Patel, V.K.; Sen, D.J.; Patel, H.U.; Patel, C.N. *J. Chem. Pharm. Res.*, **2010,** *2*, 573.

(129) Rosenthal, I.; Sostaric, J.Z.; Riesz, P. *Res. Chem. Intermed.*, **2004**, *7*, 685.

(130) Thompson, L.H.; Doraiswamy, L.K. *Ind. Eng. Chem. Res.***1999**, *38*, 1215.

(131) Zhao, D.; Wang, J.; Yang, Y.; Zhao, Y. *Energy Fuels*, **2007**, *21*, 2543.

(132) Mei, H.; Mei, B.W.; Yen, T.F. *Fuel*, **2003**, *82*, 405.

(133) Dai, Y.; Qi, Y.; Zhao, D.; Zhang, H. *Fuel Process. Technol.*, **2008**, *89*, 927.

CHAPTER II

(1) Li, C.; Jiang, Z.; Gao, J.; Yang, Y.; Wang, S.; Tian, F.; Sun, F.; Sun, X.; Ying, P.; Han, C. *Chem. Eur. J.,* **2004**, *10*, 2277.

(2) Song, C.; Ma, X. *Appl. Catal,. B,* **2003**, *41*, 207.

(3) Lee IC, Ubanyionwu HC. *Fuel*, **2008**, *87*, 312.

(4) Velu, S.; Ma, X; Song, C., Namazian, M.; Sethuraman, S., Venkataraman, G. *Energy & Fuels*, **2005,** *19*, 1116.

(5) Muradov, N.; Ramasamy, K.; Linkous, C.; Huang, C.; Adebiyi, I.; Smith, F.; T-Raissi, A.; Stevens, J. *Fuel*, **2010**, *89*, 1221.

(6) Choudhary, T.V.; Malandra, J.; Green, J.; Parrott, S.; Johnson, B. *Angew. Chem., Int. Ed*., **2006**, *45*, 3299.

(7) Nova, A.; Novio, F.; Gonzalez-Duarte, P.; Lledos, A.; Mas-Balleste, R. *Eur. J. Inorg. Chem.*, **2007,** *53,* 5707.

(8) Babich, I.V.; Moulijn, J.A. *Fuel*, **2003**, *82*, 607.

(9) Girgis, M.J.; Gates, B.C. *Ind. Eng. Chem. Res.,* **1991**, *30*, 2021.

(10) Song, C.; Reddy, K.M. *Appl. Catal., A,* **1999,** *176,* 1.

(11) Velu, S.; Ma, X.; Song, C. *Ind. Eng. Chem. Res*. **2003**; *42*, 5293.

(12) Liu, D., Gui, J., Song, L., Zhang, X., Sun, Z. *Pet. Sci. & Tech*., **2008**, *26,* 973.

(13) Wang, H.; Prins, R. *J. Catal*., **2008,** *258,* 153.

(14) Song, C. *Catal. Today,* **2003**, *86,* 211.

(15) Knudsen, K.G.; Cooper, B.H.; Topsoe, H. *Appl. Catal., C,* **1999**, *189*, 205.

(16) Zhao, D.; Wang, J.; Zhou, E. *Green Chem.*, **2007**, *9*, 1219.

(17) Fillipis, P.D.; Scarsella, M.; Verdone, N. *Ind. Eng. Chem. Res*., **2010**, *49*, 4594.

(18) Chica, A.; Gatti, G.; Moden, B.; Marchese, L.; Iglesia, E. *Chem. Eur. J.*, **2006**, *12,* 1960.

(19) Otsuki, S.; Nonaka,, T.; Takashimi, N.; Qian, W.; Ishihara, A.; Imai, T.; Kabe, T. *Energy and Fuels,* **2000**, *14*, 1232.

(20) Qian, E.W. *J. Jpn. Pet. Inst.* **2008**, *51,* 14.

(21) Jiang, X.; Li, H.; Zhu, W.; He, L.; Lu, J. *Fuel*, **2009**, *88*, 431.

(22) R.A. Holl, Methods of Operating Surface Reactors and Reactors Employing Such Methods. U.S. Patent 7,125,527, October 24, 2006.

CHAPTER III

(1) Li, C.; Jiang, Z.; Gao. J.; Yang, Y.; Wang, S.; Tian, F.; Sun, F.; Sun, X.; Ying, P.; Han, C. *Chem. Eur. J.* **2004**, *10*, 2277.

(2) Velu, S.; Ma, X.; Song, C.; Namazian, M.; Sethuraman, S.; Venkataraman, G. *Energy & Fuels*, **2005,** *19,* 1116.

(3) Lee, I.C.; Ubanyionwu, H.C. *Fuel*, **2008**, *87*, 312.

(4) Song, C.; Ma, X. *Appl. Catal. B,* **2003**, *41*, 207.

(5) Choudhary, T.V.; Malandra, J.; Green, J.; Parrott, S.; Johnson, B. *Angew. Chem. Int. Ed.* **2006**, *45*, 3299.

(6) Nova, A.; Novio, F.; Gonzalez-Duarte, P.; Lledos, A.; Mas-Balleste, R. *Eur. J. Inorg. Chem.* **2007**, 53, 5707.

(7) Babich, I.V.; Moulijn, J.A. *Fuel* **2003**, *82*, 607.

(8) Girgis, M.J.; Gates, B.C. *Ind. Eng. Chem. Res.* **1991**, *30*, 2021.

(9) Song, C.; Reddy, K.M. *Appl. Catal. A* **1999**, *176,* 1.

(10) Velu, S. ; Ma, X.; Song, C. *Ind. Eng. Che. Res.* **2003**, *42*, 5293.

(11) Liu, D.; Gui, J.; Song, L.; Zhang, X.; Sun, Z.; *Pet. Sci. & Tech.* **2008**, *26*, 973.

(12) Wang, H.; Prins, R.; *J. Catal.*, **2008**, *258*, 153.

(13) Song, C. *Catal. Today*, **2003**, *86,* 211.

(14) Knudsen, K.G.; Cooper, B.H; Topsoe, H. *Appl. Catal. C* **1999**, *189*, 205.

(15) Wang, J.; Zhao, D.; Li, K. *Energy Fuels* **2010**, *24*, 2527.

(16) Gates, B.C.; Topsoe, H. *Polyhedron* **1997**, *16*, 3213.

(17) Ma, X.; Sakanishi, K. *Ind. Eng. Chem. Res.* **1994**, *33*, 218.

(18) Chica, A. Gatti, G. Moden, B.; Marchese, L.; Iglesia, E.; *Chem. Eur. J.* **2006**, *12*, 1960.

(19) Kong, L.; Li, G.; Wang, X. *Catal. Letters* **2004,** *92,* 163.

(20) Zhao, D.; Wang, J.; Zhou, E. *Green Chem.* **2007**, *9*, 1219.

(21) Qian, E.W. *J. Jpn. Pet. Inst.* **2008**, *51*, 14.

(22) Sundararaman, R.; Ma, X.; Song, C. *Ind. Eng. Chem. Res.* **2010**, *49*, 5561.

(23) Jiang, X.; Li, H.; Zhu, W.; He, L; Shu, H.; Lu, J. *Fuel*, **2009**, *88*, 431.

(24) Holl, R.A. Methods of Operating Surface Reactors and Reactors Employing Such Methods. U.S. Patent 7,125,527, October 24, 2006.

(25) Fox, B.R.; Sun, A.W.; Dauer, H.B.; Male, J.L.; Stewart, M.L.; Tyler, D.R. *Fuel* **2011**, *90*, 998.

(26) Hulea, V.; Fajula, F.; Bousquet, J. *Catal. Today* **2010**, *14*, 1232.

(27) Ramirez-Verduzco, L.F.; Torres-Garcia, E.; Gomez-Quintana, R.; Gonzalez-Pina, V. Murrieta-Guevera, F. *Catal. Today* **2004**, *98*, 289.

(28) Otsuki, S.; Nonaka, T.; Takashima, N.; Qian, W.; Ishihara, A.; Amai, T.; Kabe, T. *Energy & Fuels* **2000**, *14*, 1232.

(29) Xu, X.; Moulijn, J.A.; Ito, E.; Wagemans, R.; Makkee, M. *ChemSusChem* **2001**, *1*, 817.

CHAPTER IV

(1) Sehgal, C.; Steer, R.P.; Sutherland, R.G.; Verral, R.E. *J. Chem. Phys*., **1979**, *70*, 2242.

(2) Suslick, K.S.; Goodale, J.W.; Schubert, P.F.; Wang, H.H. *J. Am. Chem. Soc.*, **1983**, *105*, 5781.

(3) Lewis, K.E.; Golden, D.M.; Smith, G.P. *J. Am. Chem. Soc.*, **1984**, *106*, 3905.

(4) Suslick, K.S.; Hammerton, D.A.; Cline, R.E. *J. Am. Chem. Soc.*, **1986**, *108*, 5641.

(5) Ghoneim, F.B. *Egypt. J. Chem.* **1972**, *15,* 371.

(6) Rosen, B.M.; Percec, V. *Nature*, **2007**, *446*, 381.

(7) Hickenboth, C.R.; Moore, J.S.; White, S.R.; Sottos, N.R.; Baudry, J.; Wilson, S.R. *Nature*, **2007**, *446*, 423.

(8) Gilman, J.J. *Science*, **1996**, *274*, 65.

(9) Frank, I.; Friedrichs, J. *Nat. Chem.*, **2009**, *1*, 264.

(10) Weder, C. *Nature*, **2009**, *459*, 45.

(11) Jensen, F.R.; Coleman, W.E. *J. Org. Chem.,* **1958**, *23*, 869.

(12) Fraenkel, G.; Asahi, Y.; Mitchell, M.J.; Cava, M.P. *Tetrahedron*, **1964**, *20*, 1179.

(13) Jensen, F.R.; Coleman, W.E. *J.C.S. Perkin I*, **1974**, *3*, 415.

(14) Cava, M.P.; Napier, D.R. *J. Am. Chem. Soc.*, **1957**, *79*, 1701.

(15) Beyer, M.K.; Clausen-Schaumann, H. *Chem. Rev.*, **2005**, *105*, 2921.

(16) Wiggins, K.M.; Hudnall, T.W.; Shen, Q.; Kryger, M.J.; Moore, J.S.; Bielawski, C.W. *J. Am. Chem. Soc.*, **2010**, *132*, 3256.

(17) Brunel, J.M.; *Chem. Rev.*, **2005**, *105*, 857.

(18) Pu, L. *Chem. Rev.,* **1998**, *98*, 2405.

(19) Berkowski, K.L.; Potisek, S.L.; Hickenboth, C.R.; Moore, J.S. *Macromolecules*, **2005**, *38,* 8975.

CHAPTER V

(1) Antcliff, K.L.; Murphy, D.M.; Griffiths, E.; Giamello, E. *Phys. Chem. Chem. Phys*., **2003**, *5*, 4306.

(2) Hulea, V.; Moreau, P.; *Jour. of Mol. Catal. A* **1996**, *113*, 499.

(3) Al-Maksoud, W.; Daniele, S.; Sorokin, A.B. *Green Chem.*, **2008**, *10*, 447.

(4) Kong, L.; Li, G.; Wang, X. *Catal. Lett.*, **2004**, *92*, 163.

(5) Chen, X.; Mao, S.S. *Chem. Rev.* , **2007**, *107*, 2891.

(6) Liu, J.; Hu, Y.; Gu, F.; Li, C. *Ind. Eng. Chem. Res.*, **2009**, *48* 735.

(7) Addamo, M.; Bellardita, M.; Di Paola, A.; Palmisano, L. *Chem. Commun.*, **2006**, 4943.

(8) O'Regan, B.; Gratzel, M. *Nature*, **1991**, *353*, 737.

(9) Yamaz, H.C.; Wallis, C.; Howarth, C.R. *Chemosphere*, **2001**, *42*, 397.

(10) Chen, K.; Chen, Y. *J. Sol-Gel Sci. Tech.* **2003**, *27*, 111.

(11) Almquist, C. B.; Biswas, P. *J. Catal.*, **2002**, *212*, 145.

(12) Tai, C. Y.; Tai, C.; Liu, H.; *Chem. Eng. Sci.*, **2006**, *61*, 7479.

(13) Chen, J.; Wang, Y.; Guo, F.; Wang, X.; Zheng, C. *Ind. Eng. Chem. Res.,* **2000**, *39*, 948.

(14) Cafiero, L.M.; Baffi, G.; Chianese, A.; Jachuck, R.J.J. *Ind. Eng. Chem. Res.*, **2002**, *41*, 5240.

(15) Karuppuchamy, S.; Jeong, J.M. *Jour. Oleo Sci.*, **2006**, *55*, 263.

(16) Nag, M.; Ghosh, S.; Rana, R.K.; Manorama, S.V. *J. Phys. Chem. Lett.*, **2010**, *1*, 2881.

(17) Kim, K.D.; Lee, T.J.; Kim, H.T. *Colloids Surf., A*, **2003**, *224*, 1.

(18) Kim, K.D.; Kim, H.T. *Colloids Surf., A*, **2002**, *207*, 263.

(19) Kubo, M.; Kawakatsu, T.; Yonemoto, T. *Trans. Inst. Chem. Eng.*, **1998**, *76*, 669.

(20) Look, J.L.; Zukoski, C.F. *J. Am. Ceram. Soc.*, **1992**, *75*, 1587.

(21) Look, J.L.; Zukoski, C.F. *J. Colloid Interface Sci.*, **1992**, *153*, 461.

(22) Look, J.L.; Zukoski, C.F. *J. Am. Ceram. Soc.*, **1995**, *78*, 21

APPENDIX C

(1) Green, M. M.; Wittcoff, H. A. *Organic Chemistry Principles and Industrial Practice*; Wiley-VCH: Weinheim, 2003; p 137.

(2) Wilczynski, R.; Juliette, J. J. In *Kirk-Othmer Encyclopedia of Chemical Technology (5th Ed.)* 2006; Vol. 16, p 227.

(3) Kukushkin, V. Y.; Pombeiro, A. J. L. *Inorg. Chim. Acta* 2005, *358*, 1.

(4) Ghaffar, T.; Parkins, A. W. *Tetrahedron Lett.* 1995, *36*, 8657.

(5) Ghaffar, T.; Parkins, A. W. *J. Mol. Catal. A: Chem.* 2000, *160*, 249.

(6) Parkins, A. W.; Ghaffar, T. PCT Intl. Appl. WO 9630379, 1996.

(7) Cobley, C. J.; Van den Heuvel, M.; Abbadi, A.; De Vries, J. G. *Tetrahedron Lett.* 2000, *41*, 2467.

(8) Jiang, X.-b.; Minnaard, A. J.; Feringa, B. L.; De Vries, J. G. *J. Org. Chem.* 2004, *69*, 2327.

(9) Breno, K. L.; Pluth, M. D.; Tyler, D. R. *Organometallics* 2003, *22*, 1203.

(10) Ahmed, T. J.; Zakharov, L. N.; Tyler, D. R. *Organometallics* 2007, *26*, 5179.

(11) Ahmed, T. J.; Tyler, D. R. *Organometallics* 2008, *27*, 2608.

(12) Ren, J. G.; Tomita, H.; Minato, M.; Osakada, K.; Ito, T. *Chem. Lett.* 1994, 637.

(13) Osprian, I.; Fechter, M. H.; Griengl, H. *J. Mol. Catal. B: Enzymatic* 2003, *24-25*, 89.

(14) Schuchardt, K. L. D., B. T.; Black, G. D., A Problem-Solving Environment's Evolution Toward Grid Services and a Web Architecture. . In Concurrency and Computation: Practice and Experience, Ecce: 2002; Vol. 14, pp 1221-1239.

(15) Black, G. D. D., B. T.; Elsethagen, T.; Feller, D.; Gracio, D.; Hackler, M.; Havre, S.; Jones, D.; Jurrus, E.; Keller, T.; Lansing, C.; Matsumoto, S.; Palmer, B.; Peterson, M.; Schuchardt, K.; Stephan, E.; Taylor, H.; Thomas, G.; Vorpagel, E.; Windus, T. A Problem Solving Environment for Computational Chemistry, 3.2; Ecce: 2004.

(16) Kendall, R. A.; Apra, E.; Bernholdt, D. E.; Bylaska, E. J.; Dupuis, M.; Fann, G. I.; Harrison, R. J.; Ju, J.; Nichols, J. A.; Nieplocha, J.; Straatsma, T. P.; Windus, T. L.; Wong, A. T. *Comput. Phys. Commun.* 2000, *128*, 260.

(17) Bylaska, E. J. J., W. A. d.; Kowalski, K.; Straatsma, T. P.; Valiev, M.; Wang, D.; Aprà, E.; Windus, T. L.; Hirata, S.; Hackler, M. T.; Zhao, Y.; Fan, P.-D.; Harrison, R. J.; Dupuis, M.; Smith, D. M. A.; Nieplocha, J.; Tipparaju, V.; Krishnan, M.; Auer, A. A.; Nooijen, M.; Brown, E.; Cisneros, G.; Fann, G. I.; Früchtl, H.; Garza, J.; Hirao, K.; Kendall, R.; Nichols, J. A.; Tsemekhman, K.; Wolinski, K.; Anchell, J.; Bernholdt, D.; Hess, P. A.; Jaffe, J.; Johnson, B.; Ju, J.; Kobayashi, R.; Kutteh, R.; Lin, Z.; Littlefield, R.; Long, X.; Meng, B.; Wong, T. A.; Zhang, Z.; NWChem: 2006.

(18) Hariharan, P. C.; Pople, J. A. *Theor. Chim. Acta* 1973, *28*, 213.

(19) Krishnan, R.; Binkley, J. S.; Seeger, R.; Pople, J. A. *J. Chem. Phys.* 1980, *72*, 650.

(20) Andrae, D.; Haeussermann, U.; Dolg, M.; Stoll, H.; Preuss, H. *Theor. Chim. Acta* 1991, *78*, 247.

(21) Martin, J. M. L.; Sundermann, A. *J. Chem. Phys.* 2001, *114*, 3408.

(22) Becke, A. D. *Phys. Rev. A* 1988, *38*, 3098.

(23) Becke, A. D. *J. Chem. Phys.* 1993, *98*, 5648.

(24) Becke, A. D. *J. Chem. Phys.* 1993, *98*, 1372.

(25) Lee, C.; Yang, W.; Parr, R. G. *Physical Review B* 1988, *37*, 785.

(26) Klamt, A.; Schueuermann, G. *J. Chem. Soc., Perkin Trans. 2* 1993, 799.

(27) Stefanovich, E. V.; Truong, T. N. *Chem. Phys. Lett.* 1995, *244*, 65.

(28) Schlesinger, G.; Miller, S. L. *J. Am. Chem. Soc.* 1973, *95*, 3729.

APPENDIX D

(1) Jammot, J.; Pascal, R.; Commeyras, A. *Tetrahedron Lett.* **1989**, *30*, 563-4.

(2) Jammot, J.; Pascal, R.; Commeyras, A. *J. Chem. Soc., Perkin Trans. 2* **1990**, 157-62.

(3) Wechsberg, M.; Schoenbeck, R. Alpha hydroxycarboxylic acid amides. US Patent 4222960, 1980.

(4) Gruber, W.; Schroeder, G. alpha -Hydroxyisobutyramide from acetone cyanohydrin. US Patent 4018829, 1976.

(5) Bousquet, A.; Musolino, A. Hydroxyacetic ester derivatives, namely (R)-methyl 2-(sulfonyloxy)-2-(chlorophenyl)acetates, preparation method, and use as synthesis intermediates for clopidogrel. US Patent 20040260110, 2004.

(6) DeSantis, G.; Zhu, Z.; Greenberg, W. A.; Wong, K.; Chaplin, J.; Hanson, S. R.; Farwell, B.; Nicholson, L. W.; Rand, C. L.; Weiner, D. P.; Robertson, D. E.; Burk, M. J. *J. Am. Chem. Soc.* **2002**, *124*, 9024-9025.

(7) Layh, N.; Parratt, J.; Willetts, A. *J. Mol. Catal. B: Enzym.* **1998**, *5*, 467-474.

(8) Osprian, I.; Fechter, M. H.; Griengl, H. *J. Mol. Catal. B: Enzym.* **2003**, *24-25*, 89-98.

(9) Reisinger, C.; Osprian, I.; Glieder, A.; Schoemaker, H. E.; Griengl, H.; Schwab, H. *Biotechnol. Lett.* **2004**, *26*, 1675-1680.

(10) Ress-loeschke, M.; Friedrich, T.; Hauer, B.; Mattes, R.; Engels, D. Method for producing chiral carboxylic acids from nitriles with the assistance of a nitrilase or microoganisms which contain a gene for the nitrilase. US Patent 6869783, 2005.

(11) Tamura, K. Method of producing optically active alpha -hydroxy acid or alpha -hydroxyamide. US Patent 5736385, 1998.

(12) Yamamoto, K.; Oishi, K.; Fujimatsu, I.; Komatsu, K. Appl. Environ. Microbiol. 1991, 57, 3028-32.

(13) Harrop, T. C.; Mascharak, P. K. *Acc. Chem. Res.* **2004**, *37*, 253-260.

(14) Kovacs, J. A. *Chem Rev* **2004**, *104*, 825-48.

(15) Mascharak, P. K. *Coord. Chem. Rev.* **2002**, *225*, 201-214.

(16) Nagasawa, T.; Yamada, H. *Trends Biotechnol.* **1989**, *7*, 153-8.

(17) Kobayashi, M.; Nagasawa, T.; Yamada, H. *Trends Biotechnol.* **1992**, *10*, 402-8.

(18) Green, M. M.; Wittcoff, H. A. *Organic Chemistry Principles and Industrial Practice*, 2003.

APPENDIX E

(1) Ahmed, T.J. Investigations of Transition Metal Catalysts for the Hydration of Cyanohydrins and Ligand Effects in Aqueous Molybdocene Chemistry. Ph.D. Dissertation, University of Oregon, Eugene, OR, 2008.

(2) Ghaffar, T.; Parkins, A.W. *J. Mol. Catal. A: Chem.*, **2000**, *160*, 249.

(3) Ahmed, T.J.; Fox, B.R.; Knapp, S.M.M.; Yelle, R.; Juliette, J.J.; Tyler, D.R. *Inorg. Chem.*, **2009**, *48*, 7828.

(4) Ahmed, T.J.; Zakharov, L.N.; Tyler, D.R. *Organometallics*, **2007**, *26*, 5179.

(5) Ghaffar, T.; Parkins, A.W *Tetrahedron Letters* **1995**, *36*, 8657.

(6) Song, J.E.; Kim, B.; Ha, Y. *Mater. Sci. Eng.,* C, **2004**, *191* 24.

(7) Hays, H.R. *J. Org. Chem.*, **1968**, *33*, 3690.